Numerical and Statistical Analysis of Long-Haul Undersea Optical Communication Systems

Terence Broderick

Doctor of Philosophy

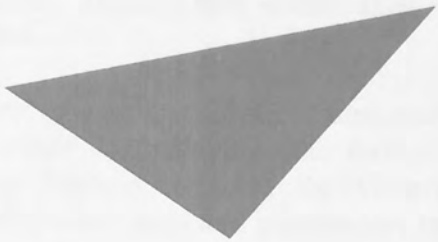

Aston University

April 2009

ASTON UNIVERSITY

Numerical and Statistical Analysis of Long-Haul Undersea Optical Transmission Systems

Terence Broderick

Doctor of Philosophy 2009

Thesis Summary

In this thesis, we numerically investigate the upgrade, to higher bit-rate, of long-haul undersea optical transmission systems. We complement our analysis with a detailed statistical investigation of the new systems, deriving new statistical estimation algorithims for BER in nonlinear transmission regimes

Firstly, we numerically model a practical 20 Gb/s undersea configuration employing the Return-to-Zero Differential Phase Shift Keying data format. The modelling is completed using the Split-Step Fourier Method to solve the Generalised Nonlinear Schrödinger Equation. We optimise the dispersion map and per-channel launch power of these channels and investigate how the choice of pre/post compensation can influence the performance. After obtaining these optimal configurations, we investigate the Bit Error Rate estimation of these systems and we see that estimation based on Gaussian electrical current systems is appropriate for systems of this type, indicating quasi-linear behaviour.

The introduction of narrower pulses due to the deployment of quasi-linear transmission decreases the tolerance to chromatic dispersion and intra-channel nonlinearity. We used tools from Mathematical Statistics to study the behaviour of these channels in order to develop new methods to estimate Bit Error Rate. We initialise this study through the close manipulation of the dispersion map in order to increase pulse broadening and enable the manifestation of intra-channel effects such as Four-Wave Mixing and Cross-Phase Modulation. We see that we can use the statistical measure of kurtosis to effectively characterise nonlinearity. This leads to the consideration of new models to estimate the Bit-Error Rate when intra-channel nonlinearity dominates the source of distortion in the transmission. Using the measure of kurtosis to characterise nonlinearity, we introduce new models for BER estimation based on the exponential and power law distributive families. We show that for different limits, these models can allow us to predict transmission errors more effectively than the popular Gaussian statistics based model.

In the final section, we consider the estimation of Eye Closure Penalty, a popular measure of signal distortion. Using a numerical example and assuming the symmetry of eye closure, we see that we can simply estimate Eye Closure Penalty using Gaussian statistics. We also see that the statistics of the logical ones dominates the statistics of signal distortion in the case of Return-to-Zero On-Off Keying configurations.

Keywords: Upgrading Undersea Systems, RZ-DPSK modulation format, BER Estimation, Nonlinearity, Power-Law Distributions

Acknowledgements

Firstly, I would like to thank my supervisor Professor Sergei K. Turitsyn for the unwavering support, encouragement and guidance offered to me during my time at Aston University. His ideas and motivation have been imperative in my completion of this thesis.

I would also like to reserve special thanks for Dr Sonia A. Boscolo for her patient and consistent support throughout my time at Aston University. I deeply appreciate her knowledge, experience and kind nature. In addition, I would like to thank Dr Vladimir K. Mezentsev, Professor Keith J. Blow, Dr Paul Harper and Dr Stanislav Derevyanko for never letting me leave their office without an answer.

My friends in the Electronics Engineering Department also deserve my gratitude for providing me with three and a half years of excellent conversation and support. In particular; Irina Nasieva, Jovana Petrovic, Edd Davies, Richard Haywood, Saty Mukherjee, Graham Smith, Pouneh Saffari, Mandana Baregheh, Guchun Zhang, Ian Johnson, Steve Grice, Scott Fowler and Brendan Slater have all proved to be firm friends. I would also like to thank the rest of my friends from Aston University.

The Mathematics department at Liverpool University deserve thanks for teaching me about a truly beautiful subject and for giving me the confidence to believe in myself and developing my ability to apply my mind.

I would like to thank my partner, Rebecca Forsyth, for her patience, love and support throughout my time at Aston, this must also be extended to all of my family and friends back in the northwest. In particular; Mum, Dad, Dorothy, Sarah, Claire and Patricia.

Contents

List of Figures

This page has been left intentionally blank

List of Tables

Chapter 1 Introduction

The demand placed on communication systems around the world is constantly increasing due to increased data stemming from internet traffic and telephone calls. Most of this data is now passed along optical fibre. The available bandwidth and low loss of optical fibres make them far more attractive than the alternatives, such as coaxial (copper) cable, for cost effective high capacity data transmission. The data rate required for a standard telephone conversation is 64 kb/s [1], therefore a single optical fibre operating at a data rate of 10 Gb/s is able to carry, simultaneously, more than one hundred and fifty thousand telephone calls. However, communication systems are now used to transmit television and radio calls in addition to computer data, substantially increasing the required capacity.

In this chapter of the thesis, we provide an overview of the rise of optical communications leading into undersea communications. We explore the main issues surrounding the upgrade of these systems and explore some performance metrics; motivating the remainder of the thesis. Starting with a brief historical overview of the growth of undersea data transmission, we cover the failed attempts to install undersea systems of vast length and the establishment of the 'blue book' which provided historical recommendations for the implementation of such systems [2].

1.1 The Rise of Optical Transmission

The first undersea cables were laid between Calais and Dover in 1850. Unfortunately, this cable was immediately recovered by a fisherman believing to have recovered a "golden alga" in his net. In 1856, the Atlantic Telegraph Company was founded by John Brett, Charles Bright, Charles Wheatstone and Cyrus Field. Work then started on a project aimed at crossing the Atlantic, this particular milestone would dominate telecommunications for years to come as part of a larger project to connect the entire world.

Activity commenced in the US, with the Western Union Telegraph Co. (hereafter referred to as WU), starting work in 1873 on a cable between Key-West and Cuba. They also leased the three transatlantic cables of both Direct United States Telegraph Co. and the American Telegraph and Cable Co. founded by Jay Gould in 1881. Supported by the most important North American domestic network, WU established partnerships wih large European companies.

The year 1873 witnessed the formation of the Commercial Cable Company, which was founded by two companies unhappy about current telegraphy tariffs. It was felt that better value and higher levels of efficiency could be given. A list of all cables laid in the Atlantic from 1858 to 1928 shows 25 cables, this demonstrated the gathering of momentum in the undersea industry. From 1875 to 1960, operators alternated between periods of very hard competition and quiet cooperation. The U.S. government strongly defended competition favourable to the interests of the two American companies, Western Union and the Commercial Cable Company. In 1912, the Anglo-American board decided to transfer the network to Western Union and the two groups worked smoothly with their associates: Western Union, Italcable and German DAT on the one hand and CCC and CFCT (Compagnie Francaise des Cables sous-marins Telegraphiques) on the other [2].

Prior to installation of the Canada-Australia cable (Vancouver-Australia, 1896), the Eastern Cable Co. objected to the laying of an expensive cable since Canada and Australia already had connections to the U.K. The cable was built by Telcon and was laid by CS Colonia, built with the intention of laying the longest section between Vancouver and Fanning Island. The capacity of this cable was 200 words per minute. This epitomised the attempts to link the

distant land masses of the world and this continued until the 1960's, when the discovery of data communications using optical fibres was made.

1.2 Optical Fibres

The key discoveries in regard to the emergence of optical communications are the laser (1960) and the optical fibre (1964-1966). In its simplest form, an optical fibre comprises a cylindrical core of silica glass surrounded by a cladding whose refractive index is lower than that of the core [3]. One type of fibre exhibits an abrupt index change at the core-cladding interface, such fibres are called step-index fibres. In a different type of fibre, known as graded-index fibre, the refractive index changes gradually inside the core. We show below (schematically) the cross-section and index profile for the two kinds of fibre.

Shown in Figure 1.1, Figure 1.2, Figure 1.3 and Figure 1.4 are the cross section and refractive index profile of a step-index fibre respectively. The main difference is the behaviour of the refractive index in the centre of the core. Step-Index and Graded-Index fibres can be used for short distances (~ 1 km) at low bit-rates.

This is expressed through the initial condition at the core-cladding interface in that for a step-index fibre the change in direction is sharp and discontinuous (Figure 1.3), whereas for a graded-index fibre the change is continuous (Figure 1.4). The propagation of the light in the respective fibres is shown in Figure 1.5. Both of these basic fibres were of limited use in optical communications and have since been superceded through consideration of the fibre mode. This is a general concept from lasers and optics. An optical mode refers to the specific solution of the radial wave equation satisfying the appropriate boundary conditions for the particular fibre geometry and also enjoys the property that the spatial distribution of the

intensity of the optical pulse doesn't change when the pulse is propagated. In strict practical language, the mode corresponds to the path which light can follow in the fibre.

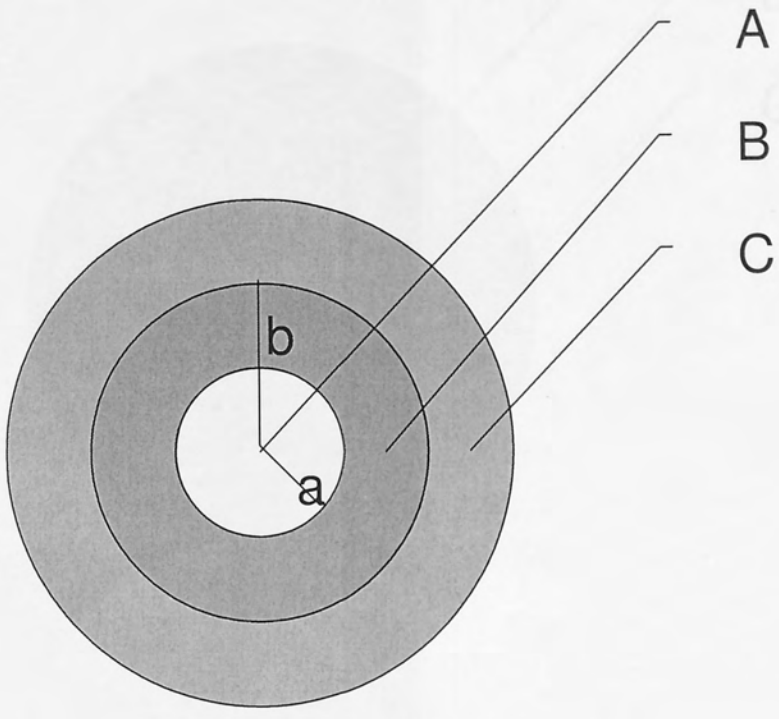

Figure 1.1: Step-index fibre with A) Jacket B) Cladding C) Core with core radius a and cladding radius b

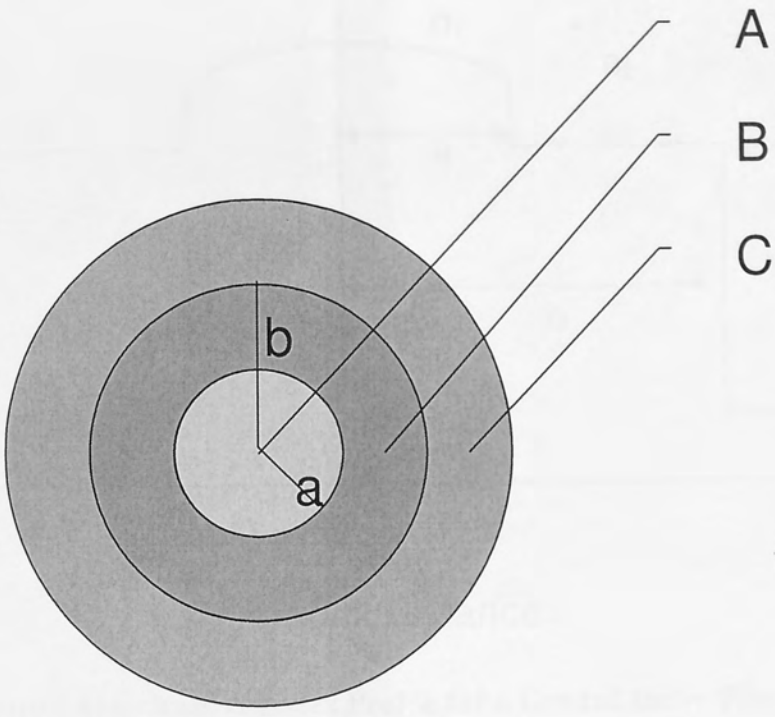

Figure 1.2: Graded Index Fibre with A) Jacket B) Cladding C) Core with core radius a and cladding radius b

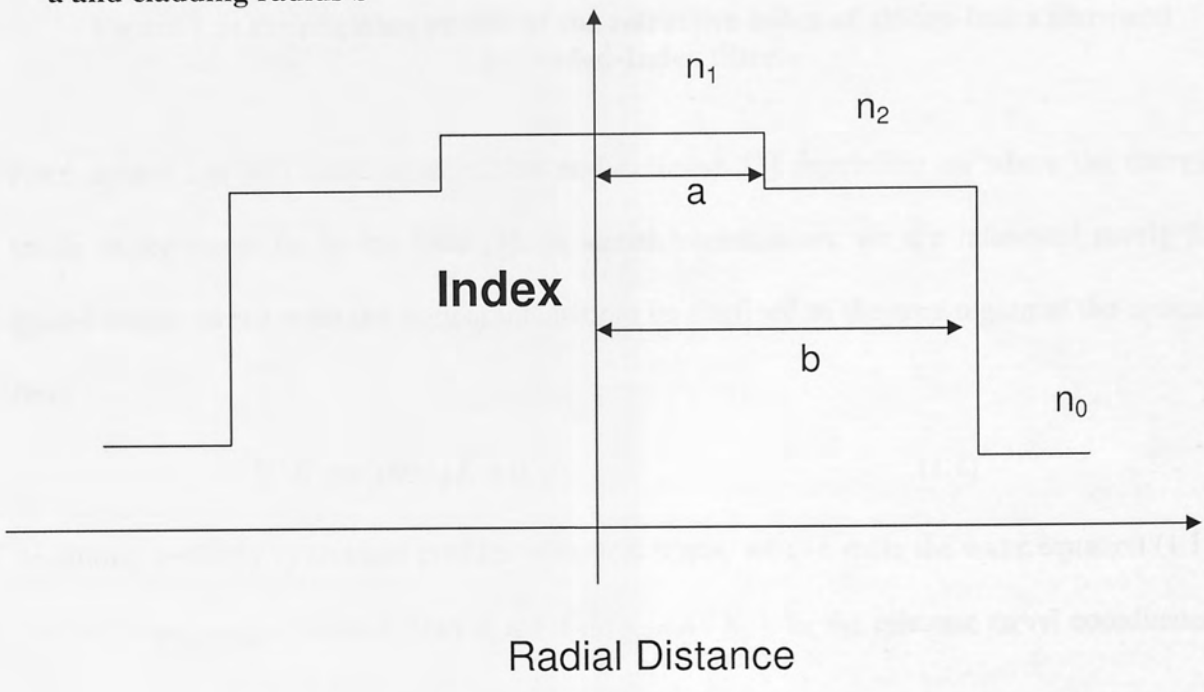

Figure 1.3: Refractive Index Profile Step-Index Fibre

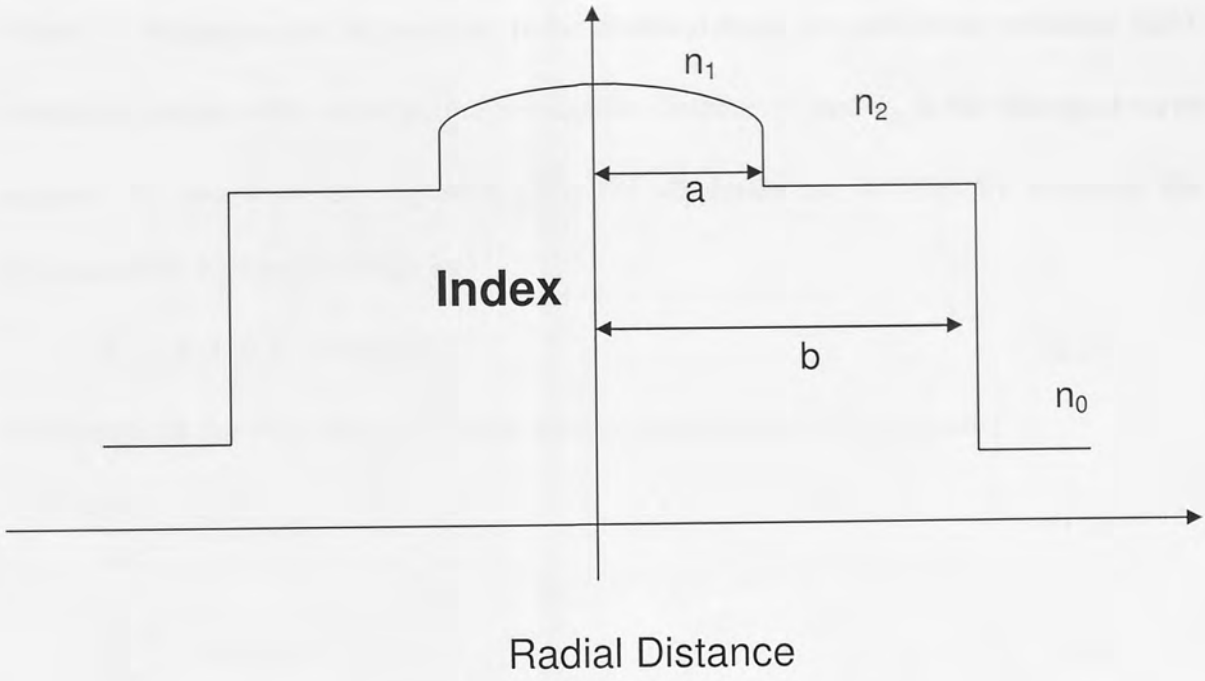

Figure 1.4: Refractive Index Profile for a Graded Index Fibres

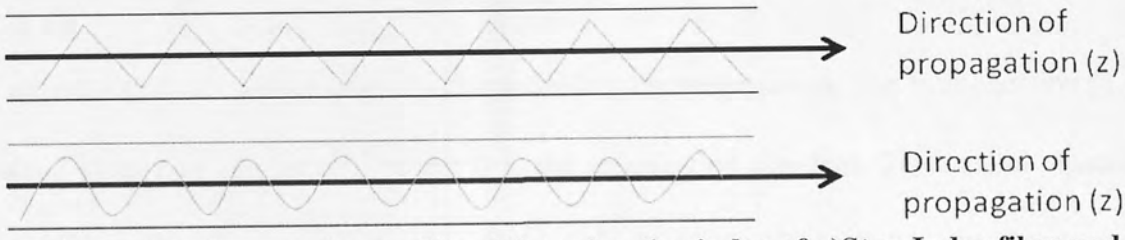

Figure 1.5: Propagation profile of the refractive index of a)Step-Index fibre and b)Graded-Index fibre.

Fibre modes can be classified as guided and radiative [3] depending on where the energy levels of the mode lie in the fibre [3]. In signal transmission, we are interested purely in guided modes as we want our optical intensity to be confined to the core region of the optical fibre.

$$\nabla^2 \tilde{E} + n^2(\varpi) k_0^2 \tilde{E} = 0 \qquad (1.1)$$

Assuming perfectly cylindrical profiles of optical fibres, we can write the wave equation (1.1) for the propagating electrical field in the z-direction (E_z), in the relevant radial coordinates as;

$$\frac{\partial^2 E_z}{\partial \rho^2} + \frac{1}{\rho}\frac{\partial E_z}{\partial \rho} + \frac{1}{\rho}\frac{\partial^2 E_z}{\partial z^2} + \frac{\partial^2 E_z}{\partial z^2} + n^2 k_0^2 E_z = 0 \qquad (1.2)$$

Where E_z (dropping the tild notation) is the electrical field, $n = n(\varpi)$ is the refractive index (which is constant with respect to the propagation distance z) and k_0 is the free-space wave number. We can solve this equation using the separation of variables by assuming the electrical field E_z can be written as;

$$E_z(\rho,\phi,z) = F(\rho)\Phi(\phi)Z(z) \tag{1.3}$$

Substitution of this form into (1.2) yields three ordinary differential equations;

$$\frac{d^2Z}{dz^2} + \beta^2 Z = 0 \tag{1.4}$$

$$\frac{d^2\Phi}{d\phi^2} + m^2\Phi = 0 \tag{1.5}$$

$$\frac{d^2F}{d\rho^2} + \frac{1}{\rho}\frac{dF}{d\rho} + (n^2k_0^2 - \beta^2 - \frac{m^2}{\rho^2})F = 0 \tag{1.6}$$

The quantity m is an integer quantity characterising the propagation. The first equation (1.4) is solved simply as $Z(z) = e^{i\beta z}$, where ß is the propagation constant. The second equation (1.5) can be solved similarly as $\Phi(\phi) = e^{im\phi}$ and the third equation (1.6) is nothing more than the Bessel equation [4] . The general solution, of course, is written in the form of Bessel functions (in the core and cladding regions respectively) [4].

$$F(\rho) = AJ_m(p\rho) + A'Y_m(p\rho) \tag{1.7}$$

For $\rho \le a$, and for $\rho > a$, we obtain this solution

$$F(\rho) = CK_m(q\rho) + C'I_m(q\rho) \tag{1.8}$$

Where A, A', C and C' are constants and I_m, J_m, Y_m, K_m are the four different kinds of Bessel functions [5], given in integral form by the equations.

$$J_n(z) = \frac{1}{\pi}\int_0^{\pi}\cos(n\tau - z\sin\tau)d\tau \tag{1.9}$$

$$Y_n(z) = \frac{1}{\pi}\int_0^{\pi}\sin(z\sin\tau - n\tau)d\tau - \frac{1}{\pi}\int_0^{\infty}\left(e^{n\tau} + (-1)^n e^{-n\tau}\right)e^{-z\sinh\tau}d\tau \tag{1.10}$$

$$I_n(z) = \frac{1}{\pi}\int_0^{\pi} e^{z\cos\tau}\cos(n\tau)d\tau - \frac{\sin(n\pi)}{\pi}\int_0^{\infty} e^{-z\cosh\tau - n\tau}d\tau \tag{1.11}$$

$$K_n(z) = \frac{\Gamma\left(n+\frac{1}{2}\right)(2z)^n}{\sqrt{\pi}}\int_0^{\infty}\frac{\cos\tau}{\left(\tau^2+z^2\right)^{n+1/2}}d\tau \tag{1.12}$$

The parameters p and q are defined by[3];

$$p^2 = n_1^2 k_0^2 - \beta^2 \tag{1.13}$$

$$q^2 = \beta^2 - n_2^2 k_0^2 \tag{1.14}$$

Considerable simplification of (1.7) occurs when we use the boundary condition that the optical field for a guided mode should be finite at $\rho = 0$ and decay to zero as $\rho \to \infty$. Since $Y_m(p\rho)$ has a singularity at $\rho = 0$ [5], $F'(0)$ can only remain finite provided that $A' = 0$. Similarly, $F(\rho) = 0$ vanishes at infinity only if $\rho = 0$. Therefore, we can write the general solution of (1.2) as

$$E_z = AJ_m(p\rho)e^{i(m\phi+\beta z)} \tag{1.15}$$

Inside of the core, yet outside of the core, we write a similar solution as;

$$E_z = CK_m(q\rho)e^{i(m\phi+\beta z)} \tag{1.16}$$

We can use the same method to obtain H_z, the magnetic field component in the z-direction which satisfies the same equation (1.2), but uses different constants B and D;

$$H_z = BJ_m(p\rho)e^{i(m\phi+\beta z)} \tag{1.17}$$

$$H_z = DK_m(q\rho)e^{i(m\phi+\beta z)} \tag{1.18}$$

For $\rho \le a$, and for $\rho > a$, respectively. The solutions to equation (1.2) for both E_z and H_z suggest the dependence of the mode propagation is largely in the direction of the radius of the core, which is consistent with the definition of a mode. The other four components, $(E_\rho, E_\phi, H_\rho, H_\phi)$, can be expressed in terms of Maxwell's equations for an electrical field [6]. In the core region, we obtain the components as;

$$E_\rho = \frac{i}{\rho^2}\left(\beta\frac{\partial E_z}{\partial\rho} + \mu_0\frac{\varpi}{\rho}\frac{\partial H_z}{\partial\phi}\right) \tag{1.19}$$

$$E_\phi = \frac{i}{\rho^2}\left(\frac{\beta}{\rho}\frac{\partial E_z}{\partial\phi} - \mu_0\varpi\frac{\partial H_z}{\partial\rho}\right) \tag{1.20}$$

$$H_\rho = \frac{i}{\rho^2}\left(\beta\frac{\partial H_z}{\partial\rho} - \varepsilon_o n^2\frac{\varpi}{\rho}\frac{\partial E_z}{\partial\phi}\right) \tag{1.21}$$

$$H_\phi = \frac{i}{\rho^2}\left(\frac{\beta}{\rho}\frac{\partial H_z}{\partial\phi} + \varepsilon_o n^2\varpi\frac{\partial E_z}{\partial\rho}\right) \tag{1.22}$$

The quantities μ_0 and ε_0 represent the vacuum permeability and vacuum permittivity of the optical medium respectively. These equations express the electromagnetic field in the core and cladding regions of an optical fibre in terms of the four constants A, B, C and D; which are determined by applying the boundary conditions that the tangential components of the vectors **E** and **H** be continuous across the core-cladding interface. This requirement of continuity gives us four homogenous ordinary differential equations satisfied by A, B, C and D [3]. These equations have a nontrivial solution only if the determinant of the coefficient matrix vanishes. Such a condition gives the following eigenvalue equation[3];

$$\left[\frac{J_m'(pa)}{pJ_m(pa)} + \frac{K_m'(qa)}{qK_m(qa)}\right]\left[\frac{J_m'(pa)}{pJ_m(pa)} + \frac{n_2^2}{n_1^2}\frac{K_m'(qa)}{qK_m(qa)}\right] = \frac{m^2}{a^2}\left(\frac{1}{p^2} + \frac{1}{q^2}\right)\left(\frac{1}{p^2} + \frac{n_2^2}{n_1^2}\frac{1}{q^2}\right) \tag{1.23}$$

Given the parameters k_0, a, n_1 and n_2, these equations can be solved numerically to give the propagation constant β. Generally, the solution of the equations is non-unique and is denoted β_{mn} for each (m,n) combination. These are called fibre modes. Since this doesn't change with respect to pulse propagation and satisfies the boundary conditions, these are optical modes. Generally, E_z and H_z are non-zero. Modes are often denoted as EH and HE, dependent on which mode dominates the propagation. Any mode is uniquely determined by the propagation constant β.

Single Mode Fibre (SMF) supports only one mode (the HE_{11} mode) [3]. This is also known as the fundamental mode of the fibre. These fibres are designed such that all higher order modes are cut off at the operating wavelength. The fundamental mode has no cutoff and is always supported by a fibre.

Methods such as Chemical Vapour Deposition (CVD) allowed the custom configuration of such fibres as opposed to traditional glass forming techniques [2]. CVD has the advantage of allowing the deposition of metals in very thin layers, an obvious advantage in fibres with radius of the order of a few microns. There are a wide range of metals that can be deposited in order to configure fibres such as silicon and germanium.

Fibre Loss

The key obstacle in the development of optical fibres was the losses due to intrinsic properties of the material. The loss-wavelength profile of single-mode fibre is given, Figure 1.6. The birth date of optical communications systems is 1970 with the demonstration of the first continuous wave (CW) operation at room temperature, of a gallium arsenide (GaAs) based laser on one hand, and of the possibility of obtaining very low loss (20 dB/km) silica optical fibre on the other hand. The miracle was that the so-called first transmission window matched the wavelength of the GaAs laser (~850 nm) (shown in Figure 1.6).

Fibre loss is a measure of the loss of power experienced by the optical signal throughout transmission and is also known as attenuation. The reasons for attenuation are material absorption and Rayleigh scattering, with the former being due to metal impurities placed into the fibre during manufacture and the latter arising from density fluctuations frozen into the fibre during manufacture.

Attenuation is characterised by the quantity α, expressed in dB/km as;

$$\alpha[dB/km] = \frac{1}{L} 10 \log_{10}\left(\frac{P_1}{P_0}\right)$$

Where P_1 is the signal power after some fixed distance, L, and P_0 is the initial power.

Resulting local fluctuations in the refractive index scatter light in all directions throughout the fibre. Attenuation was the first obstacle in the use of these fibres and we can use this quantity to characterise the progress of optical communications from its beginnings to what we have today.

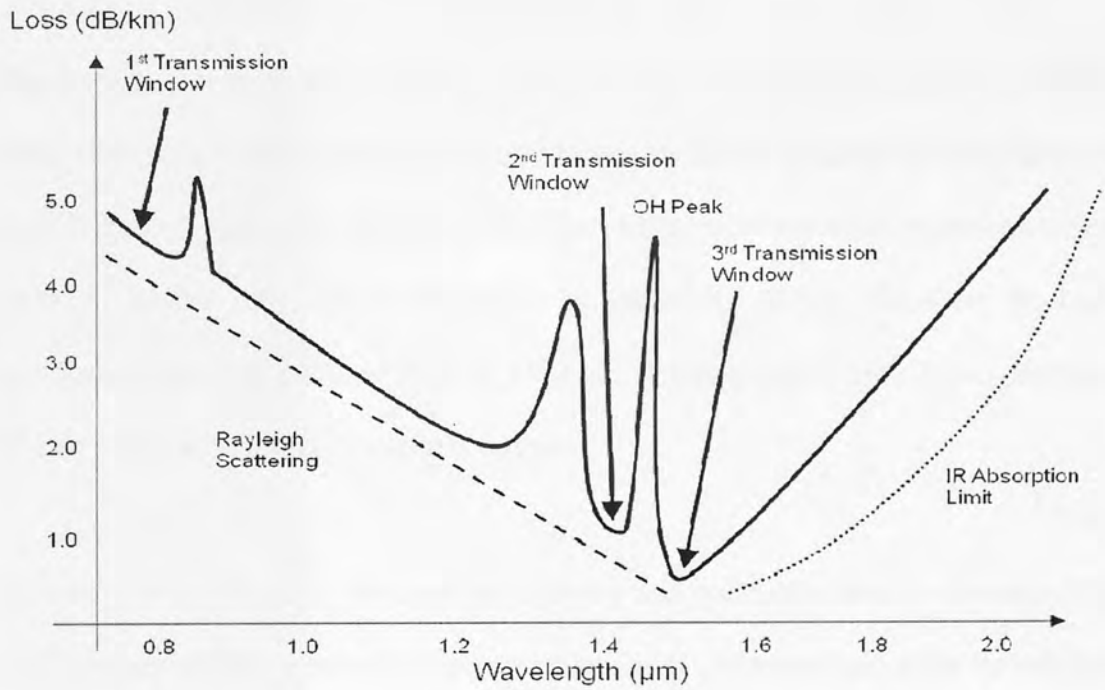

Figure 1.6: Loss Profile of Single Mode Fibre. Optimal conditions for transmission are found at a loss of 0.2 dB/km at 1.55 μm

Second and Third Transmission Window

Semi-conductor lasers such as the GaA laser are very attractive provided they can be operated in a continuous-wave mode at room-temperature. The first demonstration was made in 1962: It was in a pulsed operation at liquid helium with a temperature of 4K, far away from the

required conditions. The laser was a p-n junction with direct polarization, and because of the intrinsic properties of the bulk material (temperature dependence of the minority carriers diffusion length), there was no hope of significant improvement in the laser characteristics. The lasers first demonstration at room temperature was obtained at Bell Laboratories in 1970. This fulfilled the conditions for the testing of optical transmission systems.

The simplification of fibre splicing and the subsequent connection of components (emitter to receiver), multimode fibres (core diameter of 50 to 62.5 μm) were chosen [2]. Test-beds for about 10-km links at 34 or 45 Mbps were realised in the second half of the 1970s, followed by the first mid-distance repeater-less industrial systems in the early 1980s.

Rapid progress was made in splicing and connecting techniques [7], promoting SMFs as the likely choice for further development. Additionally, further progress in fibre manufacturing (mainly through improved material purification) led to evidence of the second window around 1300 nm (Figure 1.6), with an attenuation of around 0.4 dB/km. Moreover, the bulk silica chromatic dispersion vanished close to 1300 nm; it was therefore possible to propagate high bit-rate pulses with minimum pulse broadening.

In view of such progress, the undersea industry and operators dared to decide to build the TAT-8 (trans-atlantic) system by pioneering the use of 1300nm single mode techniques at 280 Mbps (Anon., 1984). This decision demanded the solution of a number of technical problems, from connectors to branching units. The most severe challenge was the repeater, with the need to make an optical/electrical conversion, then to electrically regenerate the signal, and finally to make an optical/electrical conversion. Two key points needed to be addressed:

- Electronic circuits at 280 Mbps with good reliability were needed.

- The emitters and receivers inside the repeater needed to be reliable and have a long lifetime.

Extensive research and development was undertook over many years. This led to the successful installation and implementation of TAT-8 at the end of 1987, quickly followed by TPC-3 (trans-pacific link) with identical technology. In the meantime, the minimum absorption of silica fibres was shown to be 0.2 dB/km [8] with a relatively small chromatic dispersion at 1550nm (Figure 1.6), the third window and a wavelength range compatible with the delicate technology of GaInAsP lasers. Consequently, the TAT-9 and TPC-5 systems were installed and operated in late 1989 at 560 Mbps per fibre. TAT-9 employed a Y configuration, with one end in the United States and the other two in Great Britain and France. The branching unit was an undersea active multiplexer, allowing for adjustable bit-rate allocation between Great Britain and France, a unique feature that was not reproduced later.

Optical Amplification

Upon completion of the 560 Mbps configuration, industrialists thought in a very naïve way that the newly developed system would cope with the needs for some time and, consequently, it was not urgent to think about a new higher performance system for some time. The rise of information technology rendered this an incorrect assumption to make, as it became obvious that a 2.5 Gbps system was required, with questions raised about the ability of the legacy system to satisfy these requirements. Traditional methods of signal regeneration had in their favour the "known technology" argument. A system CANTAT-3 was developed along these lines and installed by STC, but it was only a "one-shot action".

The second possibility was to jump into the ambitious approach of optical amplification. For a number of years, laboratories had been working on the natural scheme of the semi-conductor

amplifier. However, it turned out that some basic physical properties (such as the bandwidth and the loss of information due to electro-optic reconversion) of these amplifiers were not compatible with the requirements of long-distance systems, especially when taking into account the possibility of WDM. Optical amplification enhances incident lightwaves through stimulated emission, the process about which lasers are based. In contrast, the already well-known erbium-doped fibre amplifier with a metastable (1ms) upper level was very promising and is now a key technology of optical communications [9].

The erbium doped fibre amplifier (EDFA) was first reported in 1987 [10] and has since transformed the optical communications arena. The EDFA is used in a number of ways, but by far the most popular was their use as repeaters to compensate for transmission loss. Other applications now include nonlinear regenerative devices [11]. They offered a unique combination of features that would revolutionize lightwave communication systems such as high gain, low noise and polarization independence. Other amplification schemes have been proposed for optical communication systems.

One of these schemes is Raman amplification [12], which is expected to become very important for the next generation undersea transmission system [13]. Raman amplification utilises the effect of Stimulated Raman Scattering (SRS) to transfer energy from a co-propagating pump wave to the carrier wave. SRS is discussed later in the context of its physical manifestation as an optical nonlinearity.

Scheme	Advantages	Disadvantages
Raman	**Useful at any wavelength provided the pump is suitably aligned**	**Backscattering of the copropagating waves can result in noise.**
Brillouin	**High Gain when threshold is exceeded**	**Very low bandwidth < 100 MHz**
Distributed	**Potential for lower noise accumulation.**	**Requires substantial pump power from either end of the transmission link**
Erbium-Doped	**Large bandwidth**	**Accumulation of ASE noise**

Table 1.1: Advantages and Disadvantages of Amplification Schemes

Another proposed scheme is distributed amplification. The implementation of such a scheme involves doping all of the transmission fibre with erbium, but at significantly lower concentrations, thus providing a continuous amplification scheme. EDFA provided benefits compared to the other optical amplifier technologies, as explored in the Table 1.1.

The choice of amplifier in undersea transmission is dominated by the EDFA configuration. The EDFA is a nearly ideal building block for providing optical gain in a lightwave communication system [12]. EDFAs can be made with a variety of gains in the low-loss 1550 nm wavelength window of telecommunication fibres. With nearly ideal noise performance. EDFA's amplify high speed signals without distortion or cross talk between wavelengths. The undersea portion of the transmission system is essentially a chain of concatenated amplifiers and cable sections, providing optical gain to overcome attenuation in the lightwave cable.

Several phenomena limit the transmission performance of long-haul optical transmission systems, including noise (due largely to EDFAs), dispersion and nonlinearities.

The use of EDFA's in optical transmission systems has its benefits in the simple fact that it can be used for what is known as 1-R regeneration [14] without the need for opto-electrical reconversion and compensate exactly for fibre losses. Regeneration such as 1-R refers to simple re-amplification of optical signals. In undersea optical transmission systems, EDFA's are used to compensate for fibre losses. However, there is a problem with the use of such apparatus.

Figure 1.7: Energy Level Diagram describing Amplified Spontaneous Emission (ASE)

Physically, the excited ions from the erbium can spontaneously relax from the upper state to the ground state by emitting a photon that is uncorrelated with the signal photons [15], as shown in Figure 1.7. This spontaneously emitted photon can be amplified as it travels down the fibre and stimulates the emission of more photons from excited ions, photons that belong to the same mode of the electromagnetic field as the original spontaneous photon. This process is parasitic to the optical signal, and can occur at any frequency within the fluorescence spectrum of the amplifier[9]. It reduces the gain of the optical amplifier because it robs photons that would otherwise participate in stimulated emission with the signal photon.

This phenomenon is referred to as ASE (or ASE noise) and we now define it in terms of the Optical Signal to Noise Ratio (OSNR).

The detrimental effect of ASE is commonly characterised through the noise figure, this is defined as the ratio between the *OSNR* at the input and output of the optical amplifier;

$$F_n = \frac{OSNR_{in}}{OSNR_{out}} \tag{1.24}$$

This noise figure will always be greater than one because $OSNR_{in}$ will always be greater than $OSNR_{out}$. We can demonstrate this through the following proof by contradiction simply by considering a fictitious amplifier with no output noise and Gain (G) > 1. The output SNR would then be given by shot noise, which is the random fluctuation of the phase of the photons [15]. The dominance of the shot noise means that the variance of the noise would be given by $\sigma^2 = G < n(0) >$, where $< n(0) >$ is the average number of photons in the launched signal. The output SNR for an amplifier is given by the equation [9];

$$SNR_{out}(z) = \frac{<< n(z) > - < n(z) >_{ASE} >_T^2}{\sigma^2(z)} = \frac{G^2(z) < n(0) >^2}{\sigma^2(z)} \tag{1.25}$$

Where $\langle n(z) \rangle_{ASE}$ is the background ASE noise, $\langle n(0) \rangle$ is the mean number of photons in the modulated signal [15] and T is the bit-slot. The quantity $\sigma^2(z)$ is the noise power measured over the bit period. So we can use equation 1.25 to produce an equation for $OSNR_{out}$;

$$OSNR_{out} = \frac{[G\langle n(0) \rangle]^2}{\sigma^2} = G\langle n(0) \rangle \tag{1.26}$$

If we assume that input signal photons follow Poisson statistics [9], then we know that (variance equals mean);

$$\sigma^2(0) = \langle n(0) \rangle \tag{1.27}$$

So from equation 1.26, we can say that;

$$OSNR_{in} = \langle n(0) \rangle \tag{1.28}$$

Upon substitution into the equation for F_n (1.24);

$$F_n = \frac{1}{G} \tag{1.29}$$

Under our previous assumption on G, $F_n < 1$. This is a contradiction because we have already said that $F_n > 1$ due to its nature as a method of degradation in OSNR. The amplifier always adds noise. The noise figure is usually quoted in dB;

$$F_n[dB] = 10\log_{10}(\frac{OSNR_{in}}{OSNR_{out}}) \tag{1.30}$$

In a more realistic configuration, the noise figure is computed under the assumption that the input signal is shot-noise limited. In this case we can say the following [9];

$$OSNR_{in} = \frac{I_s^2}{2eI_sB_e} = \frac{I_s}{2eB_e} \tag{1.31}$$

Where I_s is the input signal current, and B_e is the electrical bandwidth of the signal [9]. The signal-to-noise ratio at the output of the amplifier is given by the expression [16];

$$OSNR_{out} = \frac{(GI_s)^2}{N_{s-sp} + N_{sp-sp} + N_{shot}} \tag{1.32}$$

Where the noise powers due to signal-noise beating (N_{s-sp}), noise-noise beating (N_{sp-sp}) and shot noise (N_{shot}) are given by [16];

$$N_{s-sp} = 2GI_sI_{sp}\frac{B_e}{B_o} \tag{1.33}$$

$$N_{sp-sp} = \frac{1}{2}I_{sp}^2\frac{B_e(2B_o - B_e)}{B_o^2} \tag{1.34}$$

$$N_{shot} = 2B_e(GI_s + I_{sp})e \tag{1.35}$$

Where I_{sp} is the current of the spontaneous emission, B_o is the optical bandwidth of the signal and G is the gain of the pertinent optical amplifier. Using these expressions, we can say that;

$$F_n = \frac{G\frac{I_s^2}{e} I_{sp} \frac{1}{B_0} + \frac{1}{4}\frac{I_s}{e} I_{sp}^2 \frac{(2B_o - B_e)}{B_o^2} + I_s(GI_s + I_{sp})}{(GI_s)^2} \tag{1.36}$$

We can then use that the current of the spontaneous emission can be given as [15];

$$I_{sp} = 2n_{sp}(G-1)eB_0 \tag{1.37}$$

Where n_{sp} is the spontaneous emission factor. Upon substitution into equation (1.36), we obtain;

$$F_n = 2n_{sp}\frac{(G-1)}{G} + \frac{1}{G} + \frac{n_{sp}(G-1)^2 e(2B_o - B_e)}{G^2 I_s} + \frac{2(G-1)n_{sp}eB_0}{G^2 I_s} \tag{1.38}$$

Assuming high amplifier gain (G >> 1), we can deliver a good approximation of practical interest for the noise figure. For high amplifier gain, the first term reduces to $2n_{sp}$, the second term becomes negligible, the last term disappears due to the dominance of large G and the third term tends to zero if we assume that the denominator becomes large if the input power is suitably large. Under this limit, we can say;

$$F_n \approx 2n_{sp} \tag{1.39}$$

The spontaneous emission factor n_{sp} is always greater than or equal to unity, so the noise figure of a high gain optical amplifier must be at least 3 dB. The dominance of ASE is a concern later on when we study the performance of optical communication systems. We will see that a useful approximation can be made through the consideration of Additive White Gaussian Noise (AWGN) for the frequencies of interest.

The decision was made to progress with the erbium-doped fibre optical amplifier approach in view of the promise. It was applied to TAT12/13 as well as for TPC5. Besides the challenge to design a non-regenerated system and to define its characteristics including noise accumulation (as in the old analog systems), two technologies had to be designed:

- A high-quality dispersion shifted fibre with low attenuation and low polarization effects was needed because the signal needed to be transmitted end-to-end across the ocean.
- The second enabling technology was the semi-conductor optical pumps for the erbium amplifier.

The choice has been a GaInAsp quaternary alloy, for which the materials technology was in a more advanced and safer state. At the same time, the introduction of terrestrial SDH systems with improved operation administration and maintenance characteristics led to the need to make undersea and terrestrial systems compatible for an overall network efficiency. TAT-12/13 and TPC-5 were laid in 1995, finally carrying a 5 Gbps bit-rate per fibre [17].

WDM Technology

The race for more capacity gathered momentum in 1995 and the optical amplifiers permitted a new scheme based on WDM that is simply the transmission together of a set of coloured signals at different wavelengths on the same fibre [18]. The transmission link known as Sea-Me-We-3, a huge system linking Europe to the Mediterranean countries, to Asia, and to Japan and Australia, was based on WDM technology at 8 x 2.5Gbps per fibre. Sea-Me-We-3 in addition has implemented a new WDM branching unit based on wavelength add and drops.

Since the introduction of WDM, the demand for new systems has expanded with tens of systems now linking the continents, each new system having more capacity than the old. This progress in WDM technology resulted simply from a smooth improvement of the amplifier and the maturity of other technologies.

Particularly, semi-conductor and passive optical components have been specifically designed with GaAs lasers replacing completely the GaInAsP to pump optical amplifiers, and WDM lasers became better controlled, so channel density could be increased. At the same time, the development of extremely powerful signal processing to correct errors in the terminal after transmission (forward error correction (FEC)) was a key enabling technology [19].

1.3 Evolution of Undersea Systems

Optical amplification and WDM technology provided a well-needed boost to the undersea transmission industry. Optical amplification offered the chance to include longer repeater spacing within configurations. The great advantage being that the fibre loss is compensated without electrical re-configuration of the signal. This technology was not accepted without trial. The dominant technology at the time was amplification using rare-earth dopants such as erbium or ytterbium (or a compound of both). It offered significant advantages compared to the semi-conductor laser equivalent, such as ease of operation and superior performance. The new era starting with TAT12/13 (U.S to U.K/France) and TPC5, laid during the years 1994 and 1995. These configurations offered a capacity of 5 Gbps per fibre on a single wavelength.

Whilst these amplified systems were being completed, research into WDM technologies in these long-haul systems showed that capacity could be increased significantly using this technology.

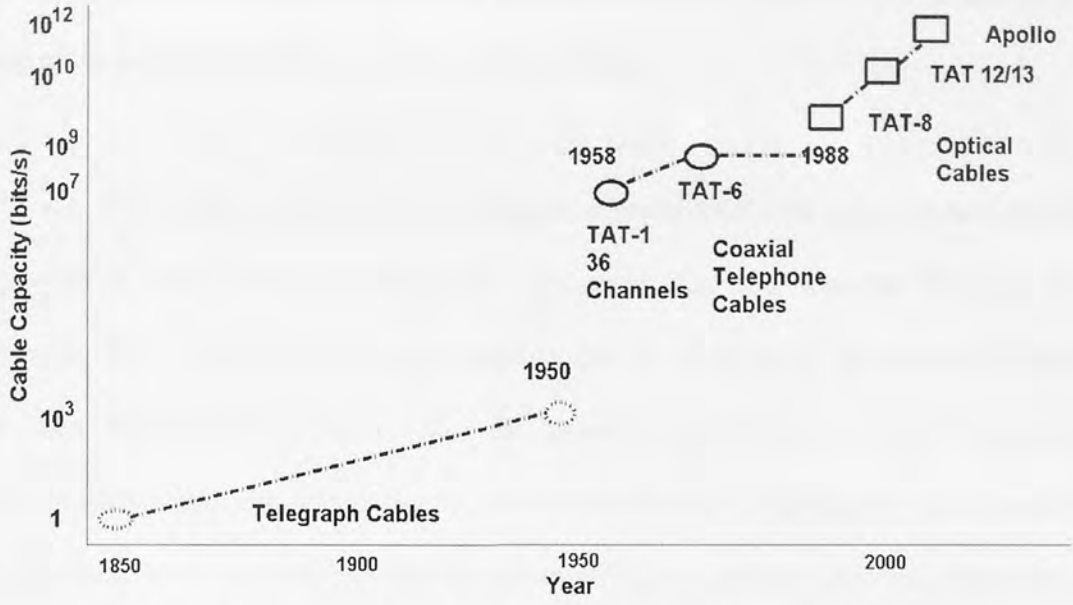

Figure 1.8: Evolution of System Capacity in Undersea Systems

WDM technologies offered new opportunities to upgrade systems by adding wavelengths. This was done for TAT12/13 in 1999, upgrading each fibre by 3 wavelengths. The second opportunity was the increase of capacity per wavelength and the increase in numbers of wavelengths. The rise in system capacity is illustrated in Figure 1.8.

The evolution of undersea transmission systems appeared to pause at the turn of the 21st century. However, due to WDM technology, increasing the overall capacity of a transmission system was not difficult. Indeed, the search for even higher capacity is of great importance due to the increasing demand on these transmission links due to the increased use of the internet in addition to the increased media due to mobile communications and advanced video and voice technologies.

Any data transmission system consists roughly of 3 broad components, a transmitter, a transmission medium and a receiver. The transmitter encodes the data into a stream of optical pulses, ready for propagation in the optical fibre based transmission medium. The transmission medium consists of sections of optical fibres and amplifiers. Following

transmission, the data must be deciphered from the received optical power which will be a mixture of the accumulated noise and the pertinent signal.

One of the main differences between undersea transmission and conventional terrestrial transmission is how the components are optimised and the required lifetime of the components. The lifetime of the transmission system is designed to be around 25 years. In reality, from Figure 1.8, we can see that the bit-rate is growing at a much faster rate. In wealthy countries, they can afford to respond to such growth by fitting new systems with far higher bit-rates, however poorer countries cannot afford to upgrade with such regularity and need a system that they can rely on for a long enough period of time to justify the expense involved. Upgrading such transmission links (as discussed later) is often done by means of adjusting the transmitter or receiver through the use of narrower pulses, adjustment of the dispersion map and the addition of new optical channels through the WDM technique.

As opposed to terrestrial optical systems, undersea systems are generally manufactured like their prototypes, with a specific design for each link. This means a specific adjustment of the amplifier bandwidth, a specific channel spacing, a specific fibre length between two consecutive amplifiers (span length), which all naturally depend on the targeted link capacity and on the system length. One particularity of undersea systems compared to terrestrial ones is also the power supply issue. High-voltage (~10 KV) power stations are located at each end of the system to feed the repeaters (which can amount to 100 or more) along the line. The reliability constraints are also much more stringent for undersea systems than for terrestrial ones, because of the difficulties involved in the repair of the cable, especially in deep waters.

The configuration of an undersea system appears to have changed little since the establishment of the industry, but in fact the WDM fibre technology that is used has led to a

full in-depth revolution. Figure 1.9 gives a general view of the main equipment involved. Amongst the differences to undersea components are the structure of the transmission cable containing the plethora of optical fibres, whilst stories of shark attacks [20] may appear far-fetched, the different atmospheric conditions at the bottom of deep oceans admit a different kind of mechanical problem when producing a casing for optical fibres [21].

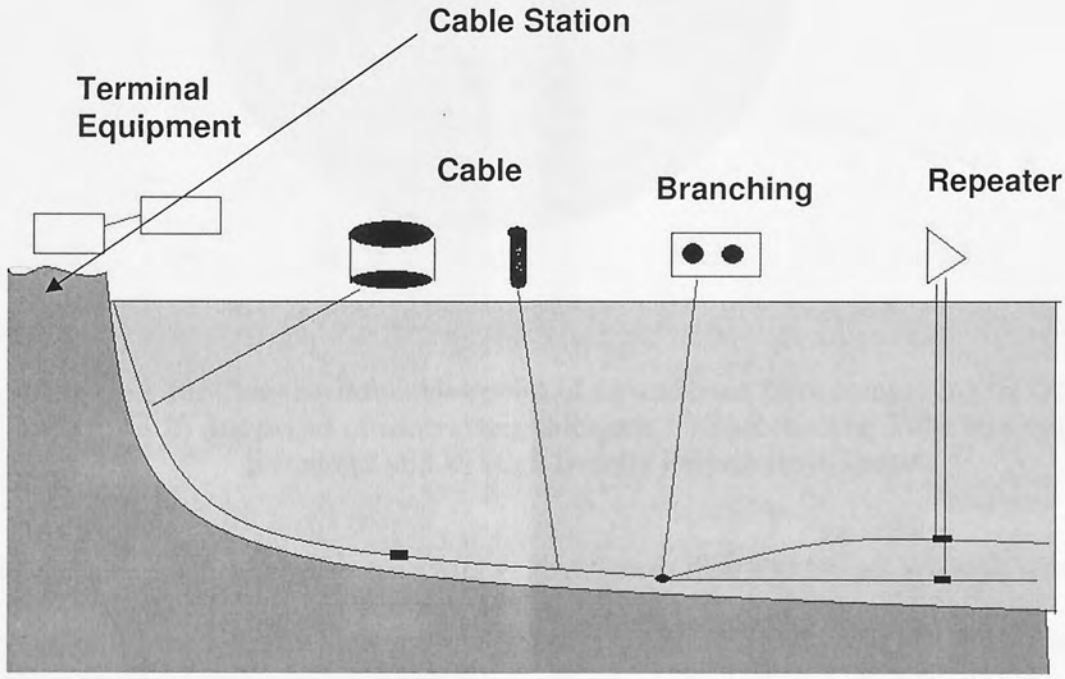

Figure 1.9: Configuration of an Undersea Transmission System

The design of modern optical undersea repeatered cables concentrates on providing a stable low-pass optical transmission path, a power-feeding conductor for the submerged amplifiers, and sufficient strength and robustness to facilitate safe and successful installation.

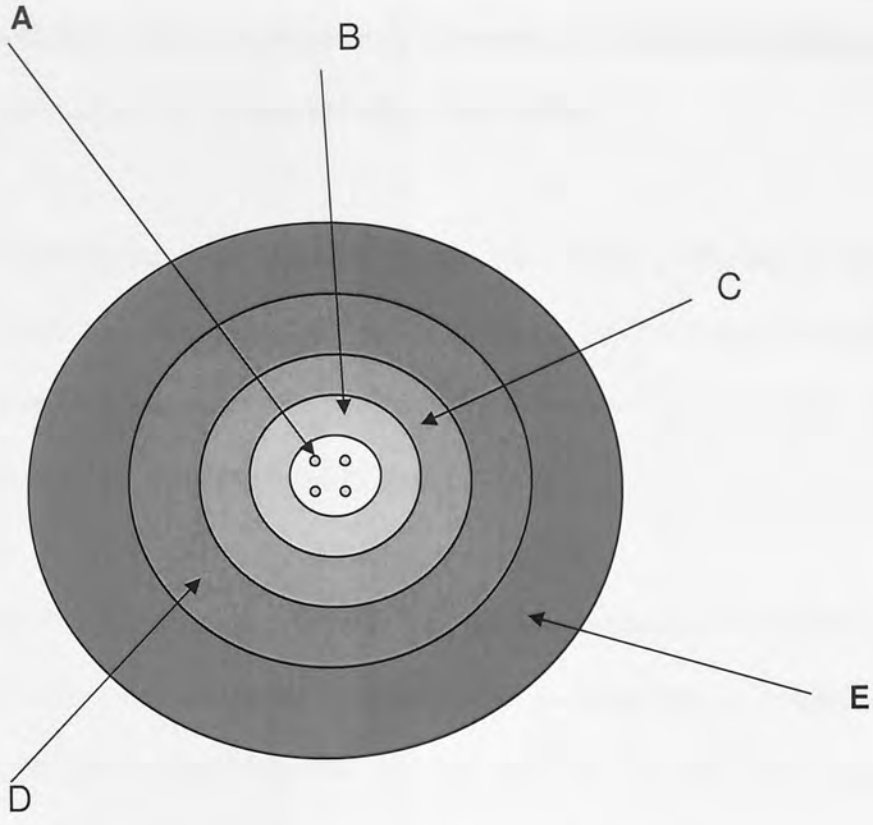

Figure 1.10: Cross sectional viewpoint of an undersea fibre comprising A) Optical Fibres B) Steelwires of contrasting thickness C) Surrounding Tube D) Copper Surround and E) High Density Polyethylene Jacket

These cables are employed on long-haul systems (more than 400 km per section), where it is necessary to power feed submerged equipment for optical amplification and deploy in water depths of down to 8000 m. The general requirements of these cables are simple, they need to protect the fibres from the outside world and a means to connect the terminal stations through the wet-plant equipment. They need to fulfil these objectives throughout the lifetime of the system, which is approximately 25 years. Sea-based trials are required to implement these configurations as it is almost impossible to recreate deep-sea conditions in a laboratory.

These deep-sea conditions relate to the pressure (800 MPa), temperature (between -5 and 35^0C). These values change dependent on the depth of the cable. An example of such a configuration is the deep-water lightweight cable specified for depths of greater than 8000 m

specified in [21]. This type of cable is required for operation in such depths due to the pressure it can withstand. These depths are only observed at the intersection between tectonic plates, but most sea-bed is soft, flat and has little or no current.

The deep-water lightweight cable characterises the basic design, offering an optical core containing the fibres and protecting them against pressure. Such a design also comprises a layer of conductive material in order to power other components such as optical amplifiers. Other designs are based on this most basic of configurations.

The cable is composed of an optical core protecting the optical fibres, surrounded by a copper conductor to power-feed the submerged equipment from the shore and an insulator to isolate the workings of the optical fibre from the sea. The repeaters are units that regenerate the optical signals, after attenuation by propagation through each span, at regular positions along the cable. The repeaters contain optical amplifiers based on laser amplification through a doped fibre pumped by semi-conductor laser pumps fed electrically by the cable. Optical equalising equipment is also inserted regularly to control the optical spectral response of the system.

The branching units are submerged equipment that permit connections between more than two points, that is, double landing to two different locations on the coast or distribution of part of the traffic to a secondary landing point. Branching units are complex pieces of equipment not only at the optical level but also at the electrical level since they are key elements for powering reconfiguration.

Branching units are required because undersea systems demand topologies that are more complex than the traditional point-to-point connections. Branching units are commonly deployed with the idea of deploying three cables (each with many fibre pairs).

A passive branching unit usually comprises no electronics, but it is simply a three port pressure vessel that provides the facility for splicing optical fibres and the cables power conductors. Other types include a power-switching branching unit, a fibre switched branching unit and an optical add/drop branching unit [2, 22].

The cable usually lands on a beach and the fibres arrive in a cable station with:

- Power-feed equipment that electrically feeds all the active submerged equipment, particularly the repeaters.
- Terminal transmission equipment that emits the laser light modulated by the communication signal and receives from the received fibre the communication signal arriving from the other continent.
- Network management system that allows the operator to monitor the systems through a computer by getting the status information and the alarms in case of failure.

At the cable station, the undersea system is connected to the terrestrial network, and the information flow is distributed to the different terrestrial destinations. All submerged equipment is designed for extreme conditions of depth, up to 8000 m (that means 800 atmospheres of pressure) and corrosion resistance. Reliability qualification testing is performed to ensure a lifetime of 25 years with practically no ship repairs for internal faults.

1.4 Issues Surrounding Undersea Systems

Legacy undersea transmission systems employ large numbers of optical amplifiers to account for the losses in fibre sections and to maintain a reasonable level of OSNR (Q~6 dB). Unfortunately, the use of large numbers of amplifiers results in an accumulation of ASE which will eventually destroy the signal, this is a serious issue for undersea transmission systems. The physical manifestation of ASE is explored previously. Other options to EDFA based 1-R regeneration include Raman amplification and distributed amplification (Table 1.1)

In this section, we explore the other issues surrounding the upgrade of undersea systems. When bit-rate increases and the use of the quasi-linear regime becomes important, control of the dispersion and nonlinearity becomes more important as we seek to mitigate signal distortion due to these effects. Ensuring the OSNR remains at a suitable level, pulse average power must be kept at a suitable level. The high power levels result in the onset of the effects of fibre nonlinearity.

Nonlinearity

Any dielectric material exhibits nonlinearity in the presence of electromagnetic fields, with optical fibres being no exception. Despite silica being an intrinsically linear material, the small core area to which light is confined within the fibre makes nonlinear effects quite important, particularly at long distances [3, 23], a clear concern for undersea configurations. We can categorise the sources of nonlinearity into 2 distinct categories; Stimulated Light Scattering and Kerr Effects.

Stimulated Light Scattering

For optical transmission systems, there are generally two types of light scattering; Stimulated Raman Scattering (SRS) and Stimulated Brillouin Scattering (SBS). Both can be understood

through the notion of inelastic scattering, the term used to describe the shift of light photons to lower frequencies. When optical power is high, both SRS and SBS become important, the intensity of the scattered light in each case becomes more intense when the optical power exceeds some threshold [24]. Both phenomena were observed in optical fibres during the 1970's [25, 26]. Although, SBS and SRS are quite similar in their origin, different dispersion relations for acoustic and optical phonons lead to differences[23];

- SBS occurs in only one direction, whereas SRS occurs in both directions.
- The scattered light is shifted by about 10 GHz for SBS and by about 13 THz for SRS [3](this is known as the Stokes shift)
- The Brillouin gain spectrum is extremely narrow (bandwidth < 100 MHz) compared to the Raman gain spectrum (bandwidth ~ 20 - 30 THz).

Stimulated Brillouin Scattering (SBS)

The physical process behind Brillouin scattering is the tendency of materials to become compressed in the presence of an electrical field, this is known as electrostriction [27]. Given an oscillating electrical field at frequency Ω_p, this process generates an acoustic wave at some frequency Ω through this process. SBS can be viewed as the scattering of a pump wave from this acoustic wave; this results in the creation of a new wave at pump frequency Ω_s. The scattering process conserves both energy and momentum [3], meaning that the Stokes shift is given by $\Omega=\omega_p-\omega_s$.

Once the scattered wave is generated, it beats with the pump and creates a frequency component at the beat frequency $\omega_p-\omega_s$, which is automatically equal to the acoustic frequency. As a result, the beating term acts as a source that increases the amplitude of the sound wave, resulting in a positive feedback loop. The feedback process is governed by the following system of coupled equations [27];

$$\frac{dI_p}{dz} = -g_B I_p I_s - \alpha_P I_p \tag{1.40}$$

$$-\frac{dI_s}{dz} = g_B I_p I_s - \alpha_s I_s \tag{1.41}$$

Where I_p and I_s are the intensities of the pump and Stokes fields, g_B is the SBS gain, and α_P accounts for fibre losses. The SBS gain g_B is frequency dependent because of the finite damping time T_B of acoustic waves (the lifetime of acoustic phonons). If the acoustic waves decay as $\exp(-t/T_B)$, the Brillouin gain has a Lorentzian spectral profile given by [28];

$$g_B(\Omega) = \frac{g_B(\Omega_B)}{1+(\Omega-\Omega_B)^2 T_B^2} \tag{1.42}$$

For optical transmission systems, this creates problems. SBS can be reduced in fibres where their is a higher concentration of germanium dopant at the core [3], but this is not usually the case in undersea transmission systems. Due to the threshold being at 1 mW [3], launch power of optical signals is limited to only a few milliwatts. The threshold value also depends on how the data is encoded.

Stimulated Raman Scattering

Stimulated Raman Scattering (SRS) occurs in optical fibres when a pump wave is scattered by the molecules of the pertinent silica fibre. Some photons give up their energy to create other photons of reduced energy at a lower frequency; the remaining energy is absorbed by silica molecules, which manifest in an excited vibrational state. This process is isotropic and occurs in all directions throughout the fibre. The value of the Raman frequency shift is given by [3];

$$\Omega_R = \varpi_p - \varpi_s \tag{1.43}$$

Similar to SBS, SRS becomes influential upon the signal if the pump power exceeds a particular value. Physically speaking, the beating of the pump and forward propagating signal in optical fibres creates a frequency component at the beat frequency given in (1.30). This acts as a source that derives molecular oscillations. Since the amplitude of the scattered wave

increases in response to these oscillations, a positive feedback loop sets in. In the case of forward SRS, the feedback process is governed the following system of coupled ordinary differential equations [23];

$$\frac{dI_p}{dz} = -g_R I_p I_s - \alpha_p I_p \tag{1.44}$$

$$\frac{dI_s}{dz} = g_R I_p I_s - \alpha_s I_s \tag{1.45}$$

We denote g_R as the gain of the process. In the case of backward SRS, a minus sign is added in front of the derivative in (1.45), making this system of equations identical to the SBS equations given in (1.40,1.41). In the case of optical fibres, the bandwidth exceeds 10 THz, the spectrum of the Raman gain exceeds 10 THz. This is a useful property and can be exploited in the construction of Raman amplifiers [23]. The main difference between SRS and SBS is that optical phonons participate in SRS whilst acoustic phonons participate in SBS. They were amongst the first effects to be studied in the context of optical fibres [24-26].

The threshold for SRS is significantly higher than the equivalent value for SBS (~ 570 mW for SMF [3]). Due to this, single channel configurations are not exposed to this phenomenon. However, WDM configurations do suffer, making SRS a serious consideration for the installation of undersea optical transmission systems.

For our modelling, we assume that both effects are negligible in the transmission system. The power shift down the spectrum due to SRS between higher and lower energy wavelengths is only significant in systems with many channels. We will only work with systems operating over a maximum of 7 channels. Whilst we assume only a small number of channels, our bandwidth is large enough for SBS to also play a negligible part in the transmission. It is known [3] that SBS only works over a bandwidth of ~ 10 GHz, which limits its influence on channels spaced further apart. Typically for high-speed transmission (> 10 Gb/s), channels are

spaced at least 30 GHz apart [3], making interchannel cross-talk due to SBS inconsequential. It is also possible to mitigate SBS via appreciation of its nature as a narrowband (<100 MHz) resonator [29]. Due to this, the back-reflection can be reduced through the gentle modulation of the laser current with a small amplitude and low frequency. This induces laser chirp and permits higher launch powers [29].

Kerr-Type Effects

For long systems, the nonlinear refractive index can couple different signal channels and additionally couple the signal with noise [3]. The conventional single-mode fibre is slightly nonlinear as a result of dependence of the fibres index on the intensity of the light propagating through it. This behaviour is expressed as

$$n = n_0 + \frac{N_2 P}{A_{eff}} \tag{1.46}$$

Where n_0 is the linear part of the refractive index, N_2 is the nonlinear coefficient (~2.6 x 10^{-16} cm^2/W), P is the light power in the fibre, and A_{eff} is the effective area over which the power is distributed [30]. This nonlinear behaviour causes only minute changes in the phase velocity of the fibre. The measured equivalent length change of 3.5 μm over 10,000 km transmission of SMF is of little direct consequence to the transmission performance [31], however, the resultant time-shifts in the signal are of considerable consequence to the optical phase. The nonlinear index change leads to important phenomena such as self-phase modulation, cross-phase modulation and four-wave mixing [32].

Self-Phase Modulation

At long fibre lengths, the shape of the underlying fibre mode does not undergo change [3], however, the phase of the signal becomes time dependent, inducing a phase shift ϕ_{NL};

$$\phi_{NL} = \int_0^L (\beta' - \beta) dz = \int_0^L \gamma P(z) dz = \gamma P_{in} L_{eff} \tag{1.47}$$

Where $P(z) = P_{in} e^{-\alpha z}$ accounts for fibre losses and L_{eff} is the effective fibre length defined as;

$$L_{eff} = \frac{1 - e^{-\alpha L}}{\alpha} \tag{1.48}$$

Since this nonlinear phase modulation is self-induced, this phenomenon is known as self-phase modulation (SPM). This leads to the frequency chirping of optical pulses. The theoretical implications of this are explored in the next chapter in the context of modelling optical pulse propagation. SPM induced chirp affects the pulse shape through chromatic dispersion and often leads additionally to pulse broadening. This phenomenon has been used previously in the context of optical pulse regeneration [33].

Generally, spectral broadening of pulses due to SPM increases the signal bandwidth [23] and limits the performance of lightwave system. SPM can be used in some cases to mitigate the effects of chromatic dispersion [23].

Four Wave Mixing

The power dependence of the refractive index as seen in equation (1.46) has its origins in the third order nonlinear susceptibility denoted by $\chi^{(3)}$. The nonlinear phenomena known as Four Wave Mixing also occurs as a result of $\chi^{(3)}$. If three optical fields with carrier frequencies ω_1, ω_2 and ω_3 co-propagate inside the fibre simultaneously, $\chi^{(3)}$ generates a fourth field whose frequency is related to the other three frequencies by the relationship

$$\varpi_4 = \varpi_1 \pm \varpi_2 \pm \varpi_3 \tag{1.49}$$

There are several combinations as suggested by the plus/minus notation given above. Most of these combinations will never occur due to the phase matching requirement [3]. However, for multichannel communications, these combinations can become troublesome due to the phase

matching as they become almost phase matched when channels converge on the zero dispersion wavelength. Due to this, FWM can be mitigated effectively by dispersion management.

Cross Phase Modulation

The intensity dependence of the refractive index in (1.34) can lead to another nonlinear phenomenon known as cross-phase modulation (XPM). This occurs when two or more optical channels are transmitted simultaneously inside an optical fibre using the WDM technique. In such systems, the nonlinear phase shift for a specific channel depends not only on the power of that channel but also on the power of other channels [34]. The phase shift for the jth channel becomes;

$$\phi_{NL} = \gamma L_{eff}\left(P_j + 2\sum_{m\neq j} P_m\right) \tag{1.50}$$

This sum extends over the number of channels. The factor of 2 in equation (1.50) comes from the nonlinear susceptibility $\chi^{(3)}$ and suggests that XPM is twice as effective as SPM for the same wavelength configuration. The phase shift due to XPM can only occur when two pulses are overlapping one another, so is derived from neighbouring channels, again suggesting that XPM can be effectively mitigated through effective dispersion management in order to prevent frequency components from influencing the transmission. This can be achieved through the use of fibres of opposite dispersion signage (D+/D-/D+).

Intra-channel Nonlinearity

In high bit-rate systems, other types of nonlinearity can dominate the transmission, these effects are due to intra-channel pulse collision. These effects are known as intra-channel four-wave mixing (IFWM) and intra-channel cross-phase modulation (IXPM).

IFWM is due to dispersion causing small fractions of an individual pulses field being shifted into an adjacent time-slot. If the adjacent time-slot is empty, then the shifted field will appear as a ghost pulse. If the time-slot is occupied by a pulse then the two pulses will beat together to form another pulse, generating amplitude fluctuations in the time-slot [35]. IXPM occurs when pulses broaden rapidly with high localised dispersion, this causes frequency shifting which is converted to timing shifts (timing jitter) through dispersion [35]. These effects have been demonstrated experimentally [36] using two differing types of fibre. IFWM was shown using an 80 km section of SMF (D = 17 ps/nm/km) and 100% dispersion compensation. IXPM was shown using an 80 km section of True-Wave Fibre (TWF) (D = 4 ps/nm/km) and 100% dispersion compensation. Full details of these experiments can be found in [36], but using a numerical model for optical pulse propagation which will be derived in Chapter 2 we have reproduced the results in Figure 1.11.

The mitigation of these effects has attracted substantial attention in the literature due to their influence on high bit-rate systems. IXPM can be mitigated effectively through the use of equal energy in all bit-slots [37], Fibre Bragg Gratings to control the dispersion [38], alternating polarization [39], symmetric dispersion maps [40] or Raman amplification [41]. Indeed, IFWM can also be mitigated through the use of Raman amplification and symmetric dispersion maps.

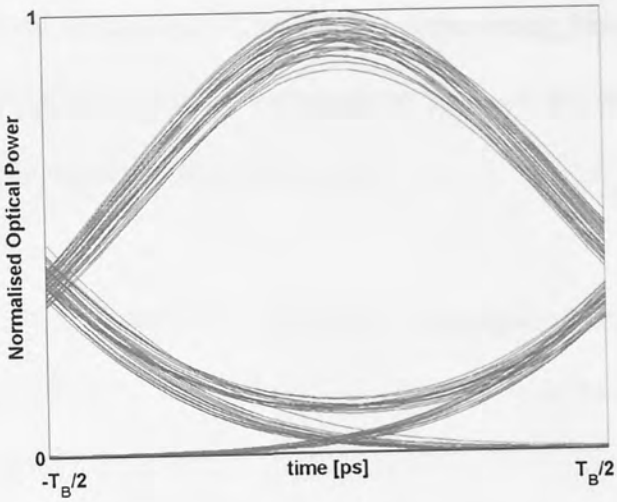

a)

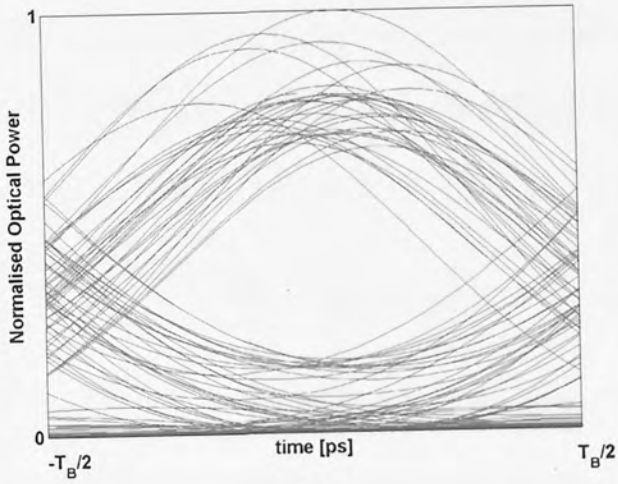

b)

Figure 1.11: Eye Diagrams displaying the two main nonlinear effects prevalent within quasi-linear transmission: a) IFWM and b) IXPM

Dispersion

During pulse propagation through optical fibre, the individual wavelengths composing each pulse travel at different speeds, causing the pulse to broaden. This is known as chromatic dispersion, causing impairment to the transmission of optical pulses as it introduces a limitation on the maximum admissible bit-rate [2]. The management of the chromatic dispersion in an undersea transmission link is of paramount importance to the successful operation of the transmission system and achieving the optimal performance.

Dispersion compensation can be achieved through usage of fibres with dispersion of opposing sign. This very often involves the use of dispersion compensating fibres (DCFs). These may be used inline as a passive dispersion management tool, or actively at the receiver to compensate for dispersion accumulated in the system.

DCF's provide an all-optical dispersion compensation technique which is useful for periodic compensation of dispersion such as what is required in long-haul systems where the chromatic dispersion must be periodically compensated for. It is possible to compensate for the dispersion completely if the average optical power is low enough to render the nonlinear effects inside the optical fibres as negligible. It can be easily understood when considering a two-stage fibre link, the second of which is the DCF. Assuming the total dispersion in the system can be given by $D_1 L_1 + D_2 L_2$, then we can say that [3]

$$A(L,t) = \frac{1}{2\pi} \int_{-\infty}^{\infty} \tilde{A}(0,\varpi) e^{\frac{i}{2}\varpi^2(\beta_{21}L_1+\beta_{22}L_2)-i\varpi t} d\varpi \qquad (1.51)$$

Where $L = L_1 + L_2$ and β_{2j} is the GVD parameter for the fibre segment of length L_j. If the DCF is configured such that the term in ω^2 vanishes, then the pulse will regain its initial shape after propagation over L km. This is perfect dispersion compensation and is characterised by the equation given in [42];

$$D_1 L_1 + D_2 L_2 = 0 \qquad (1.52)$$

The idea of using DCF's for this purpose is well developed, however, compensation at just one wavelength is not adequate for WDM transmission systems. In long-haul WDM transmission, where large sections of fibre may be used, the slope of dispersion assumes greater importance so large amounts of dispersion are added at the transmitter and receiver in order to fully compensate the dispersion despite the slope dependence. Such higher-order dispersion causes a spread in accumulated dispersion for various channels in a WDM configuration.

The first generation of installed optically amplified undersea systems used dispersion shifted fibre (DSF) with a chromatic dispersion around 0 ps/nm/km at 1550 nm. This approximately corresponded with the channel wavelength, in order to minimise the chromatic dispersion accumulation at the end of the link. The first generation of WDM systems necessitated the need for a new fibre, named Non-Zero Dispersion Shifted Fibre (NZ-DSF). This fibre had the feature of D ~ -3 ps/nm/km at the 1550 nm wavelength. After propagation over several spans of NZDSF, chromatic dispersion needs to be compensated. This was achieved through Standard Single Mode Fibre (SMF), which offered chromatic dispersion of 18 ps/nm/km at 1550 nm. There exists other approaches to dispersion compensation; such as those relying on the functionality of Fibre Bragg Gratings (FBGs) or Optical Phase Conjugation (OPC).

FBGs are a useful device in the operation of dispersion management as they offer what is known as a stop-band, a frequency region in which most of the incident light is reflected back. The stop band is centred at a wavelength known as the Bragg wavelength [3]. Using the periodic nature of refractive index variations, we can couple forward and backward propagating waves in such a way that we provide frequency dependent reflectivity to the incident signal over a bandwidth determined by the strength of the grating. FBGs act effectively as a reflection filter for the incident light.

The dispersion of an FBG is dependent on the wavelength concerned. It has been shown [42] that uniform FBGs can be used to compensate both anomalous and normal dispersion through the use of the GVD induced by the grating at either side of the stop band. Unfortunately, the use of uniform FBGs in high bit-rate systems is limited because the width of the stop band is ~ 0.1 nm [43].

Another type of FBG is the chirped FBG, unlike uniform FBGs they offer a wider stop band. Since the Bragg wavelength of chirped FBGs is dependent on the grating length, different frequency components of an incident optical pulse are reflected at different points. The main limitation to the installation and operation of chirped FBGs is the insertion loss imposed (~6 dB [42]).

The method of OPC was proposed long ago [44], but was only implemented experimentally much later (see [45] for example). It is simply understood when considering the complex form of the field envelope $A(z,t)$. For an optical pulse propagating in a dispersive nonlinear optical medium, we can say that $A(z,t)$ satisfies the Generalised Nonlinear Schroedinger Equaton for pulse propagation afflicted purely by dispersion (second order, β_2 and third order β_3) (derived in Chapter 2);

$$\frac{\partial A}{\partial z} + i\frac{\beta_2}{2}\frac{\partial^2 A}{\partial t^2} - \frac{\beta_3}{6}\frac{\partial^3 A}{\partial t^3} = 0 \qquad (1.53)$$

If we consider the complex conjugate of this equation;

$$\frac{\partial A^*}{\partial z} - i\frac{\beta_2}{2}\frac{\partial^2 A^*}{\partial t^2} - \frac{\beta_3}{6}\frac{\partial^3 A^*}{\partial t^3} = 0 \qquad (1.54)$$

We see that the sign of the second order dispersion (GVD) is reversed. This means that if the amplitude field is conjugated in the middle of a transmission link, the dispersion from the first half of the link will be compensated exactly in the second half. However, third order dispersion doesn't change sign so sloping effects cannot be considered for OPC.

From all of the methods proposed, it is plain to see that pre and post compensation, mixed with fibre based dispersion management, will provide the ideal mitigation for chromatic dispersion. In addition to maintaining low dispersion over a fibre span there are also benefits to achieving high local dispersion in individual fibre sections. The interplay between

dispersion and nonlinearity is probably the most important challenge for undersea WDM systems.

Interplay between Dispersion and Nonlinearity

The interplay between dispersion and nonlinearity is perhaps the biggest issue for the implementation of undersea transmission systems. The conflicting behaviour can offer both positive and negative influences on the transmission.

The relationship between XPM and dispersion is important for long-haul WDM optical transmission systems, such as those that operate undersea. Fibre dispersion converts phase variations into amplitude fluctuations, so understanding the relationship between the two is of great importance to the design of such systems [23].

XPM occurs when pulses operating over multiple wavelengths overlap, the possibility of this occurring is reduced when pulses are travelling at different group velocities i.e non-zero GVD. When pulses operating at multiple wavelengths overlap, the adjacent channels will exchange power and modulate the phase of the adjacent channels. With this in mind, we know that maintaining non-zero local dispersion is important in order to manage the nonlinear behaviour within a transmission link.

Four-wave mixing occurs when multiple pulses travel through one another if phase matched, an exchange of energy takes place which generates the appearance of another pulse. It has been shown that the FWM mixing is related directly to the channel spacing and the chromatic dispersion [23]. For large GVD fibres, the FWM efficiency becomes very small due to the reduced phase matching. Contrarily, FWM efficiency is approximately 1 near to the zero dispersion wavelength of the pertinent fibre, this means that the FWM component becomes significant in the transmission. For this reason, dispersion management is important so as to

reduce the occurrence of FWM in the transmission whilst maintaining acceptable levels of dispersion.

It is clear that the interplay between dispersion and nonlinearity are of vital importance to undersea transmission systems. Over such large distances, nonlinearity becomes more influential even at lower powers due to the Kerr effect. The quasi-linear transmission regime offers the unique setting in which we can use the two limiting factors as tools to further our ability to upgrade undersea systems. Later in the thesis, we will see that manipulation of this delicate interplay can enable us to gain insight into these important effects.

Polarization Mode Dispersion

Apart from dispersion and nonlinearity, there is another physical phenomenon which afflicts high bit-rate transmission. Small departures from perfectly cylindrical symmetry in optical fibres lead to birefringence because the different mode indices associated with the orthogonally polarized components of the propagating fibre modes.

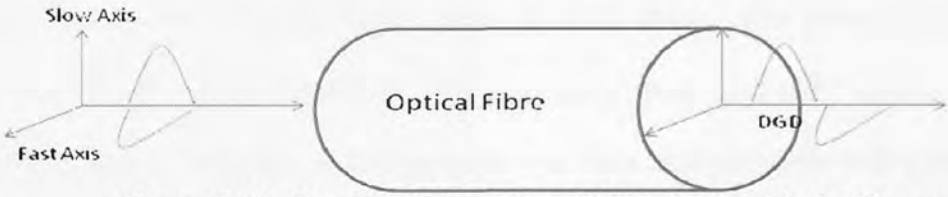

Figure 1.12: Graphical Depiction of Polarization Mode Dispersion

If the input pulse excites both components of the polarization, the birefringence grows and creates a delay between the two components. In a practical sense, we explain this in the schematic Figure 1.12. The input pulse is split into two sub-pulses due to the differing speeds at which the components propagate in the fibre. This is a result of randomly varying birefringence. This quantity is known as Polarization Mode Dispersion (PMD). It is characterised by the quantity known as differential group delay (DGD), which we define as ;

$$DGD = \left| \frac{L}{v_{gx}} - \frac{L}{v_{gy}} \right| = L\left|\beta_{1x} - \beta_{1y}\right| = L\Delta\beta_1 \qquad (1.55)$$

Where L is the fibre length, x and y identify the two orthogonally polarized modes and $\Delta\beta_1$ is related to the difference in group velocities along the two polarization modes. The quantity σ_T defines the RMS average of the DGD;

$$\sigma_T^2 = \langle (DGD)^2 \rangle \tag{1.56}$$

This expression has been calculated, for all fibre types as [3];

$$\sigma_T^2(z) = 2(\Delta\beta_1)^2 l_c^2 [e^{-\frac{z}{l_c}+\frac{z}{l_c}-1}] \tag{1.56}$$

Where l_c is the length over which two orthogonally polarized modes are correlated (correlation length). The value of this quantity is typically ~10 m, however it can range between 1m and 1 km. For distances greater than 1 km, a good approximation can be obtained as;

$$\sigma_T \approx D_p \sqrt{L} \tag{1.57}$$

The largely random nature of PMD just adds to its complexity. However, there is a developed theory [3, 46] on the subject and we can make some observations. PMD pulse broadening is characterised by the root-mean square value of DGD, this is often stated in the specification of optical fibres and is calculated after averaging over randomly varying birefringence changes. In fact, averaging over a large amount of fibre configurations with randomly varying birefringence changes has yielded a reliable, exact statistical model for DGD [46-48]. DGD is distributed as a Maxwell random variable, with a probability function given by [48];

$$P(DGD > k < DGD >) = \frac{4k}{\pi} \exp\left(-\frac{4k^2}{\pi}\right) + erfc\left(\frac{4k}{\pi}\right) \tag{1.58}$$

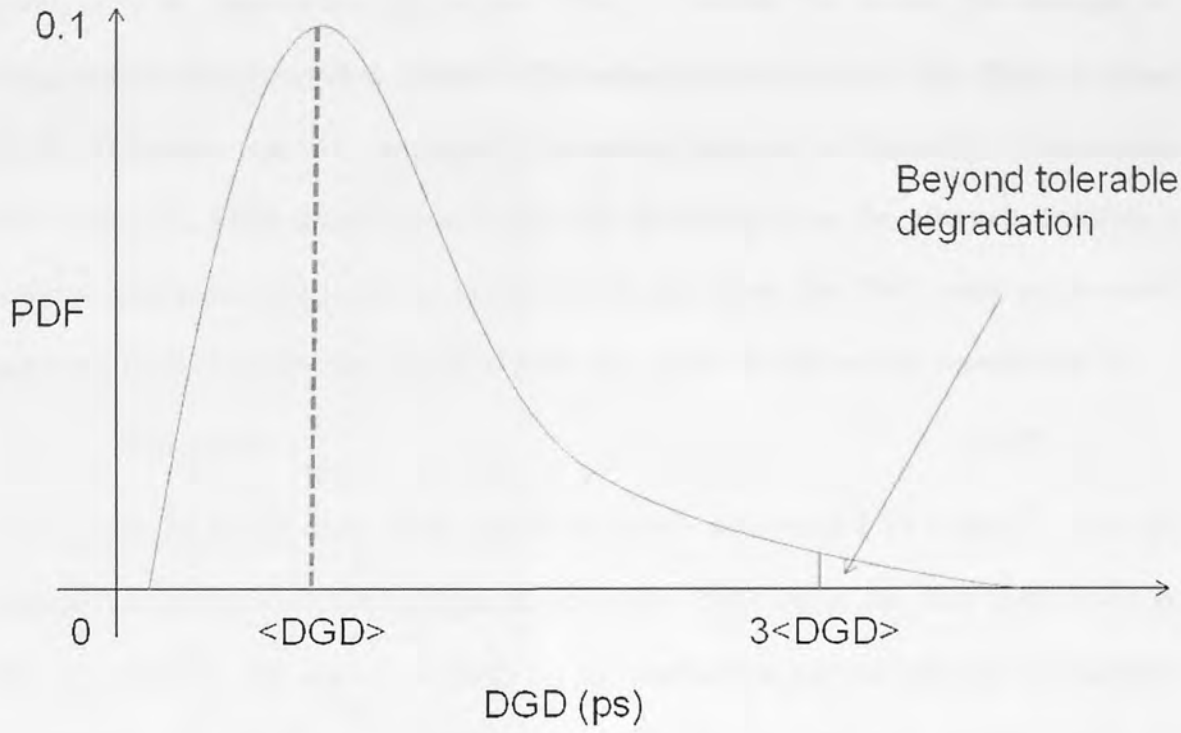

Figure 1.13: Maxwellian Distribution of DGD

The complexity of PMD means any understanding is usually attained through the use of stochastic modelling [49]. It is said to follow a Maxwellian distribution [48] which enables us to draw conclusions about its occurrence. Whilst PMD is prevalent, it tends to oscillate around the mean value <DGD> according to the Maxwellian distribution, but due to this model, very large PMD is unlikely. If the DGD goes beyond 2-3<DGD>, then the systems become inoperable. For 10 Gb/s systems, this is around a few minutes per year. The probability of systems running into these problems are ~ 10^{-5} [46]. When we increase the bit-rate, the tolerance to PMD decreases proportionally. This means that for legacy systems which are intent on operating at 20 Gb/s, we need to multiply the PMD tolerance by 1/2. There are techniques proposed for PMD mitigation [3], but for our understanding it is important to consider its impact on the system. We can say [3] that the RMS pulse broadening due to PMD can be expressed with the equation (1.56). Due to σ_T being being given in ps, this means that the units of D_p are in ps / $(km)^{1/2}$. We note, importantly, that σ_T is a RMS average value of the DGD. The instantaneous PMD value of the fibre ΔT fluctuates over time

according to the Maxwellian distribution. When ΔT exceeds the bit-slot, this becomes an outage and the probability of at outage P(ΔT) has been studied in detail [49]. When an outage occurs, the system stops working properly, fortunately this is only observed for a few minutes every year for a PMD limited system [39]. The modelling using the Maxwell distribution provides insight into the limits on this value [3] and shows the RMS value σ_T shouldn't exceed 10-15 % of the bit-slot in order to avoid the impact of PMD on the transmission [3].

$$B^2 L < (10 D_p)^{-2} \tag{1.59}$$

Fibres produced in the early 1990s had PMD values of around 1 ps / $(km)^{1/2}$, however, modern systems enjoy significantly greater tolerance. PMD values are often seen as low as 0.05 ps / $(km)^{1/2}$. The impact of PMD on the modulation formats relevant to undersea transmission (RZ-OOK and RZ-DPSK) is similar [3, 39, 46, 49]. System PMD, or accumulated PMD, is calculated through the equation;

$$PMD_{acc} = \left[\frac{1}{L} \sum_{i=1}^{N} L_i PMD_i \right]^{1/2} \tag{1.60}$$

Where PMD_i is the PMD of the i-th component, L_i is the length of i-th component and L is the overall length of the system, the integer N is equal to the number of components in the system. The issue of PMD is important for the installation of 40 Gb/s transmission [39], but can be overlooked for 20 Gb/s transmission [50]. One idea for the mitigation of PMD was to use a low-PMD fibre but progress in this area is limited. Low clad ovality has been selected as a feature of the pertinent fibre that can be adjusted in order to mitigate PMD [51]. PMD compensators can also be used [39, 50], but they are complex devices that operate on a per channel basis and would require installation with the fibres. PMD can also be effectively mitigated through the use of XPM due to the nonlinear Kerr effect in Non-Return-to-Zero (NRZ) [52] and soliton [53, 54] transmission systems. However, for high bit-rate systems, PMD transmission often limits the bit-rate, particularly over large distances.

A known effect of PMD is nonlinear polarization rotation [39, 55], which occurs when XPM and PMD combine to induce time-dependent state changes on the time scale of a single bit [39]. This limits the use of polarization multiplexing [56] as a means of upgrading the bit-rate, since PMD becomes more prevalent in the transmission

1.5 Upgrading from RZ-OOK to RZ-DPSK

The upgrade of legacy undersea transmission systems has attracted large amounts of attention due to the commercial importance of such systems [39, 50, 57]. Legacy systems originally operated at a bit-rate of 2.5 Gb/s WDM [2, 39], which was subsequently upgraded to 5 Gb/s WDM and then 10 Gb/s WDM. These upgrades have been achieved through the addition of channels or fibres [50, 57]. Such systems are expensive and complete replacement may be seen as frivolous given that technology exists to upgrade these systems through adjustment of the transmitter and receiver.

The transmission of optical data involves the modulation of electrical data into optical pulses. As in standard copper wire based transmission, we restrict ourselves to the binary alphabet as a means to encode and transmit data. The simplest method of data encoding is Return-to-Zero On-Off Keying (RZ-OOK), this is used in the current generation of undersea optical transmission systems. Put in simple terms, it involves assigning a power level to a logical one and zero power to a logical zero. This gives an infinite extinction ratio. Of course, in reality, this is very difficult to achieve because noise and fluctuations in the initial pulse carving will inevitably assign some power to the bit slots occupied by logical zeros. The RZ-OOK constellation and pulse train will resemble Figure 1.14 & Figure 1.15;

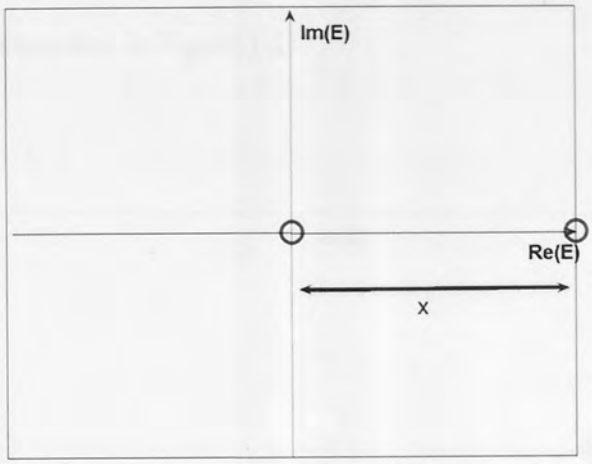

Figure 1.14: Constellation Diagram of the Amplitude Envelope E(z,t) for RZ-OOK Encoded Data

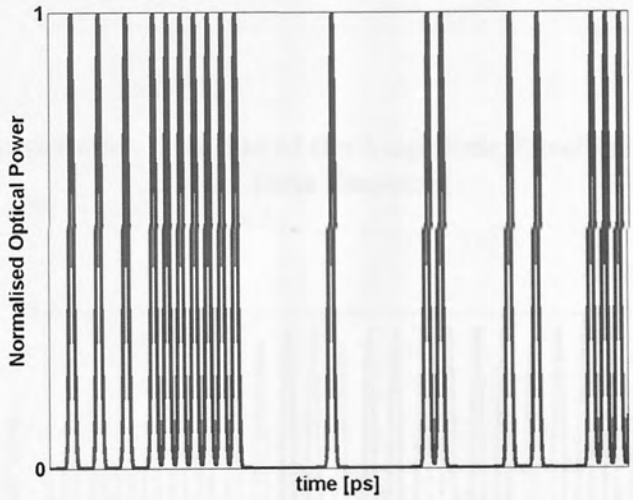

Figure 1.15: Bit-Pattern for RZ-OOK Data Encoding

Ultimately, the reliance on RZ-OOK modulation is limiting the capacity of legacy systems due to its susceptibility to nonlinear effects [57-59]. The required growth in bit-rate of communication systems can be achieved through the propagation of shorter pulses, which are more prone to the effects of fibre dispersion. Subsequently, the carrier pulse power spreads over many bit-slots, inducing interaction between pulses. However, due to the spreading, the nonlinearity on average becomes negligible. This transmission regime is defined as the quasi-

linear regime. The use of the quasi-linear regime renders the transmission vulnerable to IXPM and IFWM [35, 36] demonstrated in Figure 1.11.

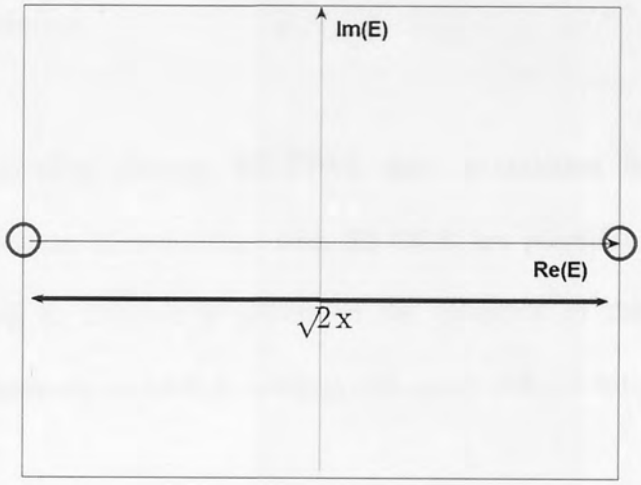

Figure 1.16: Constellation Diagram of the Amplitude Envelope E(z,t) for RZ-DPSK Data Encoding

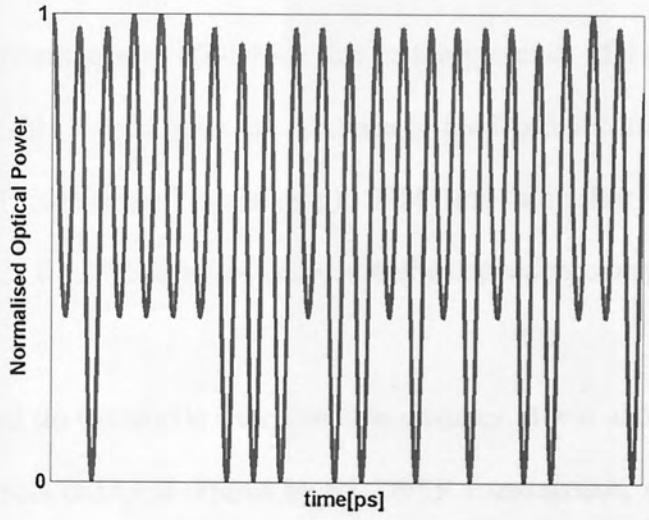

Figure 1.17: Bit Pattern for RZ-DPSK Data Encoding

Recently, it has been shown that RZ-DPSK has been shown to be a promising candidate for the upgrade of such systems to the higher bit-rate. Its symmetric power distribution makes it less prone to IXPM [37], one of the dominant sources of nonlinearity in quasi-linear

transmission. A comparison of RZ-OOK and RZ-DPSK, as given in Appendix B, reveals a 3 dB benefit in receiver sensitivity, meaning that approximately half of the optical power is required per pulse to achieve the equivalent Bit Error Rate (BER). We cover the derivation of BER in the following section. Clearly, RZ-DPSK is a definite candidate for the upgrade of legacy undersea transmission.

The potential for upgrading through RZ-DPSK data modulation has been thoroughly investigated in the literature. Comparisons with RZ-OOK are plentiful at 10 Gb/s, 40 Gb/s and 20 Gb/s, revealing an interesting picture of the potential of the upgrade of legacy configurations. The important variable is spectral efficiency (SE) (= bit-rate (Gb/s) / channel separation (GHz)).

10 Gb/s Comparison between RZ-OOK and RZ-DPSK

Currently, RZ-OOK signals are transmitted undersea at a bit-rate of 10 Gb/s over a large number of channels. At low SE (0.2 b/s/Hz), it has been shown [59] that RZ-OOK offers at least comparable performance to RZ-DPSK due to the presence of 1-dB less power margin [60]. The reason for this is seen to be the presence of the Gordon-Mollenauer effect, namely the combination of (self-phase modulation) SPM and amplifier noise. Such physical behaviour only effects RZ-DPSK pulses because of the dependence on phase.

When SE is increased (to 0.4 b/s/Hz), the situation changes. It was shown in [61], that due to the increased robustness to IXPM offered by RZ-DPSK transmission, respective performance compared to RZ-OOK increased. This made RZ-DPSK a feasible option for high SE, offering the potential for upgrading to increased capacity using the same undersea configuration.

Nonlinearity such as IXPM, IFWM in addition to PMD are negligible at 10 Gb/s [39], and scattering effects such as SRS and SBS would require considerable numbers of channels per fibre to represent an issue at this bit-rate.

40 Gb/s Comparison between RZ-OOK and RZ-DPSK

Upgrading the bit-rate of channels to 40 Gb/s opens the optical pulses up to new types of physical phenomena. Indeed, the use of narrower pulses introduces wider bandwidth into the system, which could take on the effect of Stimulated Raman Scattering (SRS) [39]. This manifests as a transfer of signal power from high frequency channels to low frequency channels.

A demonstration of 40 Gb/s transmission has been achieved at the laboratory level using more complex fibre arrangements configured to compensate inline for nonlinearity and the accumulation of dispersion [62, 63]. These fibres were configured purposely with this application in mind using very large effective area (A_{eff} ~ 200 μm^2) and ultra low loss (α ~ 0.16 dB/km) [64]. The use of such large effective area meant that nonlinear effects were significantly mitigated, yielding a larger signal to noise ratio at the receiver.

It is clear that 40 Gb/s can be achieved for undersea distances, but this requires the re-design of the transmission configuration, meaning that its infeasible for upgrading legacy transmission links.

20 Gb/s Comparison between RZ-OOK and RZ-DPSK

Most recently, 20 Gb/s RZ-DPSK was indicated as a strong candidate for upgrading non-slope matched undersea transmission links [50], by offering the potential for similar performance as 10 Gb/s RZ-ASK at twice the spectral efficiency, and higher performance than 40 Gb/s RZ-DPSK at the same spectral efficiency. Since currently it does not seem

possible to achieve translatantic transmission at 40 Gbit/s with any comfortable margin, it may be that 20 Gb/s is the bit rate of choice for long-haul undersea transmissions.

So, we can say that RZ-DPSK is a definite option for us, and we will proceed with the investigation of 20 Gb/s WDM RZ-DPSK transmission at undersea distances. Despite the higher tolerance of RZ-DPSK to nonlinearity, we cannot discount the possibility of fibre nonlinearity developing and impairing our transmission. One of the main benefits of using RZ-DPSK as an upgrade to RZ-OOK is that we can transmit over twice the distance for the equivalent pulse power [58]. The use of higher distances, in addition to the presence of considerable chains of amplifiers and narrower pulses using higher pulse average powers suggesting further nonlinearity will manifest within the transmission [31].

The upgrade of older legacy systems using RZ-DPSK is well illustrated in the literature [57, 65] and attracts some of its own physical issues. Care needs to be taken when the upgrade takes place. Mixed formats, such as that explored in [50] between RZ-OOK and RZ-DPSK can attract XPM caused by intensity modulated RZ-OOK channels [57] particularly when systems employ the traditional NZ-DSF fibre sections. This occurs mostly near to the zero-dispersion wavelength and channels far from this wavelength don't exhibit such a penalty [57]. This suggests that for such mixed configurations, RZ-DPSK channels should be placed at wavelengths away from the central, zero-dispersion wavelength. However, the sole use of RZ-DPSK channels doesn't experience such penalty because the effect of XPM is averaged out due to the symmetry of the pulses [58].

1.6 Measuring Performance

Prior to the consideration of BER estimation, it is imperative to explore what causes transmission errors. In addition to signal distortion due to nonlinearity and dispersion, the

issue of noise is of great concern to undersea systems due to the large number of amplifiers used to compensate for fibre losses. Prior to the discussion of amplifiers, we must define what is meant by noise and its manifestation in optical communications.

The study of noise was initially concentrated on electron movements than photon movements, but due to the quantum-mechanical nature of photons and their statistical movements, they were seen as 'conceptually similar'.

Noise is seen as omnipresent in any conductor, even in the absence of external voltage across it. Thus, when a signal travels in a conductor, is it the noise that contaminates the signal, or is it the signal that contaminates the noise. Noise was becoming better understood and the generating mechanism was identified. It can be classified according to origin, generating mechanism, and effect that it has on the propagating signal.

Generally, based on the generating mechanism, noise was classified as extrinsic or intrinsic. Extrinsic noise is unwanted frequencies superimposed on the signal from external sources, such as electromagnetic interference, amplifier noise (ASE), cross talk, four-wave mixing, or detector noise. We will discuss ASE in depth later as it dominates the source of noise in the systems under consideration.

Intrinsic noise is unwanted random energy fluctuation of the signal degradation of the signal electrons or photons caused by temperature, by the nonlinearity and gradient nonlinearity of the transmission medium, or by contaminants in the matrix of the medium; such noise is thermal noise, shot noise, and flicker or 1/f noise. All sources of noise degrade transmission in different ways, such as cross-talk, jitter and wander [66],

Crosstalk is the name given to the transfer of power between channels. This can occur due to nonlinear effects in optical fibres but also due to linear effects such as imperfect multiplexing and de-multiplexing. This can result in SRS, SBS, FWM and XPM.

Jitter is defined as the short-term (> 10 Hz) variation of the signals significant instants from their ideal position in time. This may be the amplitude or the timing of the bit-slot. Such phenomena may be due to inter-channel or intra-channel nonlinear effects.

Wander is defined as the long-term (< 10 Hz) variation of the signals significant instants from their idea position in time. It can be due to long-term environmental variations and component aging. Given that our systems of interest are built to last 25 years in very deep water, component aging and environmental variations do not represent a problem for our analysis.

The important quantity when measuring the performance of an optical transmission system is the electrical Q-factor (Q for Quality), which we will now introduce in the context of the BER, prior to discussion of other alternative measures of performance.

The quantification of BER is perhaps the most important challenge for optical engineers working on high capacity transmission systems. The literature is somewhat confusing its definition of this term; two definitions are often given. There is bit error ratio (BERatio), defined as the number of received bits in error over a large number of bits transmitted. There is also bit error rate (BERate) defined as the ratio of errored bits to the total transmitted in a time interval. We will use the bit error rate definition, as we will always be clear about our bit-rate.

Knowledge of the channel statistics is of utmost importance for the estimation of BER, but first we must appreciate what contributory factors influence transmission error. Clearly, attenuation weakens optical signals, but we can negate this affect using optical amplifiers. However, as we have already mentioned, optical amplifiers (or EDFA's) contribute their own type of noise. For undersea transmission, the noise contribution from EDFA's, as detailed on page 21, is one of the dominant factors limiting the reach of the system.

For undersea systems, ASE is the dominant contributor to the overall noise level in the system. Every amplifier contributes its own noise and this is concatenated with the preceding and succeeding amplifiers to saturate signals, ultimately limiting the transmission distance.

As previously mentioned, the characteristic quantity of any EDFA is the noise figure. This was defined [16] as the ratio between the OSNR of the signal entering the amplifier and the OSNR leaving the amplifier. For large Gain amplifiers, the noise figure can be calculated easily through knowledge of the spontaneous emission ($F_n \approx 2n_{sp}$).

Due to the aforementioned reasons, it is important to consider the statistical nature of ASE prior to the proposal of any statistical models. This is particularly pertinent in the linear regime [15, 66, 67] where ASE will represent the dominant source of distortion.

Practically, many sources of noise in optical transmission systems can be approximated by AWGN and this is often applied to the statistical analysis of optical signals [68]. This is a commonly used approximation because many sources of noise afflicting optical signals have what is known as a flat spectral profile for the frequencies of interest and ASE is no different.

We can illustrate noisy signals effectively through an understanding of the power spectral density and the covariance. The covariance allows us to measure the variation between successive samples of the spectral profile of the signal. It can easily be understood through the following explanation. Consider successive samples of a random variable V_1 and V_2, if we assume that the random process is defined by the deviation from the expectancy (mean) and V_1 and V_2 are both above (below) the expectancy; then this variable is said to have positive covariance. Contrarily, if V_1 is below (above) the expectancy and V_2 is above (below) the expectancy; the variable is said to have negative covariance. The covariance function of a random process $V(t)$ characterises the covariance and is defined generally as;

$$C(\tau) = \langle [V(\tau_1) - \mu][V(\tau_2) - \mu] \rangle \tag{1.61}$$

Where the $\langle V \rangle$ denotes the first moment of V and μ denotes the mean value of V, $V(\tau_1) = V_1$ and $V(\tau_2) = V_2$. AWGN is illustrated mathematically through consideration of the covariance function, which comprises a delta function multiplied by a positive constant $N_0/2$ [69]. We state this (using τ as a normalised time unit) [69];

$$C(\tau) = \frac{N_0}{2}\delta(\tau) \tag{1.62}$$

A covariance function of this form suggests neither positive or negative covariance, but rather a random variable that can change very rapidly meaning that two instants of the same random variable are uncorrelated at any point in time. The Power Spectral Density (PSD) of a random process if defined as the Fourier transform of the covariance function. Using this definition, and the sifting property of the delta function, we can easily calculate the PSD (from the Wiener-Klinchin theorem [69]) of AWGN;

$$S(\varpi) = \int_{-\infty}^{\infty} C(\tau) e^{-j\varpi\tau} d\tau = C(0) = \frac{N_0}{2} = const \tag{1.63}$$

Practically, this says that AWGN characterises an absolutely random process. As is seen from equation (1.63), the PSD is constant for all frequencies. This process is known as "white",

similar to the white light which is composed of all possible chromatic lines with approximately equal power. For a AWGN process, the variance can be calculated as [69];

$$\sigma^2 = \frac{1}{2\pi}\int_{-\infty}^{\infty} S(\varpi)d\varpi = \infty \qquad (1.64)$$

Infinite variance of AWGN is not important as we only require the noise profile to be flat for the frequencies of interest. Calculating the variance gives a singular result, showing us that the variance of white noise is equal to infinity. We are not interested in such abstraction. ASE has a flat spectral profile over the range of frequencies considered, the C-band (1525-1565 nm) [9]. Outside of this band, the use of EDFA's is not advised because of the varying gain profile. For this reason, most statistical analysis of optical transmission systems assumes that the main source of noise is AWGN.

Consider a chain of amplifiers of increasing length complementing a section of fibre of length 32.3 km, we consider an Single Mode Fibre (SMF) with loss coefficient α = 0.2 dB/km, D = 16 ps/(nm km) and A_{eff} = 80 μm^2.

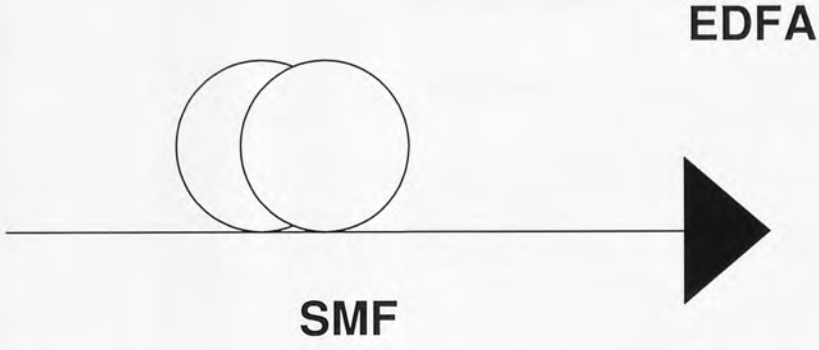

Figure 1.18: Graphical Depiction of a Simple SMF Configuration

We launch Gaussian pulses into the fibre with average launch power of -3 dBm at a duty cycle of 50% and expose the signal to extensive amounts of ASE noise through the use of amplifier with noise set to 4.5 dB which will compensate exactly for the losses in the previous fibre section.

We see from Figure 1.19 how the noise saturates the signal over large distances. ASE dominates the linear transmission regime and limits the distance of undersea transmission systems. EDFA's are often cascaded to overcome fibre losses in a long-haul lightwave system. The build-up of amplifier induced noise is one of the most critical factors for systems of this type.

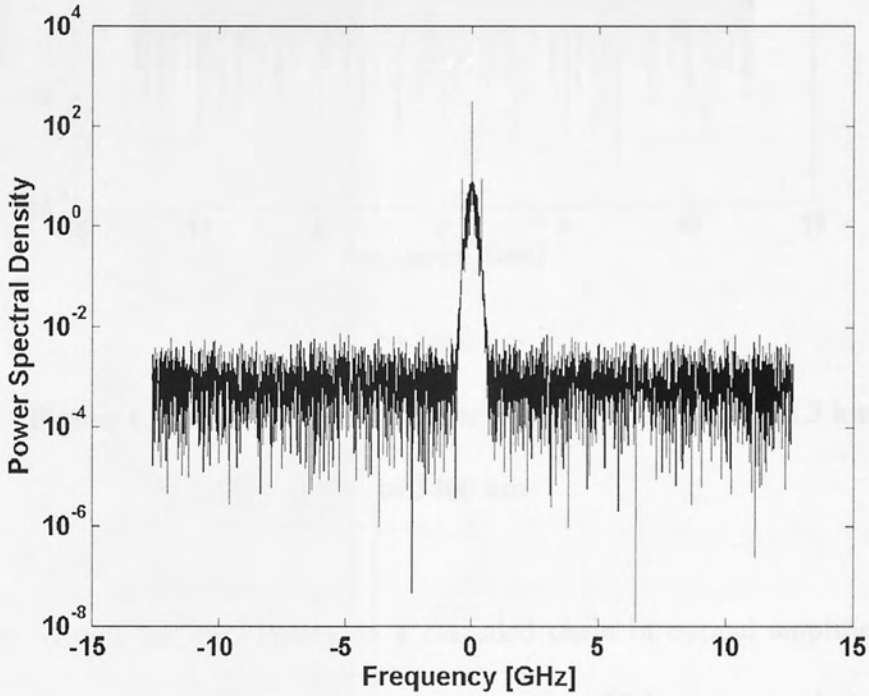

a)32 km

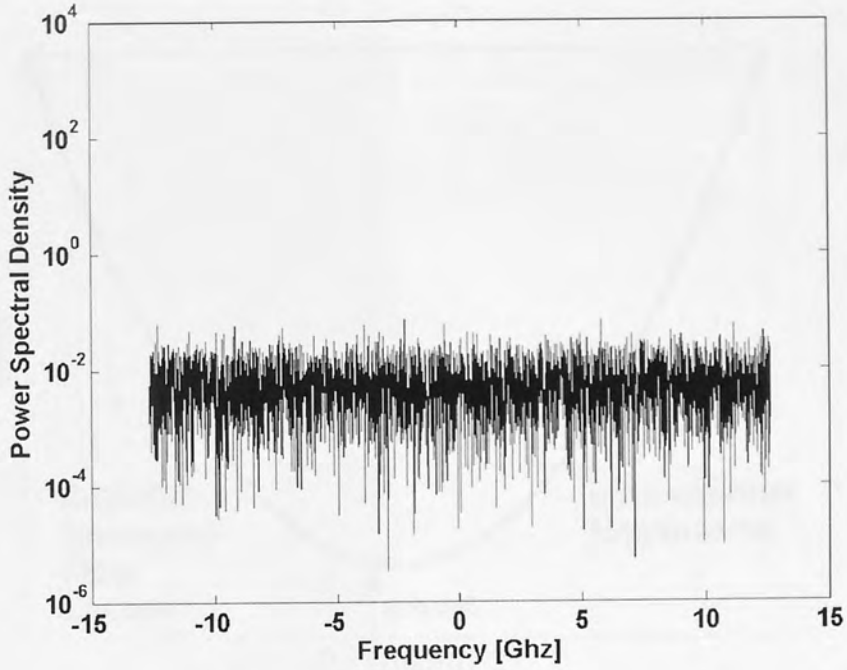

b) 2400 km

Figure 1.19: Evolution of ASE for System of Length a) 32.3 km

b) 2400 km

There are two reasons for this. Firstly, in a cascaded chain of optical amplifiers, the ASE accumulates over many amplifiers and degrades the optical SNR as the number of amplifiers increases [42]. Secondly, as the level of ASE grows it begins to saturate optical amplifiers and reduce the gain of amplifiers located further down the fibre link. An added concern is that of optical nonlinearity, SRS and SBS influence signal behaviour in addition to Kerr nonlinearity (XPM and FWM). These factors are controlled largely by effective dispersion management and appropriate channel spacing [70]. It would not be prudent to explore each and every source of noise and signal distortion in detail. Initially, we concentrate on what is relevant to the quasi-linear transmission regime, such as IXPM and IFWM

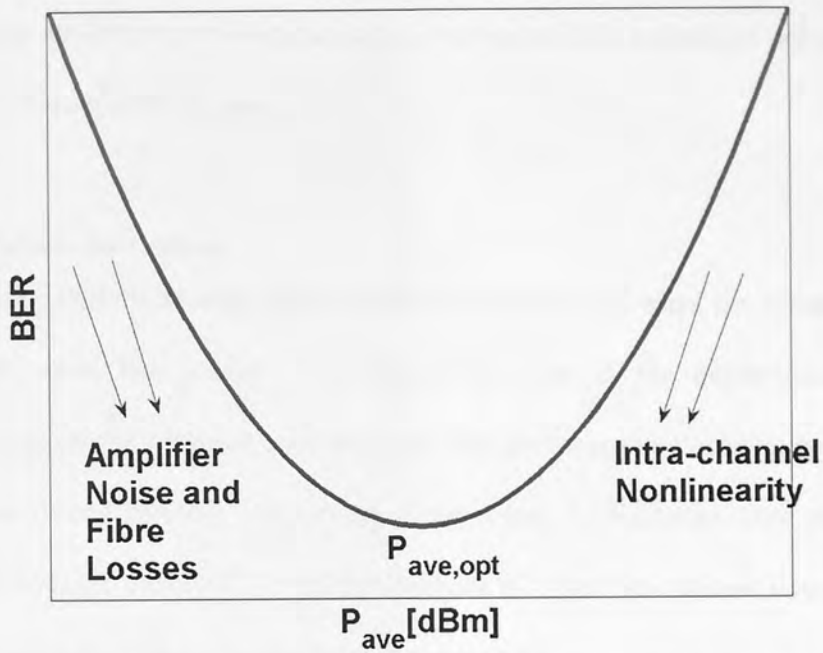

Figure 1.20: Definition of the 3 transmission regimes for optical communications

One of the main benefits of RZ-DPSK, in addition to the 3 dB receiver sensitivity improvement as detailed in Appendix B, is the increased tolerance to nonlinearity. Due to this, our use of the quasi-linear regime is a sensible base from which to work when considering BER estimation.

The estimation of BER in these channels is of great importance to the installation of these systems. As in RZ-OOK transmission, RZ-DPSK involves the use of square–law integrate and dump receivers. The statistics of which are traditionally non-Gaussian [68]. It has however, been shown, for RZ-OOK signals that the Gaussian estimate based on electrical Q-factor can be used [71].

To effectively estimate the BER, accurate knowledge of the channel statistics is required and as such BER estimation in RZ-DPSK systems is very open to debate [72-74]. Whilst BER estimation for RZ-OOK transmission is simple and well known [71], the same cannot be said of RZ-DPSK [75]. The emergence of RZ-DPSK as an option for high-capacity long-haul

quasi-linear transmission has prompted substantial investigation [72]. It is shown that several key choices are important when choosing a particular BER estimation procedure such as duty cycle and transmission distance.

BER Estimate Derivation

If we assume that the average received power is equal to P_1 when the symbol 1 is transmitted and to P_0 when the symbol 0 is transmitted. Due to the dependence of some noise contributions on the received optical power, the photocurrent fluctuations are also functions of the transmitted symbol. The output photocurrent, I, fluctuates from one bit to another, around an average value of I_1 with the variance σ_1 when the symbol 1 is transmitted and I_0 with the variance σ_0 when the symbol 0 is transmitted.

At the time decision time t_d determined by the clock recovery circuit, the decision circuit compares the observed current value I with the threshold value I_d. When I is found to be above the threshold value I_d the firm decision that a 1 is transmitted can be made. When I is found to be below the threshold value I_d the firm decision is taken that a 0 is transmitted can be made.

When, due to the signal and receiver noises, I is found to be above the threshold value I_d, whereas the symbol 0 has been transmitted, an error occurs. In the same way, when I is found to be below the threshold value I_d, whereas the symbol 1 has been transmitted, an error also occurs. Both of these two error sources degrade the performance of communication systems. The performance of a digital communication system is expressed in terms of bit error probability (bit error rate). This is defined as the ratio of the number of wrong decisions to the number of transmitted bits.

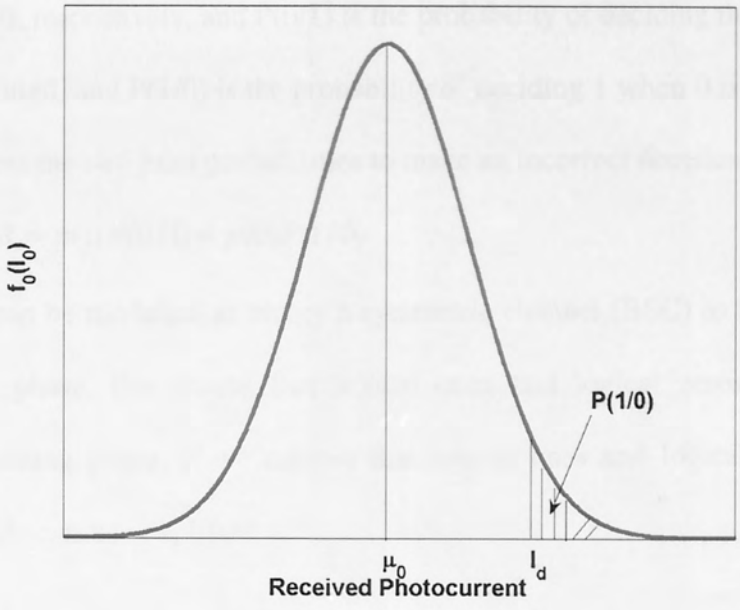

a)

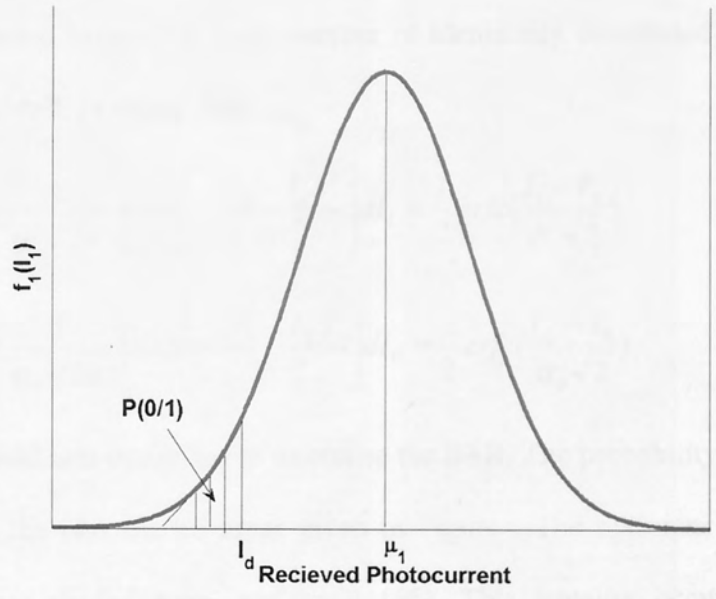

b)

Figure 1.21: Probability density functions (pdfs) of the received photocurrent:

a)Distribution of zeros with received threshold at I_d

b) Distribution of ones with received photocurrent threshold at I_d

The equation describing BER is given in (1.65), where p(1) and p(0) are the probabilities of transmitting 1 and 0, respectively, and P(0/1) is the probability of deciding that a 0 is received when a 1 is transmitted, and P(1/0) is the probability of deciding 1 when 0 is transmitted. The two products express the two joint probabilities to make an incorrect decision.

$$BER = p(1)P(0/1) + p(0)P(1/0) \tag{1.65}$$

A DPSK channel can be modelled as binary a symmetric channel (BSC) as they are complex fields encoded in phase, this means that logical ones and logical zeros have the same amplitude but opposing phase. If we assume that logical ones and logical zeros are equi-probable, then (1.65) can be simplified;

$$BER = \frac{1}{2}(P(0/1) + P(1/0)) \tag{1.66}$$

If a Gaussian model is assumed, logical for a quasi-linear transmission regime due to the statistical independence between a large number of identically distributed pulses (samples), then we can use Figure 1.21 to say that:

$$P(0/1) = \frac{1}{\sigma_1\sqrt{2\pi}}\int_{-\infty}^{I_d}\exp\left[-\frac{(I_1 - I_d)^2}{2\sigma_1^2}\right]dI_1 = \frac{1}{2}erfc(\frac{I_1 - I_d}{\sigma_1\sqrt{2}}) \tag{1.67}$$

$$P(1/0) = \frac{1}{\sigma_0\sqrt{2\pi}}\int_{I_d}^{\infty}\exp\left[-\frac{(I_0 - I_d)^2}{2\sigma_0^2}\right]dI_0 = \frac{1}{2}erfc(\frac{I_d - I_0}{\sigma_0\sqrt{2}}) \tag{1.68}$$

The decision threshold I_d is optimised to minimise the BER. The probability P(0/1) and P(1/0) are proportional to the two shaded areas given in Figure . The optimum value is obtained when when the two shaded areas are equal [66]. This equality occurs when the two distributions coincide;

$$f_1(I_d) = f_0(I_d) \tag{1.69}$$

If the two shaded regions are identical, this can be simply understood by observing that any departure from the optimal value leads to an increase of one of them being larger than the reduction for the other. The Q-factor, governing the quality of transmitted signals, can be defined using the following system of equations

$$Q = \frac{I_d - I_0}{\sigma_0} \tag{1.70}$$

$$Q = \frac{I_1 - I_d}{\sigma_1} \tag{1.71}$$

Solution of equation (1.70, 1.71) for the two unknown required variables gives;

$$I_d = \frac{\sigma_0 I_1 + \sigma_1 I_0}{\sigma_0 + \sigma_1} \tag{1.72}$$

Then from equations (1.70,1.71), we can say that the BER for the idealised channel described can be estimated using the formula;

$$BER = \frac{1}{2} erfc(\frac{Q}{\sqrt{2}}) \tag{1.73}$$

As

$$erfc(x) = 1 - erf(x) \tag{1.74}$$

Where

$$erf(x) = \frac{1}{\sqrt{\pi}} \int_x^{\infty} e^{-u^2} du \tag{1.75}$$

Alternative Q-factor Estimation

Electrical Q-factor based estimates for BER have long been questioned in the context of RZ-DPSK transmission [67, 72, 75], where the accuracy is seen as 'highly system dependent'. This has lead to the development of alternative BER estimation techniques for RZ-DPSK transmission. A Q-factor based on the optical phase of the signal was introduced [67]. This assumes a Gaussian distribution of phase in RZ-DPSK systems. The derivation of phase Q-factor is based on the assumption that the phase shifts are distributed about a centre value at π or 0 and is stated in a similar way to electrical Q-factor. The is known as $Q_{\Delta\varphi}$;

$$Q_{\Delta\varphi} = \frac{\pi}{\sigma_{\Delta\varphi,\pi} + \sigma_{\Delta\varphi,0}} \tag{1.76}$$

Similarities to Q_{el} mean that any derivation is quite unneccesary here, we can simply say that $BER(Q_{\Delta\varphi})$ can be defined as;

$$BER(Q_{\Delta\varphi}) = \frac{1}{2} erfc(\frac{Q_{\Delta\varphi}}{\sqrt{2}}) \tag{1.77}$$

Phase Q-factor measures performance based on the distance of the respective phase difference rails $\Delta\varphi$,0 and $\Delta\varphi$,π. This was introduced in addition to the assumption of a Gaussian noise distribution at the centre of each bit-slot. It was shown [76] that such an estimate works particularly well in regimes dominated by phase noise and phase fluctuation due to nonlinearity such as SPM and XPM [67, 76].

Alternatively, a linear approximation for an RZ-DPSK channel provided another alternative in the shape of amplitude Q-factor (Q_A). Balanced detection (identical priority given to both arms of the Mach-Zehnder detector) was used [67] to derive an alternative expression based on the moments of the field amplitude distribution. This Q-factor is defined as;

$$Q_A = \frac{<|f_n|>}{\sigma_{|f_n|}} \tag{1.78}$$

Where f_n is the field amplitude, $\langle x \rangle$ denotes the expectancy of x and σ_x denotes the standard deviation of x. Direct substitution of Q_A into the Gaussian BER estimate [67] provides a BER estimate based on amplitude Q-factor.

$$BER(Q_A) = \frac{1}{2} erfc(\frac{Q_A}{2}) \tag{1.79}$$

This is shown to be effective in the low power (linear) regime, but insufficient when power is increased and distortion due to phase modulation or phase noise are prevalent.

A fourth direct method of estimating Q-factor in the nonlinear regime is that of the modified phase Q-factor [76]. This is based on the inference from [67] that the standard phase Q-factor

often under-estimates the BER directly but correctly predicts qualitative behaviour. This lead to the modification of the two phase rails by approximately 15% [76], hence an overall modification to the phase Q-factor of 0.87. The modified phase Q-factor is therefore stated as;

$$Q_{\Delta\varphi,\mathrm{mod}} = \frac{\pi}{1.15(\sigma_{\Delta\varphi,0} + \sigma_{\Delta\varphi,\pi})} \tag{1.80}$$

This is then used in the formula for phase Q-factor of;

$$BER(Q_{\Delta\varphi,\mathrm{mod}}) = \frac{1}{2} erfc(\frac{Q_{\Delta\varphi,\mathrm{mod}}}{\sqrt{2}}) \tag{1.81}$$

Despite the choice on offer from the literature, a broad comparison of the 4 Q-factor dependent methods shows no particular superior choice [72]. However, BER estimation based on the electrical Q-factor, for quasi-linear transmission, is shown to be effective [67, 72]. For such regions, only optimal, dispersion managed transmission in the optimal power regime is considered. It can be accepted here, from our initial introduction to the quasi-linear regime, that the effects of the dispersion are averaged out over all of the pulses in the pattern and that as such, fibre nonlinearity is averaged out.

We identified that RZ-DPSK is an option for the upgrade of legacy undersea transmission systems. The most important parameter for measuring performance of optical communications is the BER i.e. the probability of transmission error. During simulation, an important method of assessing the performance of new technologies and transmission configurations, it is computationally expensive to generate transmission errors when the quality of transmission (characterised by the Q-factor) is high. With this in mind, we need to explore BER estimation for RZ-DPSK transmission, in the limit of the quasi-linear transmission regime.

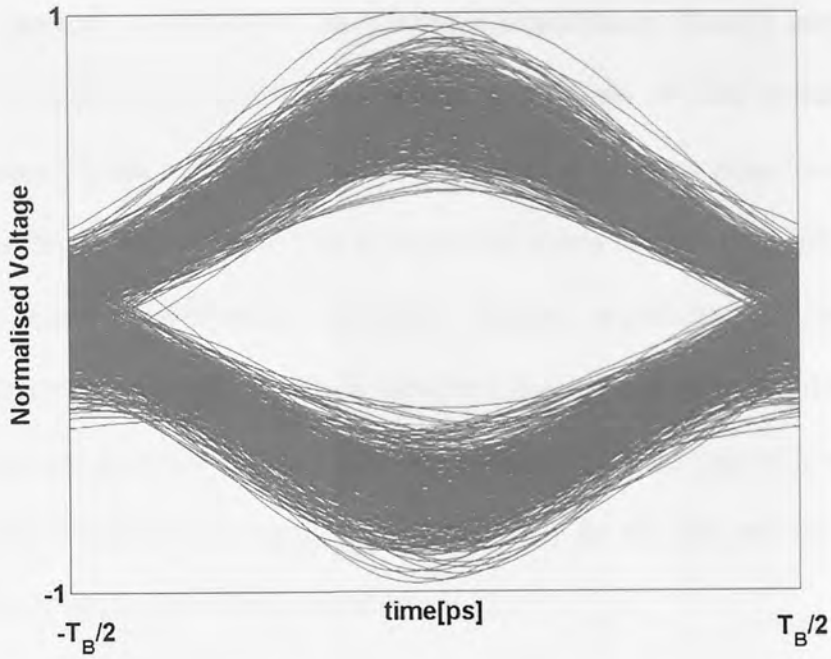

Figure 1.22 Typical RZ-DPSK Eye Diagram

Statistically, RZ-DPSK enjoys several statistical differences compared to RZ-OOK. Amongst them is symmetry, as shown in the traditional eye diagram shown in Figure 1.22. If we move away from this transmission region, to where dispersion is not properly managed or where nonlinearity is increased due to an increase in average pulse power over large distances, not much is known about the statistical behaviour of the channel. If we assume that the dominant sources of nonlinearity are IXPM and IFWM [36], this provides insight into the structure of the underlying statistics over a single channel as we can study the statistics of pulse-to-pulse interaction. This would also make a useful tool in the analysis of 40 Gb/s RZ-DPSK transmission over long-haul transmission distances, since the use of yet narrower pulses introduces the pulse-to-pulse interactions at significantly lower distances and at lower BER.

1.7 High-Capacity Long-Haul RZ-OOK Transmission

Despite identifying RZ-DPSK as a key technology for the upgrade of undersea transmission configurations. We see that 40 Gb/s transmission over large distances using such a format is

Missing page(s) from the bound copy

The improved tolerance of RZ-DPSK to nonlinear impairments doesn't necessitate the assumption that such problems do not exist. Following a review of BER estimation within RZ-DPSK transmission, we see that the use of the electrical Q-factor based estimation can work within quasi-linear transmission. This is supported within the literature [67]. However, BER estimation when pulse-to-pulse interaction becomes significant due to nonlinear impairments is sparse in the literature, this is identified as important when the time comes to switch again to higher capacities, enlisting narrower pulses and the subsequent introduction of new physical phenomena into the transmission, which may be due not only to IFWM and IXPM, but also self-steeping, or Raman-based effects [3].

We then returned to the idea of transmitting RZ-OOK pulses at 40 Gb/s channel capacity. We identified the statistics of eye closure as an important consideration for assessing the impact of distortion and Q-degradation on high capacity RZ-OOK transmission. Such transmission, again an example of the quasi-linear transmission regime, is subject to distortion. The analysis of the transmission, or comparison with other formats or the assessment of transmission impairments, will require the estimate of ECP. One of the dominant intrachannel impairments that dominate this transmission, amongst other quasi-linear transmission configurations using RZ-DPSK, is FWM [36]. This manifests as amplitude fluctuations [36], so an analysis of ECP due to such amplitude fluctuations is an important next step in the analysis of high capacity RZ-OOK transmission.

We can now identify objectives for the remainder of the thesis:

- To assess the performance of 20 Gb/s RZ-DPSK transmission over undersea transmission distances

- To further investigate BER estimation in quasi-linear transmission using the RZ-DPSK data format and 20 Gb/s capacity
- Study the impact of dispersion and nonlinearity on BER estimation using an analysis of the channel statistics.
- Derive an estimate of ECP for RZ-OOK transmission systems in the quasi-linear regime, dominated by FWM.

In this thesis, we will first assess the performance of 20 Gb/s RZ-DPSK WDM undersea transmission through numerical simulation of the Generalised Nonlinear Schrödinger Equation (GNLS), assessing the flexibility due to changes in both pulse duty cycle and pre-/post-compensation, and assessing the performance of BER estimation methodologies mentioned in the literature [72]. Following this, we return to the study of single channel 20 Gb/s RZ-DPSK in order to study the impact of both chromatic dispersion and nonlinearity on channel statistics. Finally, we derive an estimate of ECP in the limit of 40 Gb/s transmission dominated by amplitude fluctuations due to IFWM using an examplary dispersion managed RZ-OOK transmission configuration.

Chapter 2 Numerical and Mathematical Analysis of Optical Pulse Propagation

Our analysis of undersea optical transmission systems is guided by mathematical modeling. Such analysis of these systems is a useful as they are too big for detailed physical investigation without some guidance from preceding modeling. In this section, we demonstrate how we model optical pulse propagation in nonlinear dispersive optical fibres.

Firstly, we derive the Generalised Nonlinear Schrödinger Equation (GNLS) using a perturbation analysis of the wave equation for an optical pulse. Using the idea of isotropic nonlinear susceptibility of the pertinent optical material and the convergence of the propagation constant defined by the fibre mode, we derive the full GNLS.

Secondly, we make some assumptions about the behaviour of our pulses in order to simplify our equation in some limits, such as nonlinear and dispersive transmission. However, we also see that the combination of nonlinearity and dispersion creates a very complicated regime inside which we cannot explicitly solve the GNLS.

In such a situation, we need to use numerical algorithms, such as the Split-Step Fourier Method to solve the GNLS. This provides insight into the solution of the GNLS for complicated transmission configurations, allowing the inclusion of inline devices and new fibres in order to manage dispersion and nonlinearity.

2.1 Generalized Nonlinear Schrödinger Equation (GNLS)

The propagation of optical pulses propagating in an optical fibre is modeled using the nonlinear wave equation [23];

$$\nabla^2 \hat{E} - \frac{1}{c^2}\frac{\partial^2 \hat{E}}{\partial t^2} = -\mu_0 \frac{\partial^2 P(\hat{E})}{\partial t^2} \tag{2.1}$$

Where E (dropping the tilde notation) is the electrical field vector, μ_0 is the vacuum permeability, c is the speed of light and P is the polarization density field. We can expand the polarization density field in a Taylor series;

$$P(t) = \chi^{(1)} E(r,t) + \chi^{(2)} E^2(r,t) + \chi^{(3)} E^3(r,t) + \ldots$$

At low optical powers, the induced polarization has a linear relationship with E such that [23] (i.e the first term in the Taylor series);

$$P_L(r,t) = \varepsilon_0 \int_{-\infty}^{\infty} \chi^{(1)}(t-t') \cdot E(r,t')dt' \tag{2.2}$$

Where ε_0 is the vacuum permittivity and $\chi^{(1)}$ is the first order susceptibility. To account for fibre nonlinearity, the polarization can be written in two parts.

$$P(r,t) = P_L(r,t) + P_{NL}(r,t) \tag{2.3}$$

Where $P_{NL}(r,t)$ is the nonlinear part of the polarization. In silica fibre, the nonlinear part of the polarization always comes from the third order susceptibility [42], which comes from the third term in the Taylor series expansion of the polarization density field [27]. This is due to the fact that second-order susceptibility, $\chi^{(2)}$ (responsible for second term in the Taylor series of the polarization density field [27]) is exactly zero in a material with molecular centro-symmetry such as silica [27]. Therefore;

$$P_{NL}(r,t) = \varepsilon_0 \int_{-\infty}^{\infty}\int_{-\infty}^{\infty}\int_{-\infty}^{\infty} \chi^{(3)}(t-t_1, t-t_2, t-t_3) E(r,t_1) E(r,t_2) E(r,t_3) dt_1 dt_2 dt_3 \tag{2.4}$$

Third order susceptibility is responsible for producing the nonlinear effects which we discussed in the first chapter such as FWM, XPM, SPM and light scattering such as SRS and SBS. We use (2.2), (2.3) and (2.4) in (2.1) to derive the propagation equation in nonlinear dispersive fibres. A few simplifying assumptions are generally made to solve (2.1). Firstly, P_{NL} is treated as a small perturbation of P_L, and the field polarization is maintained along the

fibre. We also make the weakly guiding approximation, namely that the difference in the refractive index between the core and the cladding is very small.

A second assumption, known as the quasi-monochromatic assumption, places the condition upon the channel that the overall spectral width of the wave is much smaller than the centre frequency. In many modern systems, using narrow pulses, the quasi-monochromatic assumption is false and the spectral width of the wave can be as much as 1/3 rd of the centre frequency. However, we maintain the assumption to ensure mathematical convenience. With this in mind, we can still proceed with our analysis. In the time domain, this is interpreted as a slowly varying amplitude envelope. The propagation constant, $\beta(\varpi)$, is approximated by a low order Taylor series expansion about the carrier frequency;

$$\beta(\varpi) = \beta_0 + (\varpi - \varpi_0)\beta_1 + \frac{1}{2}(\varpi - \varpi_0)^2\beta_2 + \frac{1}{6}(\varpi - \varpi_0)^3\beta_3 + \ldots \qquad (2.5)$$

Where β_n denotes the Taylor coefficients given by;

$$\beta_n = \left[\frac{d^n\beta}{d\varpi^n}\right]_{\varpi=\varpi_0} \qquad (2.6)$$

The second order propagation constant β_2 [ps/km], accounts for the chromatic dispersion effects in fibre-optic communication systems. Depending on the sign of β_2, the dispersion region can be classified into two regions, normal ($\beta_2>0$) and anomalous ($\beta_2<0$). Qualitatively, in the normal-dispersion region, the higher frequency components of an optical signal travel slower than the lower frequency components. In the anomalous dispersion region, the opposite occurs. Fibre dispersion is often expressed by another parameter, D [ps/(nm-km)], which is called the dispersion parameter. Where D is defined as:

$$D = \frac{d}{d\lambda}\left(\frac{1}{v_g}\right) \tag{2.7}$$

$$\beta_2 = -\frac{\lambda^2}{2\pi c} D \tag{2.8}$$

The relationship between β_2 and D is given (2.8) [79], where λ is the wavelength and v_g is the group velocity. The cubic and higher-order terms in (2.5) are generally negligible as long as the quasi-monochromatic assumption holds. However, if the centre wavelength of an optical signal is in the vicinity of the zero-dispersion wavelength (i.e. $\beta_2 \approx 0$), the β_3 term due to third-order dispersion should be included. If the input electric field is assumed to propagate in the positive z direction and is polarized in the x direction, then equation (2.1) becomes;

$$\frac{\partial A(z,t)}{\partial z} = -\frac{\alpha}{2} A(z,t) \qquad \text{(linear attenuation)} \tag{2.9}$$

$$+ j\frac{\beta_2}{2}\frac{\partial^2}{\partial t^2} A(z,t) \quad \text{(second order dispersion)}$$

$$+ \frac{\beta_3}{6}\frac{\partial^3}{\partial t^3} A(z,t) \qquad \text{(third order dispersion)}$$

$$- j\gamma |A(z,t)|^2 A(z,t) \qquad \text{(Kerr effect)}$$

$$+ j\gamma T_R \frac{\partial}{\partial t} |A(z,t)|^2 A(z,t) \qquad \text{(SRS)}$$

Where A(z,t) is the slowly varying envelope of the electric field. This assumption removes the need for any potential homogenization of the equation as we don't need to compensate for heavy changes in the gradient of the envelope of the electrical field. The term z corresponds to the the propagation distance, t is the normalized physical time, α [1/km] is the fibre loss, β_2[ps^2/km] is the second order propagation constant and β_3[ps^3/km] is the third order propagation constant, γ[W/km] is the nonlinear coefficient, n_2 is the nonlinear index

coefficient, A_{eff} is the effective core area of fibre, λ_0 is the centre wavelength, ω_0 is the centre angular frequency and T_R is the slope of the Raman gain (~ 5 fs).

This equation (2.9) is the generalized nonlinear Schrödinger equation [23], and is known to be applicable for the propagation of pulses as short as ~50 fs, corresponding to a spectral width of ~20 THz. When the pulse-width (T_0) is greater than 1 ps, equation (2.9) can be considerably simplified (as indicated below) because the Raman effect term [3] and the self-steepening [3] terms are negligible compared to the Kerr effect term [79]. Systems under this consideration do not occupy enough bandwidth to be vulnerable to SRS or self-steepening, so we can simplify equation (2.9) to

$$\frac{\partial A}{\partial z} = -\frac{i}{2}\beta_2 \frac{\partial^2 A}{\partial t^2} - \frac{\alpha}{2} A + i\gamma |A|^2 A \qquad (2.10)$$

This is the equation that we deal with in this thesis, third order dispersion is neglected as we don't always operate at the zero dispersion wavelength. Given that we are concerned with 20 Gb/s bit-rate systems operating with a bit-period of 50 ps, we can use this equation as a guide for our numerical modeling. Next, we examine the cases of lossy and lossless transmission. For these cases, equation (2.9) can be solved exactly using some simple initial conditions.

2.2 Normalised GNLS

Our equation (2.10) models the pulse under the influence of the three main factors of dispersion, nonlinearity and fibre loss, the most important 3 factors in modern optical communication systems. We simplify our analysis by introducing normalized quantities in the shape of dispersion length L_D (the length of fibre at which dispersive effects become important) and nonlinear length L_N(the length of fibre at which nonlinear effects become important):

$$L_D = \frac{T_0^2}{|\beta_2|} \tag{2.11}$$

$$L_N = \frac{1}{\gamma P_0} \tag{2.12}$$

Where β_2 is the second order propagation constant, γ is the nonlinear coefficient and P_0 is the peak power of the slowly varying envelope, A(z,t). If the amplitude envelope A(z,t) is normalized by its peak value such that:

$$A(z,t) = \sqrt{P_0}U(z,t) \tag{2.13}$$

We can express equation (2.10) as (in terms of L_D and L_N);

$$i\frac{\partial U}{\partial z} = \frac{\mathrm{sgn}(\beta_2)}{2L_D}\frac{\partial^2 U}{\partial \tau^2} - \frac{e^{-\alpha z}}{L_N}|U|^2 U \tag{2.14}$$

Where $\mathrm{sgn}(\beta_2)=+1$ when $\beta_2 > 0$ and $\mathrm{sgn}(\beta_2)=-1$ when $\beta_2 < 0$. The unit τ is a normalized time unit such that $\tau=t/T_0$. Within optical transmission systems, the fibre loss α is compensated through the use of amplifiers. If optical amplifiers are placed at equal spacing throughout the transmission, such as in the case of undersea transmission, then we can use the average optical power throughout the transmission;

$$P_{avg} = \frac{1}{z_a}\int_0^z P_0 e^{-\alpha z}dz = \frac{P_0}{\alpha z_a}(1 - e^{-\alpha z_a}) \tag{2.15}$$

This is based on the assumption that the Erbium-doped fibre which is used to configure the amplifier is of negligible length when compared to the transmission fibre length. The normalized GNLS is then given as:

$$i\frac{\partial U}{\partial z} = \frac{\mathrm{sgn}(\beta_2)}{2L_D}\frac{\partial^2 U}{\partial \tau^2} - \frac{1}{L_N}|U|^2 U \tag{2.16}$$

Where

$$\bar{L}_N = \frac{1}{\gamma P_{avg}} \tag{2.17}$$

This equation is equivalent to (2.14) without a loss term, but with constant optical power, P_{avg}, modeling a lossless transmission systems We illustrate the power evolution of both a lossless and a loss-limited system in Figure 2.1. We check the validity of these equations below using the SSFM using a Gaussian input pulse of 70 ps initial half width at 1/e-intensity point. To exaggerate power fluctuations, we set fibre loss to 0.2 [dB/km], which is larger than the typical value at 0.2 [dB/km] and the distance to 50 km. Amplifier gain (G) is set to compensate fibre loss exactly such that $G = \exp(\alpha z)$, where z is the inter-amplifier distance. In this case, the average power can be obtained either by Eq(2.4) or by the relationship $P_{ave} = P_0(G-1)/(G \ln G)$. We also include a wide (~ 0.1 THz) optical bandpass filter after the amplifier to alleviate the influence of the ASE. We show (Figure 2.1) the different evolution behaviour for both the lossless and lossy transmission regimes;

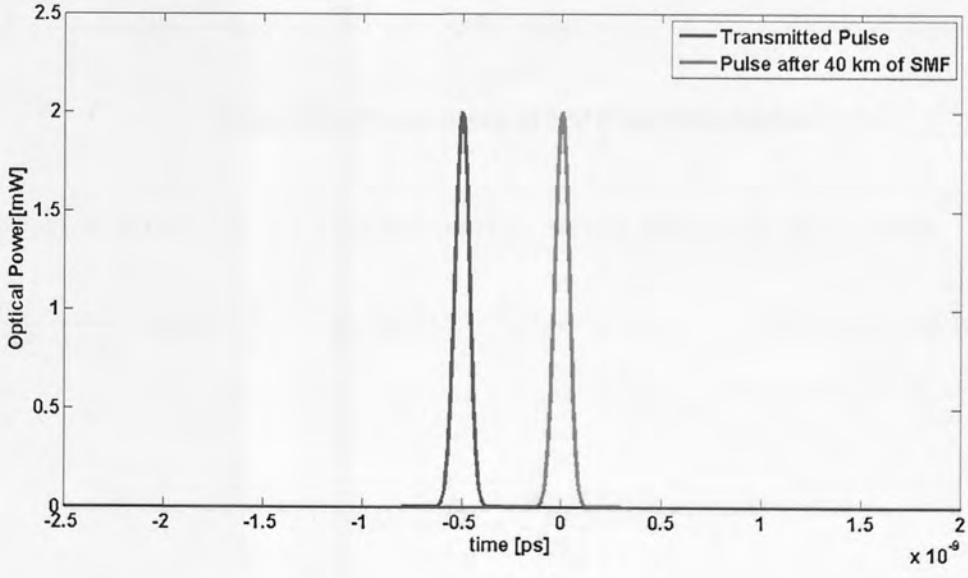

a)

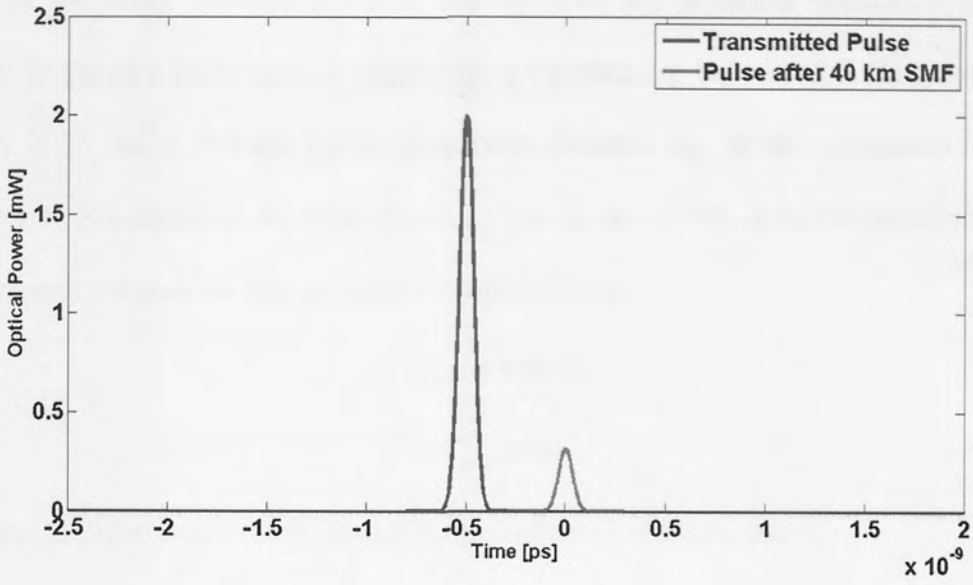

b)

Figure 2.1: Power Evolution for a Gaussian Optical Pulse at 50% Duty Cycle for a) lossless transmission and b) lossy transmission.

	D[ps/nm km]	α[dB/km]	$A_{eff}[\mu m^2]$	P[mW]
SMF	16	0.2	80	2

Table 2.1: Parameters of SMF for Simulation

If we normalize distance by, L_D, such that $\xi=z/L_D$, we can simplify (2.16) to obtain;

$$\frac{\partial U}{\partial \xi} = -\frac{1}{2} i \cdot \mathrm{sgn}(\beta_2) \frac{\partial^2 U}{\partial \tau^2} + iN^2 |U|^2 U \tag{2.18}$$

Where

$$N^2 = \frac{L_D}{L_N} = \frac{\gamma P_{avg} T_0^2}{|\beta_2|}$$

This equation is known as the normalized NLSE. It has an advantage over the previous equations in that it involves only one dimensionless parameter, N. The range of N values depends on the particular configuration.

If we consider an SMF, then typical values of β_2=-20 [ps^2/nm] and γ = 2 [1/W km] and signal powers in the range between 0.1 mW and 10 mW, the nonlinear distance (L_N), ranges between 50 km and 5,000 km [3]. Similarly, if bit-rates are between 2.5 Gb/s and 10 Gb/s result in 31.25 km to 500 km for the dispersion distance, L_D. In the calculation of L_D, the parameter T_0 is assumed as the pulse rise time. This is set to 25% of the bit-period in a typical NRZ transmission system. The calculated L_D and L_N give;

$$N_{\min}^2 = 0.0625$$

$$N_{\max}^2 = 10$$

In the case of dispersion shifted fibres (DSF), similar calculations reveal;

$$N_{\min}^2 = 0.0135$$

$$N_{\max}^2 = 135$$

The GNLS can also be explored using perturbative analysis [79], this provides insight into the analysis of highly nonlinear systems employing other types of pulses such as solitons [79]. We now move onto some special cases which can be solved using standard analytical techniques.

We now study the cases of dispersive transmission and we see that, given a Gaussian pulse shape, propagation through a dispersive medium can maintain this Gaussian pulse shape. We also see how dispersion influences the phase of the pulse, which leads into the study of SPM and XPM.

2.3 Dispersive Transmission

We identified in Chapter 1 that the interplay between chromatic dispersion and nonlinearity was a key concern for undersea optical transmission systems, so understanding the mathematical models underpinning such phenomena is of great importance. We now discuss

the effects of dispersion on optical pulses propagation inside a fibre using the pulse-propagation equation derived (2.10).

$$i\frac{\partial A}{\partial z} = -\frac{i\alpha}{2}A + \frac{\beta_2}{2}\frac{\partial^2 A}{\partial T^2} - \gamma|A|^2 A \tag{2.19}$$

Where A is the slowly varying amplitude of the pulse envelope and T is measured in a frame of reference moving with the pulse at the group velocity v_g ($T=t-z/v_g$). Depending on the initial width T_0 and the peak power P_0 of the incident pulse, either dispersive or nonlinear effects may dominate along the length of the fibre. We again use the length scales L_N and L_D. Depending on the relative magnitudes of L_D and L_N, and the fibre length L, pulses can evolve quite differently. We introduce a time scale normalized to the input pulse width T_0 as

$$\tau = \frac{T}{T_0} = \frac{t - z/v_g}{T_0} \tag{2.20}$$

We also introduce a normalized field amplitude U as:

$$A(z,t) = \sqrt{P_0}e^{-\alpha z/2}U(z,t) \tag{2.21}$$

Where P_0 is the peak power of the incident pulse. The exponential factor in accounts for fibre losses. Using (2.19, 2.21), U(z,t) is found to satisfy:

$$i\frac{\partial U}{\partial z} = \frac{\mathrm{sgn}(\beta_2)}{2L_D}\frac{\partial^2 U}{\partial \tau^2} - \frac{e^{-\alpha z}}{L_{NL}}|U|^2 U \tag{2.22}$$

Depending on the relative magnitudes of L, L_D and L_N, the propagation behavior can be classified into four categories; $L \ll L_N$ and $L \ll L_D$, $L \ll L_N$ and $L \sim L_D$, $L \ll L_D$ and $L \sim L_N$ and L longer or comparable to $L_{N,D}$.

For the first category, $L \ll L_N$ and $L \ll L_D$, neither dispersive nor nonlinear effects play a significant role during pulse propagation. This can be seen by noting that both terms on the right hand side of 2.22 can be neglected in this case. It is assumed that a pulse has a smooth temporal profile so that $\partial^2 U/\partial\tau^2 \sim 1$. As a result $U(z,\tau) = U(0,\tau)$, i.e the pulse maintains its shape during propagation. The fibre plays a passive role in this regime and acts purely as a

transport medium for optical pulses. The only concern in such a regime is fibre losses which reduce the energy of optical pulses.

This regime is useful for optical communication systems. For L ~ 50 km (SMF), L_D and L_N should be larger than 500 km for distortion free transmission. We can estimate T_0 and P_0 from equations (2.11,2.12) for given values of β_2 and γ. If we use standard values of β_2 and γ, then dispersive and nonlinear effects are negligible for L < 50 km if T_0 > 100 ps and P_0~ 1 mW. However, L_D and L_N become smaller as pulses become shorter and more intense. This is a detail which will become more apparent in the following chapter. For such short pulses, i.e at bit-rate > 10 Gb/s, both dispersive and nonlinear effects need to be included if fibre length exceeds 1 km [23].

For the second category, $L << L_N$ and $L \sim L_D$, the last term in (2.22) is negligible compared with the other two. The pulse evolution is then governed by GVD, and the nonlinear effects play a relatively minor role. The effect of GVD on propagation of optical pulses will be discussed shortly. The dispersion dominated regime occurs when

$$\frac{L_D}{L_{NL}} = \frac{\gamma P_0 T_0^2}{|\beta_2|} << 1 \qquad (2.25)$$

For the third category, $L << L_D$ and $L \sim L_N$, the dispersion term in (2.22) is negligible compared to the nonlinear term (as long as the pulse maintains the smooth temporal profile). In which case, the pulse evolution in the fibre is governed by SPM leading to spectral broadening of the pulse. The nonlinearity dominant regime occurs when;

$$\frac{L_D}{L_{NL}} = \frac{\gamma P_0 T_0^2}{|\beta_2|} >> 1 \qquad (2.26)$$

This condition is readily satisfied for relatively wide pulses (T_0 > 100 ps) with a peak power P_0 ~ 1 mW [23]. In such a limit, SPM-induced chirping can lead to spectral broadening. This

effect has been used to great effect in optical regeneration [33]. For long-haul systems, the fourth category is often realized, as transmission length L is long compared to both L_D and L_N, dispersion and nonlinearity act together as the pulse propagates along the fibre. This can lead to the realization of SPM or other nonlinear effects such as XPM and FWM.

It is simple to study the impact of chromatic dispersion on optical pulses propagating in a linear dispersive medium simply by setting $\gamma = 0$ in equation 2.19. Using the normalized amplitude equation (2.22), we obtain the simple partial differential equation;

$$i\frac{\partial U}{\partial z} = \frac{\beta_2}{2}\frac{\partial^2 U}{\partial T^2} \tag{2.27}$$

This equation can be solved by letting U(z,t) be an inverse Fourier transform:

$$U(z,T) = \frac{1}{2\pi}\int_{-\infty}^{\infty}\tilde{U}(z,\varpi)e^{-i\varpi T}\,d\varpi \tag{2.28}$$

Upon substitution into (2.27), we obtain the simple, first order partial differential equation;

$$i\frac{\partial \tilde{U}}{\partial z} = -\frac{1}{2}\beta_2\varpi^2\tilde{U} \tag{2.29}$$

The solution of this partial differential equation is given by;

$$\tilde{U}(z,\varpi) = \tilde{U}(0,\varpi)e^{\frac{i}{2}\beta_2\varpi^2 z} \tag{2.30}$$

Despite its simplicity, equation (2.29) shows that chromatic dispersion changes the phase of each spectral component by an amount proportional to both the frequency and the propagated distance. This means that the rate of change of optical phase, chirp, is also dependent on chromatic dispersion and propagation distance. Although such phase changes do not effect the pulse spectrum, they can modify the pulse shape. If we substitute (2.30) into (2.28), then we can obtain;

$$U(z,T) = \frac{1}{2\pi}\int_{-\infty}^{\infty}\tilde{U}(0,\varpi)e^{\frac{i}{2}\beta_2\varpi^2 z - i\varpi T}\,d\varpi \tag{2.31}$$

So we use the initial condition of the incident field at z=0. This is obtained simply using;

$$\tilde{U}(0,\varpi) = \int_{-\infty}^{\infty} U(0,T)e^{i\varpi T}\,dT \tag{2.32}$$

Using the relationships developed in (2.31) and (2.32), we can investigate the dispersive behaviour of a pulse of arbitrary shape. Consider, for example the Gaussian pulse, given by the initial condition;

$$U(0,T) = e^{-\frac{T^2}{2T_0^2}} \tag{2.33}$$

Where T_0 is the half width (at 1/e intensity point) introduced earlier (equation (2.13)). Practically, it is customary to use the full width at half maximum (FWHM) in place of T_0. For a Gaussian pulse, the two can be related through the equation stated below [23].

$$T_{FWHM} = 2(\ln 2)^{1/2} T_0 \approx 1.665 T_0$$

If we substitute 2.32 into 2.31, we obtain the integral.

$$\tilde{U}(0,\varpi) = \int_{-\infty}^{\infty} e^{-\frac{T^2}{2T_0^2}+i\varpi T}\,dT \tag{2.34}$$

We need to calculate this Fourier transform in order to understand the spectral broadening of such a signal. We now detail this simple procedure.

Fourier Transform of a Gaussian Function

This integral is simple to evaluate by considering the function

$$f(x) = e^{-\frac{ax^2}{2}}$$

Obtaining the Fourier transform of this function can be achieved by means of observing that it satisfies the differential equation;

$$\frac{df}{dx} + axf(x) = 0$$

This differential equation can be solved using Fourier transforms [80], the resulting transformed equation is given by;

$$i\xi\hat{f}(\xi)+i\frac{1}{a}\frac{d\hat{f}}{d\xi}=0$$

This equation is solved simply, using separation of variables, to obtain the solution;

$$\hat{f}(\xi)=Ce^{-\frac{\xi^2}{2a}}$$

The constant C is found using the definition of the Fourier transform;

$$C=\hat{f}(0)=\sqrt{\frac{2\pi}{a}}$$

Having found the Fourier transform of a general Gaussian function, we can evaluate the integral in equation (2.31) and use the convolution theorem [80] to obtain;

$$U(z,T)=\frac{T_0}{(T_0-i\beta_2 z)^{1/2}}e^{-\frac{T^2}{2(T_0^2-i\beta_2 z)}} \qquad (2.35)$$

This suggests that a Gaussian pulse will maintain its shape on propagation but its width T_1 increases with z as;

$$T_1(z)=T_0[1+\left(\frac{z}{L_D}\right)^2]^{1/2} \qquad (2.36)$$

This equation also tells us that the extent of broadening is governed by the dispersion length L_D. The key result here is that for a given fibre length, short pulses broaden more because of a smaller dispersion length. At $z = L_D$, Gaussian pulses broaden by a factor of the square root of 2. We show below the extent of dispersion induced broadening for differing values of D for a section of SMF fibre of length 1000 km with launch peak power 2 mW.

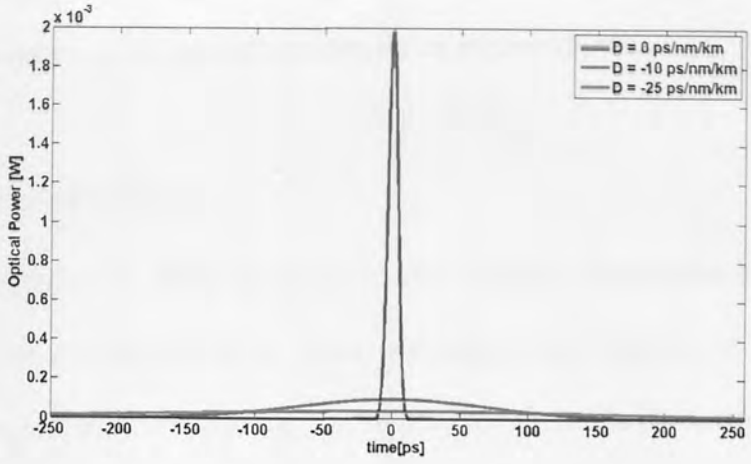

Figure 2.2: Pulse at given values of D after 1000 km transmission over SMF with launch peak power 2 mW.

Figure 2.2 shows the evolution of a Gaussian optical pulse with launch peak power 2 mw over 1000 km of SMF for varying values of D. It is clear that over this distance, uncompensated dispersion will cause the pulse to broaden out of the initial bit-slot. The SMF length of 1000 km is much longer than the dispersion length, so any transmission I this system would be dominated by dispersive effects. We can study the influence of D on the phase behavior by introducing the Euler form of a complex field;

$$U(z,T) = |U(z,T)|e^{i\phi(z,T)}$$

Where

$$\phi(z,T) = -\frac{\mathrm{sgn}(\beta_2)(z/L_D)}{1+(z/L_D)^2}\frac{T^2}{T_0^2} + \frac{1}{2}\tan^{-1}(\frac{z}{L_D}) \qquad (2.37)$$

This enables us to analyse the phase behaviour. The time dependence of the phase implies that the instantaneous frequency differs across the pulse from the central frequency ω_0. The difference $\delta\omega$ is simply the time derivative of the phase given by;

$$\delta w(T) = -\frac{\partial\phi}{\partial T} = \frac{\mathrm{sgn}(\beta_2)(2z/L_D)}{1+(z/L_D)^2}\frac{T}{T_0^2} \qquad (2.38)$$

This equation demonstrates that the frequency changes linearly across the pulse. The chirp $\delta\omega$ depends on the sign of $ß_2$ and is responsible for SPM and XPM. In the normal-dispersion

regime ($ß_2$>0), $\delta\omega$ is negative at the leading edge (T < 0) and increases linearly across the pulse; the opposite occurs in the anomalous-dispersion regime ($ß_2$<0).

2.4 SPM Solution of GNLS

As mentioned in Chapter 1, SPM results from the intensity dependence of the refractive index, this results in modulation of the phase and subsequent chirping of the propagating pulse. Due to the modulation of the phase, spectral broadening takes place which can limit the transmission bit-rate dramatically [3]. Here, we examine the solution of equation (2.10) in the limit of SPM. We see, as expected from the description in Chapter 1, that this results in temporally varying phase (chirp). Consider again 2.10;

$$i\frac{\partial A}{\partial z}-\frac{\beta_2}{2}\frac{\partial^2 A}{\partial T^2}+\gamma|A|^2A=-i\frac{\alpha}{2}A \tag{2.39}$$

In solution of this equation, we propose an ansatz;

$$A(z,T)=\sqrt{P_0}e^{-\alpha z/2}U(z,T)$$

Differentiation and substitution yields;

$$-i\frac{\alpha}{2}U+i\frac{\partial U}{\partial z}-\frac{\beta_2}{2}\frac{\partial^2 U}{\partial T^2}+\gamma P_0 e^{-\alpha z}|U|^2U=-i\frac{\alpha}{2}U \tag{2.40}$$

From this equation, we can clearly identify the terms responsible for dispersion (second time derivative), loss (loss coefficient of the field) and nonlinearity (nonlinear term). The terms in the loss will cancel, leaving only dispersion and nonlinearity. This equation is unsolvable, generally. However, if we set the dispersion $\beta_2=0$, we can use a second ansatz ($U=Ve^{i\phi_{NL}}$) to fully solve equation (2.40). The term in the exponent, ϕ_{NL} , is responsible for phase shift. The V is responsible for the amplitude of the field. This gives the equation (setting $p(z)=e^{-\alpha z}$);

$$i\frac{\partial V}{\partial z}-V\frac{\partial \phi_{NL}}{\partial z}+\gamma P_0 p(z)|V|^2V=0 \tag{2.41}$$

Matching the real and imaginary parts on both sides and we obtain;

$$\frac{\partial V}{\partial z} = 0 \tag{2.42}$$

$$\frac{\partial \phi_{NL}}{\partial z} = \gamma P_0 p(z)|V|^2 \tag{2.43}$$

This provides a system of equations from which to work in order to find the final solution of 2.40. Equation 2.42 tells us that amplitude V is constant with respect to z. This is expected from the initial assumption about zero dispersion as we want that phase to modulate the pulse. Using the fact that V is constant with respect to z, we can then say;

$$\phi_{NL} = \int_0^L \frac{e^{-\alpha z}}{L_{Nl}} V^2 dz = \frac{V^2}{L_{NL}} \int_0^L e^{-\alpha z} dz = \frac{V^2}{L_{NL}} L_{eff} \tag{2.44}$$

Where

$$L_{eff} = \frac{1 - e^{-\alpha L}}{\alpha}$$

We know that V is a constant amplitude. So we can say that ϕ_{NL} is calculated from;

$$\phi_{NL} = |U(0,T)|^2 \frac{L_{eff}}{L_{NL}}$$

So the solution of equation 2.40 is given by;

$$U(z,T) = |U(0,T)|^2 e^{i\phi_{NL}(z,T)} \tag{2.45}$$

This solution tells us the SPM imposes an intensity dependent phase shift on the pulse, but doesn't influence pulse shape. The spectral dependence induced by SPM are a direct consequence of the time dependence of ϕ_{NL}.

2.5 XPM Solution of GNLS

As already reviewed in Chapter 1, XPM is known as a multichannel effect which entails the modulation of the phase of adjacent pulses from the intensity field of another pulse. This

results in timing jitter due to the associated chirp being converted into timing shifts through fibre dispersion. Again, we start with the GNLS equation (2.10);

$$i\frac{\partial A}{\partial z}-\frac{\beta_2}{2}\frac{\partial^2 A}{\partial T^2}+\gamma|A|^2A=-i\frac{\alpha}{2}A$$

Following on from our analysis of SPM limited pulse evolution, our ansatz considers the evolution of two pulses at two frequency seperations Ω_1 and Ω_2 from the centre channel.

$$A(z,T)=A_1(z,T)e^{-i\Omega_1 T}+A_2(z,T)e^{-i\Omega_2 T} \tag{2.46}$$

Upon substitution, we match terms beating at frequencies Ω_1 and Ω_2 whilst neglecting the terms beating at frequencies of $\Omega_1-2\Omega_2$ and $\Omega_2-2\Omega_1$ as we don't want to consider FWM. We obtain the coupled system of nonlinear PDE's;

$$\frac{\partial A_1}{\partial z}+\Omega_1\beta_2\frac{\partial A_1}{\partial t}+i\frac{\beta_2}{2}\frac{\partial^2 A_1}{\partial t^2}=i\gamma(|A_1|^2+2|A_2|^2)A_1+\frac{i}{2}\beta_2\Omega_1^2A_1 \tag{2.47}$$

$$\frac{\partial A_2}{\partial z}+\Omega_2\beta_2\frac{\partial A_2}{\partial t}+i\frac{\beta_2}{2}\frac{\partial^2 A_2}{\partial t^2}=i\gamma(|A_2|^2+2|A_1|^2)A_2+\frac{i}{2}\beta_2\Omega_2^2A_2 \tag{2.48}$$

We have derived two equations (2.47 & 2.48) for the amplitude envelope of two co-propagating optical pulses. If we study the nonlinear terms on the right-hand side, then we can identify the terms responsible for SPM and XPM. The terms beating in only one field envelope contribute to SPM ($i\gamma|A_1|^2A_1$) and the terms beating in two field envelopes contribute to XPM ($2i\gamma|A_2|^2A_1$). It is clear that XPM is a multi-channel analogy of SPM and has twice the impact (hence the factor of two) on the nonlinear behaviour of the pulse. These equations cannot be solved in general as their propagation regimes are too complicated for conventional analytical methods, this leads us naturally to our numerical algorithm which will be used for the remainder of the thesis.

2.6 Split-Step Fourier Method

The special cases mentioned are limited in their scope due to the particular conditions under which they are solved, we need to explore the method of solution of 2.10 for any case given we will be concerned with transmission configurations comprising several fibre types and other devices such as amplifiers and filters. These devices impose separate conditions upon the pertinent optical pulses. We are required to solve the GNLS in order to understand various impairments occurring during signal transmission. However, the solution when both dispersion and nonlinearity are at play is not available using classical methods. For this reason, we use the Split-Step Fourier Method (SSFM) [23]. This method is identified as the best [23] amongst many [81-84] .We first state the version of the equation in which we are so interested;

$$i\frac{\partial A}{\partial z} = -\frac{i\alpha}{2}A + \frac{\beta_2}{2}\frac{\partial^2 A}{\partial T^2} - \gamma|A|^2 A \tag{2.49}$$

This equation can be expressed as:

$$\frac{\partial A(z,t)}{\partial z} = (\hat{L} + \hat{N})A(z,t) \tag{2.50}$$

Where the linear operator, L and nonlinear operator, N are defined below

$$\hat{L} = -\frac{\alpha}{2} - \frac{j}{2}\beta_2\frac{\partial^2}{\partial t^2} \tag{2.51}$$

$$\hat{N} = j\gamma|A(z,t)|^2 \tag{2.52}$$

When the electric field envelope, A(z,t), has propagated from z to Δz, the analytical solution of 2.49 will have a form of;

$$A(z+\Delta z,t) = e^{(\Delta z(\hat{L}+\hat{N}))}A(z,t) \tag{2.53}$$

The main assumption of the SSFM is the commutation of the operators L and N, using this we can expand 2.53 to give;

$$A(z+\Delta z,t) \approx e^{\Delta z\hat{L}} e^{\Delta z\hat{N}} A(z,t) \tag{2.54}$$

This would suggest that A(z+δz,t) can be estimated by applying the two operators independently. If δz represents only a small increment in z, then 2.54 provides a good approximation to the analytical result [23]. We now use the case of perfect dispersion management to test the algorithm we have proposed.

Test Case: Loss-Managed Transmission

We propagate pulses with a launch peak power of 2 mW along a 200 km section of SMF with loss-management due to EDFA's. The fibre parameter are identical to those given in Table 2.1 but we neglect dispersion. If a pulse is propagated along an optical fibre with attenuation α with initial pulse peak power P_0, then the peak power after propagation over z km is given by;

$$P(z) = P_0 e^{-\alpha z}$$

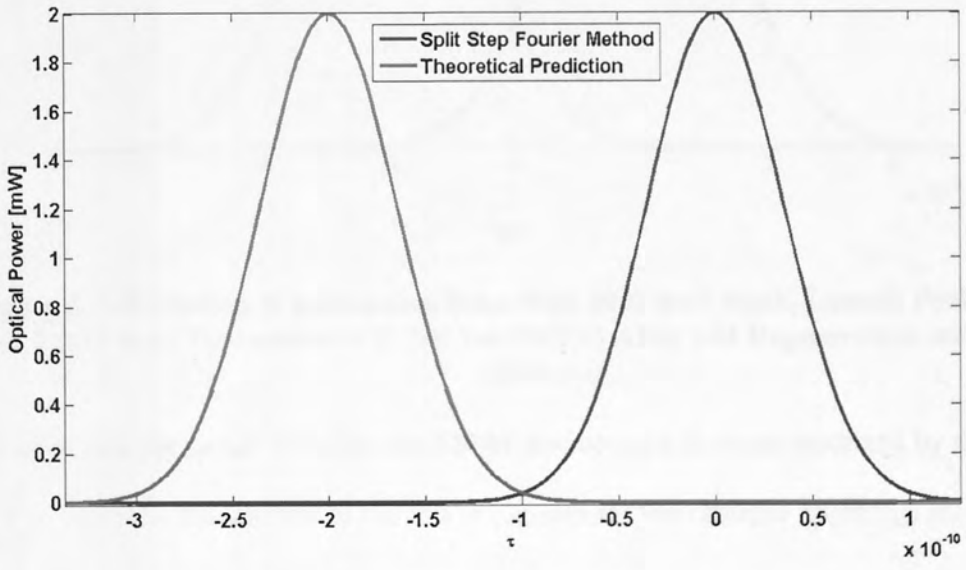

a)

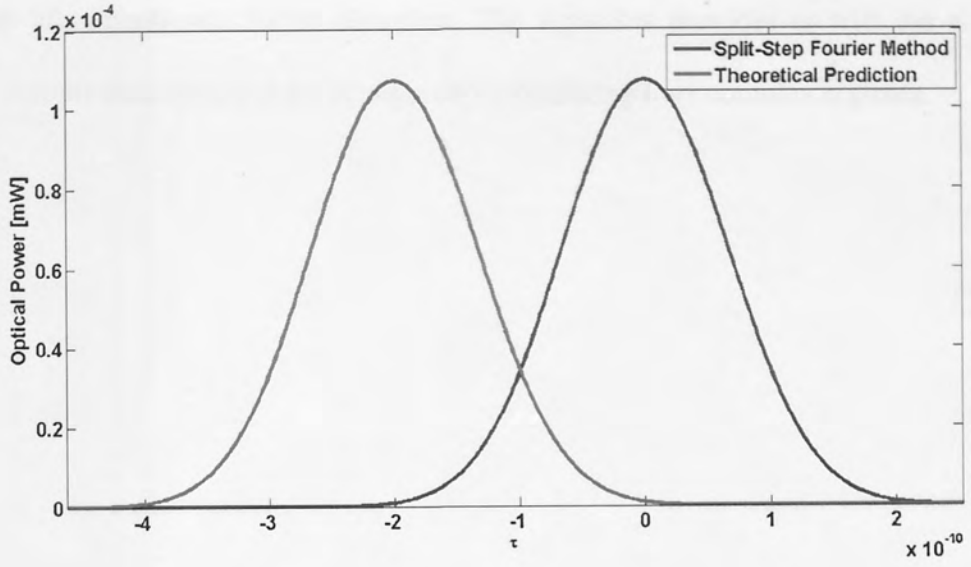

b)

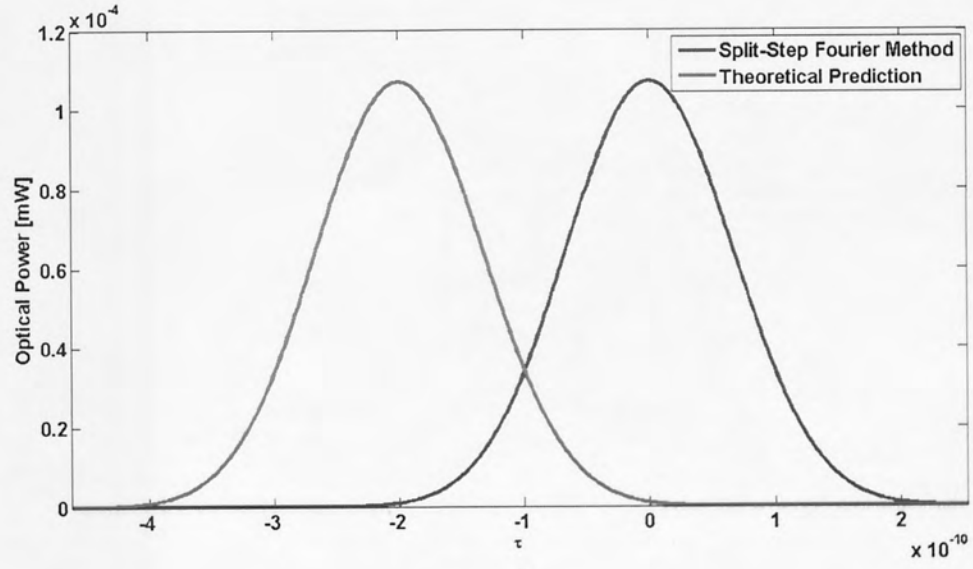

c)

Figure 2.3: Evolution of a Gaussian Pulse with 50% duty cycle, Launch Peak Power of 2 mW at a) Transmission b) 200 km SMF c) After 1-R Regeneration using an EDFA.

We see from that the pulses given by the SSFM are identical to those predicted by the theory given. This confirms the validity of the SSFM algorithim. We can now apply this algorithm to the study of realistic optical transmission configurations.

In the next chapter, we analyse the potential for upgrading legacy undersea transmission links using the aforementioned SSFM algorithm. The algorithm provides us with the platform to analyse complicated optical fibre configurations operating over complex regimes.

Chapter 3 Performance Analysis of Non-Slope Matched RZ-DPSK Undersea Transmission Systems

3.1 Review

The application of differential phase-shift keying (DPSK) [58, 61, 85] - a format shown to have about 3-dB improved receiver sensitivity and enhanced tolerance to nonlinear impairments over ASK [58] - to legacy undersea systems using the conventional non-slope matched DSFs has already been demonstrated at both 10 Gbit/s [86] and 40 Gbit/s [87] [88]. However, recently a side-by-side comparison of 10 Gb/s and 40 Gb/s return-to-zero (RZ) DPSK using the same nominal spectral efficiency over transoceanic distances showed a lower net bit-error rate (BER) for 40 Gbit/s [89].

Most recently, 20 Gbit/s RZ-DPSK was indicated as a strong candidate for upgrading non-slope matched undersea transmission links [50], by offering the potential for similar performance as 10 Gbit/s RZ-ASK at twice the spectral efficiency, and higher performance than 40 Gbit/s RZ-DPSK at the same spectral efficiency. The upgrade to 40 Gb/s transmission is considered to be infeasible at this moment due to the requirement for inline compensation of PMD and intra-channel nonlinearity [50].

In this section, we consider two systems of the proposed type; the first system is a 7-channel WDM configuration using NZ-DSF and SMF sections. Such a fibre map is typical of an undersea configuration as it allows simple dispersion management and substantive minimisation of the nonlinear length L_N[32].

The second system is a 5-channel WDM configuration using a mixture of fibres including the aforementioned mixture of NZ-DSF sections and SMF sections. The other fibre sections will comprise short sections of Large Effective Area Fibre (LEAF) and True-Wave Fibre (TWF). LEAF is useful for us in the sense it enjoys a larger effective core area than NZ-DSF fibre, allowing the introduction of increased nonlinearity management, which is useful when introducing quasi-linear transmission. However, when considering the full C-band (1525 nm to 1565 nm), the net dispersion of LEAF has a higher curvature than that of NZ-DSF, meaning that appropriate dispersion management is needed to ensure that slope dependence across the WDM band becomes a problem. True-Wave Fibre was designed specifically for undersea systems to introduce reduced slope behaviour in order to help compensate for the increased slope involved due to the introduction of LEAF whilst offering similar performance in respect to nonlinearity

3.2 Performance of a 7-channel Non-Slope Matched RZ-DPSK Undersea Transmission Link at 20 Gb/s

Our first system emulates the fibre map of a practical, legacy undersea transmission link. The study of a single-channel embodiment [65] found that the 33% duty cycle pulses performed at a superior level to both 20% duty cycle and 50% duty cycle pulses. It was also shown for the widest duty cycle that large flexibility in both pulse power and pre-compensation dispersion, although Q-factor is slightly lower. Our aim is to expand this study to that of a full 7 channel WDM embodiment, in order to make recommendations about the upgrade of legacy undersea transmission systems and the estimation of BER for systems of this type.

System Description

The transmission link used in our analysis is depicted in Figure 3.1. It emulates a typical non-slope matched undersea type link [32] and resembles a real system currently installed on a transatlantic setup. The unit cell of the system comprises nine sections of NZ-DSF, followed

by a section of standard SMF. We use the SSFM to simulate such a transmission links as we aim to realise the natural behaviour of the link as a realistic fibre configuration.

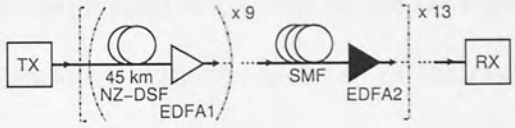

Figure 3.1 Setup of the Transmission Link

The values of D, α and A_{eff} are given at 1550 nm in Table 3.1. The nonlinear Kerr coefficient is 2.35×10^{-20} m^2/W. The residual path-averaged dispersion of the line at 1550 nm is zero, the average dispersion of the outermost channel is shown in Figure 3.2.

	D[ps/nm km]	S[ps/nm^2]	A[dB/km]	A_{eff}[μm^2]	L[km]
NZ-DSF	-3	0.09	0.2	54	45
SMF	16	0.057	0.2	80	78

Table 3.1: Fibre Parameters

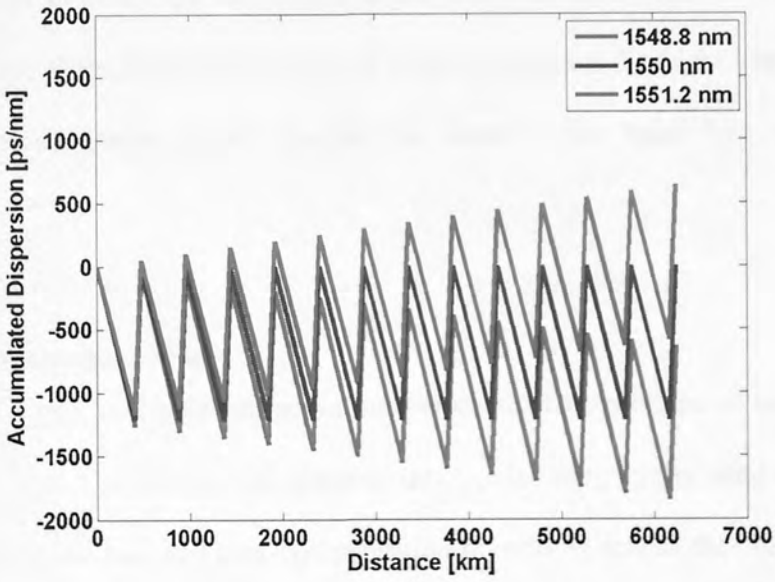

Figure 3.2: Accumulated Dispersion at Channels 1 (1548.8 nm) Channel 4 (1550 nm) and Channel 7 (1551.2 nm)

Erbium-doped fibre amplifiers (EDFAs) with a noise figure of 4.5dB are used at the end of each fibre section to compensate for the energy losses in the fibres. The amplifier spacing is 45 km for the NZ-DSF part of the unit cell and 75 km for the SMF part of the unit cell, this is typical for an undersea configuration [32]. The unit cell of the system is repeated thirteen times to yield a total transmission length of approximately 6300 km. Seven wavelength 20 Gbit/s RZ-DPSK data channels symmetrically distributed around 1550 nm and with a spacing of 50 GHz (0.4 nm) are transmitted over the line. Each channel is modelled by a pseudo-random bit sequence (PRBS) formed with Gaussian pulses. The input pulses have the duty cycles of 20%, 33% and 50%, which enables us to realise 3 distinct propagation regimes.

Signal multiplexing is accomplished by use of a Gaussian optical bandpass filter (OBPF). At the receiver, the signal is filtered using an OBPF/demultiplexer (DEMUX) identical to the multiplexer (MUX), detected using a balanced Mach-Zehnder delay interferometer, and then filtered electrically by a fourth-order Butterworth filter with a cut-off frequency equal to the bit rate. Usually, the electrical filter bandwidth would be some fraction of the bit-rate (~70%), however we wish to study the worst case scenario in this work and we push the allowable boundaries on the filter bandwidth, this will help to generate the noise required in order to generate the transmission errors needed to observe the behaviour of the installed configuration.

Pre-/Post-Compensation Map

We optimize the pre- and post-compensation per-channel dispersions of the system and the launch average signal power for the different input pulse duty cycles used in this work. It is imperative to optimise pre- and post-compensation in order to realise the optimal performance due to the dispersion slope of the fibres involved. We use the electrical Q-factor (Q_{el}),

calculated at the end of the unit cell of the link, as an indicator of system performance. The Q-factor is averaged over 10 1024-bit pattern runs.

The 3-dB bandwidth of the MUX/DEMUX is optimized for each duty cycle through back-to-back simulations. Figure 3.6 shows contour-plots of the Q_{el}^2-factor of the weakest channel at the output of the transmission link in the plane pre-compensation dispersion (D_{pre}, given at 1550 nm) – launch average power per channel. Here, the post-compensation dispersion, D_{post}, is selected such that $D_{post} = -D_{pre} + \delta D$ (at zero line average dispersion), i.e. fine tuning of the 50/50 pre/post-compensation ratio is performed by addition of a dispersion amount δD.

The results are shown at the optimum δD and for the weakest channel in this configuration, which turns out to fall around 50 ps/nm for the 20% and 33% duty cycles, and around 300 ps/nm for the widest duty cycle (see Figure 3.7). It can be seen that the optimum pre-compensation and average power vary from approximately (400 ps/nm, -2.4 dBm) for the 20% duty cycle, to approximately (700 ps, -4.5 dBm) for the 33% duty cycle, and to (700 ps/nm, -6.2 dBm) for the 50% duty cycle, while there are sufficiently large power margins within the dispersion range 300 ps/nm to 1000 ps/nm for all duty cycles. Comparison with values obtained from the optimisation of the single channel configuration confirm that this system is limited by intra-channel effects [65]. This implies that we are dealing with quasi-linear transmission [35].

The values of power obtained here are counter-intuitive in the sense that we use higher peak power for narrower duty cycles. However, when we normalise the optical power with respect to the peak power for each pulse, we see that the situation is reversed, It is also observed that narrower pulses than the conventional 50% duty-cycle pulses offer superior performance in terms of higher Q-values, as it is observed in the case of single-channel transmission [65].

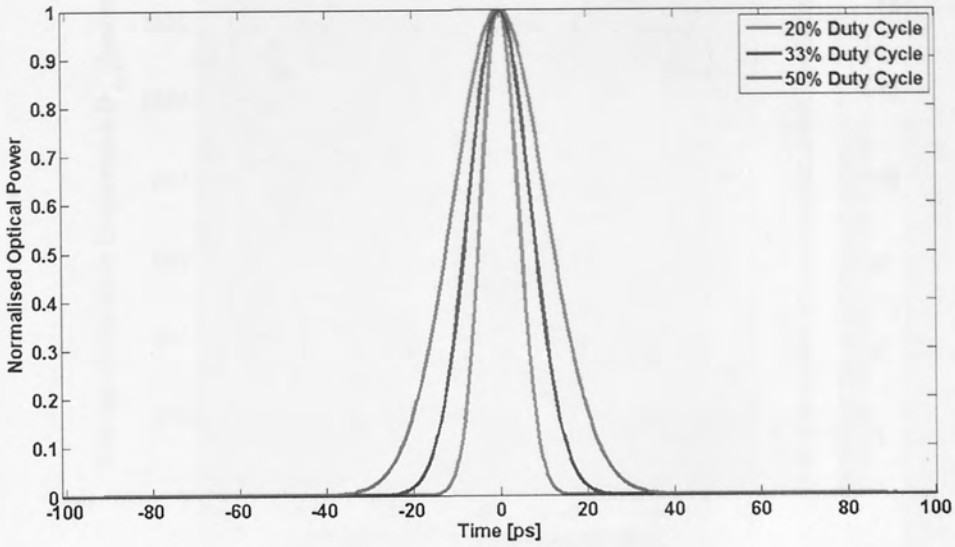

Figure 3.3: Normalised Optical Power at Optimal Values for each duty cycle.

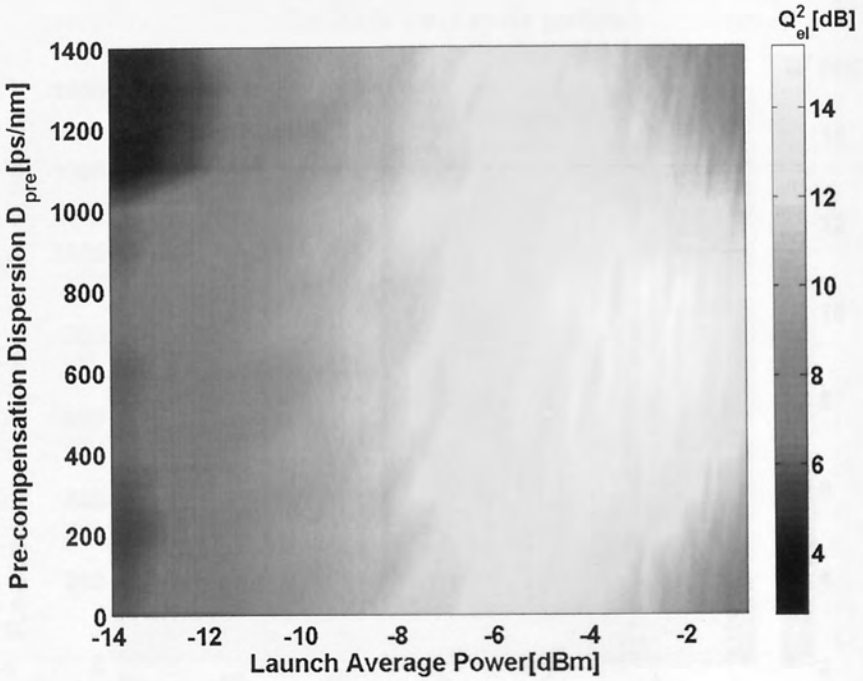

Figure 3.4: Electrical Q^2-factor versus launch average power per channel and pre-compensation dispersion for 50 Ghz spaced 20 Gb/s WDM RZ-DPSK Transmission at 20% duty cycle pulses

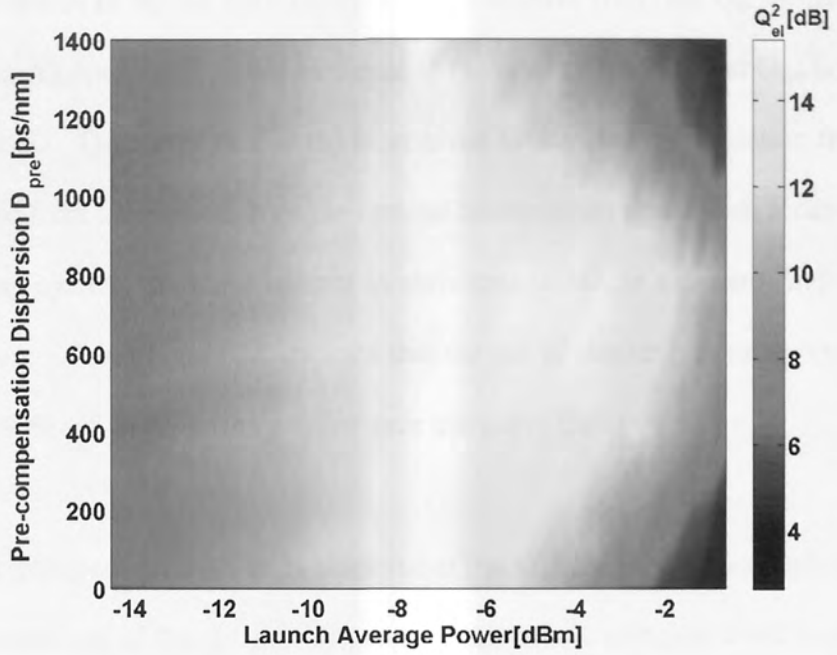

Figure 3.5: Electrical Q^2-factor versus launch average power per channel and pre-compensation dispersion for 50 Ghz spaced 20 Gb/s WDM RZ-DPSK Transmission for 33% duty cycle pulses.

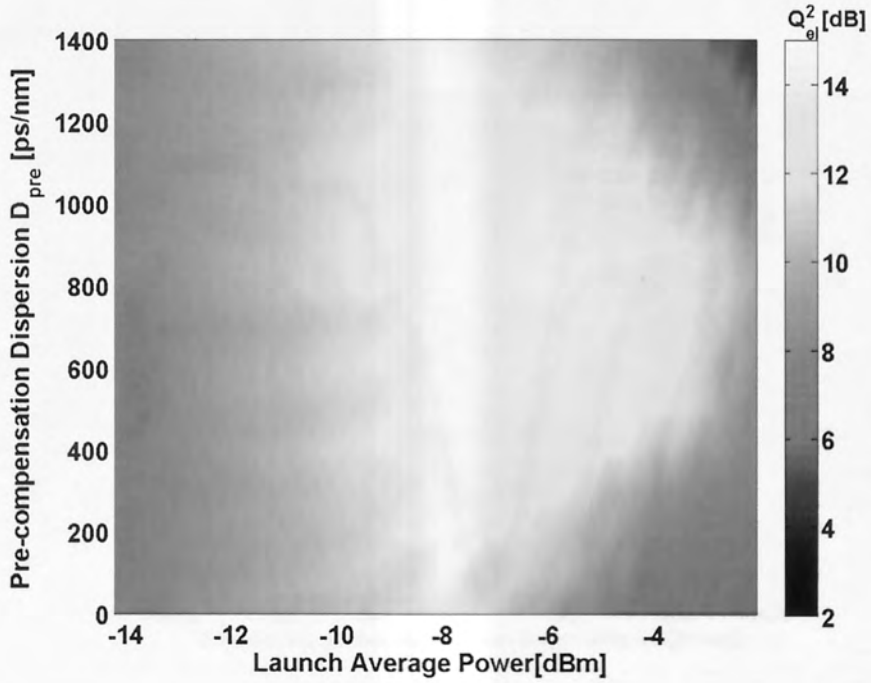

Figure 3.6 Electrical Q^2-factor versus launch average power per channel and pre-compensation dispersion for 50 Ghz spaced 20 Gb/s WDM RZ-DPSK Transmission for 50% duty cycle pulses

The tolerance of the system performance to deviations of the fine-tuning post-compensation dispersion δD from its optimal value is illustrated in Figure 3.7, which shows the Q^2-factor

penalty as a function of δD for the three duty cycles studied. Here, the Q_{el}^2-penalty is defined as 20 $\log_{10}$ (Q_{opt}/Q_{el}),where Q_{el} is the electrical Q-factor at a given δD and Q_{opt} is the Q-factor at the optimal δD. Q-penalty here is the term given to describe the deviation from Q-factor that is obtained from a deviation from the optimal transmission conditions. It can be seen that the largest duty cycle is the most tolerant to variations in δD, as expected [23]. Overall, the results of Figure 3.6 and Figure 3.7 indicate that the use of shorter pulse duty cycles than the conventional 50% can improve the performance margin of the system.

This gain in performance, however, is achieved at the expense of a reduced tolerance against variations/fluctuations of the net link dispersion and, hence, stringent conditions need to be imposed on the post-compensation of chromatic dispersion to realise the performance improvement. Selection of the duty cycle should therefore be performed in accordance with availability of tuneable dispersion post-compensating devices.

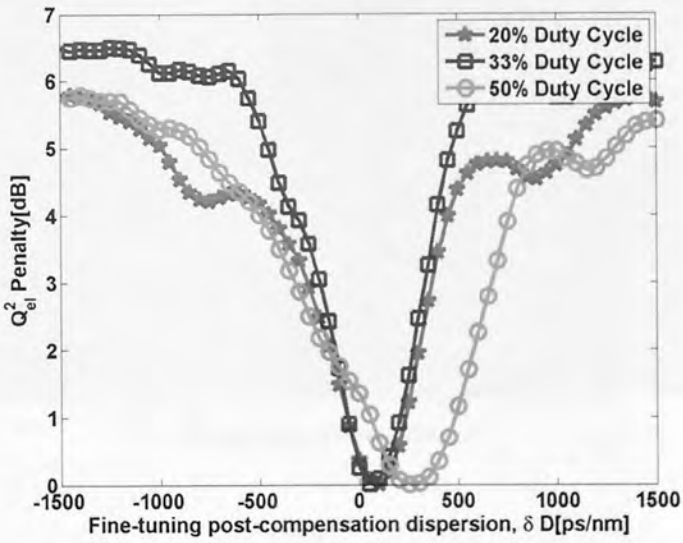

Figure 3.7: Q_{el}^2-factor penalty of deviation from optimal fine-tuning post-compensation dispersion

The difference for the 50% duty cycle pulses is clear, this is simply due to our results being based on the weakest channel. In the narrower duty cycles, the weakest channel is observed to be channel 4 (1550 nm), whilst for the 50% duty cycle the weakest channel is at channel 5

(1550.4 nm). The difference in the optimal fine-tuning can be attributed to the additional sloping effects than can be observed.

We can see in Figure 3.8 that there is approximately a 3-dB loss as a result of increasing the bit-rate to 20 Gb/s, this is as a result of doubling the bandwidth to achieve the higher bit-rate. We observe this at the 50% duty cycle and would anticipate that it is the case for both duty cycles. However, through exploration of other duty cycles we can expect to increase Q-factor further by comparison to the 50% duty cycle configuration.

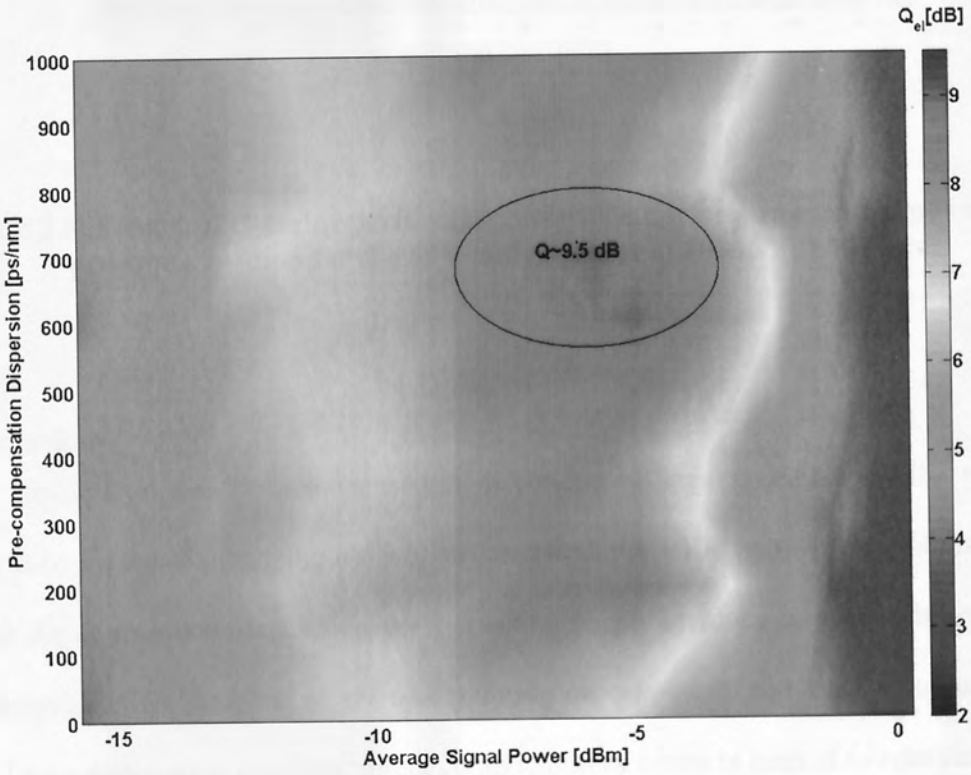

a)

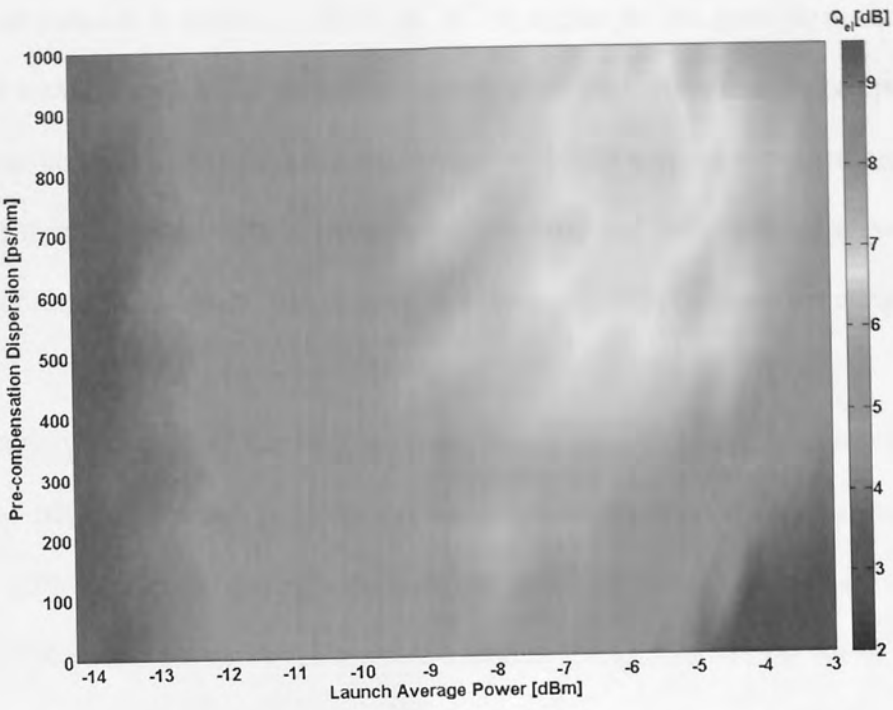

b)

Figure 3.8: Electrical Q-factor performance versus launch average signal power and pre-compensation for the 50% duty cycle at a) 10 Gb/s b) 20 Gb/s

Bit Error Rate

Using the optimal pre-/post-compensation dispersion settings suggested by the results in Figure 3.6, Figure 3.5 and Figure 3.6, we assessed the BER performance of the system through direct error counting. Direct error counting simply involves comparing bit-patterns at the transmission and receiver stages and counting the number of bits that are transmitted in error. Using direct error counting, direct computation of errors is limited to reliable BERs of 10^{-5} or higher, but the precision is 100%. The practical limitations are perfectly evident, but for simulation purposes the benefits are obvious and using direct counting we can evaluate the precision of models both proposed in the literature [67, 72] and newly proposed models which we will explore in Chapter 5.

Direct computation is limited to BERs of 10^{-5} or higher so that good error statistics can be obtained within a reasonable amount of computation time. Note that this corresponds to an acceptable error level before FEC. Sequences of 16384 bits were transmitted over larger distances than the total length of the transmission link, and the results were averaged over a number of runs. In our modelling, we compute the signal BER by direct counting of errors.

An exemplary variation of the BER with the launch average power is shown in Figure 3.9, where the BER is recorded at 11500 km transmission distance. It appears from Figure 3.9 that the 33% duty cycle outperforms both the 20% and 50% duty cycles by offering the highest BER margin as well as substantial tolerance to variations in the signal power. It can also be noted that the optimal launch power and pre-compensation combination suggested by the Q-factor estimates of Figure 3.7 is not necessarily adhered to when the actual BER is computed. We can highlight from Figure 3.9 that we have achieved a BER of 10^{-5} for the 33% duty cycle at 11500 km, this is a strong result as it suggests that the upgrade is a feasible solution and will offer high levels of performance over large distances without the assistance of FEC or other technologies.

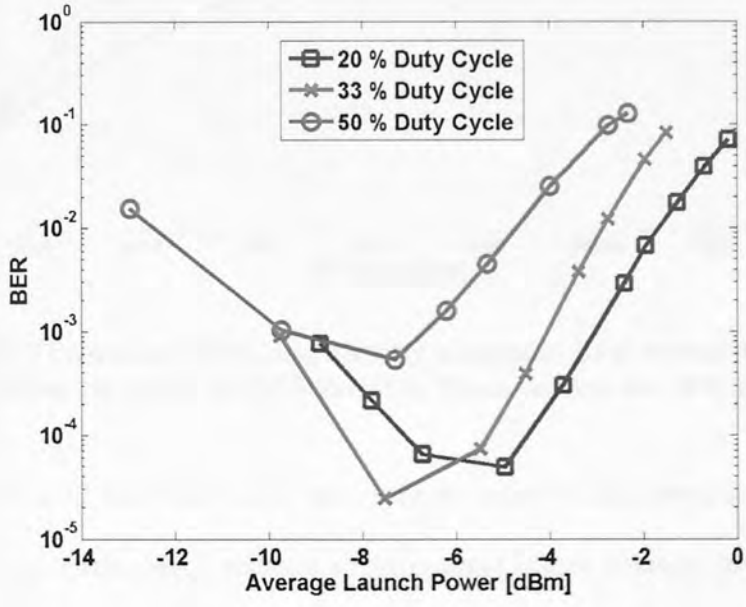

Figure 3.9: BER variation with launch average power per channel at 11500 km transmission distance

Next, we compare the accuracy of the electrical, differential phase, and amplitude Q-factor models versus the directly computed BER. We use here the standard Q-factor of the received electrical signal (Q_{el}) [71], and the Q-factors defined for the optical (differential) phase ($Q_{\Delta\varphi}$) and the field amplitude before demodulation (Q_A) of the signal, which were introduced in [67] to estimate the BER in a DPSK channel in the nonlinear and linear regimes, respectively. These Q-factor models and their related BER estimation formulae are explored in Chapter 1.

The BER is estimated from Q_{el}, $Q_{\Delta\varphi}$ and Q_A using the expressions: BER (Q_{el}) = (1/2) erfc ($Q_{el}/\sqrt{2}$), BER ($Q_{\Delta\varphi}$) = erfc ($Q_{\Delta\varphi}/\sqrt{2}$) and BER ($Q_A$) = (1/2) exp ($-Q^2_A/2$) [72], which are calculated using the Gaussian approximation of the intensity noise, the field amplitude noise and the noise at the centre of each rail of the differential phase eye diagram, respectively.

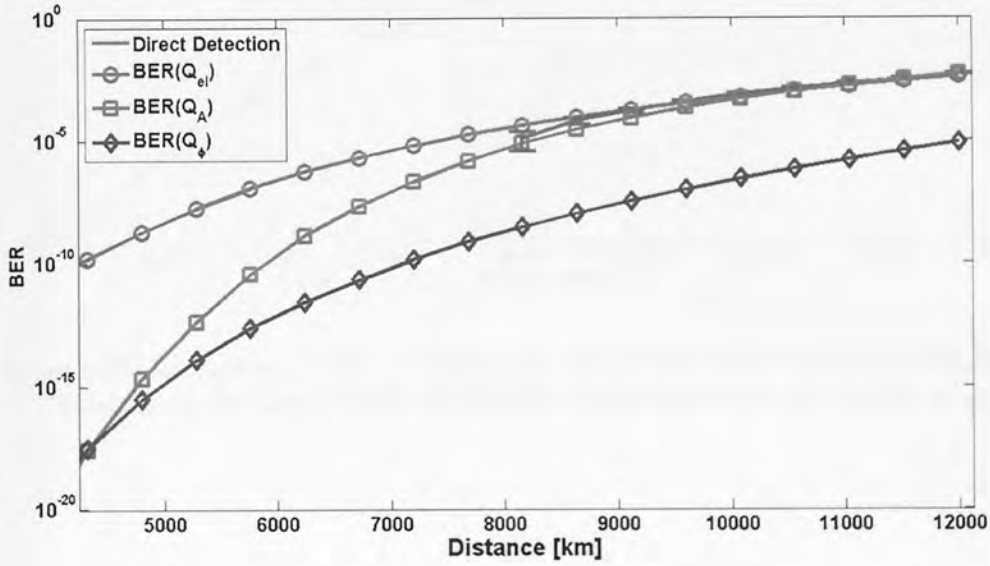

Figure 3.10: Theoretical BERs and directly computed BER versus distance for 50 GHz-spaced 20 Gbit/s WDM RZ-DPSK Transmission for 20% duty cycle.

Figure 3.10, Figure 3.11 and Figure 3.12 shows the evolution of the theoretical BERs and the actual BER over the transmission distance at the optimal launch average power given by the results derived previously (Figure 3.4, Figure 3.5 and Figure 3.6). It can be seen that for all

duty cycles Q_A and Q_{el} compete with one another at yielding the most reliable estimate of the actual BER, and the predictions based on these Q-factor models are more accurate at large distances. On the other hand, $Q_{\Delta\varphi}$ significantly underestimates the actual BER. We also show the relative error within the statistics It is shown, particularly at the two narrowest duty cycles, that the estimates are even valid within the order of the statistical error. The 50% duty cycle is somewhat different to the others in that the two most effective estimation methodologies underestimate the BER, but we can say that the difference is less than one order of magnitude, particularly at higher distances

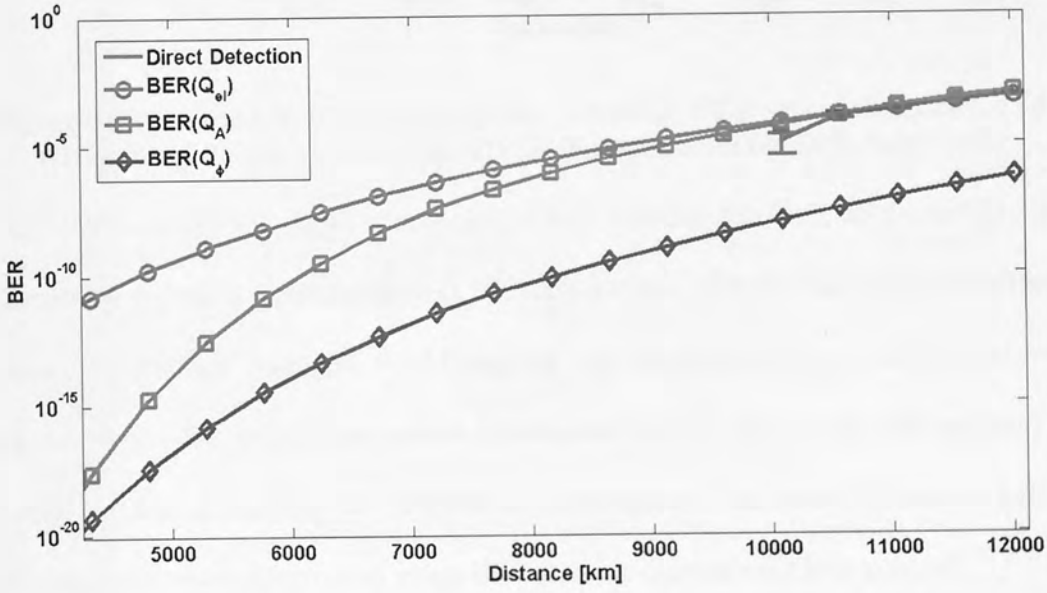

Figure 3.11: Theoretical BERs and directly computed BER versus distance for 50 GHz-spaced 20 Gbit/s WDM RZ-DPSK Transmission for 33% duty cycle.

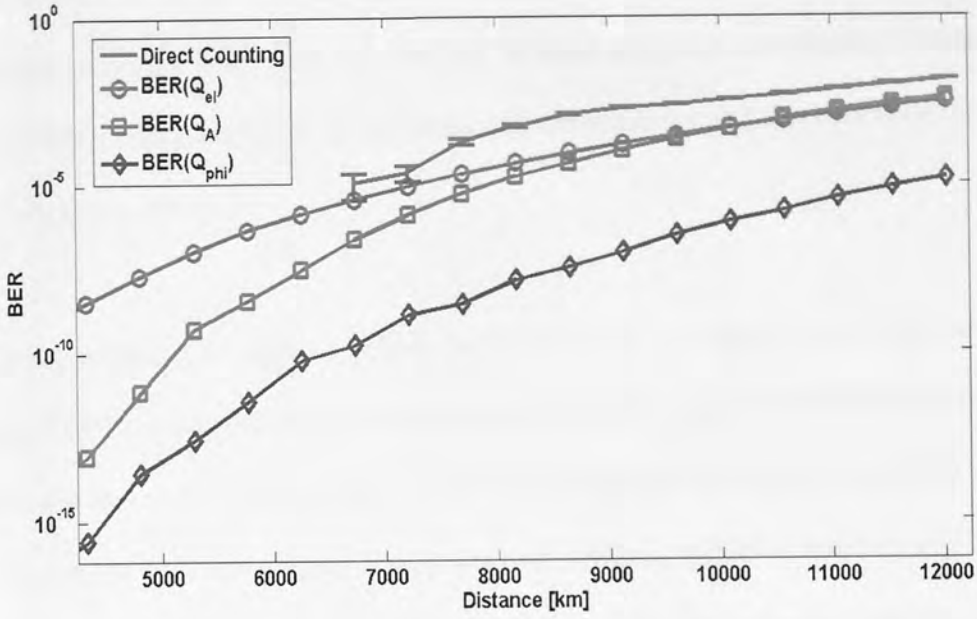

Figure 3.12 Theoretical BERs and directly computed BER versus distance for 50 GHz-spaced 20 Gbit/s WDM RZ-DPSK Transmission for 50% duty cycle.

Generally, electrical current statistics provide the best estimate for BER, so we can say that the transmission regime is quasi-linear [67]. The fact that the conventional electrical Q-factor is a useful performance indicator would suggest that electrical current statistics in such channels are largely Gaussian, assumptions investigated later in this thesis. The accuracy of the Q-factor estimation methods can be better explored through the study of the error bars of the BER data. This would allow us to gauge how accurate our estimate is in general.

It is also seen clearly from Figure 3.9 that the 33% duty cycle pulses achieve the highest BER margin, which confirms the conclusion drawn from Figure 3.5. Indeed, supposing an extension of the directly computed BER curves to the region of short distances with either BER(Q_A) or BER(Q_el) as a reference curve, a BER of 10^{-9} would relate to a transmission distance of approximately 5500 km for the 20% duty cycle, 6500 km for the 33% duty cycle, and 5000km for the widest duty cycle.

Conclusions

In any case, the results for the three duty cycles studied show that error-free 20 Gbit/s RZ-DPSK transmission at 50 GHz channel separation is feasible beyond the design length of typical installed undersea links with no need for in-band slope compensation of chromatic dispersion or PMD, which confirms the experimental observations and theoretical predictions of previous works [50, 65].

Through direct counting of errors, BER performance of a typical non-slope matched transoceanic WDM undersea transmission link using 50-GHz spaced RZ-DPSK at a bit rate of 20 Gbit/s was assessed. The important issue of the impact of the duty cycle of the carrier pulses on the system performance has been addressed. Overall, we have observed that shorter duty cycles (33%) than the conventional 50% improve the performance margins of the system, at the expenses of a reduced tolerance against dispersion variations. This highlighted with the achievement of a BER of 10^{-5} over 11500 km transmission without the aid of FEC or additional compensation of nonlinearity.

PMD is neglected in the numerical code (see Chapter 2), as is justified in the literature [50]. PMD is not seen as a significant threat in systems at this bit-rate. These results indicate that the pulse width can and should be chosen carefully to tune the system performance for RZ-DPSK transmission, in accordance with available channel bandwidth and availability of tuneable dispersion post-compensating devices. The validity of different existing numerical Q-factor approaches to the BER estimation for RZ-DPSK was analysed, with the results indicating that the conventional Q-factor of the received electrical signal and the Q-factor defined for the field amplitude before demodulation compete to one another at offering the most reliable indication of the system performance in the considered range of parameters. The results obtained in this paper confirm and extend further the results of previous work [50, 65]

where 20 Gbit/s RZ-DPSK transmission has been indicated as a feasible technique for the upgrade of existing undersea links.

3.3 5-channel WDM RZ-DPSK Non-Slope Matched Configuration at a Bit-Rate of 21.4 Gb/s

Again, the major goal of this section is to theoretically assess the bit-error rate (BER) performance of a typical non-slope matched transoceanic WDM undersea transmission link using 50-GHz spaced RZ-DPSK at a bit rate of 21.4 Gbit/s (~0.4 bit/(s Hz) spectral efficiency) with different duty cycles of the signal pulses.

A configuration comprising a mixture of fibre sections is employed. Still dominated by NZ-DSF and SMF sections in order to minimise nonlinear interaction length and effectively manage dispersion, we add a section of LEAF and TWF to offer additional nonlinearity management due to the contrasting effective core areas and negative dispersions compared to NZ-DSF.

TWF is a fibre designed to allow transmission at higher powers but restrictive of nonlinear behaviour. It enjoys negative dispersion and large effective area so it removes nonlinear effects due to phase matching such as FWM. It also offers a flat dispersive profile which is a feature that differentiates it from LEAF. LEAF is a fibre designed to have large effective area (reducing nonlinear behaviour) even compare to TWF but it also has a steeper dispersion slope. We will comment at the end of the chapter on the differences this brings to the system.

We also discuss the reliability of different available Q-factor approaches to the BER estimation for the RZ-DPSK format [72], and investigate their accuracy with respect to the different duty cycles by comparing their predictions to the results of direct error counting.

Firstly, we optimize the pre/post compensation map. This allows the study of the operational regimes allowed for the three duty cycles considered 33%, 50% and 67%. We then show the evolution of the BER for increased distances, demonstrating the validity of the three BER estimation methods explored in [72].

System Description

The transmission link used in our analysis is depicted in Figure 3.15. We choose to emulate a non-slope matched undersea type link that is implemented in our experiments as a re-circulating fibre twin-loop. This offers the advantage of high flexibility and allows replication of the dispersion and optical signal-to-noise ratio maps of a typical transoceanic undersea link.

The unit cell comprises nine NZ-DSF sections with negative dispersion. Each of them has a length of 45.7 km and is composed of a mix of large effective core area fibre (LEAF), standard NZ-DSF and reduced slope fibre (True-Wave fibre), followed by a SSMF section of length 73.2 km. The residual path average dispersion of the line at 1550 nm is -0.025 ps/nm. The unit cell of the system is iterated M times in order to realise practical undersea transmission distances The difference between this system and the previous system is the use of sections of TWF and LEAF. The features of these fibres are important in the installation of undersea transmission systems. TWF offers high nonlinearity with an almost constant dispersion, whilst LEAF offers more linear behavior (compared to NZ-DSF) with a high dispersion slope, this is shown in Figure 3.13 & Figure 3.14. Sections of TWF and LEAF with comparable length offer additional nonlinearity management whilst providing some compensation of dispersion slope effects. We can see in Figure 3.14 that within our wavelength configuration the dispersion slope is almost non-existent.

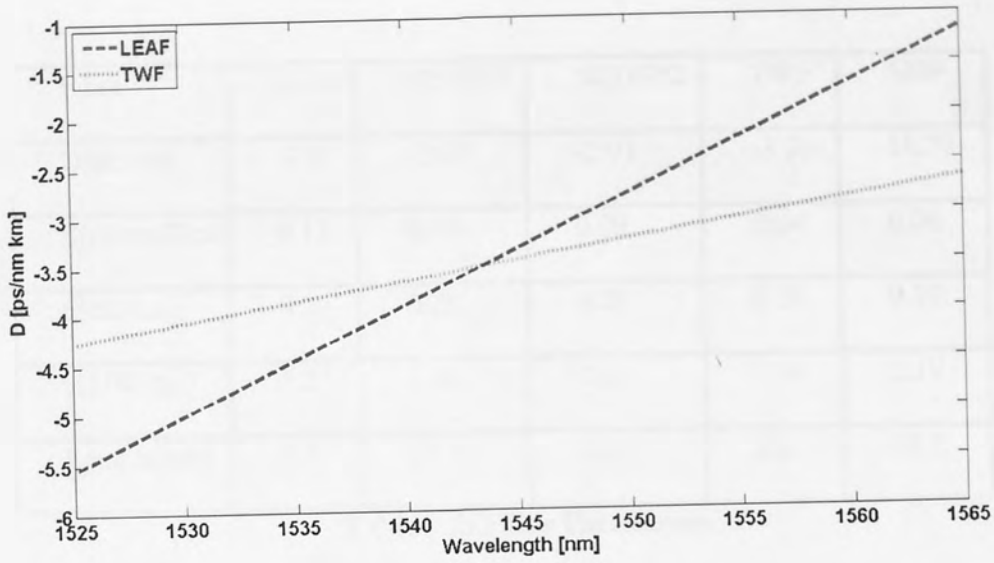

Figure 3.13: Values of Group Velocity Dispersion for LEAF and TWF inside the C-band

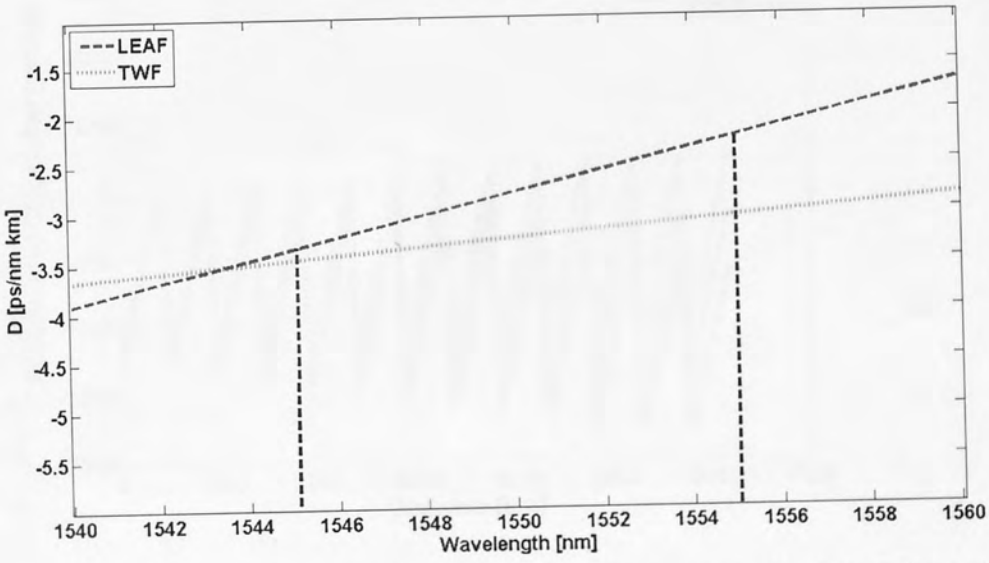

Figure 3.14: Dispersion for TWF and LEAF in the wavelength region of most interest

Figure 3.15 Graphical Depiction of the Fibre Map

Erbium-doped fibre amplifiers (EDFAs) with a noise figure of 4.5 dB are employed to compensate for the losses in both the fibres and the splicing associated with the fibre joins.

Fibre	LEAF	NZDSF1	NZDSF2	TWF	SMF
D[ps/nm]	-2.8	-3.07	-2.91	-3.26	16.79
S[ps/nm2km]	0.11	0.09	0.09	0.04	0.06
α[dB/km]	0.21	0.20	0.21	0.20	0.19
γ[1/W km]	1.27	1.88	1.85	1.99	1.19
Length[km]	5.5	25.1	10.1	5.0	73.2

Table 3.2: Fibre Parameters

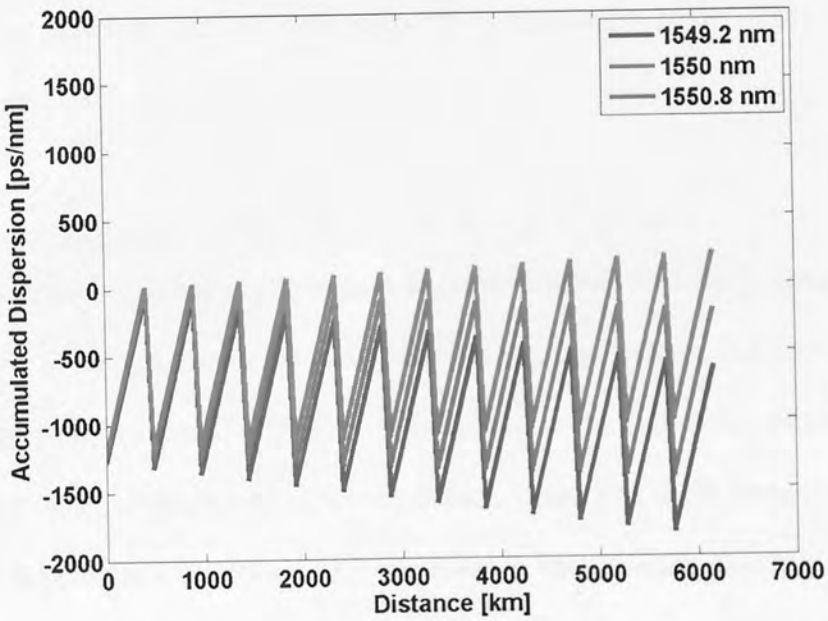

Figure 3.16: Accumulated Dispersion of the Fibre Map at Channel 1 (1549.2 nm) Channel 3 (1550 nm) and Channel 5 (1550.8 nm)

The transmitter is modelled as the concatenation of a distributed feedback laser, a dual-drive Mach-Zehnder modulator-based pulse carver with an extinction ratio of 30 dB, and an ideal phase modulator. Three biasing configurations of the pulse carver are used to create RZ pulses with duty cycles 33%, 50% and 67% at a 21.4 Gb/s bit-rate in accordance with the power transfer function given below

$$T(t) = \left|\frac{u_{out}}{u_{in}}\right|^2 = \frac{1}{4}\left\{1+\gamma^2+2\gamma\cos[\frac{\pi(2V_1\cos(2\pi\varpi t+\theta))-V_b}{V_\pi}]\right\} \qquad (3.1)$$

where the subscripts on the u fields correspond to the input and output fields respectively, V_π is the voltage required to produce a π phase shift, V_b is a constant bias voltage and we define γ, the depth of the modulation, as below;

$$\gamma = \frac{\sqrt{\varepsilon}-1}{\sqrt{\varepsilon}+1} \qquad (3.2)$$

Where ε is the extinction ratio. We consider 5 equally spaced (0.4 nm) channels centred symmetrically upon 1550 nm. The channels are de-multiplexed using a second-order Gaussian optical band-pass filter, detected using a balanced Mach-Zehnder delay interferometer, and then filtered electrically by a third-order Bessel filter with a cut-off frequency equal to the bit-rate.

Pre-/Post-Compensation

The pre- and post-compensation dispersions of the system and the launch signal power for the different input pulse duty cycles are optimised. We use the electrical Q-factor as an indicator of the system performance. The Q-factor is calculated at the end of the unit cell of the link, and averaged over a number of 1024-bit pattern runs. The 3-dB bandwidth of the de-multiplexer is optimized for each duty cycle through back-to-back simulations. Figure 3.19 shows contour-plots of the Q^2-factor of the weakest channel at the output of the transmission link in the plane pre-compensation dispersion (D_{pre}, given at 1550 nm) – launch average power per channel. Here, the post-compensation dispersion, D_{post}, is selected such that $D_{post} = -D_{pre} - D_{ave}L + \delta D$, i.e. fine tuning of the pre/post compensation ratio is performed by addition of a dispersion amount δD in addition to the product $D_{ave}L$. The results are shown at the optimum δD. D_{ave} is the net-link dispersion (-0.025 ps/nm at 1550 nm) and L is the length of one span (484 km).

It can be seen (Figure 3.17, Figure 3.18, Figure 3.19) that the optimum pre-compensation and average power vary from approximately (600 ps/nm, -4.8 dBm) for the 33% duty cycle, to approximately (700 ps, -3.7 dBm) for the 50% duty cycle, and to (700 ps/nm, -3.5 dBm) for the 67% duty cycle, while there are sufficiently large power margins within the dispersion range 400 ps/nm to 900 ps/nm for all duty cycles.

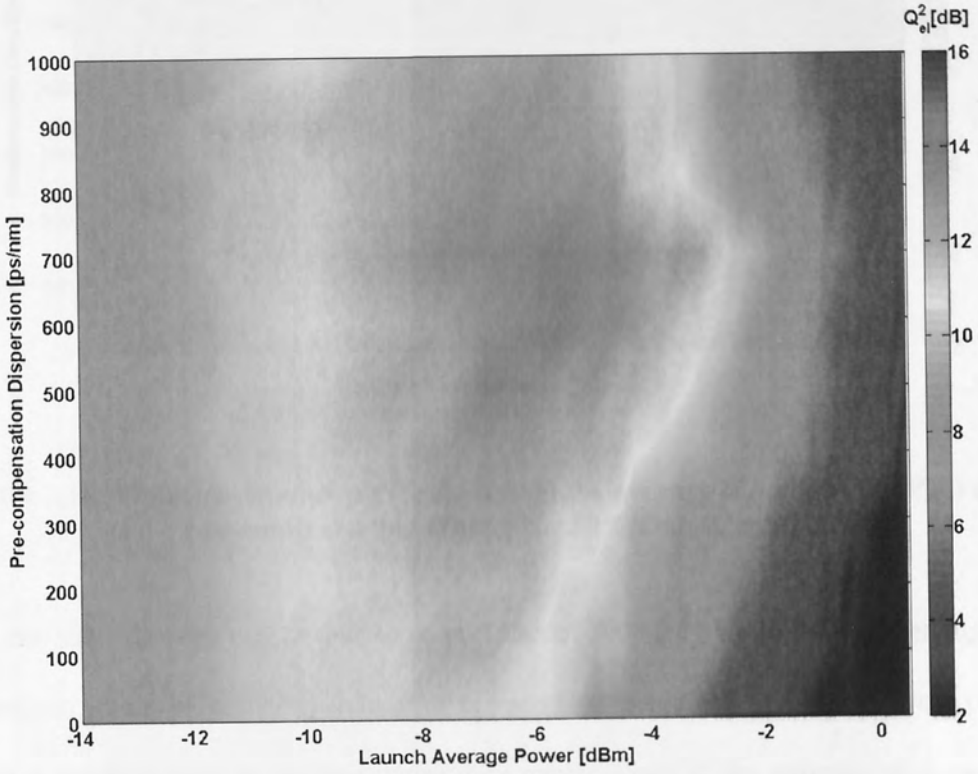

Figure 3.17: Weakest channel performance versus average signal power (P_{ave}) and pre-compensation (Dpre) for 33% Duty Cycle

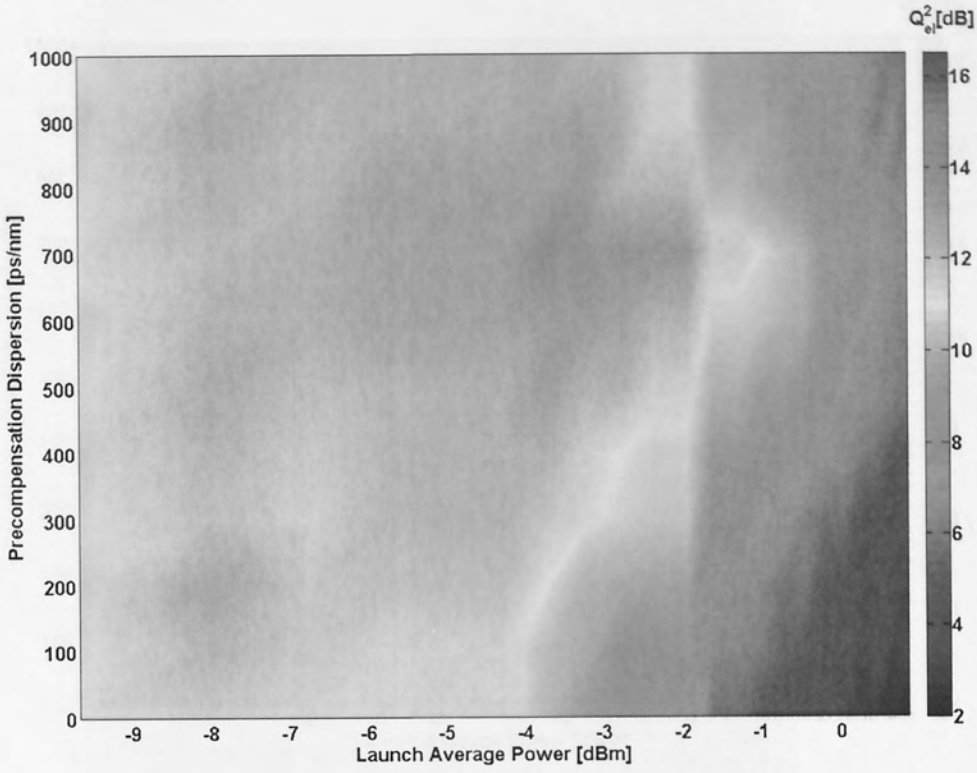

Figure 3.18: Weakest channel performance versus average signal power (P_{ave}) and pre-compensation (Dpre) for 50% Duty Cycle

It is also seen that narrower pulses than the conventional 50% duty-cycle pulses offer superior performance in terms of higher Q-values. It is seen that generally, 33% duty cycle pulses perform at a superior level to the two wider duty cycles albeit at the expense of dispersion tolerance.

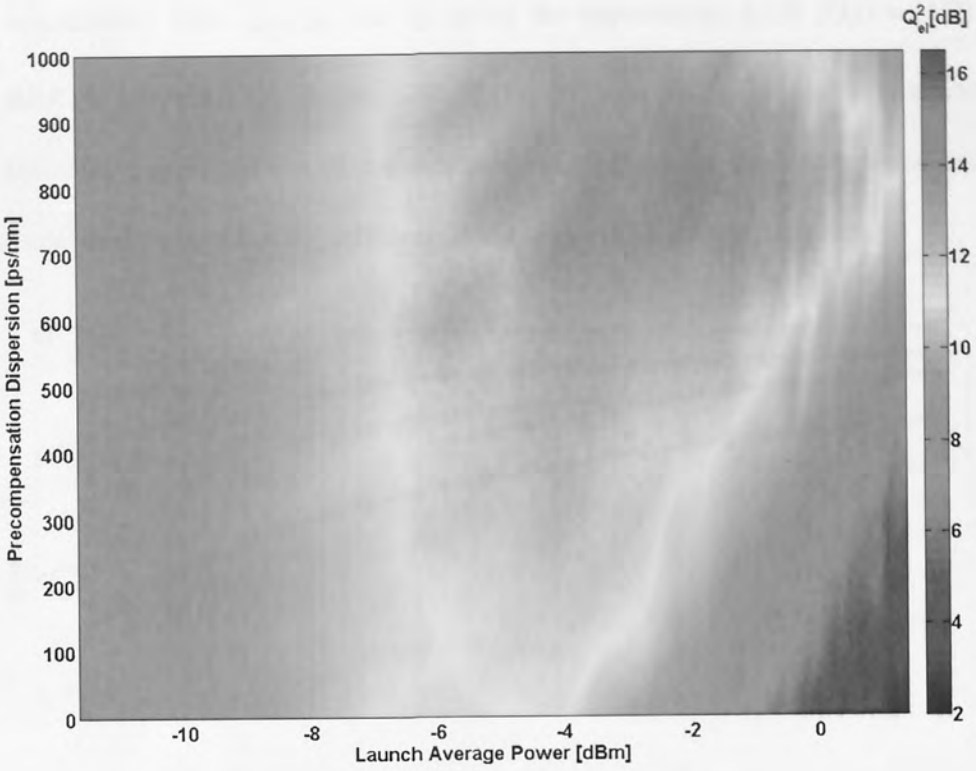

Figure 3.19: Weakest channel performance versus average signal power (P_{ave}) and pre-compensation (D_{pre}) for 67% Duty Cycle

Bit Error Rate

In our modelling, we compute the signal BER by direct counting of errors. We also use BER estimates in terms of the signal Q-factor, which is closely related to the error probability and is a widely used tool to estimate the performance of optical transmission systems because it is relatively easy to evaluate, thus preventing the need for time-consuming direct counting. Again, we use here the standard Q-factor of the received electrical signal (Q_{el}), and the Q-factors defined for the optical (differential) phase (Q_{φ}) and the field amplitude before demodulation (Q_A) of the signal, which were introduced in [67] to estimate the BER in a DPSK channel in the nonlinear and linear regimes, respectively.

The BER is estimated from Q_{el}, Q_{φ} and Q_A using the expressions: BER (Q_{el}) = (1/2) erfc ($Q_{el}/\sqrt{2}$), BER (Q_{φ}) = erfc ($Q_{\varphi}/\sqrt{2}$) and BER (Q_A) = (1/2) exp ($-Q^2_A/2$), which are calculated using the Gaussian approximation of the intensity noise, the field amplitude noise and the noise at the centre of each rail of the differential phase eye diagram, respectively.

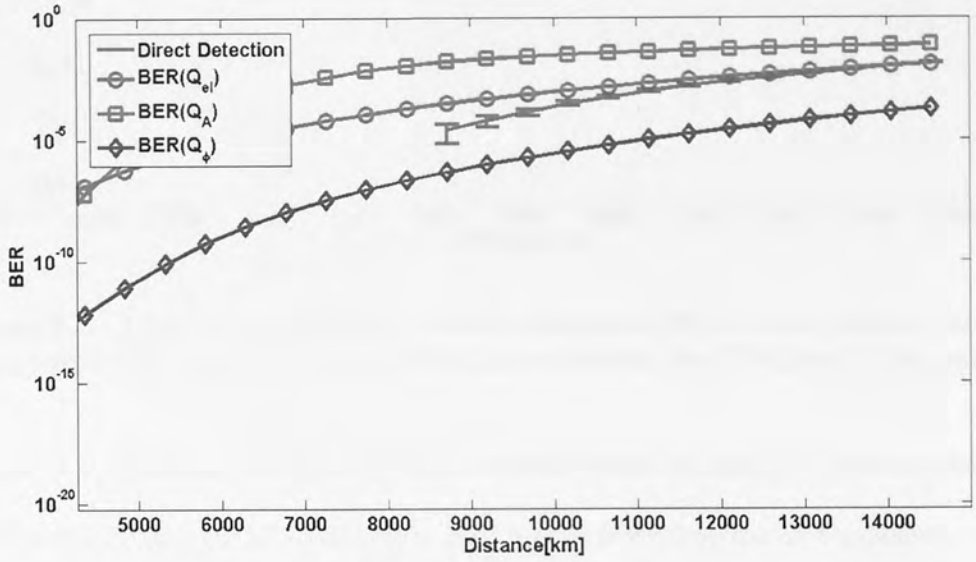

Figure 3.20: Theoretical BERs and directly computed BER versus distance for 50 GHz-spaced 21.4 Gbit/s WDM RZ-DPSK transmission for 33% Duty Cycle pulses.

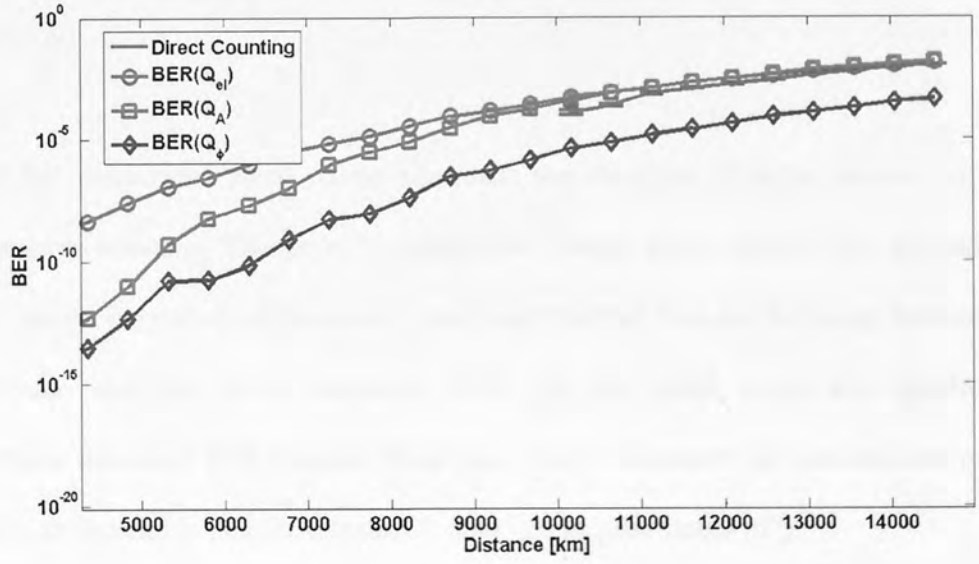

Figure 3.21: Theoretical BERs and directly computed BER versus distance for 50 GHz-spaced 21.4 Gbit/s WDM RZ-DPSK transmission for 50% Duty Cycle pulses

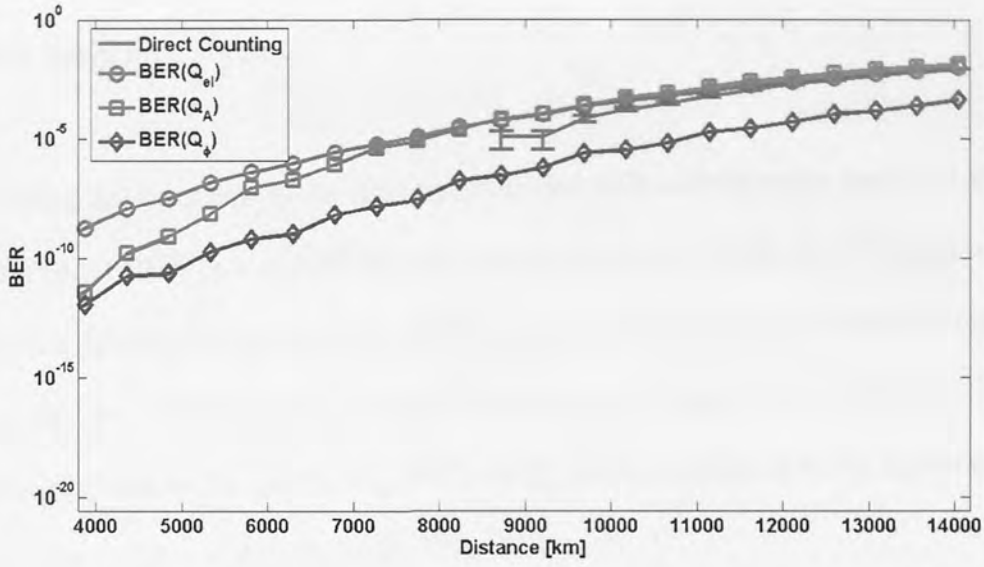

Figure 3.22: Theoretical BERs and directly computed BER versus distance for 50 GHz-spaced 21.4 Gbit/s WDM RZ-DPSK transmission for 67% Duty Cycle pulses.

Comparison of the accuracy of these Q-factor models versus the directly computed BER is given in Figure 3.20, Figure 3.21 and Figure 3.22 for the three duty cycles considered, which shows the evolution of the theoretical BERs and the actual BER over the transmission distance at the optimal launch average power given by the results in Figure 3.17, Figure 3.18 and Figure 3.19.

It is clear that predictions based on the amplitude and electrical Q-factor models are more accurate at large distances. This point is strengthened further when the error bars are included as we see that the magnitude of the error is much smaller than than the difference between the BER estimate and the direct counting BER. On the other hand, Q_φ significantly underestimates the actual BER because phase noise doesn't dominate our transmission regime [67]. This is an indication that the transmission regime is quasi-linear [67].

That the conventional electrical Q-factor is a reliable performance indicator suggests that electrical current statistics in our channels are largely Gaussian. It is also seen clearly from

Figure 3.17 that the 33% duty cycle pulses achieve the highest BER margin, which confirms the conclusion drawn from Figure 3.9.

Indeed, supposing an extension of the directly computed BER curves to the region of short distances with either BER(Q_A) or BER(Q_{el}) as a reference curve, a BER of 10^{-9} would relate to a transmission distance of approximately 4500 km for the 33% duty cycle, 5000 km for the 50% duty cycle, and 5000 km for the widest duty cycle. Again, this is without inline compensation of PMD or the addition of FEC. PMD is not considered to be important in transmission links of this type [50] at the 20 Gb/s bit-rate.

Overall, the results for the three duty cycles demonstrate that error-free 21.4 Gbit/s RZ-DPSK transmission at 50 GHz channel separation is feasible beyond the design length of typical installed undersea links with no need for in-band slope compensation of chromatic dispersion, which confirms the experimental observations and theoretical predictions of previous works [50, 65].

Comparison of the Two Fibre Configurations

Comparison of the two systems can be illustrated simply through the BER evolution. If we study the BER at 10000 km for the 33% duty cycle at the optimal power for both configurations, we see that we achieve a BER ~ 10^{-5} for the first configuration, whilst for the second configuration we achieve a BER ~ 10^{-4}.

One of the differences across the configurations, apart from the inclusion of the LEAF and TWF sections, is the difference in accumulated dispersion. By happy coincidence, the weakest channel when 33% duty cycle is used on both occasions is the centre channel, so the

wider bandwidth of the first makes no difference against the second particularly when neither is wide enough to make SRS account for any distortion. Due to the long distances we propagate over, the dispersion accumulates quite substantially at the centre wavelength for the second system. This may account for the increased BER at the distance 10000 km. The influence of the extra dispersion is not linearly dependent on the distance because the Q-factor given in the initial optimisations are similar for both transmission configurations.

3.4 Conclusions

We have studied the performance of two RZ-DPSK WDM undersea transmission links. The first at a bit-rate of 20 Gb/s using a fibre map comprising a pure mixture of NZ-DSF and SMF sections. The second at a bit-rate of 21.4 Gb/s using a fibre map comprising largely sections of NZ-DSF and SMF, but additional sections of LEAF and TWF.

We first investigate the electrical Q-factor performance of a transmission link by varying the pre-/post-compensation dispersion to accommodate dispersion slope. Using 3 separate duty cycles, we realise three different transmission regimes. It is observed that the use of wider duty cycles allows for more dispersion tolerance at the expense of Q-factor performance, but the comparison of the performance of 50% duty cycle regime with its equivalent at 10 Gb/s reveals a 3- dB penalty in Q-factor performance. This is expected due to the expansion of the bandwidth.

The best performing duty cycle in both systems is identified as 33%. This is highlighted for the first system when we see that we can achieve a BER as low as 10^{-5} at a transmission distance of 11500 km. This is about the distance between the UK and the middle of South America. To achieve this performance over that distance is testament to the ability of RZ-DPSK to transmit at high bit-rates over undersea distances.

BER performance and estimation is studied. It is seen that the optimal (P_{ave}, D_{pre}) configuration is not necessarily adhered to when BER is studied with regard to the evolution of both transmission and distance. The important issue of BER estimation is addressed and it is seen that Q-factor estimation based on electrical current or amplitude statistics provides the best indicator for BER, confirming the initial suggestion that we are investigating quasi-linear transmission. Using the optimised configurations, we then studied the evolution of the BER using direct error counting. It was shown that without any in-line compensation of chromatic dispersion, optical regeneration at the receiver or forward-error correction, a BER of 10^{-9} was obtainable at transmission distances of at least 4500 km. By comparison to the four traditional methods of Q-factor based BER estimation, we saw that estimation based on the electrical Q-factor was the most accurate, suggesting Gaussian electrical statistics.

Upon comparison of both systems, we see that the small amount of uncompensated dispersion in the second fibre map can account for increased BER, particularly over longer distances. It is now important to further investigate this idea of quasi-linear transmission by considering the limitations of this BER estimation when the two main impairments of dispersion and nonlinearity are imposed onto the transmission configuration.

Chapter 4 Statistical Analysis of RZ-DPSK Fibre Communication

4.1 Review

One of the main benefits of DPSK is the doubling of transmission distance is the increased tolerance to nonlinearity due to the reduced requirement for optical power compared to RZ-OOK at comparable distances and the symmetric power profile across pulses. However due to the vast distances over which undersea transmission operates, the two main impairments of dispersion and nonlinearity are still realised.

The estimation of BER in these channels is of great importance to the installation of these transmission systems. If signals are going to be transmitted in regimes where pulses are vulnerable to dispersion and nonlinearity, it is essential to understand channel statistics in such channels, particularly if the traditional Gaussian estimate is no longer valid.

As in RZ-OOK transmission, RZ-DPSK involves the use of square–law integrate and dump receivers. The statistics of which are traditionally non-Gaussian [68]. It has however, been shown, for RZ-OOK signals that the Gaussian estimate based on electrical Q-factor can be used [71].

To effectively estimate the BER, accurate knowledge of the channel statistics is required and as such BER estimation in RZ-DPSK systems is very open to debate [72] [73, 74]. Whilst BER estimation for RZ-OOK transmission is simple and well known [71], the same cannot be said of RZ-DPSK [75]. The emergence of RZ-DPSK as an option for high-capacity long-haul quasi-linear transmission has prompted substantial investigation [72].

It is shown that several key choices are important when choosing a particular BER estimation procedure such as duty cycle and transmission distance. Several Q-factor based estimates have been introduced in the literature, in addition to the use of the conventional electrical Q-factor based estimate, amplitude Q-factor has been proposed (Q_A) [67] in addition to phase Q-factor (Q_φ) [67] and the modifed phase Q-factor ($Q_{mod\text{-}\varphi}$) [76]. However, BER estimation based on the electrical Q-factor is shown to be effective [67] for quasi-linear transmission. In these papers, only optimal, dispersion managed transmission in the optimal power regime is considered. It can be accepted here that the affects of the dispersion are averaged out over all of the pulses in the pattern and that as such, fibre nonlinearity is averaged out.

We have identified that RZ-DPSK is an option for the upgrade of legacy undersea transmission systems. The most important parameter for measuring performance of optical communications is the BER i.e. the probability of transmission error. During simulation, an important method of assessing the performance of new technologies and transmission configurations, it is computationally expensive to generate transmission errors when the quality of transmission (characterised by the Q-factor) is high. With this in mind, we need to explore BER estimation for RZ-DPSK transmission, at the limit of the quasi-linear transmission regime in order to produce a parametric estimate for BER.

Most recently, 20 Gb/s RZ-DPSK was indicated as a strong candidate for upgrading non-slope matched undersea transmission links [50], by offering the potential for similar performance as 10 Gb/s RZ-ASK at twice the spectral efficiency, and higher performance than 40 Gb/s RZ-DPSK at the same spectral efficiency. Since currently it does not seem possible to achieve transatlantic transmission at 40 Gbit/s with any comfortable margin, it may be that 20 Gb/s is the bit rate of choice for long-haul undersea transmissions.

We investigated the performance of 20 Gb/s WDM RZ-DPSK in the previous chapter and we found that the use of narrower pulses (~33% duty cycle) was the optimal choice of duty cycle, but at the expense of dispersion tolerance. We also found the optimal method of estimating the BER in quasi-linear regime was using the electrical Q-factor method derived earlier for quasi-linear RZ-DPSK and so common in the literature [71, 72].

In this chapter, we would like to expand on the conclusions of the previous chapter by focusing on the important situation occurring when Gaussian estimation cannot be applied. We attempt to realise non-Gaussian behaviour by adjusting both the levels of dispersion and nonlinearity within the transmission regime and, in doing this, we hope to realise interesting statistical behaviour and ultimately both characterise nonlinearity and produce an estimate for BER under the influence of such phenomena.

We start by focusing on the important matter of appropriate dispersion management, through the analysis of channel statistics of a channel where the dispersion is not well managed. Optimally, in the quasi-linear regime, chromatic dispersion and fibre nonlinearity will be averaged out. However, when we introduce a small change in this regime and force an increased interaction between pulses, there is a net occurrence in Kerr effect which, in the quasi-linear regime, will manifest as IXPM and IFWM. Thus, using the technique of pre-/post-compensation to realise dispersive transmission regimes, we will encourage phenomena such as IFWM and IXPM to manifest in the transmission as pulse-spreading will prevail throughout the transmission and introduce interaction between pulses. Usually, IXPM can be neglected due to the symmetry of RZ-DPSK transmission [37], but that is based on the assumption of effective dispersion management. We saw in the previous chapter that by using an asymmetric dispersion map $D_{post} = -D_{pre} + D_{ave}L + \delta D$, where δD is some fine-tuning dispersion amount, we can realise truly optimal transmission regimes. If we neglect this

quantity, such that $D_{post} = -D_{pre} + D_{ave}L$. We incur a penalty in the Q-factor (Figure 3.7). Using this notion, we study the impact on the statistics of introducing IXPM and IFWM into the transmission regime.

In the second part of this section, we induce the occurrence of nonlinear phenomena naturally through the long term imposition of Kerr nonlinearity [31]. Due to this dependence, it can be said that nonlinearity naturally increases, independent of the data format, through an increase of both pulse power and transmission distance [31]. We assess this behaviour using an optimised undersea configuration at the pertinent bit-rate of 21.4 Gb/s. We increase the pulse average power to the very limit of the optimal transmission regime, thus intra-channel nonlinearity is realised and changes the statistical behaviour of the channel. The new behaviour is assessed through study of the kurtosis of the electrical current and we use these results to intuitively derive two new estimates for the BER in such channels, one will reduce to the optimal transmission regime as a limiting case and the other only models statistical behaviour when pulse-to-pulse interaction is significant in the transmission.

For both transmission configurations, we can neglect the influence of SBS, SRS and PMD because we utilise only a narrow part of the C-band. Transfer of power across the band will not have much impact on our results.

4.2 Statistical Analysis of BER

As previously mentioned in Chapter 1, BER is one of the most important performance indicators for optical communication systems. Often, the problem is addressed statistically [66, 72, 74, 75, 90, 91] with the emphasis on the derivation of parametric models aimed at the estimation of BER in order to reduce the computational time associated with running large bit patterns to generate errors.

It has been shown that for reliable BER statistics, the number of bits that is to be simulated should be 2 orders of magnitude higher than the minimum BER to be achieved (10^{11} bits simulated for reliable estimation at BER = 10^{-9}). Practically, this is impossible and other methods are required. A particular class of such methods is the Monte Carlo methods.

Monte Carlo methods are based on the principle that physical systems with random behaviour can be approximated using partial differential equations (PDE's) with random terms that are simulated through the generation of random numbers. A non-parametric or parametric approach can be taken, with the former being more appropriate than the latter as it assumes no information about the underlying distributional shape of the physical process.

The idea behind the Monte Carlo method is to evaluate the expectation of the underlying random variable through the integral;

$$E[f(X)] = \int_{-\infty}^{\infty} xf(x)dx \tag{4.1}$$

This integral can be approximated as;

$$E[f(X)] = \frac{1}{N}\sum_{i=1}^{N} f(X_i) \tag{4.2}$$

In order to successfully Monte Carlo simulate the integral (4.1), we generate a random sample (often uniform or normally distributed sampling) between the limits of the integral, and use the discrete approximation to the integral (4.2) to calculate the value of interest. Such a method is useful when the only value is needed is the expectation of the underlying random variable, however for events which lie in the tails of the underlying probability distribution this method is computationally very expensive. For BER calculation, this is exactly the case and other approaches have been proposed.

One such method is the Multicanonical Monte Carlo (MMC) technique, which was originally used in the solution of Statistical Physics problems of high dimension [92], but has since been applied to problems in optical communications [49, 90, 91, 93].

MMC Technique

In this section, a short introduction to MMC is given. In particular, we apply the MMC to the evaluation of the probability density function of a control quantity $V(x)$, where x can represent a multi-dimensional vector sampled from a multi-dimensional state space Γ with the distribution $\rho(x)$. The state space Γ can be partitioned into a union of M subsets such that;

$$\Gamma_k = \{x \in \Gamma \mid ((k-1)\Delta V \leq V(x) \leq k\Delta V\}$$

Practically Γ_k represents a set of samples x such that $V(x)$ falls into the kth bin, H_k of the histogram H. This is a set defined as;

$$H_k = \{V \mid (k-1)\Delta V \leq V(x) \leq k\Delta V\}$$

Then the probability of a random realisation x to be sampled from Γ_k is defined by the integral;

$$P_k = \int_{\Gamma_k} \rho(x)dx = \int_{\Gamma} \rho(x)\chi_k(x)dx \tag{4.3}$$

Where $\chi_k(x)$ is the characteristic function defined by;

$$\chi_k(x) = 1, x \in \Gamma_k \tag{4.4}$$
$$\chi_k(x) = 0, otherwise \tag{4.5}$$

Conventional Monte Carlo would use the discrete approximation to this integral given by;

$$P_k = \frac{1}{N}\sum_{i=1}^{N} \chi_k(x^i) \tag{4.6}$$

Where x^i are N realizations of the random variable x sampled according to the probability density $\rho(x)$. A substantial increase in the performance of the Monte Carlo can be obtained through the use of a biasing pdf $\rho^*(x)$ for the vector x. Through proper selection of the biasing pdf, it is possible to reduce the variance of P_k. This is the inventive feature of the MMC algorithm. The equation 4.3 can be written as;

$$P_k = \int_{\Gamma} \chi_k(x) \frac{\rho(x)}{\rho^*(x)} \rho^*(x) dx \tag{4.7}$$

If we apply the conventional Monte Carlo discretisation of the integral (4.2), then we obtain a formula for P_k.

$$P_k = \frac{1}{N} \sum_{i=1}^{N} \chi_k(x) \frac{\rho(x_*^i)}{\rho^*(x_*^i)} \tag{4.8}$$

Where x_*^i are sampled from a biased distribution $\rho^*(x)$. Zero variance can be obtained for this estimate for an optimal choice of the biasing pdf, $\rho^*(x)$ [90], given by;

$$\rho_{opt}(x) = \chi_k(x) \frac{\rho(x)}{P_k} \tag{4.9}$$

The problem is that the optimal biasing pdf, $\rho_{opt}(x)$, is dependent on the unknown probabilities, inspiring an iterative procedure that we will now detail, which comprises the main part of the MMC procedure. The iterative procedure will converge monotonically to the optimal biasing pdf detailed in equation [90]. Based on [90], we detail this procedure using the equation;

$$\rho^{*,j}(x) = \frac{\rho(x)}{c^j P_j^k} \tag{4.10}$$

Where P_j^k represent the approximate probabilities found at the jth iteration and c^j is the normalising constant allowing the satisfaction of one of the basic features of a probability density function;

$$\int_{\Gamma} \rho^{*,j}(x)dx = 1 \tag{4.11}$$

Moreover, it is customary to use $\rho(x)$ as an initial guess to the biasing pdf $\rho^*(x)$, through this we can use the uniform distribution as an initial guess ($P_1^1 = \ldots = P_M^1 = \frac{1}{M}$). It is observed that the choice of initial distribution doesn't significantly effect the convergence of the overall algorithm [90]. Following each iteration, the probabilities P_k^j are updated by the latest information from the simulation. Due to the constant updates of the information, a more uniform sampling of the sample space takes place, meaning rare events in the state space are explored compared to the unbiased case characteristic of standard Monte Carlo. Eventually, the algorithim approaches a state when the expected number of entries into each bin H_k of the histogram H becomes equal to N/M [90]. Substitution into equations 4.9 & 4.10 yield $c^j \to M$ and $P_k^j \to P_k$. The recursive relations for the update of P_k^j are given by [49];

$$P_{k+1}^{j+1} = \frac{P_k^{j+1} P_{k+1}^j}{P_k^j} \left(\frac{H_{k+1}^j}{H_k^j} \right)^{g_k^j} \tag{4.12}$$

$$\hat{g}_k^j = \frac{g_k^j}{\sum_{l=1}^{j} g_k^1} \tag{4.13}$$

$$g_k^1 = \frac{H_k^l H_{k+1}^l}{H_k^1 + H_{k+1}^l} \tag{4.14}$$

In addition, we define $\hat{g}_k^j = 0$ if $g_k^j = 0$ and $g_k^1 = 0$ if $H_k^1 + H_{k+!}^l = 0$. Moreover, before applying these relations to recalculating the probabilities P_k^{j+1}, we set P_1^{j+1} to an arbitrary

positive constant. The exact value of the number is not important since afterwards we renormalize the approximate probabilities P_k^{j+1} so that;

$$\sum_{k=1}^{M} P_k^{j+1} = 1 \tag{4.15}$$

In each iteration we accomplish sampling from the distribution $\rho^{*,j}(x)$ using the Metropolis algorithm [94], this is an example of Markov Chain Monte Carlo (MCMC). The Metropolis algorithm entails drawing samples from any probability distribution $P(x)$, the only requirement being that the function dominating the density can be calculated at x. The algorithm generates a Markov chain in which each state depends only on its previous state [69, 95].

In essence, we produce a random walk of samples $\hat{x}^i$. Each transition goes from $\hat{x}^i = x_a$ to $x_b = x_a + \varepsilon^j \Delta x$ where ε^j is a random step that doesn't favour any direction in the sample space Γ. The transition is accepted with probability π_{ab} and $\hat{x}^i = x_b$. In problems pertaining to optical communications the state space Γ may represent a set of all possible noise realizations at all amplifiers and all frequencies [90, 93]. It may also represent the rotation of polarization [49] states. This will govern the proposal distribution of the Metropolis algorithm.

The beauty of the MMC procedure lies in its ability to equally sample the state space in a relatively short space of time. In this section, we are more interested in the statistics of the system under the influence of particular distortions. To this end, we rely upon the direct counting method explored in Chapter 3 and alter the physical regime of the system in order to realise particular effects. We feel this is a more organic method of studying the physical

regime. The implementation of MMC for this task is beyond the scope of the thesis, but is covered elsewhere [49, 90, 91].

4.3 Statistics and Dispersion

We study a dispersion managed link, a similar configuration is considered in Chapter 3 when a 7-channel 20 Gb/s RZ-DPSK undersea link is examined. The single channel embodiment of this configuration has been studied [65] in the context of optimisation and performance. The first step was to optimise the pre-/post-compensation dispersion where $D_{post} = -D_{pre} - D_{ave}L$. Indeed, for this particular map, $D_{ave}=0$, so $D_{post} = -D_{pre}$. Optimal configurations are suggested for the single channel embodiment for three duty cycles, allowing the realisation of 3 seperate transmission regimes. We continue the analysis of the seperate regimes using statistical analysis techniques often published in the financial [96] or meteorological [97] literature.

In the previous chapter, we concluded that the use of narrow duty cycles could be employed at the expense of dispersion tolerance, providing that tunable chromatic dispersion devices could be inserted into the receiver to allow for the lower dispersion tolerance of pulses with narrow duty cycles. In this section, we start with a study of the symmetric postcompensation map ($D_{post}=-D_{pre}$) and analyse the optimised dispersion regimes identified in [65]. We use advanced statistical techniques to study the underlying structure of the distribution when distances become higher than the original optimisation length (6300 km).

We first introduce the statistical techniques and the theory behind the analysis we undertake, we then apply the analysis to the same single channel configuration considered in [65], using the optimised parameters for both pre-/post-compensation dispersion and pulse average power.

Statistical Theory

The most importance statistical quantity connected to any optical transmission system is the the BER, this is estimated from the tails of the underlying channel probability density function. From this, we can assume that when the Gaussian based electrical Q-factor based estimate, derived from Gaussian statistics, holds, the distribution of the electrical current maintains a Gaussian structure in both the logical ones and logical zeros due to the symmetry of the RZ-DPSK transmission format. Mathematical statistics tells us that higher-order standardised moments (all moments apart from mean and variance) for a Gaussian-distributed sample, are exactly equal to zero. We can use this feature to facilitate the analysis of our transmission systems. The typical measure of tail behaviour in the literature is the kurtosis, defined as the fourth standardised moment of the underlying data. We set I to be the received current and σ to be the standard deviation of the pertinent data set and define kurtosis (κ) as [98]:

$$\kappa = \frac{E(I-\mu_I)^4}{\sigma^4} - 3 \tag{4.16}$$

Where

$$E(I-\mu_I)^n = \mu_n = \sum_{i=1}^{N}(I_i - \mu)^n \tag{4.17}$$

For Gaussian distributed data, the kurtosis (4.16) will be exactly 0. This gives us the required reference value for our data analysis. Distributions can be characterised in terms of κ; where they are described as lepto-kurtic if $\kappa>0$, platy-kurtic when $\kappa<0$ and meso-kurtic when $\kappa=0$. Gaussian tail behaviour suggests that all values in the data set will be statistically independent and identically distributed due to the central limit theorem. This is redolent of pulses which, even when averaged over their time slot [99] retain statistical independence from other pulses and the resultant electrical current retains a Gaussian shape without any extreme variations due to the energy transfer caused by nonlinearity.

Therefore, consistent with this logic is the notion that any distributions not following a Gaussian structure will exhibit lepto-kurtic behaviour, such as interacting pulses due to energy transfer stemming from pulse broadening or long-term dependence on fibre refractive index. This was identified previously as an issue when modelling extreme behaviour in stock prices, where power-law distributions were introduced as an option when modelling the nonlinear behaviour in the stock market [96]. Also considered is the example distributions given as a result of extreme value theory, which we now describe;

Extreme Value Theory

Extreme value theory is concerned with the analysis of extrema in data samples, and the subsequent distributive models. To illustrate Extreme Value Theory, we must consider the notion of the maximum of a data set

$$y = \max\{x_{i,1} \ldots, x_{i,m}\} \tag{4.18}$$

If the $x_{i,j}$ can be observed by the statistician, then taking the maxima out of the blocks is another possibility of extracting upper extreme values from a set of data (besides taking exceedances). This method is called the annual maxima, block or Gumbel method. For identically, independently distributed (iid) random variables $X_1,\ldots,X_m$ with a common cumulative distribution function F, it is simple to compute the cumulative distribution function of the maxima; we obtain

$$P\{\max_{i\le m} X_i \le x\} = P\{X_1 \le x,\ldots,X_m \le x\} = F^m(x) \tag{4.19}$$

Thus, the y_i's in (4.18) are governed by F^m if the $x_{i,j}$'s are governed by F. If the iid condition fails, then a cumulative function of the form given in (4.19) may still represent an accurate approximation of the actual cumulative function [100]. Where independent, heterogenous (taken from different distributions) random variables X_j with cumulative function F_j, holds with F^m replaced by;

$$F^m = \prod_{j \le m} F_j \tag{4.20}$$

A cumulative function F^m can be fitted to $\prod_{j \le m} F_j$ if the deviations of the F_j from each other can be neglected. Likewise, if there is a slight dependence in the data, a distributive function of the form F^m may still serve as an approximation of the actual distribution function of the maximum. It is plausible to employ this approach in more complex situations as well. We can replace the actual cumulative distribution function with another distribution function. We introduce an α-parameterization and state 3 models (for a random variable X);

Gumbel (for all x)

$$G_0(x) = \exp(-\exp(-x)) \tag{4.21}$$

Fréchet (for $x \ge 0$, α>0)

$$G_{1,\alpha}(x) = \exp(-x^{-\alpha}) \tag{4.22}$$

Weibull (for $x \le 0$,α<0)

$$G_{2,\alpha}(x) = \exp(-(-x)^{-\alpha}) \tag{4.23}$$

We can also introduce a new parameterization in terms of a quantity ξ (=1/α) which allows the unification of the three aforementioned models [100]. Through this parameterization, the Weibull distribution becomes;

$$P_\xi(I) = e^{-(1+\xi I)^{-\frac{1}{\xi}}} \tag{4.24}$$

The unifying distribution, known as the GEVT distribution, is characterises by the probability density function given below;

$$P_\xi(I) = e^{-(1+\xi\frac{I-\mu_I}{\psi})^{-\frac{1}{\xi}}} \tag{4.25}$$

The parameters (α,μ,ψ) represent shape, scale and location respectively. The ability of these distributions to model extrema of data sets means they are ideal for the modelling of transmission errors in optical data transmission systems as error occurrence represents extreme behaviour in channels, which manifest in the tails of distributions.

Numerical Analysis

Using the SSFM algorithim to model optical pulse propagation, we consider a DPSK non-slope matched undersea system with symmetric pre/post compensation ($D_{post} = -D_{pre}$):

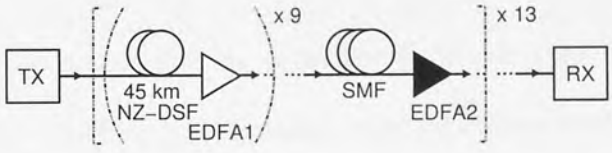

Figure 4.1: Graphical Depiction of the Fibre Map

The transmission link used in our analysis is depicted in Figure 4.1. It emulates a non-slope matched undersea type link. The unit cell of the system comprises nine sections of NZ-DSF of length 45 km each, followed by a section of standard SMF. The NZ-DSF has a dispersion of D = -3ps/(nm km), a dispersion slope of S = 0.09 ps/(nm^2 km), an attenuation of α = 0.2 dB/km, and an effective area of A_{eff} = 54 μm^2 . The parameters of the SMF are: D = 16ps/(nm km), S = 0.057 ps/(nm^2 km), α = 0.2 dB/km, and A_{eff} = 80 μm^2. The values of D, α and A_{eff} are given at 1550 nm. The nonlinear Kerr coefficient is $2.35\times10^{-20} m^2/W$. The residual path-averaged dispersion of the line at 1550 nm is zero.

Erbium-doped fibre amplifiers (EDFAs) with a noise figure of 4.5dB are used at the end of each fibre section to compensate for the energy losses in the preceding fibre section. The unit cell of the system is repeated thirteen times to yield a total transmission length of approximately 6300 km.

We transmit several PRBS sequences of length 16384 bits using Gaussian pulses at a bit-rate of 20 Gb/s, we consider distances upwards of 4800 km (~10 spans) and realise distances towards 20000 km (~40 spans). The transmission uses the optimal regimes defined by the initial optimisation completed in [65]. The narrowest duty cycle, at 20% duty cycle performs optimally when D_{pre} = 600 ps/nm and the launch average power (P_{ave}) = -2.9 dBm, the 33% duty cycle is shown to be optimal D_{pre} at 800 ps/nm and P_{ave} = -3.6 dBm. For the widest duty cycle (50%), we know that the optimal D_{pre} is 500 ps/nm with P_{ave} = -4.8 dBm.

At such high distances, we realise that our particular dispersion map will not guarantee a suitable transmission regime, but we aim to realise statistical effects redolent of the impact of dispersion upon optical pulses. At the receiver stage we measure the electrical current using a balanced Mach-Zehnder delay interferometer which provides us with an electrical current, which, following filtering, we can measure. Collating electrical currents, we analyse the kurtosis according to (4.16). This provides the first part of our analysis.

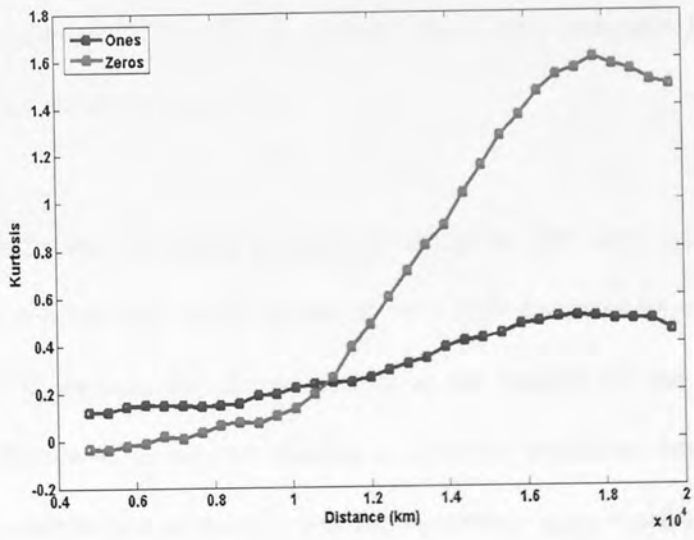

a)

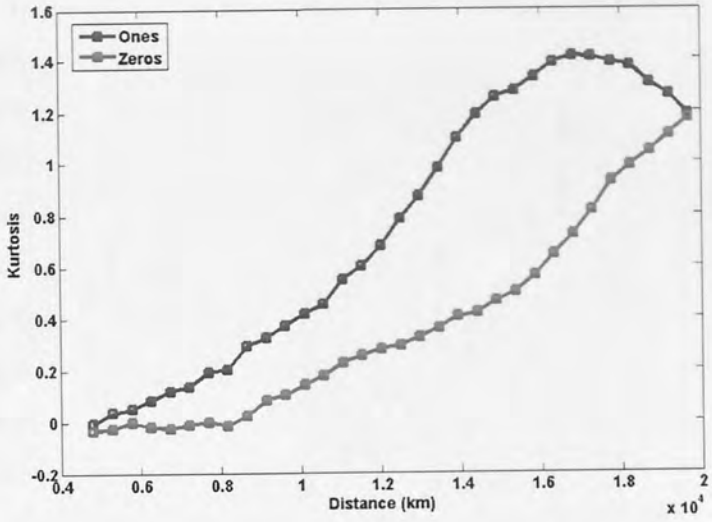

b)

Figure 4.2: Kurtosis of Electrical Current Distributions for 20 Gb/s Single Channel RZ-DPSK Pulses a) 33% Duty Cycle b) 50% Duty Cycle

We see from Figure 4.2 that interesting dynamical behaviour can be observed in both distributions. The difference in duty cycle is clear. For the 33% duty cycle, we witness interesting differences between the ones and zeros in terms of the tails of the probability density function. The measure of kurtosis providing such high values intimates that there is extreme variation in the behaviour of the pulses, but it also indicates that the extreme behaviour is not consistent across the pulses.

We study the bit patterns for increasing kurtosis, choosing the 33% duty cycle as an example for our analysis and consider the optical pulses at very high distances by comparison to the pattern at 4800 km. If we take the optical pattern at the optimal δD for the transmission distance 4800 km (Figure 4.3), we can observe a smoother transition between the pulses, intimating a smooth distribution of energy. For the symmetric map, there are fluctuations in power at the intersection between bit-slots, suggesting the presence of at least some IFWM [36].

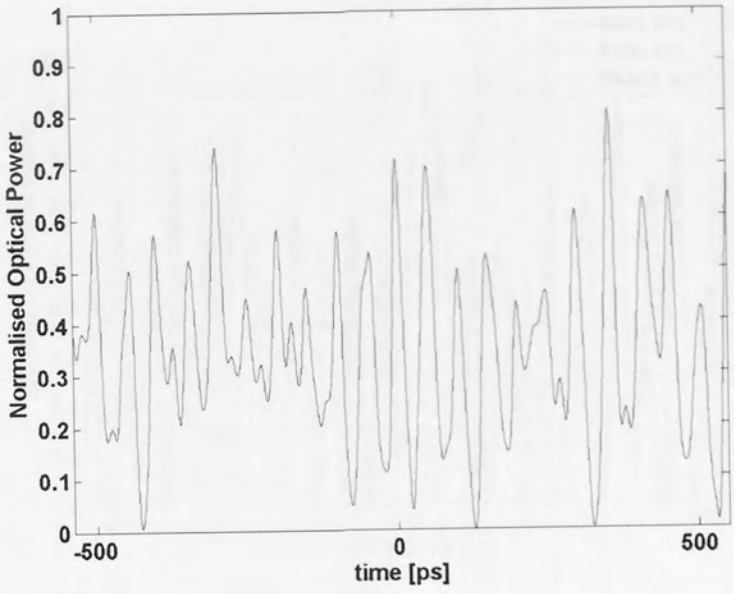

a)

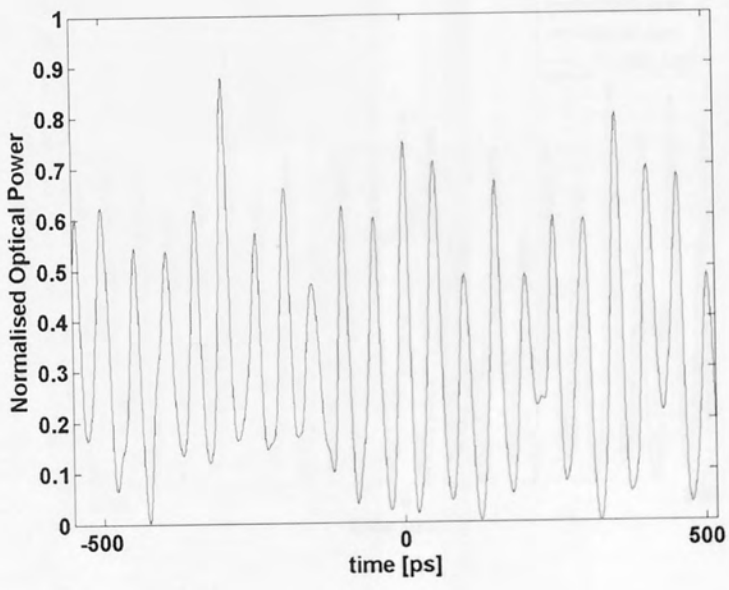

b)

Figure 4.3: Normalised optical power for 33% duty cycle RZ-DPSK pulses at 4800 km a) $D_{post} = -D_{pre}$ b) $D_{post} = -D_{pre} + \delta D$

Increasing the transmission distance demonstrates significant power fluctuations, this would infer an increase in IFWM proportionate with the increase in transmission distance. Also evident from Figure 4.4, is the presence of timing jitter, which can be attributed to IXPM [36].

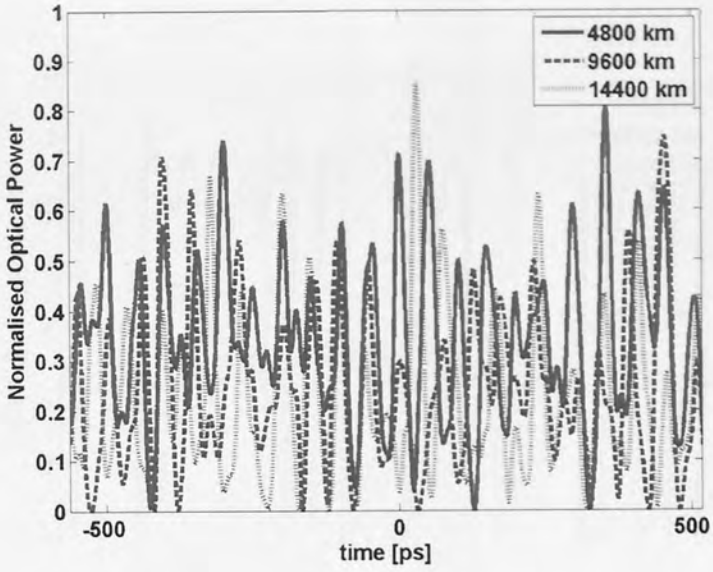

a)

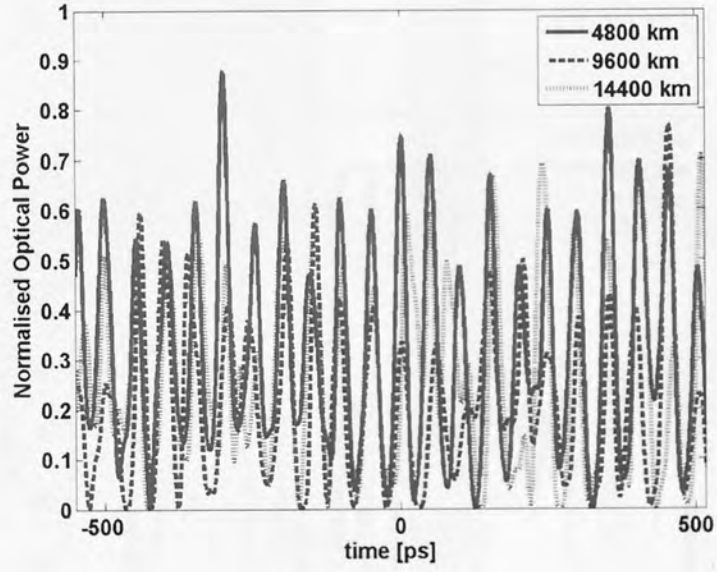

b)

Figure 4.4: Normalised optical power for 33% duty cycle RZ-DPSK pulses at distances increasing from 4800 km to 14400 km for a) $D_{post} = -D_{pre}$ b) $D_{post} = -D_{pre} + \delta D$

For an indication of the influence of IXPM, we plot the evolution of optical phase for an optical pattern at increasing distances Figure 4.5. There appears to be very little difference in the optical phase due to the presence of the additional δD to the post-compensation. Although extensive phase modulation does ensue for the ascent of the distance.

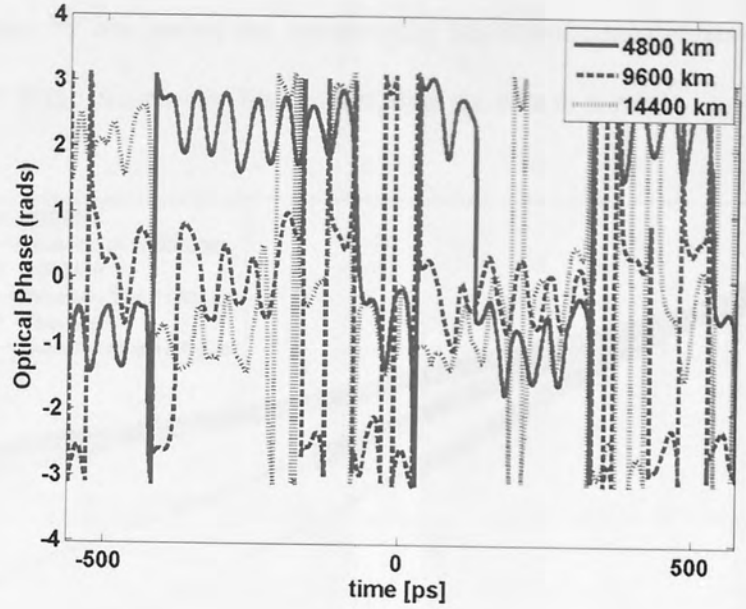

a)

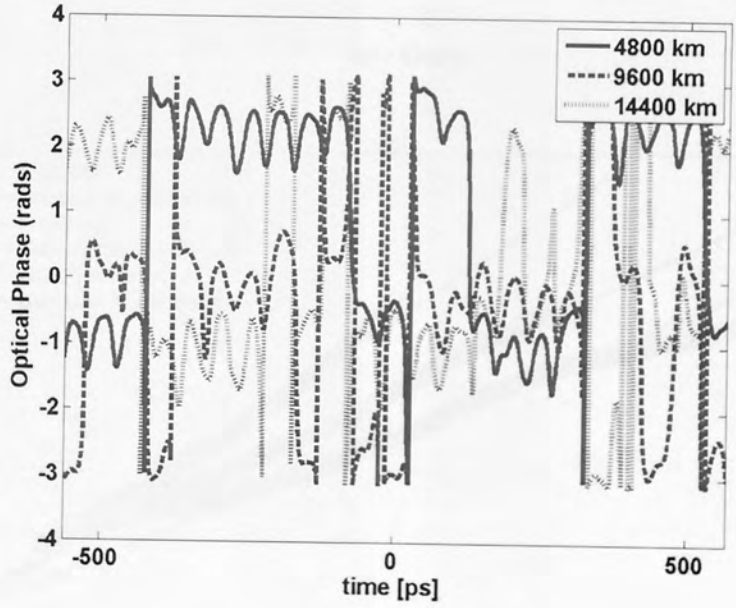

b)

Figure 4.5: Optical Phase for 33% Duty Cycle RZ-DPSK Pulses at Increasing Distance for a) $D_{post} = -D_{pre}$ b) $D_{post} = -D_{pre}+\delta D$

We can also study the behaviour of the probability density functions using the statistical construct known as the probability plot, this provides an essential method of studying the normality in data by comparing the numerically calculated probabilities with those of an assumed model. If the two curves (lines) meet, then the data is normal.

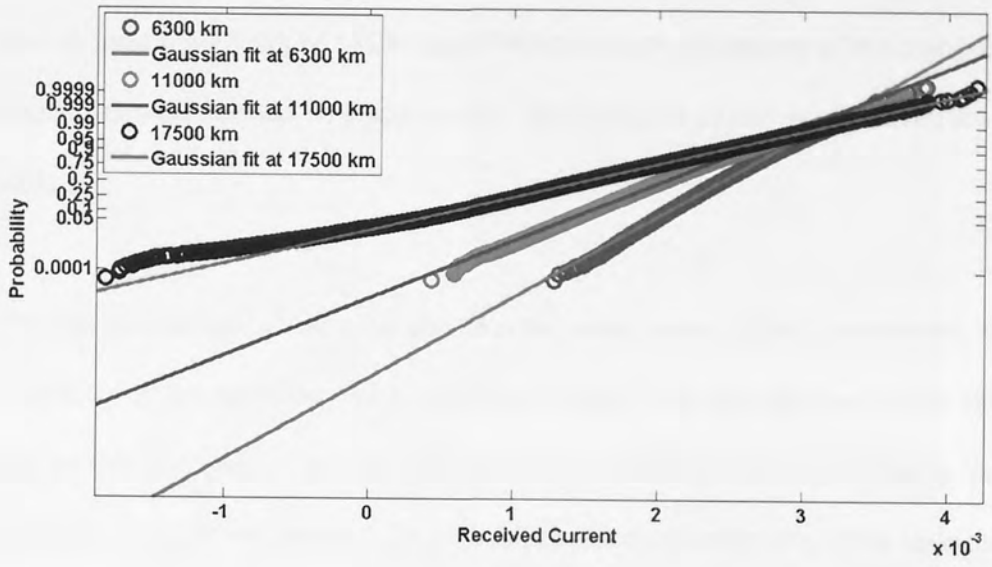

a) Ones

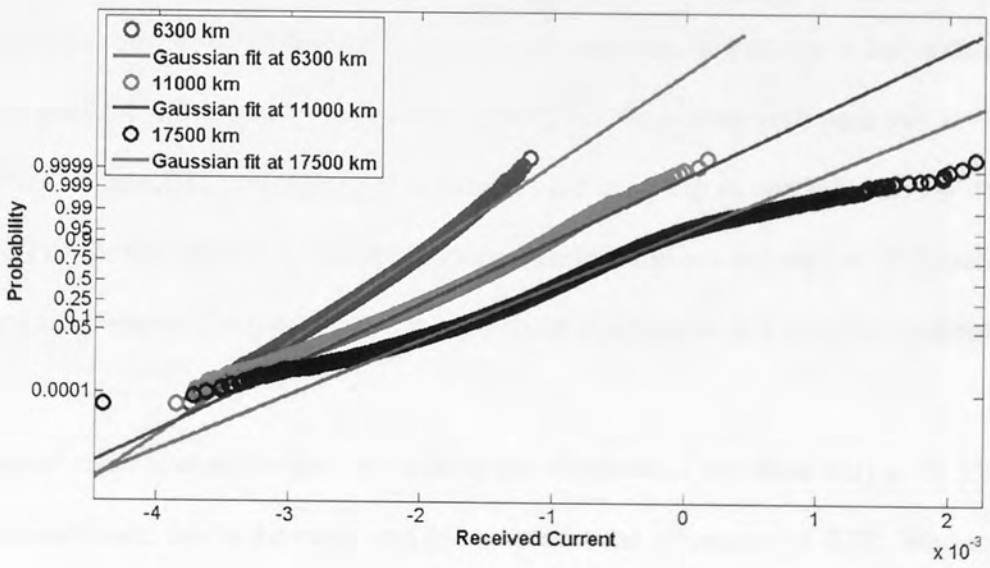

b) Zeros

Figure 4.6: Probability plots for the received current histograms at 33% duty cycle at distances 6300 km, 11000 km and 17500 km (Maximal Kurtosis) a) Logical Ones b)Logical Zeros for the dispersion map $D_{post} = -D_{pre}$

The probability plots provide a useful indicator of the structural behaviour in the underlying data. Gaussian behaviour is generally preserved for the middle of the histogram, but the tails show deviation, as demonstrated through the analysis of the kurtosis. The deviation from the Gaussian is commensurate with an increase in kurtosis, and this is concentrated in the tails of the distribution. Transmission in these regimes is not practical for the system in question, but we have realised the effects of IXPM and IFWM through adjustment of the dispersion map. This motivates our next step, to study models which may be of use as we move forward with this study.

The obvious differences between the ones and the zeros is not of great importance, as we are only interested in the occurrence of transmission errors. It is the behaviour of the extrema of the data set that is important and we seek inspiration from Extreme Value Theory to develop new predictive methods to measure the probability of transmission error. It is clear that lepto-kurtic distributions should be used to model highly nonlinear transmission from Figure 4.2.

At the widest duty cycle (50%), the kurtosis of the ones and the kurtosis of the zeros grow at a similar gradient and appear to intersect at 19960km. Suggesting both ones and zeros can be modelled as fat-tailed processes. This motivates the next step in our analysis, we wish to fit the tails of the distribution to the distributions mentioned in our description of Extreme Value Theory and compare the resulting fits to a Gaussian distribution as a reference example.

As we are concentrating on the inner tails of the distribution, we chose only to fit 33% of the data in each case, this is the main area of interest for the estimation of BER. We can assume that the centre of the distribution is Gaussian, but given the results presented in Figure 4.2, we cannot make this assumption about our tails. The results shown in Figure 4.7 are for the optimal fits for each distribution.

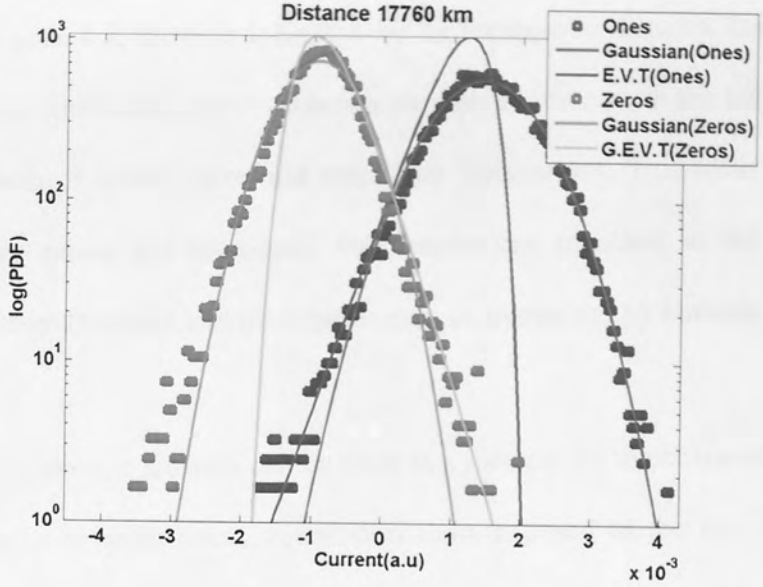

a)

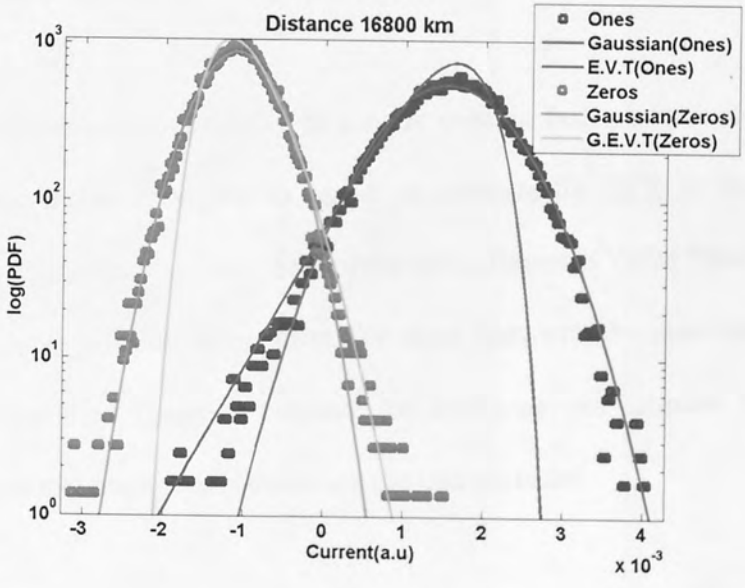

b)

Figure 4.7: Numerical Tail Fitting a) 33% Duty Cycle b) 50% Duty Cycle

Its clear from Figure 4.7 that for high kurtosis transmission, the tails are well approximated by the GEVT distribution (logical zeros) and the EVT distribution (logical ones). At such distances, transmission is not practically viable due to the high BER sustained, but we have illustrated the need for new statistical models in transmission where kurtosis is high due to significant pulse-to-pulse interaction.

As can be seen from Figure 4.2, kurtosis increases for an increase in distance and we have shown that an increase in distance is also commensurate with an increase in the intra-channel nonlinearities in the form of timing jitter and amplitude fluctuations. This leads us to the conclusion that extreme phase and amplitude fluctuations can manifest in the electrical domain in the shape of non-Gaussian statistical behaviour, characterised by kurtosis.

We have seen in this section that kurtosis can be used as a method for the characterisation of intra-channel nonlinearity in quasi-linear trasmission links exposed to the two sources of distortion created by IXPM and IFWM. Mathematically, we have shown that such nonlinearity results in lepto-kurtic distributions.

We now study the intrachannel nonlinearity in a more organic fashion by increasing pulse power and transmission distance, hoping to derive an estimate for BER in these channels which, contrary to the estimates that could be derived using Extreme Value Theory using the results of this section, have practical application. We show that, with the same information as what is given to the standard Gaussian estimate for BER, we can estimate the BER for channels where intrachannel nonlinearity dominate the transmission.

4.4 Statistics of Nonlinearity

In this section, we closely examine the accumulation of nonlinearity within the quasi-linear transmission regime, aiming to develop a statistical estimate for the BER. The statistics of RZ-DPSK have been long open to debate [37, 67, 72, 73, 101], but with the adoption of the quasi-linear regime, new physical effects will be introduced into the transmission. These effects derive from the interaction between pulses. We show that that for RZ-DPSK undersea links of this type, the underlying channel probability density functions (pdfs) possess non-

Gaussian tails. Thus, alternative methods need to be developed to accurately calculate the BER. We justify the requirement for a new distributive model with the analysis of higher order standardised moments. Following this analysis, we derive a new estimate based on the Gamma distribution and show that the new estimate accurately predicts the BER when nonlinearity dominates the transmission.

Statistical Theory

For quasi-linear DPSK transmission, it has been shown that the Gaussian estimate of BER is effective. However, when the impact of fibre nonlinearity grows due to higher pulse power or increased transmission distances, pulse-to-pulse interactions become increasingly significant and create correlation between pulses [101]. This results in decidedly non-Gaussian behaviour, which motivates the need for alternative statistical estimation procedures. Non-Gaussian behaviour can be studied via means of the higher order standardised moments of the data.

Mean and variance are standard quantities which are well defined in the engineering literature. Skewness and kurtosis relate to the asymmetry and tail behaviour of the data histogram respectively. We detail below the physical significance of the first four standardised moments Figure 4.8.

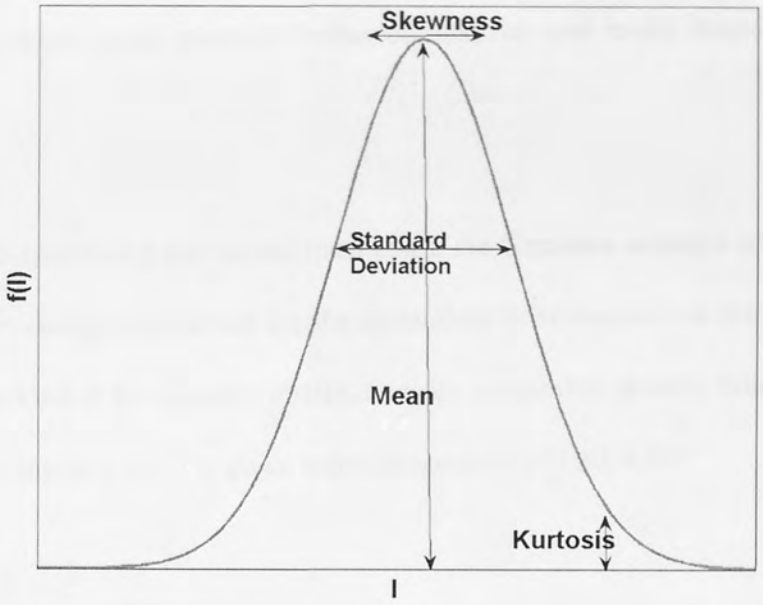

Figure 4.8: Statistical definition of the first four standardised moments

We define both quantities below (as in [98]), the kurtosis is defined slightly differently here to the previous definition, but the only difference is the value (-3). The definition from the previous section is often described as the excess kurtosis because it is used as a measure of Gaussianity.

$$K = \frac{\mu_4}{\sigma^4} \tag{4.26}$$

$$S = \frac{\mu_3}{\sigma^3} \tag{4.27}$$

$$\mu_n = \sum_{i=1}^{N} (I_i - \mu)^n \tag{4.28}$$

$$\sigma = \sqrt{\sum_{i=1}^{N} (I_i - \mu)^2} \tag{4.29}$$

Where N is the size of the data set, I_i are the individual received currents and μ is the mean of the data. For normal Gaussian distributed data, the quantity known as skewness (asymmetry) is equal to zero and the quantity known as kurtosis (tail behaviour) is equal to 3, so data can be categorised relative to the Gaussian distribution according to the measure of kurtosis. We

have already seen, using this measure, that the onset of intra-channel nonlinearity is commensurate with lepto-kurtic statistical behaviour and our new model must indulge such a requirement.

The distribution characterising this model must count the Gaussian amongst its special cases, but also be flexible enough to account for the dynamical behaviour of the transmission. One distribution of this kind is the Gamma distribution, its probability density function (pdf) and cumulative density function (cdf) is given below respectively (4.30, 4.31).

$$f(I;k,\theta) = I^{k-1}\frac{e^{-\frac{I}{\theta}}}{\theta^k \Gamma(k)} \tag{4.30}$$

$$F(I;k,\theta) = \frac{\gamma(k,\frac{I}{\theta})}{\Gamma(k)} \tag{4.31}$$

Where k is the shape parameter; θ is the scale parameter; I is the received current and $\Gamma(.)$ & $\gamma(.,.)$ are the gamma function and incomplete gamma function respectively, given below (4.32, 4.33);

$$\Gamma(z) = \int_0^\infty t^{z-1}e^{-t}dt \tag{4.32}$$

$$\gamma(a,z) = \int_0^z t^{a-1}e^{-t}dt \tag{4.33}$$

The Gamma distribution is characterised by two parameters, k and θ, the shape parameter and scale parameter respectively. Distributions described using shape and scale exhibit more stability to changing trends in the underlying random variable. The gamma distribution is perfect for our analysis, any additional physical effects particular to the quasi-linear regime, due say, to further increasing capacity, can also be integrated into such a flexible model because it makes no assumptions based on symmetry or tail behaviour within the underlying data. We limit ourselves to two-parameter distributions as we want to investigate whether or

not prediction under the influence of non-Gaussian behaviour is still possible given the same information we would provide to a Gaussian model.

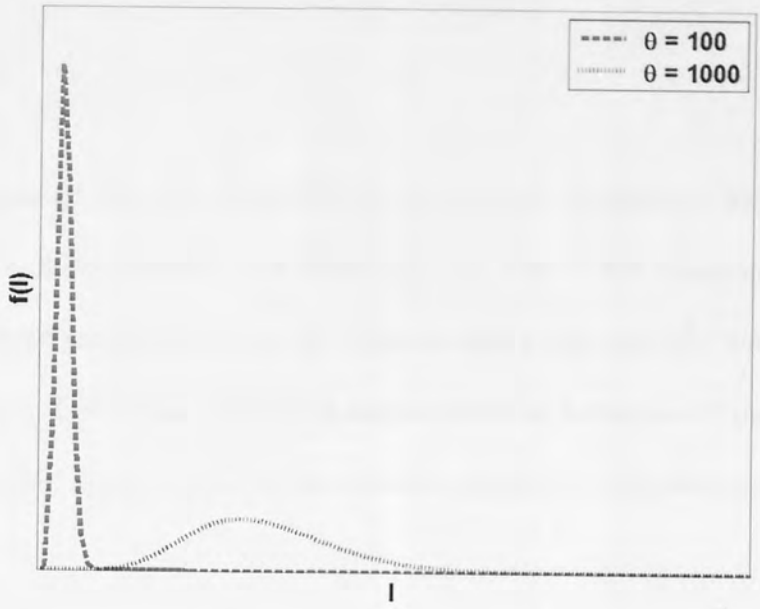

Figure 4.9: Gamma Distribution at shape parameter k =10 for varying scale parameters

It is seen from Figure 4.9 that the Gamma distribution doesn't maintain a rigid shape as its characteristics are based on shape and scale parameters. We show in Figure 4.9 that such flexibility allows dynamic behaviour within the underlying statistics. The flexibility of the Gamma distribution suggests that BER estimation based on such a model will be successful under the influence of varying nonlinear effects. All of the moments of the Gamma distribution can be characterised using the shape and scale parameters k & θ respectively. Subsequently, we can also use the mean and the variance of the sample data to estimate the correct fitting parameters of the distribution. The first two standardised moments (mean, μ and variance, σ^2) can be estimated theoretically using k and θ using the following equations [98]:

$$\mu = k\theta \tag{4.34}$$

$$\sigma^2 = k\theta^2 \tag{4.35}$$

Simple manipulation of (4.34, 4.35) reveals two estimates of the shape (k) and scale (θ) parameters

$$k = \frac{\mu^2}{\sigma^2} \tag{4.36}$$

$$\theta = \frac{\sigma^2}{\mu} \tag{4.37}$$

Substantial investigation into the behaviour of the Gamma distribution has already been performed and its limiting cases are well publicised [98]. One of the important special cases occurs when the shape parameter k becomes large. In such a case, the distribution becomes a Gaussian distribution. Given that we wish to analyse physical behaviour of our transmission relative to the Gaussian, such a feature serves immense purpose for our progression.

As a consequence, we endeavour to develop a model to predict the probability of error in transmission (BER) using the Gamma distribution.

$$BER_0 = \int_{I_d}^{\infty} P_o(y_0; k_0, \theta_0) dy_0 \tag{4.38}$$

$$BER_1 = \int_{-\infty}^{I_d} P_1(y_1; k_1, \theta_1) dy_1 \tag{4.39}$$

Where y denotes the average current for the logical ones and zeros respectively (denoted by subscript), $k_{1,0}$ and $\theta_{1,0}$ denote the respective shape parameters of the Gamma distribution and $P(y; k, \theta)$ is the probability density function describing a Gamma distributed random variable (4.30) and I_d is the decision level for the current. We echo the approach of [99] in our derivation of the expression for BER.

$$BER = \frac{1}{2}(BER_1 + BER_0) \tag{4.40}$$

We know from any standard mathematical statistics text that we can define BER_0 equivalently as:

$$BER_0 = \int_{I_d}^{\infty} P_0(y_0;k_0,\theta_0)dy_0 = 1 - \int_{-\infty}^{I_d} P_0(y_0;k_0,\theta_0)dy_0 \tag{4.41}$$

The integrals in (4.40) and (4.41) are nothing more than the cumulative density functions of the Gamma distributed random variable which we have already given in (4.31) as:

$$F(y,k,\theta) = \int_{-\infty}^{I_d} P(y;k,\theta)dy = \frac{\gamma(k,\frac{I_d}{\theta})}{\Gamma(k)} \tag{4.42}$$

From (4.40), we can say that the BER can be estimated as:

$$BER = \frac{1}{2}\left(1 - \frac{\gamma(k_0,\frac{I_d}{\theta_0})}{\Gamma(k_0)} + \frac{\gamma(k_1,\frac{I_d}{\theta_1})}{\Gamma(k_1)}\right) \tag{4.43}$$

This gives us a simple parametric estimate of BER. We must now compare the performance of this estimate with the results of direct numerical simulations.

Numerical Analysis

We consider the configuration given in Figure 4.10, it is identical to the configuration given in Figure 3.15, but we are not so interested in the optimal transmission regime, instead we study the configuration as an example of a transmission configuration which can subject signals to signal distortion at increased pulse average power.

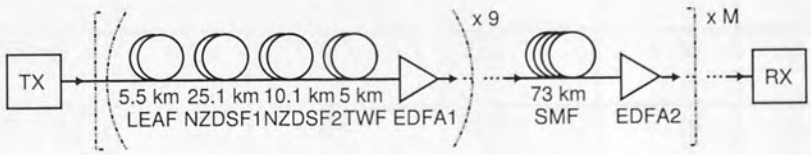

Figure 4.10: Graphical Depiction of Fibre Map

Such a fibre map emulates a non-slope matched undersea type link that is implemented in our experiments as a re-circulating fibre twin-loop. This map offers substantial flexibility and allows for the replication of the dispersion and OSNR maps of a typical transoceanic link [32]. We use the SSFM algorithim in order to model the propagation of optical pulses in the

transmission medium. The unit cell comprises nine non-zero dispersion-shifted fibre sections with negative dispersion. Each of them has a length of 45.7 km and is composed of a mix of large effective core area fibre (LEAF), standard NZDSF and reduced slope fibre (TWF), followed by a standard mono-mode fibre (SMF) section of length 73.2 km. The transmission length of one complete span is 484km. We iterate the unit cell M times to realise transoceanic distances. The residual path average dispersion of the line at 1550 nm is -0.025 ps/nm. Fibre parameters are given in Table 4.1. The domination of NZ-DSF and SMF within the fibre map enables replication of the legacy transmission links.

Erbium-Doped Fibre Amplifiers (EDFAs) with a noise figure of 4.5 dB are utilised to compensate exactly for the energy losses in the fibres and the splicing losses associated with the joining of the distinct fibre sections. The amplifiers have a flat gain spectrum over the range of wavelengths of interest and dominate the source of noise in the transmission. We consider the central channel of a symmetrically distributed 5 channel arrangement with the central channel at 1550nm, separated by 0.4 nm (50 GHz).

Fibre	LEAF	NZDSF1	NZDSF2	TWF	SMF
D[ps/nm]	-2.8	-3.07	-2.91	-3.26	16.79
S[ps/nm2km]	0.11	0.09	0.09	0.04	0.06
α[dB/km]	0.21	0.20	0.21	0.20	0.19
γ[1/W km]	1.27	1.88	1.85	1.99	1.19
Length[km]	5.5	25.1	10.1	5.0	73.2

Table 4.1: Fibre Parameters

The transmitter is modelled as the concatenation of a distributed feedback laser, a dual-drive Mach-Zehnder modulator-based pulse carver with an extinction ratio of 30 dB, and an ideal

phase modulator. The pulse carver is biased to produce RZ-pulses with a 50% duty cycle at a 21.4 Gb/s bit-rate. The channels are de-multiplexed using an optimised second order Gaussian optical band pass filter (OBPF) with 3-dB bandwidth of 30 GHz, detected using a balanced Mach-Zehnder delay interferometer, and then filtered electrically by a third order Bessel filter with a cut-off frequency equal to the bit-rate. Pre compensation is optimised to D_{pre} = 700 ps/nm at a distance of approximately 6300 km (13 unit spans of the transmission) and D_{post} = -D_{pre} +D_{ave}L + δD, (L = 484 km is the span length) with statistics given only for optimal δD. We consider average pulse power upwards from the optimised value at P_{ave}=-3.7 dBm given in Figure 4.11.

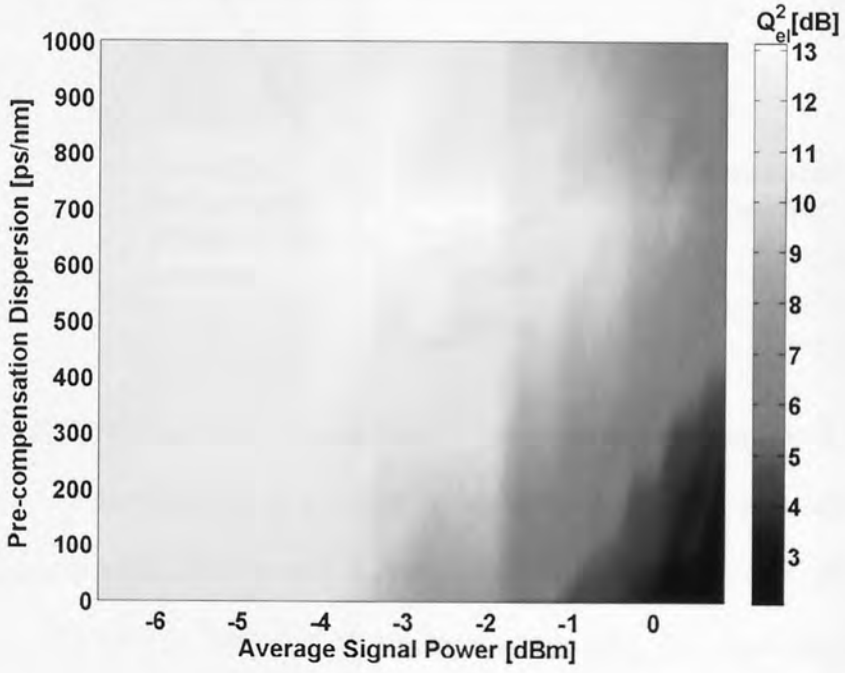

Figure 4.11: Optimisation of Centre Channel (1550 nm) for Undersea Transmission Link at 50% Duty Cycle

Examining Figure 4.11, it is simple to define our region of interest. The optimal transmission is realised when P_{ave} = -3.7 dBm and D_{pre} = 700 ps/nm. We can use such a configuration to state a reference point in accordance with. For P_{ave} < -3.7 dBm, errors are dominated by largely linear effects such as fibre loss, noise and linear dispersion, the performance of such a regime is well studied for RZ-DPSK transmission. For $P_{ave} \geq$ -3.7 dBm, the increase in pulse

power is met with a subsequent increase in nonlinearity [31]. We study the transmission regime at the limit of the boundary of the quasi-linear transmission regime, realising quite different transmission effects due to the increase in nonlinearity. It is clear from that such a transmission regime is at the limit of what would be considered an optimal configuration of the transmission link.

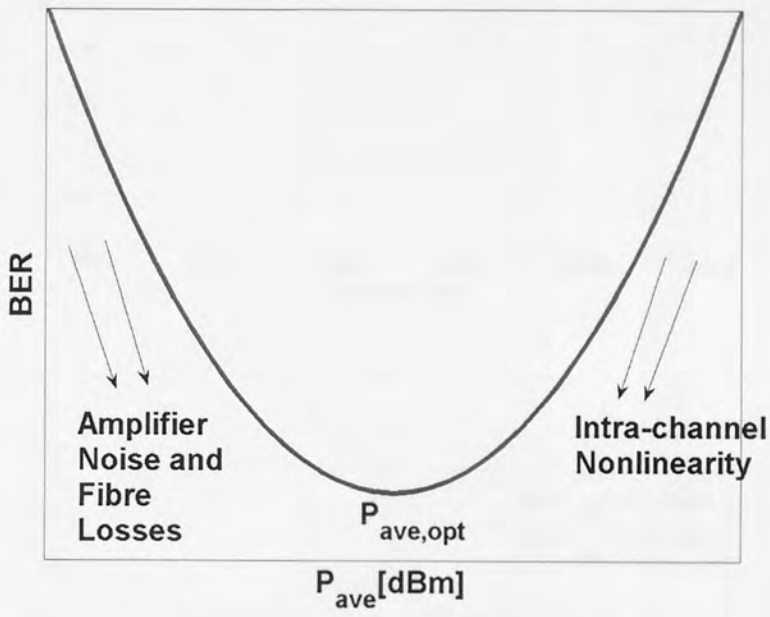

Figure 4.12: Definition of the transmission regime of interest, $P_{ave,opt}$ = -3.7 dBm

It is important to make clear that in our analysis we do not neglect the presence of amplifier noise as a source of errors, but our area of interest, defined in as the region to the right of the optimal P_{ave} at -3.7 dBm is dominated by nonlinear effects [36]. The signal distortion due to such phenomena is dominant in this region as a source of signal degradation, particularly in pseudo-linear transmission [36].

We transmit 30 PRBS random patterns of order 10 (length 1024 bits) within the transmission link depicted in Figure 4.10, we base our analysis on the numerical histograms of the received electrical current. Our simulation of the system at high distance and high pulse average power

allows the emulation of a transmission link heavily afflicted by fibre nonlinearity. We use K, given in (4.26) to investigate the tails of the received current data histogram.

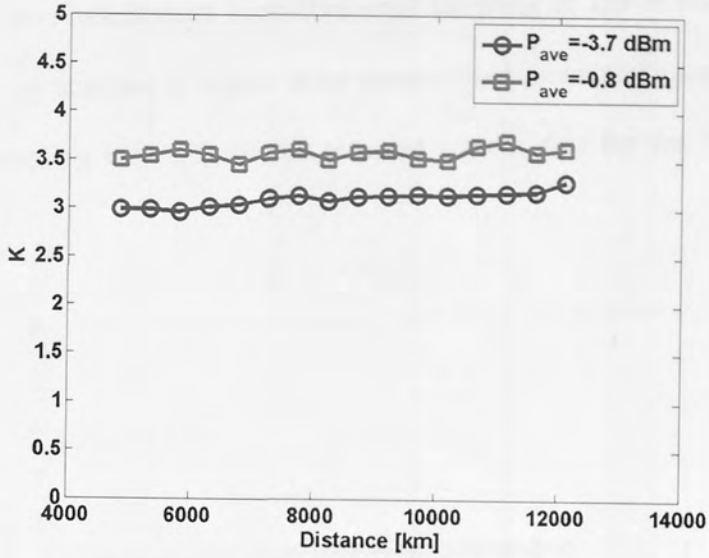

a)

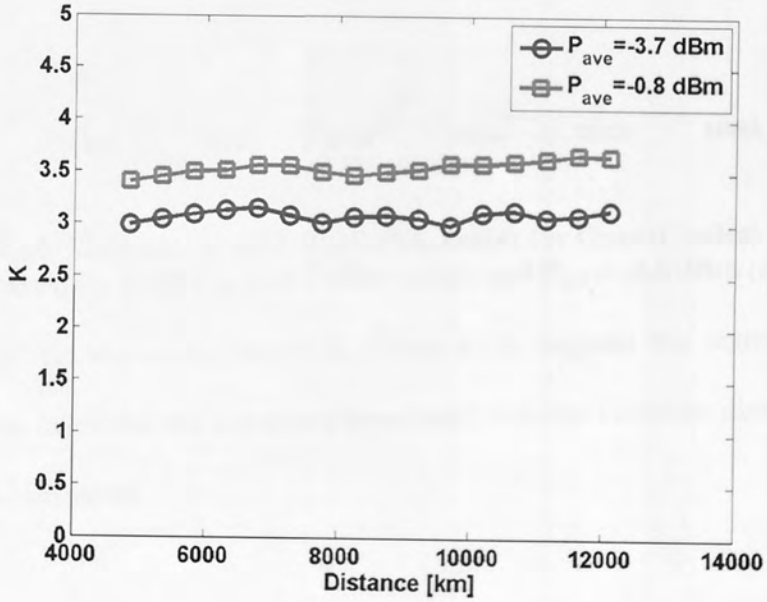

b)

Figure 4.13: Kurtosis of Received Electrical Current at 50% duty cycle for a)Logical Ones and b)Logical Zeros

We see for logical ones, Figure 4.13, an increase in K is recorded for the entire considered distance range at the higher power level for both logical ones and logical zeros. This is

expected due to the increased pulse-to-pulse interaction which occurs as a result of transmission using narrow pulses in the quasi-linear regime. Increased pulse-to-pulse interaction results in non-independent (non-Gaussian) sampling of the received pulses. For brevity, we continue the analysis of higher order standardised moments through the analysis of the skewness, according to (4.27), of the received current data for the two operational regimes in question.

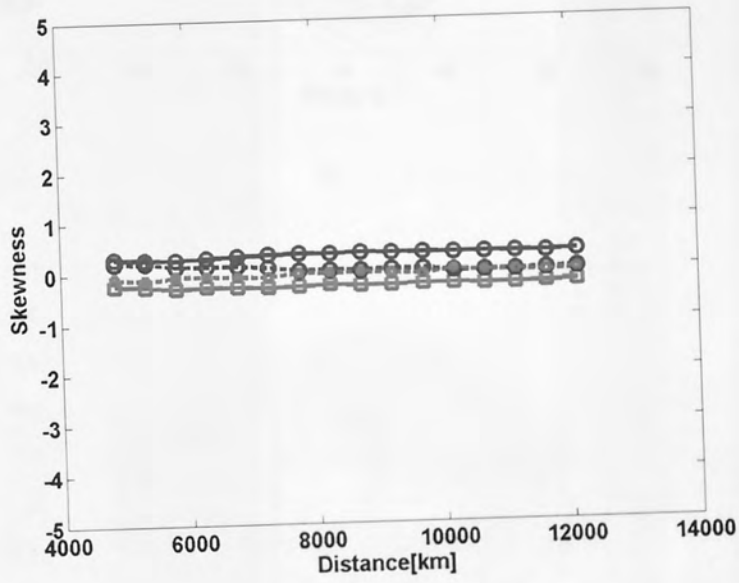

Figure 4.14: Skewness of 50% RZ-DPSK Pulses for Ones (Circles) and Zeros (Squares) for both P_{ave} = -3.7 dBm (solid) and P_{ave} = -0.8 dBm (dashed)

The evolution of the skewness, shown in Figure 4.14, suggests the underlying received current histogram maintains the symmetry associated with the Gaussian distributed channel for both powers considered.

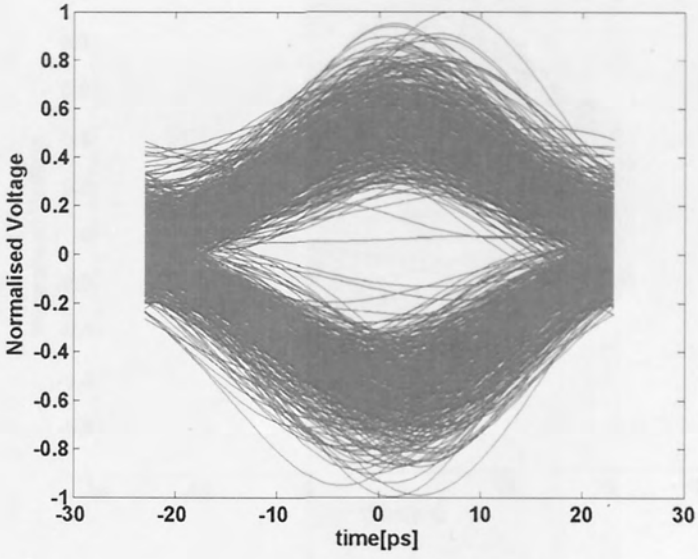

a)

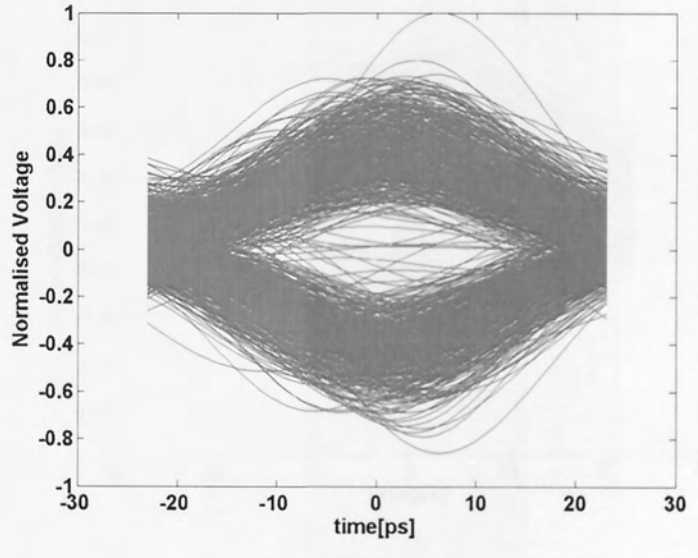

b)

Figure 4.15: Eye Diagrams at 7500 km a) P_{ave} = -3.7 dBm b) P_{ave} = -0.8 dBm

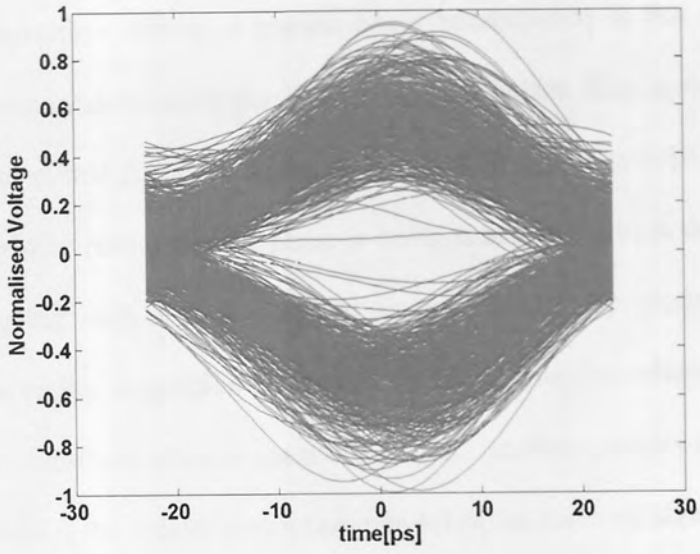

a)

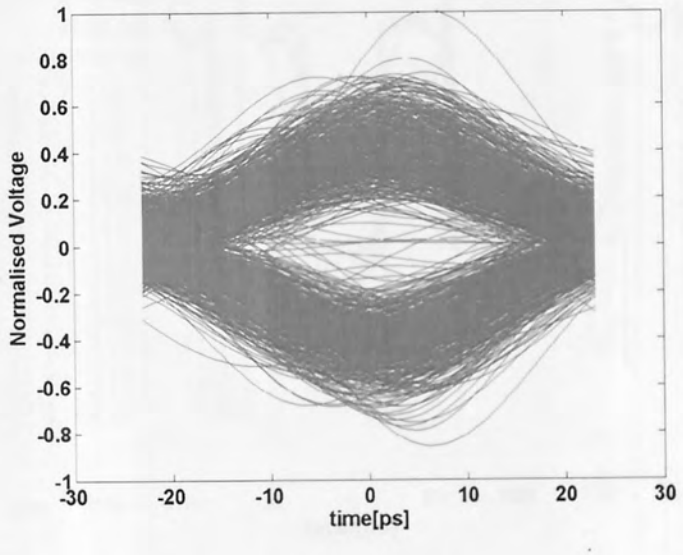

b)

Figure 4.16: Eye Diagrams at 10000 km a) P_{ave} = -3.7 dBm b) P_{ave} = -0.8 dBm

Examining the eye diagrams, Figure 4.15 & Figure 4.16, we see that the transmission dominated, as indicated in, by signal distortion, possibly due to nonlinearity. Studying the eye diagrams, it is clear that the growth of the signal distortion is commensurate with the increase in kurtosis. We can be more conclusive from the study of the optical bit patterns, in particular the important quantity of optical phase.

One of the dominant nonlinear effects in pseudo-linear transmission is that of IXPM, this occurs when the one pulse modulates the phase of its adjacent pulses. This is studied using the optical phase of the transmitted signal as shown in Figure 4.18 & Figure 4.18. The teachings of Figure 4.18 & Figure 4.18 reveal that the phase is being modulated within the transmission, and, the pulses undergoing such distortion appear grouped within the received bit pattern. This would confirm the earlier suggestion that pulses could become dependent on one another when IXPM becomes a dominant effect in the transmission. Another quantity of interest when studying nonlinear effects is the optical power (amplitude) of the received signals.

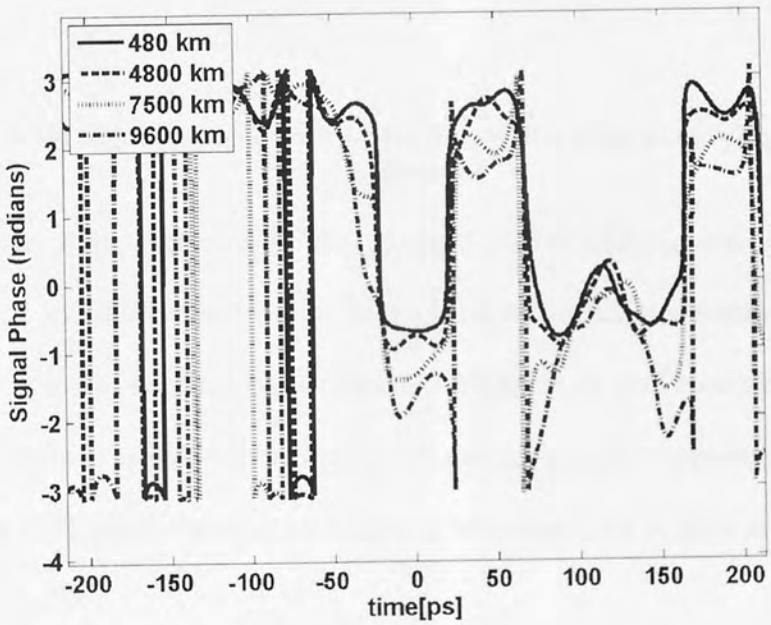

Figure 4.17: Signal phase evolution for P_{ave} = -3.7 dBm at varying transmission distance

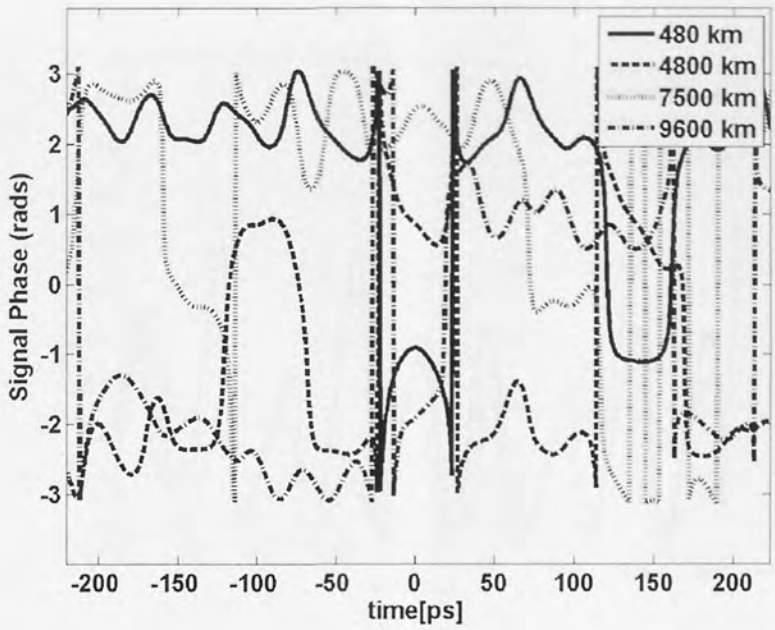

b)

Figure 4.18: Signal phase evolution for P_{ave} = -0.8 dBm at varying transmission distance

We can observe from Figure 4.19, the received signal endures considerable amplitude fluctuations. For RZ-DPSK, as it has no empty bit slots, we cannot automatically say this is due to energy transfer between pulses due to IFWM. It is however clear that excessive amplitude fluctuations appear between pulses of average height, suggesting that IFWM may be at play here [58], particularly as such typical behaviour [36] is clear at the higher power level (P_{ave} = -0.8 dBm).

We can also see that the timing jitter, so evident in the eye diagrams and said to be a result of IXPM in this transmission regime [36], is also evident in Figure 4.19. In addition, close examination of the optical phase and the optical power reveals that both phase and amplitude fluctuations are almost correlated as it occurs within corresponding pulses. This would suggest that amplitude (intensity) and phase modulation are the direct result of each other, further suggesting the presence of IXPM in the transmission, particularly in the high power regime Figure 4.18 & Figure 4.19 b).

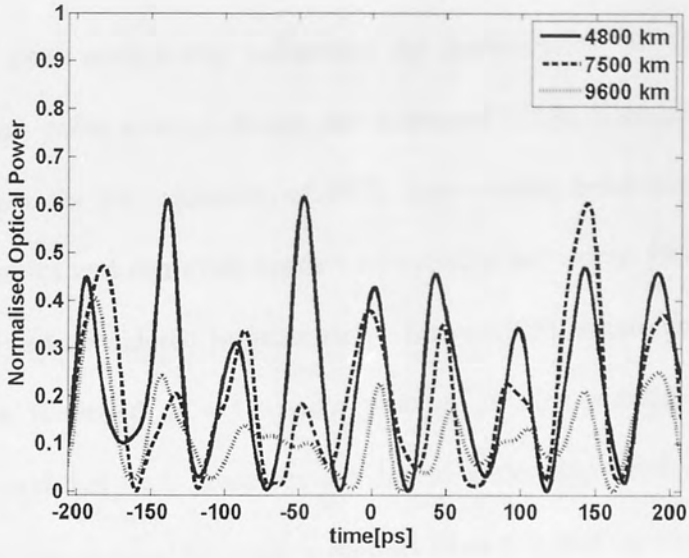

a)

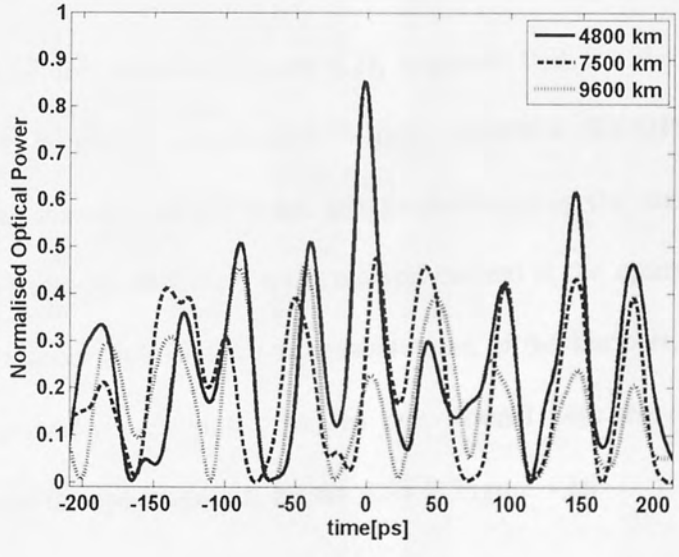

b)

Figure 4.19: Optical power evolution for a)P_{ave} = -3.7 dBm b) P_{ave} = -0.8 dBm at varying transmission distance

Using the analysis of optical phase and optical power (amplitude), we can say with conviction that the leading nonlinear effects in our transmission regime are IXPM and IFWM.

From the study of the evolution of the received optical phase and received optical power, in addition to tracking the evolution of the current statistics for increasing transmission distance, we can say that when fibre nonlinearity influences the transmission (for example when transmission distance and pulse average power are increased [31]), Gaussian statistics no longer become appropriate for the estimation of BER. Lepto-kurtic behaviour demonstrates correlation between samples and can even suggest self-similar behaviour [96]. Problems of this sort have recently been considered in quantitative finance [96], where predicting stock-market behaviour, once modelled as a Gaussian process, is now viewed as 'fat-tailed'. Recently, it was illustrated that such processes are due to underlying nonlinearity between stock prices [96], clearly our physical situation is distinct from this, but the statistical analysis can be viewed in a similar fashion using 'fat-tailed' distributions.

Our previous analysis of the kurtosis (Figure 4.2), suggests that for the transmission in question, there exists a global distribution which describes RZ-DPSK quasi-linear transmission at all pulse powers and distances. It was shown using the measure of kurtosis observed in Figure 4.13 that the distribution of received current at the optimal pulse average power of -3.7 dBm is largely Gaussian. Upon measurement of the kurtosis, it is seen that at higher pulse average power (P_{ave} = -0.8 dBm), is proportional with the increase in signal distortion as witnessed in the eye diagrams, Figure 4.15 & Figure 4.16.

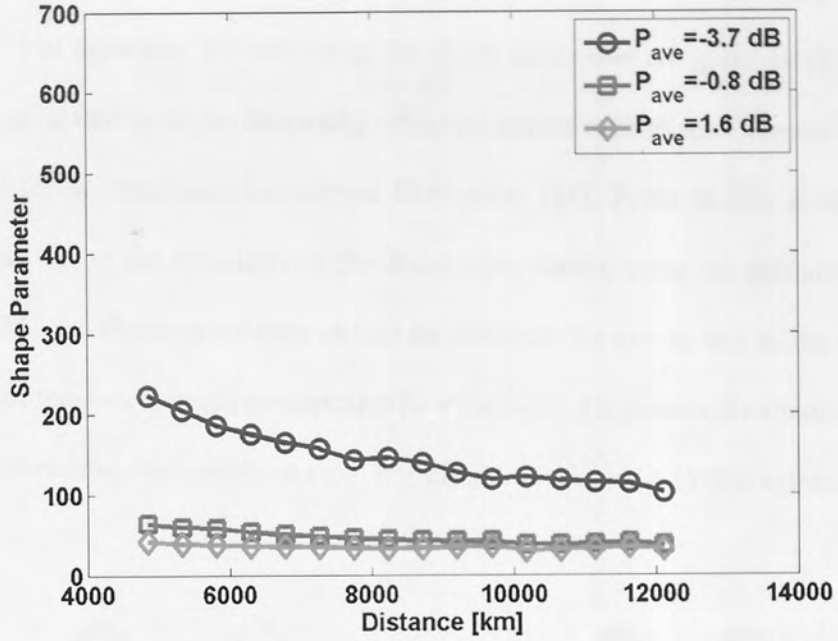

a)

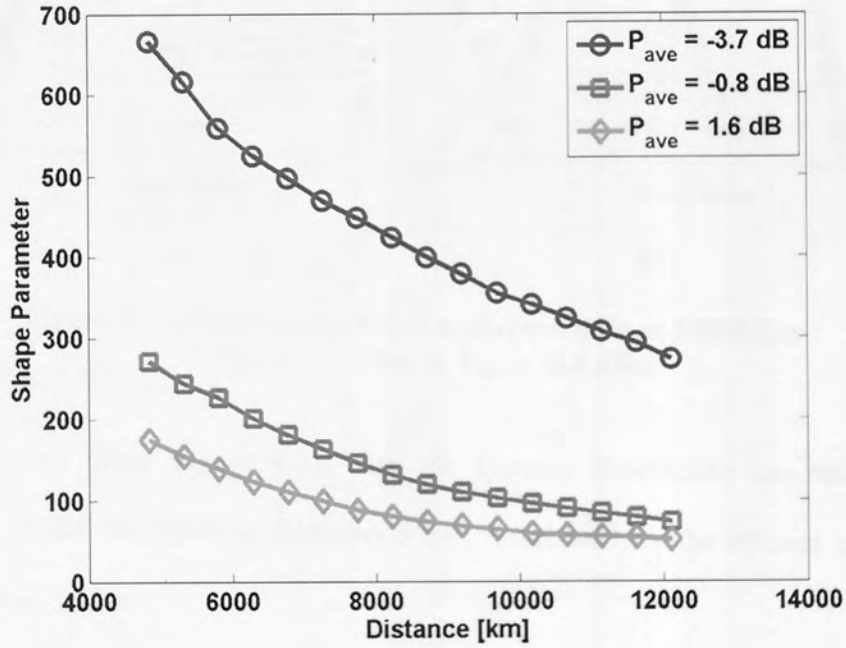

b)

Figure 4.20: Evolution of the shape parameter of the Gamma Distribution a) logical zeros b) logical ones

The fitting of the shape parameter (Figure 4.20) which describes the Gamma distribution confirms such a result as the Gaussian behaviour of the data is characterised by a larger shape

parameter than for the received current data taken for transmission at a higher pulse average power [98]. The equations for estimating the shape parameter are given in (4.36, 4.37), but can also be estimated upon the data using other techniques such as the Generalised Method of Moments [102] or Maximum Likelihood Estimation [98]. From (4.36), it should also be expected that, due to the symmetry of the distribution shown using the measure of skewness in Figure 4.14 , the shape parameters should be identical. As true as this is, the normalisation we execute on the data to avoid numerical difficulties with the gamma distributions render our samples as symmetric, but not about zero. It is clear from Figure 4.21 that symmetry is clearly observed.

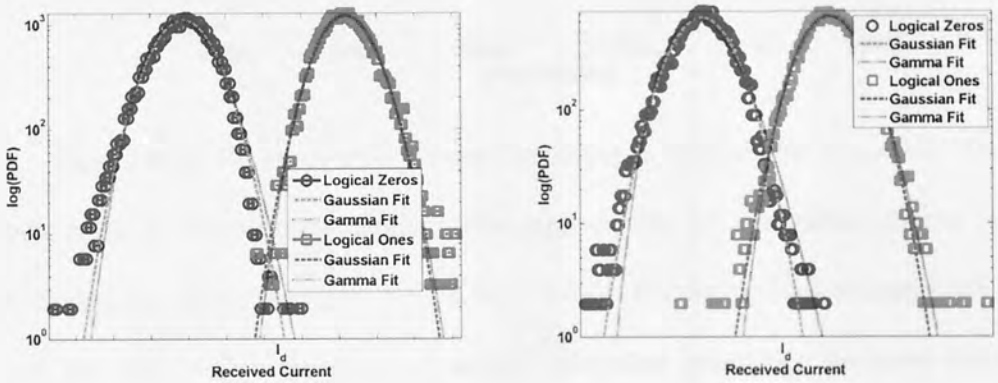

Figure 4.21: Distribution fits of numerical data at 10000 km: P_{ave} = -3.7 dBm b) P_{ave} = -0.8 dBm

We can also see from Figure 4.21, that the Gamma distribution assumes fits both distributions, whilst the Gaussian distribution only holds well for the optimal transmission regime (P_{ave} = -3.7 dBm).

Extensive Numerical Analysis

In a repeat of the initial simulation procedure, we use longer bit sequences (10240 bits) to allow for the realisation of error statistics. We compare the performance of the Gaussian

estimate against the performance of our new Gamma distribution estimate given in (4.43) and statistics taken from direct detection.

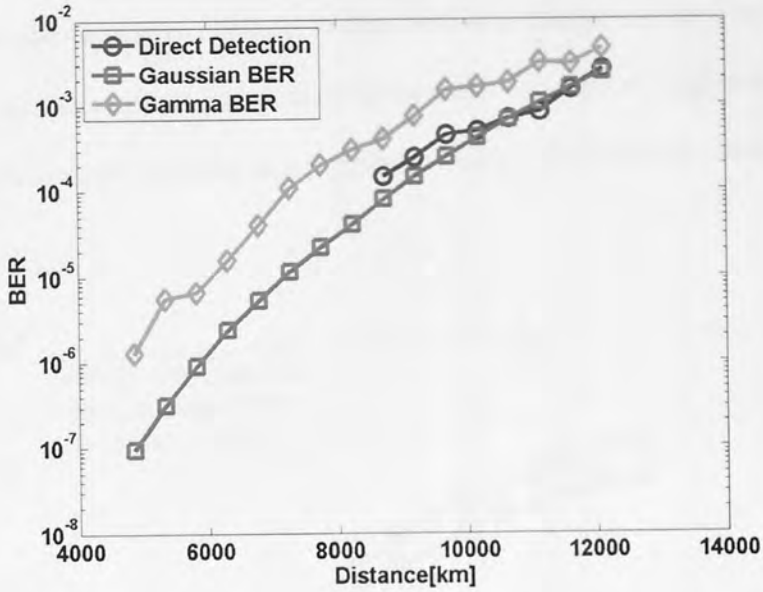

Figure 4.22: Bit error rate versus transmission distance for P_{ave} = -3.7 dBm

The behaviour of the different transmission regimes can be recognised simply from the statistical analysis given in Figure 4.22 & Figure 4.24. For the optimal transmission regime, statistics are largely Gaussian because of the controlled interaction between pulses. The interaction is not large enough to make any impact on statistical calculations of the signal properties. However, when transmission power is increased, pulse-to-pulse interaction grows for all of the transmission distances, which is explains the non-Gaussian statistics at low distances (Figure 4.24 & Figure 4.24).

We demonstrate in Figure 4.13 the dynamic behaviour of the transmission when we venture into the high power regime defined in Figure 4.11. For the optimal power, we see that Gaussian estimation of BER is valid and provides a useful means for estimating what can be computationally very expensive to simulate. We also see that for high powers (Optimal P_{ave} + 3 dBm), the Gaussian distribution fails, providing the necessity for the proposed BER estimation based on the Gamma distribution. The estimate of BER based on the Gamma

distribution accurately predicts BER when the transmission becomes dominated by IFWM and IXPM. We observe that when the dominant fibre nonlinearity influences transmission, the newly proposed BER estimate based on the Gamma distribution performs well. Such an estimate possesses the flexibility required to deal with any changes in the distribution shape due to underlying random effects prevalent in the transmission regime. Higher order moments of the transmission statistics can also be accounted for using the parameter estimates for k and θ.

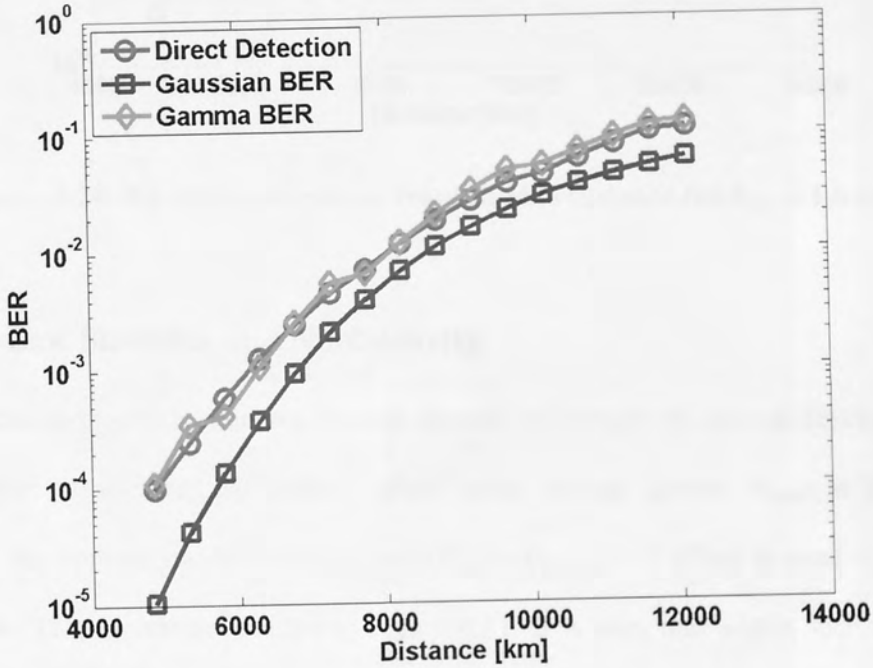

Figure 4.23: Bit error rate versus transmission distance for P_{ave} = -0.8 dBm

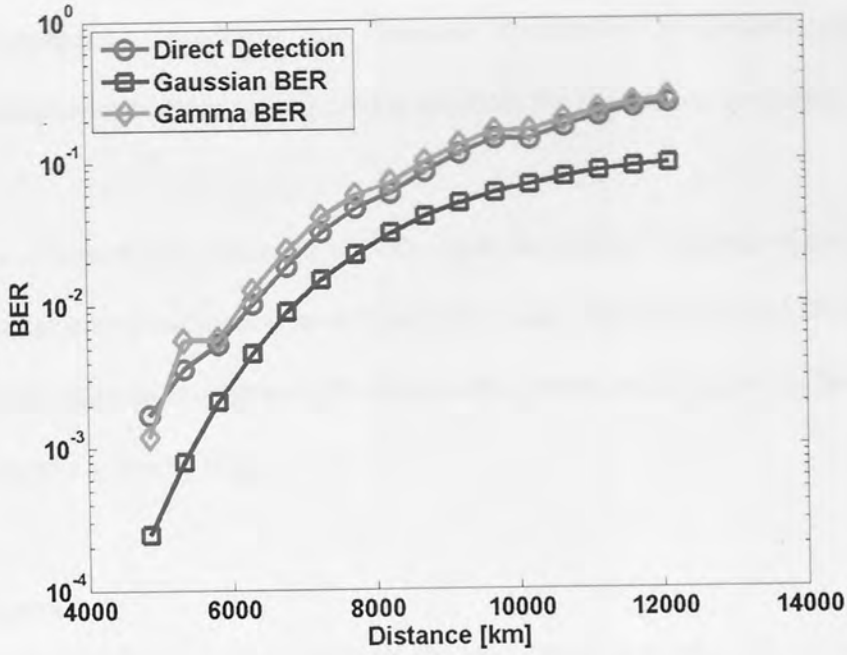

Figure 4.24: Bit error rate versus transmission distance for P_{ave} = 1.6 dBm

4.4 Power-Law Statistics and Nonlinearity

The high distances at which undersea systems operate encourages the natural development of such nonlinear phenomena, particularly when pulse average power (P_{ave}) at the upper boundary of the optimal transmission regime ($P_{ave} = P_{ave,opt} + 3$ dBm) is used to transmit optical pulses. This regime is detailed in Figure 4.11. It is seen that within such a regime, transmission impairments are dominated by such phenomena.

The conventional Gaussian distribution is successful in the quasi-linear regimes [67] because the typical distortions do not result from significant pulse-to-pulse interaction. This renders each pulse statistically independent from one another, thus statistics based on these pulses will naturally tend to the Gaussian distribution due to the Central Limit Theorem.

However, within the nonlinear transmission regime, impairments are dominated by pulse-to-pulse interactions which could result from IXPM or IFWM. Due to the potential impact of

one pulse on another, the sampling of the adjacent pulses cannot be modelled as statistically independent processes – rendering the Gaussian assumption as invalid. Subsequently, alternative statistical procedures are required to estimate the BER in such regimes.

In this work, we study transmission for high P_{ave} and, through the analysis of numerical data, we aim to propose a new estimation model for BER, valid when IFWM and IXPM dominate the source of transmission impairment. We define this transmission regime as the 'nonlinear' transmission regime given by Figure 4.11.

Statistical Theory

As mentioned previously, we can characterise the tail behaviour of any distribution relative to a Gaussian using the simple measure of kurtosis.

We demonstrated that increased nonlinearity manifests in the tails of electrical current distributions, motivating the study of the Gamma distribution and its features. A principle feature of the Gamma distribution is that it is characterised only by shape and scale parameters. We can define all moments in terms of these parameters and the introduction of new physical effects, possibly due to narrower pulses, will not hinder the validity of the model. However, a constraint of that study was the included description of the optimal transmission regime. In this section we study the purely nonlinear regime, where pulse-to-pulse interaction, likely due to IXPM and IFWM, will wholly dominate the transmission statistics.

Distributions exhibiting 'fat-tailed' behaviour model underlying quantities that are prone to high variation, such as extreme weather [97] or stock-market behaviour [96]. In this work, we are not concerned with the optimal transmission regime, we are only concerned with

transmission dominated by pulse-to-pulse interaction(s). To this end, we must follow [96] in the consideration of a power-law distribution to model our underlying data. The beta distribution is an example of such a distribution. Its probability density function is given in (4.44) and the cumulative density function is given in (4.45) [98]:

$$f(y;\alpha,\beta) = \frac{(1-y)^{\alpha-1} y^{\beta-1}}{B(\alpha,\beta)} \tag{4.44}$$

$$P(Y < y) = I_y(\alpha,\beta) \tag{4.45}$$

Where α and β are shape parameters and the function $I_y(\alpha,\beta)$ is the regularized Beta function defined below;

$$I_y(\alpha,\beta) = \frac{B_y(\alpha,\beta)}{B(\alpha,\beta)} \tag{4.46}$$

Where $B(\alpha,\beta)$ is the beta function and $B_y(\alpha,\beta)$ is the incomplete beta function, defined by the following integrals;

$$B(\alpha,\beta) = \int_0^\infty (1-t)^{\beta-1} t^{\alpha-1} dt \tag{4.47}$$

$$B_y(\alpha,\beta) = \int_0^x (1-t)^{\beta-1} t^{\alpha-1} dt \tag{4.48}$$

Dependency of a distribution on shape parameters is a useful feature for our analysis. The conventional Gaussian assumption, which holds for quasi-linear transmission in the optimal transmission configuration [72], is constrained by symmetry and exponential tail behaviour. The use of power-law distributions such as the beta distribution removes this condition and could also be extended to the modelling of other physical phenomena manifesting within the transmission media. Simple estimation of the parameters α and β is obtainable using the method of moments

$$E[y] = \frac{\alpha}{\alpha+\beta} \tag{4.49}$$

$$Var[y] = \frac{\alpha\beta}{(\alpha+\beta)^2(\alpha+\beta+1)} \tag{4.50}$$

We can use equations 4.49 and 4.50 to derive estimates for the values of α and β most appropriate for the data. The two equations form a system of nonlinear algebraic equations in the two shape parameters, the system is easily soluble using conventional algebra. We set $\mu = E[y]$ and $\sigma^2 = Var[y]$, manipulating (4.49) and (4.50) we obtain;

$$\alpha = \frac{\mu\sigma^2}{1-\sigma^2+\mu} \tag{4.51}$$

$$\beta = (\frac{1}{\mu} - 1)\frac{\mu\sigma^2}{(1-\sigma^2+\mu)} \tag{4.52}$$

It is also possible to use Maximum Likelihood Estimation (MLE) to obtain values for these parameters. Using the values of α and β obtained for the logical ones and zeros, we can evaluate the Bit Error Rate from the average probability of an error in the logical ones and the average probability of an error in the logical zeros. We denote the probability of an error in the ones by BER_1 and the probability of an error in the zeros by BER_0, where:

$$BER_0 = \int_{I_d}^{\infty} P_o(y_0;\alpha_0,\beta_0)dy_0 \tag{4.53}$$

$$BER_1 = \int_{-\infty}^{I_d} P_1(y_1;\alpha_1,\beta_1)dy_1 \tag{4.54}$$

Where y denotes the average current for the logical ones and zeros (denoted by subscript) defined by the integral;

$$y = \frac{1}{T}\int_0^T I(t)dt \tag{4.55}$$

Where α and β denote the respective shape parameters, I_d is some current threshold value and $P(y;\alpha,\beta)$ is the probability density function describing a beta distributed random

variable (given by (4.44)). We echo the approach of [99] in our derivation of the expression for BER.

$$BER = \frac{1}{2}(BER_1 + BER_0) \tag{4.56}$$

From the expression (4.56), we can estimate the BER. We know from any standard mathematical statistics [98] text that we can define BER_0 equivalently as:

$$BER_0 = \int_{I_d}^{\infty} P_0(y_0;\alpha_0,\beta_0)dy_0 = 1 - \int_{-\infty}^{I_d} P_0(y_0;\alpha_0,\beta_0) \tag{4.57}$$

The integrals in (4.53) and (4.57) are nothing more than the cumulative density functions of the beta distributed random variable which we have already given in (4.45) as:

$$P(y < I_d) = I_{I_d}(\alpha,\beta) \tag{4.58}$$

Therefore from (4.56), we can say that the BER can be estimated as:

$$BER = \frac{1}{2}(1 - I_{I_d}(\alpha_0,\beta_0) + I_{I_d}(\alpha_1,\beta_1)) \tag{4.59}$$

Numerical Analysis

Again taking the electrical current at the receiver stage and collating the electrical current data, we use (4.26) to calculate the kurtosis of the electrical current for some increasing transmission distance. We have already seen (pg. 121) that the configuration is shown to perform optimally at P_{ave} = -3.7 dBm and D_{pre} = 700 ps/nm. We increase P_{ave} beyond the optimal P_{ave} at -3.7 dBm and consider transmission at P_{ave} = -0.8 dBm and 1.6 dBm in order to realise the 'nonlinear' regime detailed in Figure 4.11.

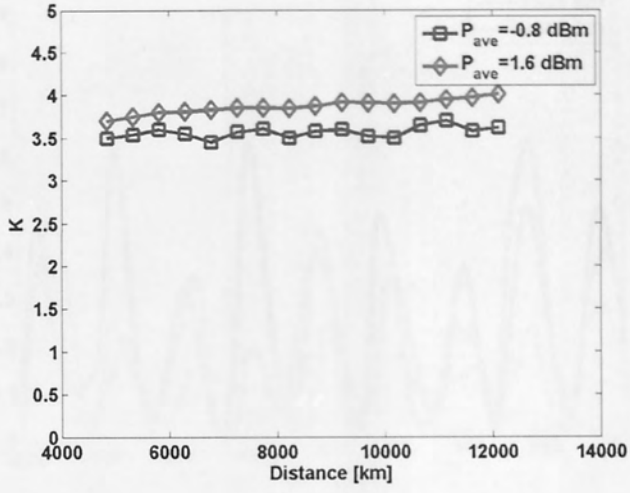

a)

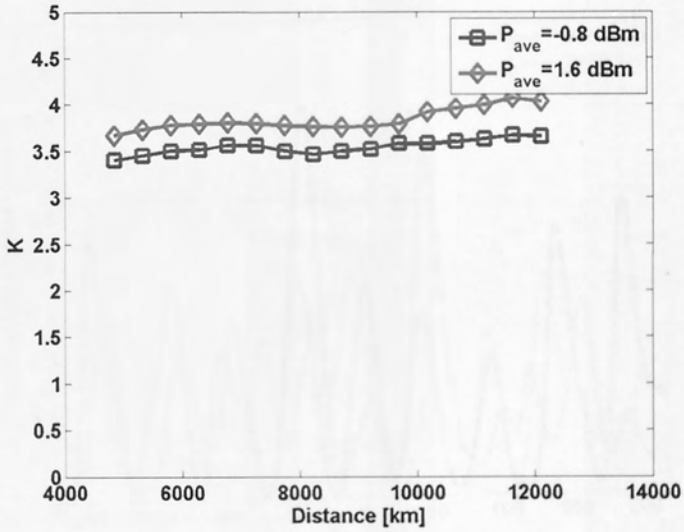

b)

Figure 4.25: Kurtosis for a) Logical Ones and b) Logical Zeros at 50% duty cycle versus transmission distance

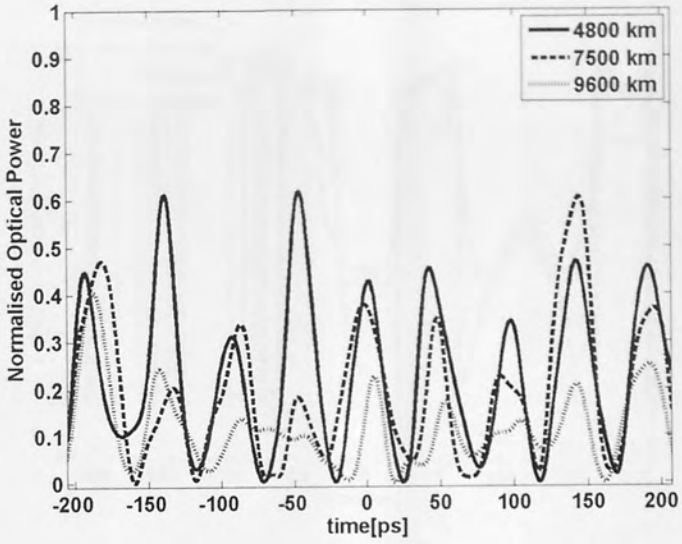

a)

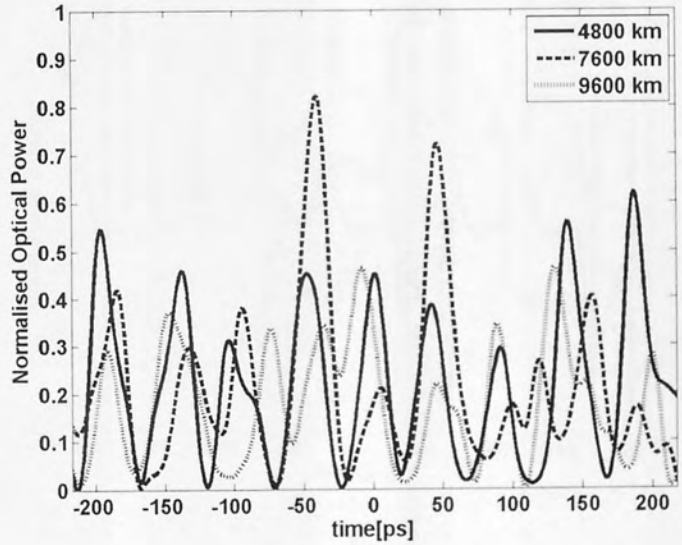

b)

Figure 4.26: Optical power evolution at increasing distance a) P_{ave} = -0.8 dBm b) P_{ave}= 1.6 dBm

We see from Figure 4.25 that kurtosis increases for higher $P_{ave,}$ this is expected due to the increasing significance of pulse-to-pulse interactions within the transmission. IXPM and IFWM manifest themselves in the tails of the underlying current distribution due to the high variations in electrical current they create (Figure 4.19).

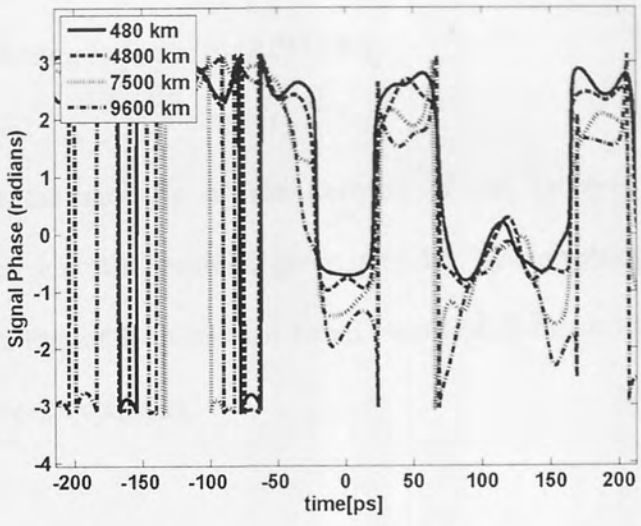

a)

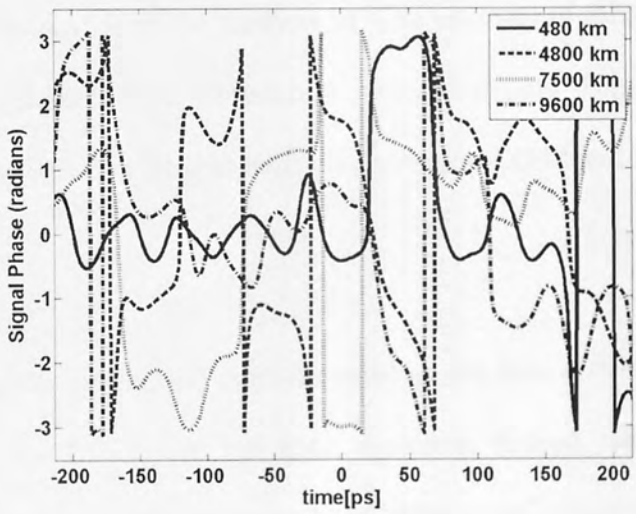

b)

Figure 4.27: Optical phase evolution for increasing distance
a)P_{ave} =-0.8 dBm b) P_{ave} = 1.6 dBm

When we increase the pulse average power at the launch stage, we see, from Figure 4.26, that we witness more extreme power (amplitude) fluctuations and also an increase in phase modulation. This is a very good indicator that the transmission impairment in the channel is indeed dominated, as predicted from [36] by IXPM and IFWM. The extreme variations in

electrical current causing the 'fat-tailed' behaviour are as a result of the amplitude fluctuations due to IFWM [36] and timing jitter due to IXPM [36].

Next, following from the analysis of the kurtosis of the received electrical current distributions, we test the new BER estimate given in (4.59), by comparing its performance in the nonlinear regime to that of the Gaussian based electrical Q-factor estimate [66] and the BER taken using direct error counting.

In the vein of the initial simulations, we repeat the simulations using longer bit sequences (10240 bits). We observe from Figure 4.28 that for the 'nonlinear' regime, the Gaussian estimate fails, as is predicted from the analysis in. The estimate of BER based on the Beta distribution accurately predicts BER for this high powered regime. This provides a basis for the future statistical analysis of nonlinear transmission where IXPM and IFWM become more significant.

We see that for high pulse power, the estimate based on the beta distribution performs well, accurately predicting the BER given by direct detection. Indeed, we are limited by our computational power to the reliable computation of BERs at 10^{-4}, however, from these results (Figure 4.28), we can extrapolate the conclusion that for nonlinear transmission, estimates based on the Beta distribution perform effectively compared to the standard Gaussian estimate.

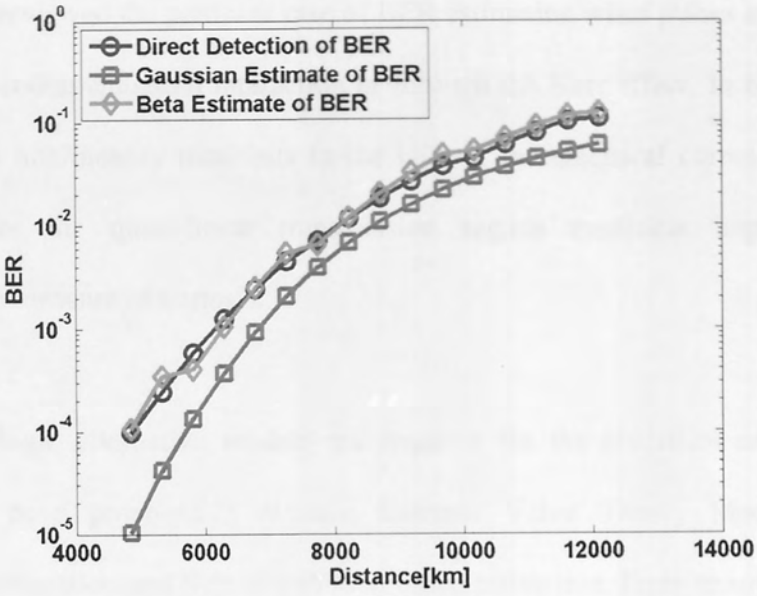

a)

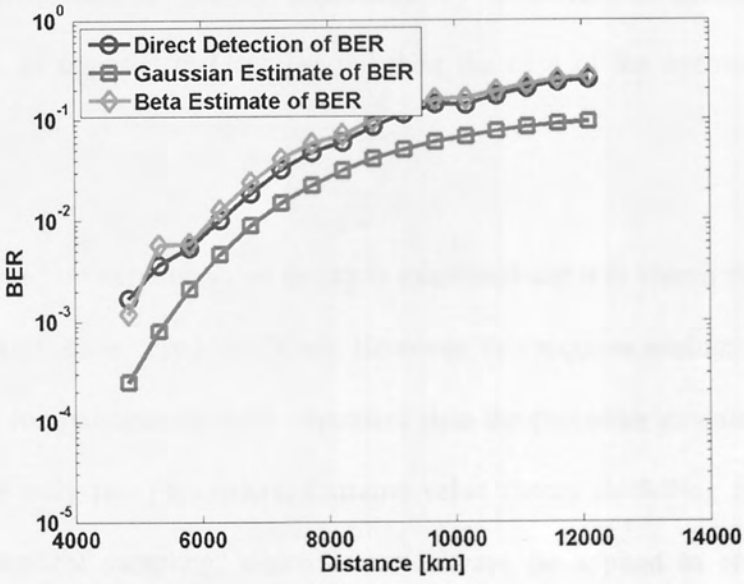

b)

Figure 4.28: BER evolution versus transmission distance
a) P_{ave} = -0.8 dBm b) P_{ave} = 1.6 dBm

4.5 Conclusions

In this chapter, we reviewed the pertinent case of BER estimation when pulses are interacting, either through dispersion enhanced interaction or through the Kerr effect. In both cases, we have observed that nonlinearity manifests in the tails of the electrical current distribution, suggesting that for the quasi-linear transmission regime nonlinear impairments are characterised by the measure of kurtosis.

When kurtosis is high, alternative models are required for the statistical analysis of the transmission. We have proposed 3 models; Extreme Value Theory Models, Gamma distribution based estimation and Beta distribution based estimation. From examination of the three models we can make some observations, the tails of the distribution within transmission regimes whose performance is heavily influenced by intra-channel nonlinearity are at exponentially tailed, as opposed to Gaussian tailed in the case of the optimal quasi-linear regime.

Firstly, modelling based on extreme value theory is examined and it is shown that we can use these models when kurtosis is very high (K>4). However, this requires evaluation of 3 fitting parameters which is computationally more expensive than the two other models, as they only require the fitting of only two parameters. Extreme value theory modelling is also heavily dependent on independent sampling, which cannot always be applied to channels where pulses are interacting.

The other two models offer solutions which are more flexible in terms of both BER prediction and their robustness to other effects. We proposed an estimate based on the Gamma distribution, this is a flexible distribution which doesn't depend on channel symmetry or distributive symmetry. The shape characterisation allow it to be considered for more complex

nonlinearity that could be introduced when pulses become narrower, such as 40 Gb/s upgrades or even 80 Gb/s upgrades. Gamma distributed statistics also become Gaussian distributed as a limiting case. The two parameters characterising the Gamma distribution are also simple and quick to evaluate based on the electrical current data.

We also explored the prospect of BER estimation using the power-law distribution for the final part of the chapter. If the tails of a distribution are high, then their tails can be approximated using a polynomial. Following this sentiment, we derive an estimate for BER based on the Beta distribution, an example of a power-law distribution. We see that this estimate accurately predicts BER for transmission regimes where intra-channel nonlinearity dominates the transmission. However, the Beta distribution only works as a mathematical curiousity and its practicality is limited due to its nature as a power-law distribution.

In the last two chapters we have managed to draw conclusions about the potential upgrade of 10 Gb/s undersea transmission using the incumbent RZ-OOK data format to a 20 Gb/s undersea transmission link using the newly proposed RZ-DPSK data format. We feel secure in the knowledge that the upgrade can take place. However, the story is not over. The ultimate challenge will be to go to 40 Gb/s RZ-DPSK channels transmitting over an undersea transmission link.

We now return to the transmission of RZ-OOK transmission at high capacity, 40 Gb/s. Again we straddle the quasi-linear transmission regime to explore the impact of nonlinearity on statistics.

Chapter 5 : Eye Closure in Amplitude Noise Dominated Transmission: A Statistical Approach

5.1 Review

Our previous analysis has been characterised by a strict investigation into the potential of RZ-DPSK transmission systems due to its promise as an upgrade technology for legacy undersea transmission systems due to the 3-dB improvement in receiver sensitivity and improvements in nonlinear tolerance [58].

However, upgrades to 40 Gb/s transmission from the legacy 10 Gb/s transmission have proved difficult due to the growth of inline nonlinearity and PMD over the large distances considered [50]. This is why we considered only 20 Gb/s RZ-DPSK transmission thus far in this thesis.

The adoption of narrower pulses in order to increase the bit rate of transmission systems naturally decreases the nonlinear and dispersion tolerance of transmission systems, particularly over large distances where Kerr nonlinearity and dispersion are a particular problem [32]. Using the quasi-linear regime introduces the dominant Kerr based effects such as IXPM and IFWM into the transmission. They manifest as timing jitter and amplitude fluctuations respectively.

The upgrade of RZ-OOK to RZ-DPSK transmission requires a means of comparing the performance of the two data formats in terms of the nonlinear signal distortion. Fibre nonlinearity within pseudo-linear transmission of RZ-OOK and RZ-DPSK pulses is dominated by Intra-channel Four-Wave Mixing (IFWM) [36, 37], leading to eye closure due to amplitude fluctuations of logical ones and ghost pulses generated within logical zeros [36].

The penalty due to such nonlinearity is of great interest due to such systems being in demand in accordance with growing requirements for capacity and increased bit-rate.

The numerical modelling of such complex lightwave communication systems is an effective and well-used tool for design and performance evaluation. While accurate, this type of simulation can also be lengthy and computationally expensive for modern fibre-optic communication links, which comprise a number of components using a variety of modulation formats and operational regimes. For this reason, it is sometimes desirable to obtain estimates of the effects of impairments that cause signal degradation by the relatively simple evaluation of the eye closure (EC) in the signal eye diagram [103].

The effects of impairments that can be assessed by propagation of optical channels without noise such as fibre dispersion or without any actual propagation distance at all such as optical filtering have been studied with simulation and analysis in the recent past by evaluation of the eye-closure penalty (ECP) [103]. In most cases, the results have been related to the Q-factor penalty or the power penalty [78]. Analytical or semi-analytical results for the system performance evaluation are of great importance even if they are derived based on simplified models. In this paper, we present a simple theoretical method for the estimation of the expected ECP for signals whose quality is mainly deteriorated by the amplitude noise accumulated during transmission due to IFWM [36].

5.2 Theoretical Model

We begin by noting the definition for EC. Supposing the centre of the bit slot is the location of maximum pulse amplitude, an appropriate measure of EC is provided by the difference between the innermost rails of the signal electrical eye diagram [42]:

$$EC = \min[V_1] - \max[V_0] \qquad (5.1)$$

Where min[V_1] is the voltage level of the minimum "ones" rail at the eye centre, and max[V_0] is the voltage level of the maximum "zeros" rail.

Let us assume now a Gaussian shape for the received-voltage distributions of the "ones" and "zeros", an approximation that usually works relatively well in communication systems using the conventional ASK modulation format [71]. We can then use simple rules governing the extrema of Gaussian distributed samples to derive an upper bound for the EC. We know, from analytical computation of the 99-percentiles of a Gaussian random variable [98], that the following inequalities exist;

$$\min[V_1] \leq E[V_1] - 3\sigma_{V_1} \tag{5.2}$$

$$\max[V_0] \geq E[V_0] + 3\sigma_{V_0} \tag{5.3}$$

Where E[V_1] & E[V_0] and σ_{V_1} & σ_{V_0} are the average voltage and the standard deviation of the "ones" and "zeros" distributions, respectively. Thus, it is straightforward to write:

$$EC \leq E[V_1] - E[V_0] - 3(\sigma_{V_1} + \sigma_{V_0}). \tag{5.4}$$

The ECP can then be calculated as the ratio of the EC before transmission to this quantity after transmission [71]:

$$ECP = 10\log_{10}(EC_{in} / EC_{out}). \tag{5.5}$$

An example of a degraded eye signal is given by Figure 5.1. Note that the validity of the derived EC estimate for general signal degradation primarily rests on the assumption that the signal eye is closed symmetrically from the top and bottom. Thus, the effects of timing jitter and of waveform distortions such as those originated from strong inter-symbol interference (ISI) and inter-channel crosstalk of wavelength-division multiplexed systems cannot be accounted for by the underlying model. The model has potential applicability in ASK systems when the dominant source of signal degradation is amplitude noise.

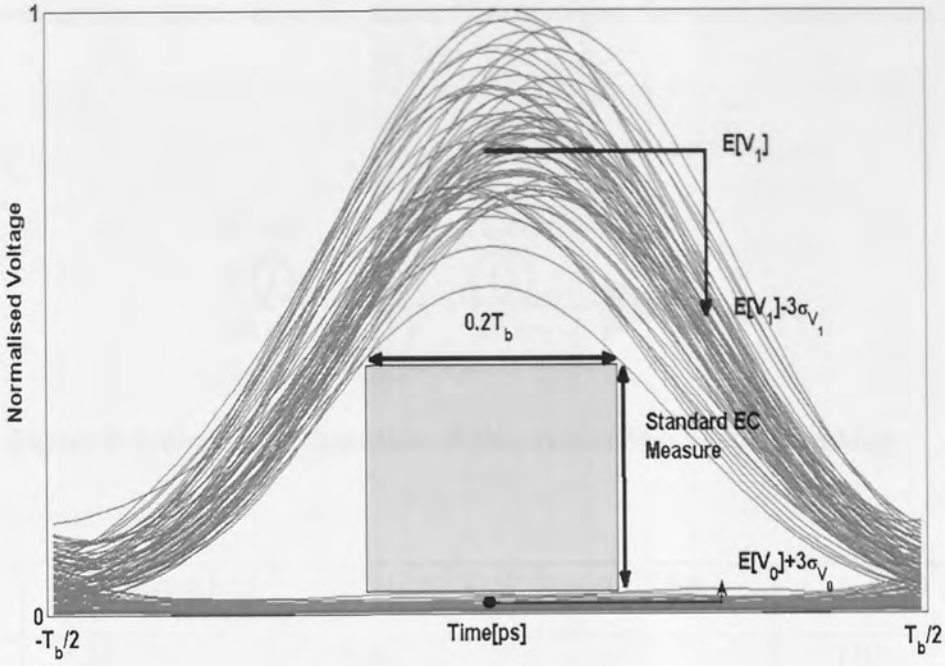

Figure 5.1: Example of a degraded signal electrical eye diagram and eye closure estimate

The EC is measured as the height of the rectangle of the largest area with a base of 0.2 T_b (T_b is the bit period) that can be fitted within the open portion of the eye [42]. This rectangle is not the largest We compare this definition with our estimate given in (5.4).

5.3 Numerical Model

In this work, the viability of the proposed theoretical model for signal degradation mainly caused by amplitude noise is evaluated with numerical simulation of of single-channel RZ-ASK signal transmission at 40 Gbit/s bit rate in a typical dispersion-managed, terrestrial link[11], therefore operating a quasi-linear transmission regime. We use the SSFM algorithim to model optical pulse propagation.

In the considered system, each amplifier span consists of 20km effective core area enlarged positive dispersion fibre and negative dispersion fibre sections. The fibre parameters are given below;

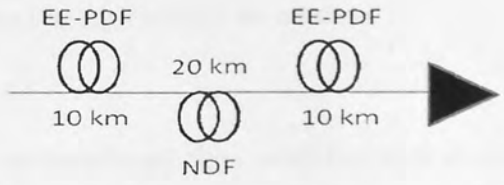

Figure 5.2: Graphical Depiction of Dispersion-Managed Fibre Map

	D [ps/nm km]	S [ps/nm^2 km]	α[dB/km]	A_{eff}[μm^2]
EE-PDF	20	0.06	0.2	110
NDF	-20	-0.06	0.24	30

Table 5.1: Fibre Parameters

Clearly, the dispersion map is designed in such a way that $D_{ave} = 0$. This arrangement is an example of a D+/D-/D+ arrangement, with the D- fibre having smaller effective core area (thus higher nonlinearity), thus more nonlinear distortion is generated in the D- section. This arrangement is familiar in wideband transmission systems [104].

We aim to realise a transmission regime which is dominated by IFWM, this is done via the use of the NDF section, the low A_{eff} will allow the inherent dispersion in the fibre section to mix and combine with the change in fibre refractive index and instigate pulse-to-pulse interaction. The pulse-to-pulse interaction will transfer energy between pulses and create amplitude fluctuations in the logical ones and generate noise in the logical zeros.

At longer distances, intra-channel cross-phase modulation will also manifest as timing jitter due to the long term change in the fibre refractive index. This will invalidate the model as we base our model on symmetric eye closure. Although this is a declaration of the limitations of our model, it is also interesting as it allows us to study the statistics of timing jitter in RZ-OOK transmission with respect to the statistics we assume.

Each span also includes an erbium-doped fibre amplifier with a noise figure of 4.5 dB with the gain configured to compensate for the energy losses in the previous fibre section. Simulations are performed here for pseudo-random data sequences (PRBS) of $(2^7\text{-}1)$ length formed with Gaussian pulses. The standard pulse duty cycles of 33%, 50%, and 67% are employed and the pulses are carved with infinite extinction ratio.

A fifth-order Bessel filter with a cut-off frequency equal to the bit rate is used as a receiver low-pass filter. The results are averaged over a number of bit patterns to obtain accurate statistics of the in-line amplifier noise. The transmission performance of the system is degraded by both intra-channel nonlinear interactions-induced amplitude noise and timing jitter [11]. This presents a good model situation to evaluate the validity and illustrate the limits of the proposed methodology.

5.4 Performance of Estimate

Shown in Figure 5.3, Figure 5.4 & Figure 5.5 is the evolution of the estimated ECP versus the transmission distance. The results of the approach commonly used for numerical simulations, where the EC is measured as the height of the rectangle of the largest area with a base of 0.2 T_b (T_b is the bit period) that can be fitted within the open portion of the eye [42] (see Figure 5.1), are shown in Figure 5.3, Figure 5.4 & Figure 5.5. The 1-dB level of ECP corresponds to to a shrinking of the initial eye-opening by 25%.

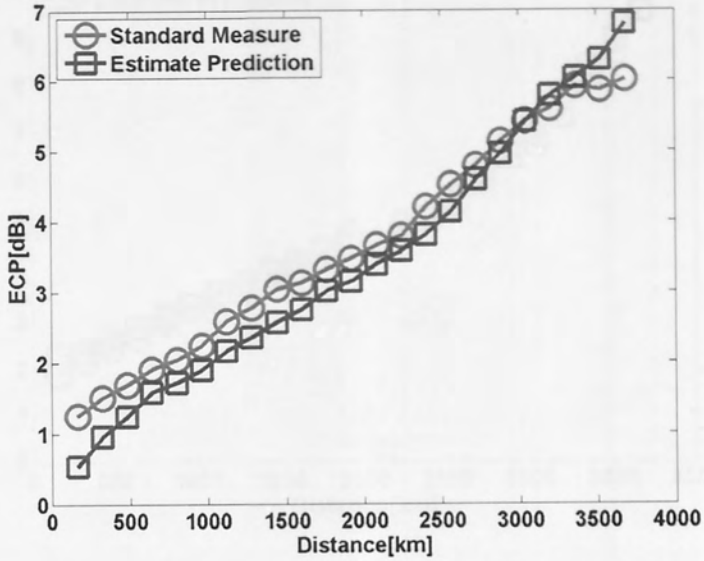

Figure 5.3: Eye-closure penalty versus distance for 40 Gbit/s RZ-ASK at 33% duty cycle

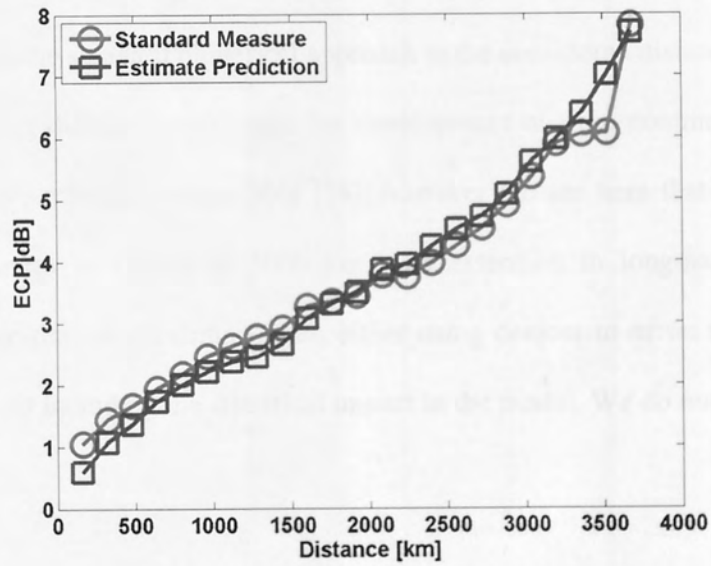

Figure 5.4: Eye-closure penalty versus distance for 40 Gbit/s RZ-ASK at 50% duty cycle

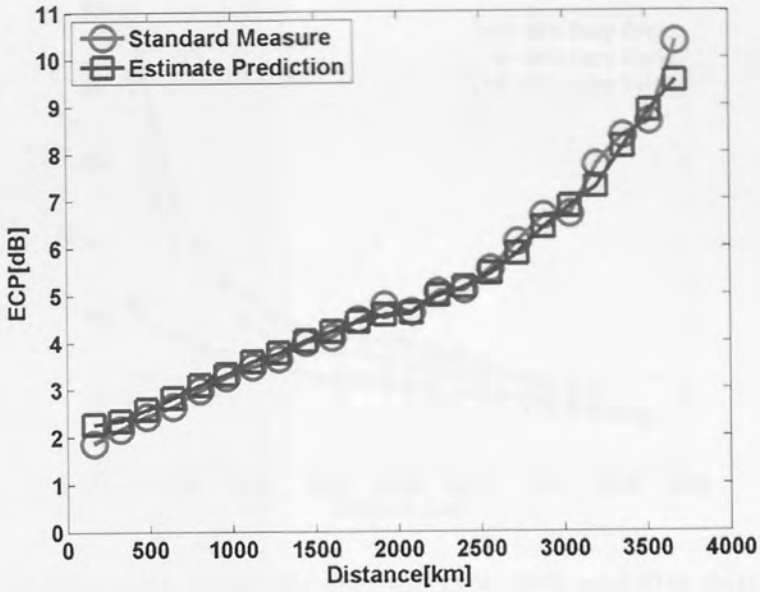

Figure 5.5: Eye-closure penalty versus distance for 40 Gbit/s RZ-ASK at 67% duty cycle

We can see that there is good agreement between the model predictions of ECP and the results obtained from the standard numerical approach at the considered distances for all pulse duty cycles. Growing distance encourages the development of fibre nonlinearity, of which RZ-OOK pulses are particularly vulnerable [58], however we see here that our estimate is valid even at distances in excess of 3000 km. The extension to long-haul transmission requires the consideration of the timing jitter, either using devices to offset the influence of timing jitter [11] or by including the statistical impact in the model. We do not consider either in this work.

One of the aims of this section was to derive an estimate of ECP for transmission regimes, dominated by amplitude noise, in high Q-factor regimes where generating signal distortions in numerical models is computationally expensive. We detail the evolution of Q-factor for all three duty cycles in Figure 5.6:

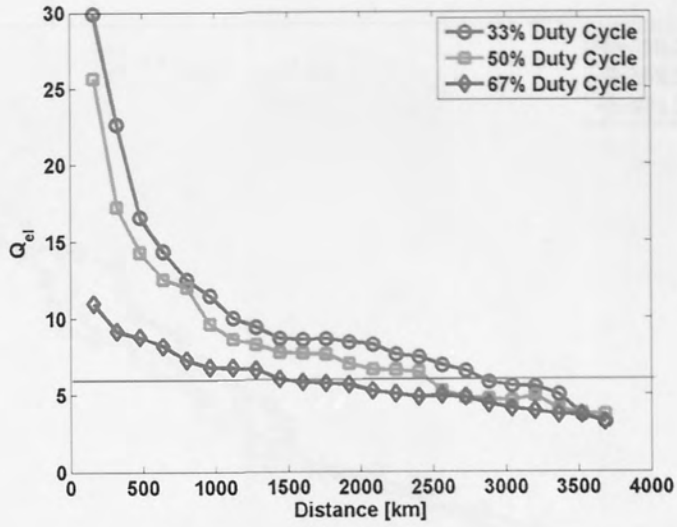

Figure 5.6: Q_{el} evolution versus distance for 33%, 50% and 67% duty cycles with Q_{el} = 6 as a reference

Comparing Figure 5.3, Figure 5.4 and Figure 5.5 with Figure 5.6, it is easy to see that part of our initial objective is achieved. Our estimate allows the prediction of signal distortion for high Q-factor transmission. From Figure 5.6, we can also extend the conclusions of [77]. In this paper, it is suggested that there is a relationship between Q-penalty and ECP, and in various limits this relationship is derived. A Gaussian approximation is shown to provide a useful estimator of Q-penalty in terms of ECP for RZ transmission. In [77], it is easily inferred that Q-factor is directly proportional to ECP, and we demonstrate this below;

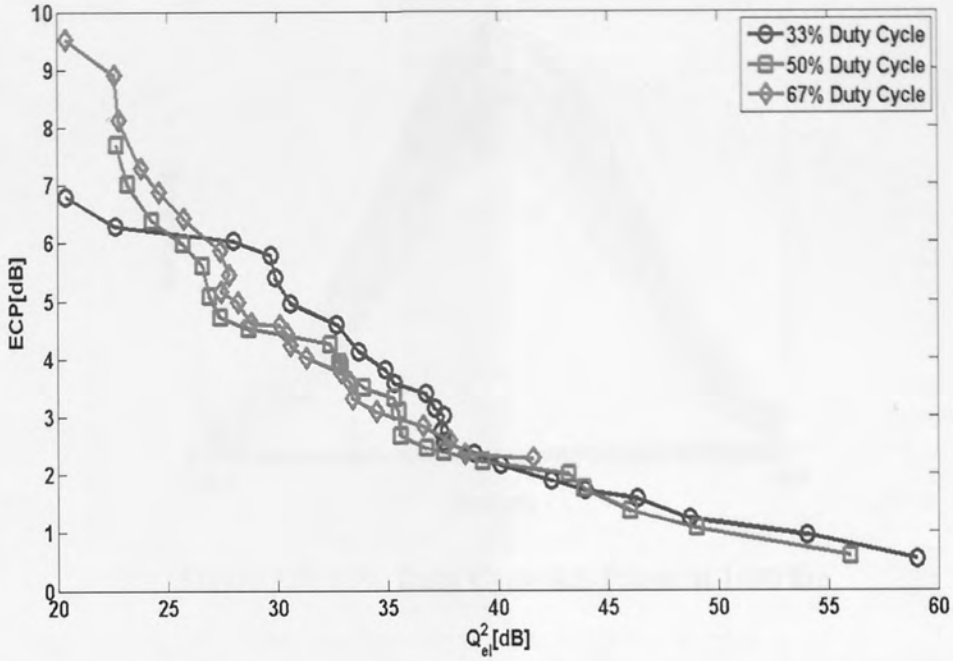

Figure 5.7: Evolution of ECP against Q^2_{el} for 40 Gb/s RZ-OOK Transmission

We can see, from Figure 5.7, that evolution of ECP for increasing Q_{el} is given by an inverse polynomial relationship. This is expected, since for similar transmission configurations given in the literature [77] the relationship between the Q-penalty and the ECP is shown to be directly proportional.

5.5 Failure of the Estimate

We observed in our study that, for the example system considered here, at distances larger than approximately 3500 km the ECP model yields incorrect predictions. The principle explanation for this is that the assumption of symmetry in the eye closing is less accurate when the effects of the accumulation of timing jitter and waveform distortion through the system become important.

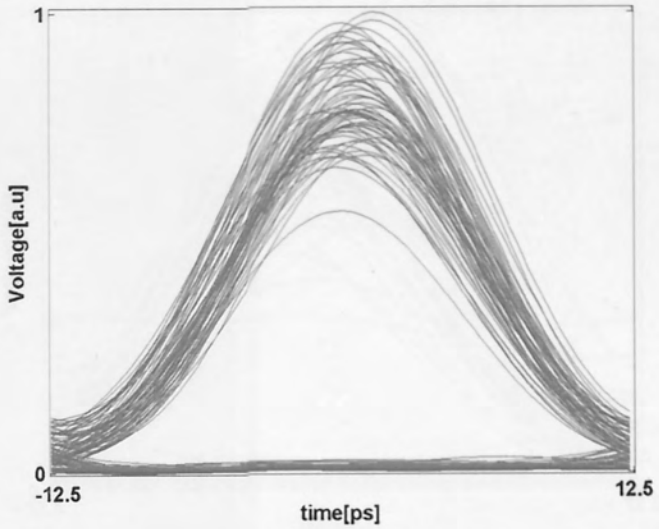

Figure 5.8: 33% Duty Cycle RZ-Pulses at 1600 km

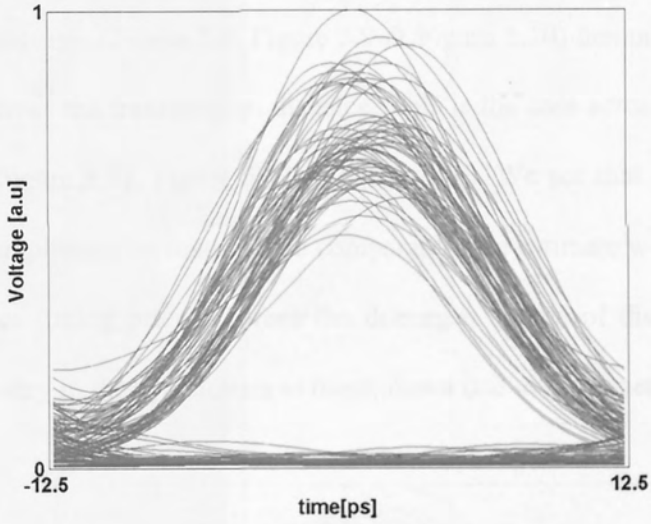

Figure 5.9: 33% Duty Cycle RZ-Pulses at 2600 km

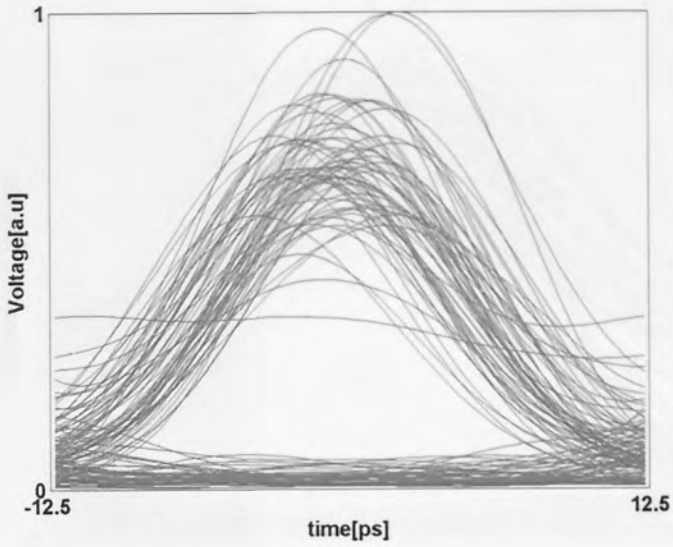

Figure 5.10: 33% Duty Cycle RZ-Pulses at 3700 km

Evidently, the eye diagrams (Figure 5.8, Figure 5.9 & Figure 5.10) demonstrate the evolution of the eye closure across the transmission distance. This is the case across all duty cycles, as explained below in Figure 5.11, Figure 5.12 & Figure 5.13. We see that whilst the influence of timing jitter and amplitude fluctuations are comparable, the estimate works well. However, at increased distances timing jitter becomes the dominant source of distortion, causing the assumption of symmetry in the eye closure to break-down due to asymmetric eye closure

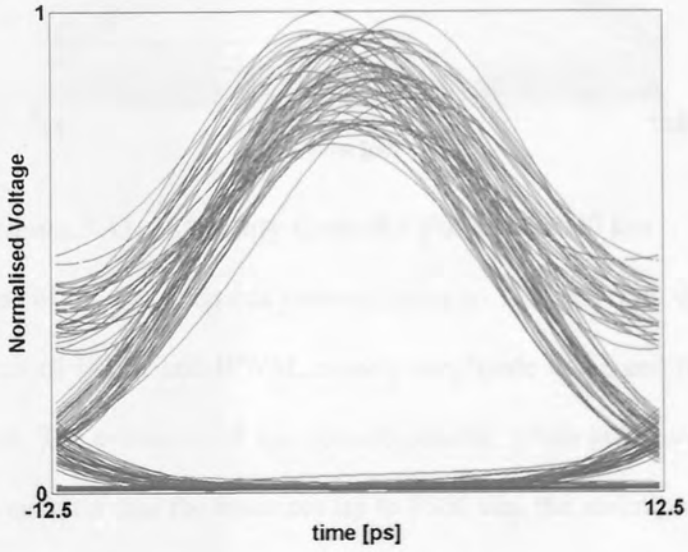

Figure 5.11: 50% Duty Cycle RZ Pulses at 1000 km

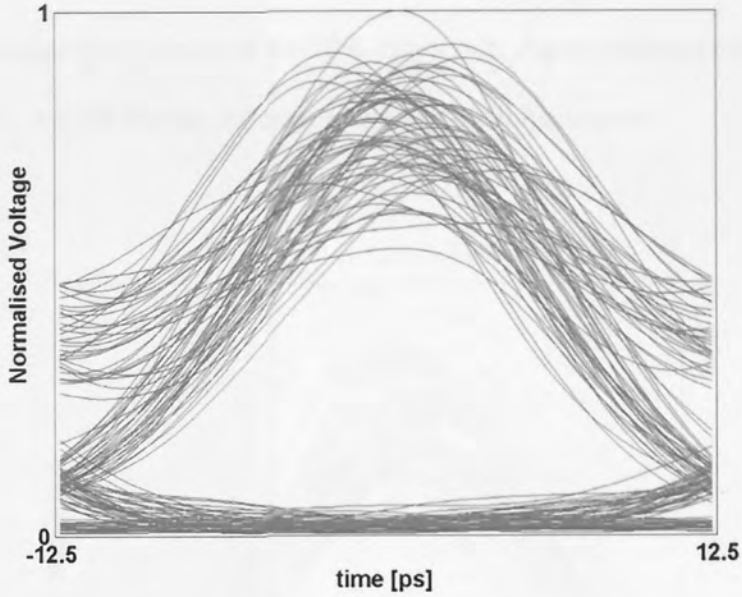

Figure 5.12: 50% Duty Cycle RZ Pulses at 2000 km

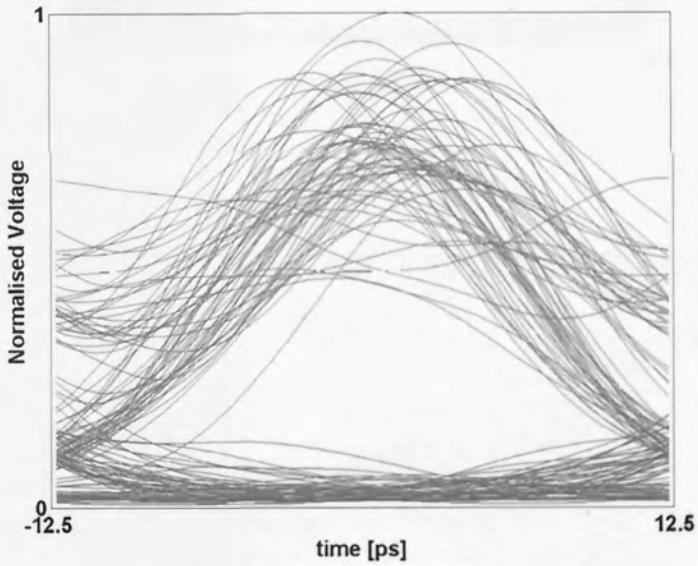

Figure 5.13: 50% Duty Cycle RZ Pulses at 3000 km

Studying the evolution of the eye diagrams corresponding to 33% and 50% duty cycle pulses, we see that the effects of IXPM and IFWM, namely amplitude noise and timing jitter [36], increase with distance. The evolution of eye closure penalty, given in Figure 5.3, Figure 5.4 and Figure 5.5, demonstrates that for distances up to 3500 km, the assumption of symmetric eye closure is upheld and our estimate is valid.

To study the failure of the estimate and the subsequent reasons behind the failure, we extend the transmission distance in the case of the 50% duty cycle. Again studying the eye diagrams for higher distances, we can see the difference between the impairments:

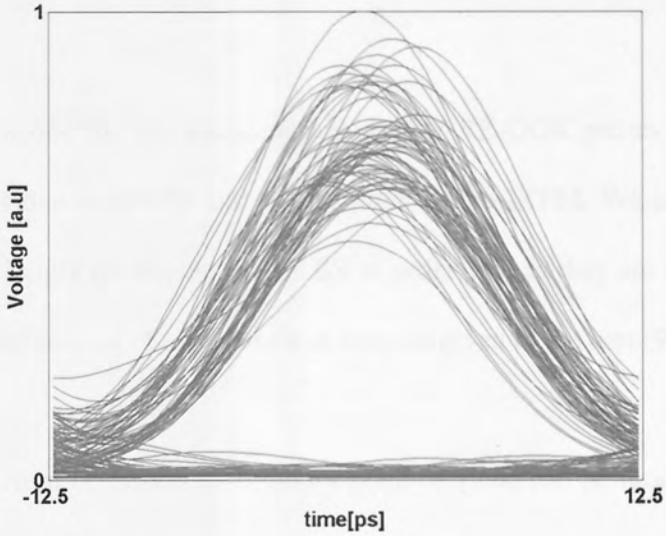

a)

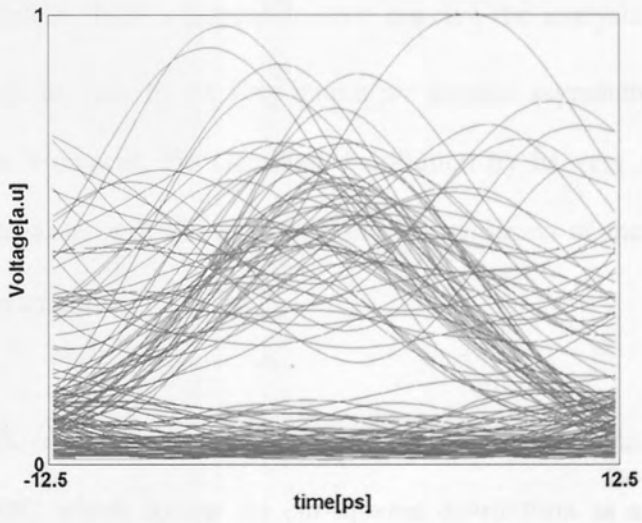

b)

Figure 5.14: Eye diagrams for 50% RZ-pulses a) 1600 km b) 4800 km

We observe simply by looking at the eye diagrams that at 1600 km (Figure 5.14 a)), the dominant source of distortion is due to amplitude fluctuations, which we identify as being due to IFWM [36]. Observing in exactly the same way, at 4800 km (Figure 5.14 b)), timing jitter becomes significant leading to the subsequent failure of the estimate as the eye closure is no longer symmetric.

The failure provides scope for the statistical analysis of RZ-OOK pulses affected by both amplitude fluctuations due to IFWM and timing jitter due to IXPM. We analyse the higher order moments using longer bit sequences (PRBS of order 10), as they are detailed in Figure 4.8, according to the definitions of skewness and kurtosis given in the text [98].

We know that OOK, from an information theory point of view, can be modelled as a Binary Asymmetric Channel (BAC), so we cannot assume any symmetry across the ones and zero. Logically, if two distributions are symmetric to one another then the magnitude of their skewness must be identical. Such a feature doesn't concern the analysis of data generated from RZ-OOK channels because by its very nature we assume asymmetry between logical ones and logical zeros. However, the Gaussian distribution by its very nature is perfectly symmetric so such a measure will allow us to study the evolution of the shape of the data relative to the initial assumption.

We know, for RZ-OOK transmission, logical ones can be modelled using a non-central chi-squared distribution [99], which counts the chi-squared distribution as a special case. The logical zeros are modelled by a chi-squared distribution [99]. Ultimately ECP is related to the BER as it models the impact of signal distortion on the transmission. For RZ-OOK transmission, errors are distributed according to a Gaussian distribution [71], despite the non-Gaussian nature of the receiver statistics given previously.

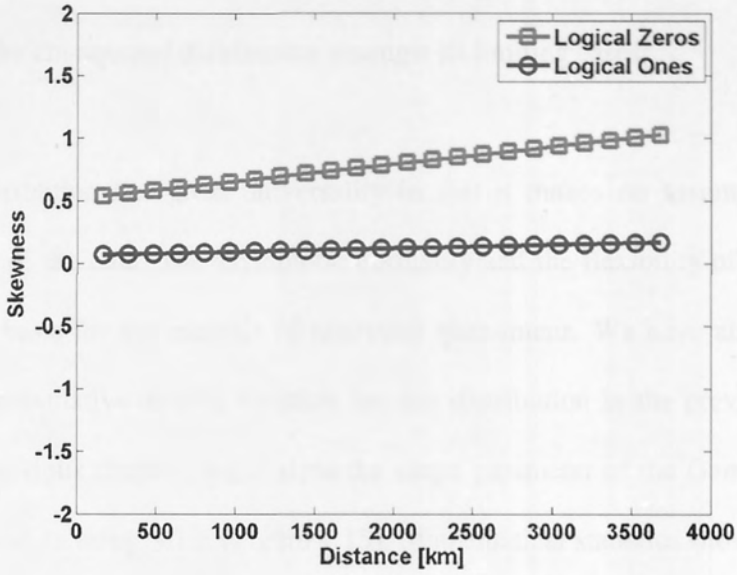

a)

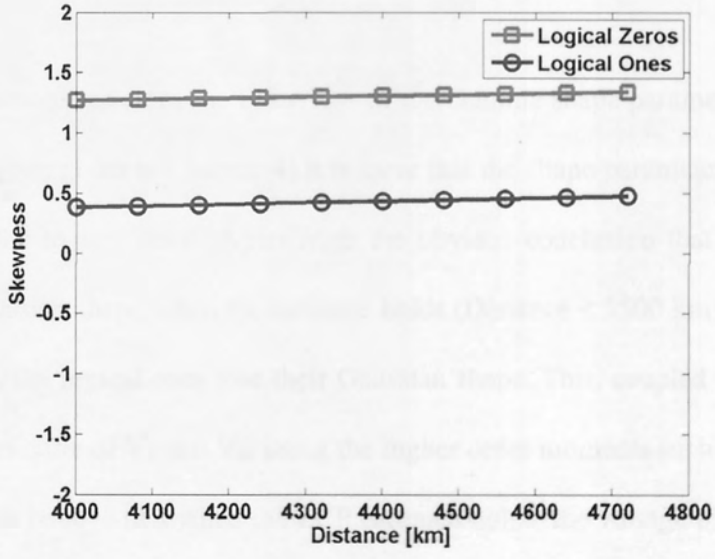

b)

Figure 5.15: Skewness of Voltage Distribution at 50% duty cycle at a) Distances < 3700 km b) Distances > 4000 km

From the literature, we see that both the chi-squared distribution and the Gaussian distribution are important in the overall evaluation of BER, so in an 'ad-hoc' fashion, we feel that we can use the Gamma distribution to facilitate further analysis given that it counts both the Gaussian distribution and the chi-squared distribution amongst its limiting cases.

The Gamma distribution has great universality in that it makes no assumption about the underlying shape of the data. The asymptotic normality and the flexibility of the distribution make it an ideal basis for the analysis of nonlinear phenomena. We have already stated the distribution and cumulative density function for this distribution in the previous chapter. In the vein of the previous chapter, we analyse the shape parameter of the Gamma distribution by fitting it to the data using MLE (Figure 5.15). Mathematical statistics shows that for large values of the shape parameter, the Gamma distribution distributively converges to the Gaussian distribution.

From the above demonstration of the behaviour of the Gamma shape parameter (denoted as k in the initial definition given in Chapter 4) it is clear that the shape parameter is larger for the logical ones that the logical zeros. Apart from the obvious conclusion that the logical ones have a strictly Gaussian shape when the estimate holds (Distance < 3500 km). However when the estimate holds, the logical ones lose their Gaussian shape. This, coupled with the analysis of the statistical structure of V_1 and V_0, using the higher order moments such as skewness and kurtosis, leads us to believe that when the ECP estimate holds, the voltage of the logical ones has an underlying Gaussian structure.

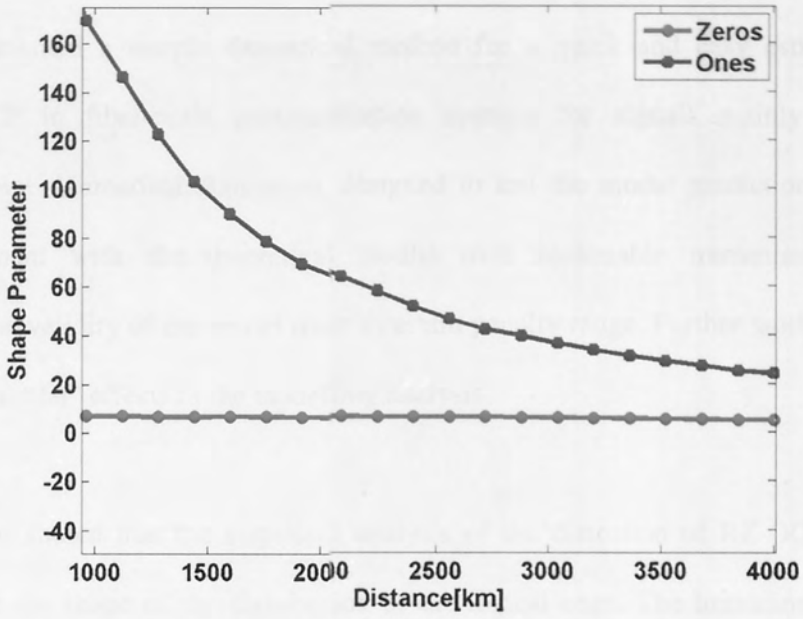

Figure 5.16: The fitted shape parameter of the electrical voltage of the received pulses at 50% duty cycle for Distances < 4000 km.

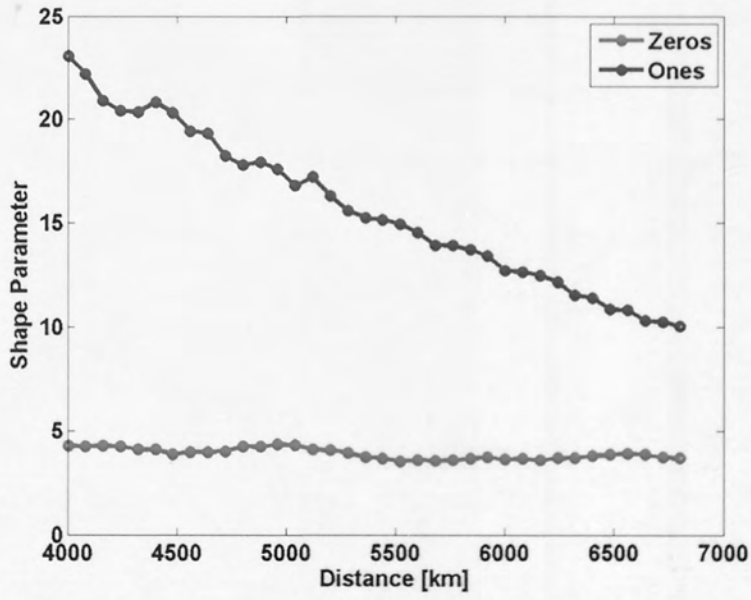

Figure 5.17: The fitted shape parameter of the electrical voltage of the received pulses at 50% duty cycle for Distances > 4000 km.

5.6 Conclusion

We have presented a simple theoretical method for a quick and easy estimation of the expected ECP in fibre-optic communication systems for signals mainly degraded by amplitude noise. Numerical simulation designed to test the model predictions have shown good agreement with the theoretical results over reasonable transmission distances, confirming the validity of the model over a certain penalty range. Further work is required to include "horizontal" effects in the modelling analysis.

We have also shown that the statistical analysis of the distortion of RZ-OOK statistics is dependent on the shape of the distribution of the logical ones. The limitation of this is the model sets an infinite extinction ratio, however, the voltage of the logical ones should always be significantly larger than the voltage of the logical zeros, so there is strength in our conclusion.

Chapter 6 Conclusions

Upon starting this thesis, we identified main objectives for the completion of the thesis:

- To assess the performance of 20 Gb/s RZ-DPSK transmission over undersea transmission distances
- To further investigate BER estimation in quasi-linear transmission using the RZ-DPSK data format and 20 Gb/s capacity
- Study the impact of dispersion and nonlinearity on BER estimation using an analysis of the channel statistics.
- Derive an estimate of ECP for RZ-OOK transmission systems in the quasi-linear regime, dominated by amplitude noise.

To facilitate the modelling of such complex configurations, we derived a mathematical model from which we could study optical pulse propagation in fibres with differing dispersion and nonlinearity. We used the wave equation to derive the GNLS equation in limit of zero Raman effect and zero third order dispersion, exploring pulse propagation in various limits before stating a numerical algorithm which we would be using to solve the GNLS equation for the complex practical configurations we were interested in. This is known as the Split-Step Fourier Method (SSFM).

We started by using the SSFM to examine the performance of a 7-channel WDM arrangement using a fibre map comprising several sections of NZ-DSF, complimented by a section of SMF. Such a configuration is redolent of the practical undersea configurations used to minimise the nonlinear interaction length and maintain zero dispersion at the 1550 nm wavelength [32].

The first step was to optimise the configuration by careful adjustment of the launch pulse average power and the pre-/post-compensation dispersion at the initial transmission distance of 6300 km. One of our first observations concerned the tolerance of the transmission link. We varied the duty cycle to allow us to realise quite different regimes within the transmission. After realising high Q-factor regimes for all three duty cycles, we confirmed the potential for 20 Gb/s RZ-DPSK WDM transmission at undersea distances earlier identified in [65]. However, we observed that whilst the potential for undersea transmission at the bit-rate is undoubted, the duty cycle essentially governs the overall performance for two reasons; narrower duty cycles improve performance but wider duty cycles are more tolerant to changes in the dispersive conditions. This is a fundamental condition for quasi-linear transmission as we would like to minimise the signal distortions due to IXPM and IFWM which can be generated through the adjustment of chromatic dispersion.

For the 3 duty cycles under consideration, we the analysed the evolution of the BER for both pulse average power and transmission distance. It was noted that tolerances towards changes in both power and dispersion are concurrent with the initial optimisation of pre-/post-compensation. This identified the 33% duty cycle as the optimal duty cycle for the undersea transmission of RZ-DPSK pulses at the newly identified 20 Gb/s bit-rate. We observed that we could transmit pulses at up to 10000 km whilst maintaining a BER < 10^{-3}. Particularly, for the 33% duty cycle, we saw that if pulse average power was chosen appropriately, performance levels of BER = 10^{-5} could be attained at a distance of 11500 km at the newly proposed 20 Gb/s per-channel bit-rate.

We also performed a (P_{ave},D_{pre}) optimisation identically for another fibre configuration, using 5-channels also employing the RZ-DPSK data format at a bit-rate of 21.4 Gb/s. This particular map was reticient of the next generation of transmission link, which comprises a

mixture of fibre sections, although it was still dominated by the traditional mixture of NZ-DSF and SMF sections. Mixtures of other fibres, such as LEAF and reduced slope TWF are a common feature of the newer undersea systems to implement a passive form of dispersion compensation and to compensate for the nonlinearity created within the NZ-DSF through the small amounts of dispersion and smaller effective area. LEAF has a smaller effective area than SMF, but larger than NZ-DSF.

Subsequently, we analyse the BER for both configurations in regard to its estimation. In the thesis, three BER estimation methods are identified; BER (Q_{el}), BER(Q_A) and BER(Q_φ). The teachings of [67] tell us that each of these estimation methods have their own merits, BER(Q_A) is appropriate for the linear regime, BER(Q_φ) is appropriate for the nonlinear regime due to the dominance of phase noise and BER(Q_{el}) is appropriate for the quasilinear regime. These estimation methods are compared [72] and no method is found to be of superior merit in regard to BER estimation over undersea transmission distances. This prompts further comparison.

Upon our own comparison of BER estimation methods, we see that BER(Q_{el}) performs the best out of the three aforementioned methods, suggesting from the teachings of [67] that the link is quasi-linear. This is exactly what we anticipate as we designed the transmission link with the quasilinear transmission regime in mind. The deployment of the quasi-linear regime means that the fibre nonlinearity is averaged over all pulses and has negligible effect on the overall transmission.

Speaking in strict numerical terms, we tentatively extrapolate our results to find that BER $<10^{-9}$ at distances of at least 4500 km, which is a considerable distance to propagate optical

pulses at a bit-rate of 20 Gb/s without any Forward Error Correction or any visible need for PMD compensation.

In short, we demonstrated that 20 Gb/s per-channel WDM RZ-DPSK is possible over undersea transmission distances without the use of FEC or physical devices such as optical regenerators or PMD compensators. We have also seen that narrower pulses can be used to improve performance, at the expense of tolerance to chromatic dispersion.

The high distances and narrow pulses used in high capacity undersea transmission, in addition to the high levels of accumulated dispersion and noise due to large chains of amplifiers, can only serve to increase the presence of nonlinearity within the transmission due to the creation of Kerr nonlinearities due to the long-term dependence of refractive index on the power.

The use of pulse-overlapped transmission is seen as a future technology for the further upgrade of such transmission systems [105], which will only increase the need for knowledge of the effects of dispersion and nonlinearity on the estimation of BER. To this end, an investigation of channel statistics under the influence of changing nonlinearity and dispersion is required. Indeed, both quantities ultimately contribute towards nonlinearity, so we re-interpret our aim as aiming to statistically characterise nonlinearity.

We considered the single channel embodiment of the 7-channel configuration investigated for its performance in (pg. 107). Investigating the single channel embodiment of this configuration removes the possible consideration of the impact of dispersion slope on the underlying nonlinearity. The dominant nonlinear effects in such a channel have previously been shown as IXPM and IFWM [36], which are both single channel effects. The effects of FWM and XPM can be effectively mitigated using dispersion management. Dispersion

management is achieved using the typical combination of NZ-DSF and SMF fibre sections [32].

We used pre-optimised values for the pre-compensation and pulse average launch power, which we ascertained in [65]. Initially, postcompensation is defined as $D_{post} = -D_{pre} - D_{ave}L$ and optimised in such a way. We collated the electrical current statistics for the transmission at successive spans of the transmission link. We then collated the electrical current statistics for $D_{post} = -D_{pre} - D_{ave}L + \delta D$ and drew a comparison. We saw that the inclusion of δD reduced the interaction between pulses due to the reduced pulse-to-pulse distortion created.

Indeed, if we increase the interaction between quasi-linear pulses we naturally seek a new distributive model for the channel because the statistical independence between pulses can no longer be assumed. As already mentioned, we can realise increased pulse-to-pulse interaction in one of two ways. We can change the dispersion to sub-optimal levels, which in turn would generate increased occurence of the two main sources of nonlinearity in a quasi-linear transmission link, namely IXPM and IFWM [36]. Alternatively, we can generate Kerr nonlinearity using the increased power and long distances involved in undersea transmission through the fibre refractive index.

The average dispersion of the transmission is $D_{ave} = 0$, with postcompensation $D_{post} = -D_{pre}$, initially, and electrical current statistics are collated with kurtosis taken on the sample for each distance between 4800 km and 20000 km.

We use advanced tools from Mathematical Statistics to study the tails of the electrical current distributions and we see that when we let dispersion manifest without ample compensation, the subsequent increase in nonlinearity due to the mis-management results in higher kurtosis.

Kurtosis is the chief characteristic of the tail behaviour of any distribution. The evolution of kurtosis is therefore plotted and the point of highest kurtosis is considered. For high kurtosis, we needed to introduce new models to measure the performance of the channel. Studying the theory of extreme values, we see that logical ones follow an extreme value distribution and the logical zeros follow a generalised extreme value distribution. These distributions are based on independent sampling, so the insinuation that the extreme value and generalised extreme value distribution fitting the situation imply that pulses are retaining their statistical independence. For highly nonlinear behaviour, we cannot assume pulse-to-pulse independence because the occurrence of IXPM and IFWM invalidate that assumption. So Extreme Value Theory is not appropriate, but we illustrated the need for deeper consideration of the statistical behaviour of these channels.

However, we did see that kurtosis could be used to characterise the nonlinearity in quasi-linear channels. This was a useful basis for our further analysis. The organic manifestation of nonlinearity is followed for further investigation of the impact of nonlinearity on the statistical analysis of undersea optical communcations. Again using the example of a WDM non-slope matched quasi-linear transmission link at a bit-rate of 21.4 Gb/s utilising the now heralded RZ-DPSK data format, we use the teachings of Forghieri [31] to emulate the occurence of intrachannel nonlinearity in undersea transmission. In plain terms, we increase the laucnh power and transmit over vast distances.

After the identification of the nonlinear transmission regime, we show that for such links, the intrachannel nonlinearity can be characterised by the kurtosis of the electrical current statistics. This leads to the consideration, again, of new distributive models to estimate the BER. Where kurtosis shows the electrical current statistics to exhibit some facets of non-Gaussian structure, we need to consider other distributive models.

We introduce the idea that idealised quasi-linear transmission can just be a limiting case of the nonlinear transmission regime by deriving a model for BER estimation using the Gamma distribution. This distribution is characterised by two parameters corresponding to shape and scale. From the mathematical statistics literature, we know that Gamma distributed random variables with large shape parameters are Gaussian in structure. We show this to be the case by fitting the shape parameter to our data. We then derive an estimate for BER based on the Gamma distribution.

Using extensive numerical simulation, we compare the performance of this estimate with the estimate based on electrical Q-factor statistics, as is shown to be valid for quasi-linear RZ-DPSK transmission. It is seen that the new Gamma distribution based estimate of BER is valid for transmission regions dominated by intrachannel nonlinearity such as IXPM and IFWM, such features manifest as timing jitter and amplitude fluctuations in the transmission.

Next, after addressing the issue of a global description of the nonlinear transmission regime in reference to the quasi-linear transmission regime, we study the nonlinear transmission regime on its own merits. Again, we use the kurtosis to characterise the impact of nonlinearity, due to its ability to simply clarify the non-Gaussian tail behaviour of the electrical current probability density function.

The identification of the nonlinear transmission regime in order to test the Gamma distribution based estimate allows us a head start in our analysis of the nonlinear transmission regime. Indeed, we already know that kurtosis is high in this region, indicating tail behaviour is not square exponential, but rather possesses power-law behaviour. This topic is covered in

the context of stock pricing in [96] and provided inspiration for the analysis of this transmission regime.

Power-law distributions are used traditionally to model phenomena which exhibit high variation, as what would be observed with the high amplitude fluctuations created by IFWM and the timing fluctuations created by IXPM. With this in mind we considered the use of the Beta distribution as an example power law distribution.

We derived an estimate of BER based on this distribution and then compared it to the predictive performance of the aforementioned Gaussian based electrical Q-factor dependent BER estimate. Studying the performance we see that the Beta distribution performs well for the nonlinear transmission regime.

The analysis of statistics in the presence of nonlinearity tells us that wherever the nonlinearity imposes itself seriously on the distribution, it manifests in the tails of the distribution. This creates a problem in that the estimation of BER must be adjusted. We have investigated three seperate methods of adjusting the BER; using extreme value theory, using the Gamma distribution or using the Beta distribution.

All three methods have their own merits and for the purpose of this thesis, it would not be prudent to be too detailed about the three new distrubitive models introduced. Extreme value theory is based on independent sampling, which rules it out as a serious model for the estimation of BER when pulse-interaction becomes significant. However, estimation of BER using the extreme value distributions also require the numerical fitting of three parameters, this can be computationally more expensive over large data sets.

The characterisation of both the Beta and Gamma distributions in terms of the shape and scale parameters means that they are not constrained by the assumption of symmetry or square exponential tails. However, just one is general enough to count the optimal regime within its remit, the Gamma distribution. From this, we can say, with conviction, that when pulse-to-pulse interaction is a serious concern for our transmission i.e pulse-overlapped transmission [105], the Gamma distribution should stand up to scrutiny. This is an issue that must be addressed when the eventual upgrade to 40 Gb/s per channel transmission is made. Indeed, narrower and narrower pulses will introduce other effects, which will require a flexible statistical model in order to correctly undertake statistical analysis of the transmission Again, Gamma distributed based statistical analysis would provide this flexibility.

On the subject of the eventual upgrade to 40 Gb/s, it is worth noting that such upgrades have been investigated, but the prevalence of intrachannel effects makes such an upgrade next to impossible without devices for the compensation of intrachannel PMD based effects. To this end, comparisons are still important between the incumbent RZ-OOK based configuration and others, such as RZ-DPSK.

Comparison can be completed by means of the ECP, which can be related to the Q-penalty, an important measure of signal degradation. One of the leading effects of quasi-linear transmission is the amplitude fluctuations that occur within the eye diagrams due to four-wave mixing and we endeavoured to derive an estimate for ECP when the distortions are dominated by amplitude fluctuations. We assumed a Gaussian distribution on the received voltage of the logical ones and the logical zeros and used the laws governing the extrema of the Gaussian distribution to derive an estimate for the ECP. We also assumed that eye closure is symmetric.

Such an estimate is useful for numerical simulation of transmission systems as it allows us to predict the influence of signal distortion even in the high Q-factor regime, which would usually require considerable computer time even to generate statistically unreliable results.

We then used a 40 Gb/s RZ-OOK dispersion managed transmission link configured using the useful D+/D-/D+ layout. This allowed the control of both the dispersion and the nonlinearity because of the low effective core area of the D- fibre section and the roughly optimised powers that are used to transmit the signals. We used distances of up to 4000 km initially to test the validity of the estimate.

The estimate held at distances of up to 3500 km, but when the influence of timing jitter grew, expected due to IXPM [36], the estimate failed. We expected this due to our initial assumption with regard to the symmetry of eye closure. However, this failure provided us with the information to further explore the statistics of eye closure.

It is well published in the literature that the statistics of RZ-OOK signals have a non-Gaussian shape but that the errors can be predicted using a Gaussian distribution [71]. This suggested that we could use statistical interplay between individual bits and errors to study the statistics of timing jitter in such transmission systems.

There is just one distribution that offers us the chance to study the interplay between the two and offer an insight into why our estimate failed when timing jitter became significant in the transmission – this is again the Gamma distribution, whose practicality is growing in the context of this thesis.

We use the mathematical statistics governing the distributive convergence of gamma distributed samples to study any underlying Gaussian structure. Initially, we assumed Gaussian shapes on both of the ones and the zeros. However, our results show that this assumption only matters when we make it on the logical ones, as, for RZ-OOK transmission anyway, the timing jitter is only visible on the logical ones and manifests only as noise on the logical zeros.

Therefore, when the estimate fails, the timing jitter grows and manifests in the distribution in the tails of the distribution, meaning that our assumptions on extrema of the sample are invalid.

Overall, the thesis indicates that high bit-rate transmission at long-haul distances is feasible within legacy configurations given some constraints; such as the bit-rate itself and the components which comprise the system.

Operation at 40 Gb/s is not seen as feasible at this point due to the growing influence of PMD at that bit-rate and increasing intra-channel nonlinearity. PMD needs to be compensated for and legacy links do not encompass such apparatus and the intra-channel nonlinearity will present a problem. Solutions have been proposed in the shape of Optical Regeneration (OR) (refer to the work of Leclerc (2002) and Boscolo (2002) for details) where the nonlinearity of optical fibre is utilised to stabilise the transmission of optical pulses and enable transmission at almost limitless range.

Raman amplification is another solution proposed as it would allow high bit-rate transmission without the need for regeneration and the bandwidth of the Raman shift is very high (~3 THz). Obviously, the use of narrower pulses over many channels will eventually exhaust the

C-band operation of the traditional EDFA, rendering it useful at the outermost channels due to the expansion of the bandwidth.

There are numerous future avenues to be explored in the context of this work. From the statistical point of view, the deployment of Extreme Value Theory in the study of BER estimation has definite potential. The theory is designed to approach rare events in a rigourous mathematical fashion, and methods traditional to fields such as economics and meteorology have enormous scope should be explored in any discipline where heavily stochastic nonlinear behaviour is influential. The use of narrower and narrower optical pulses means that pulse-to-pulse interaction will become highly prevelant in high bit-rate configurations. Such physical effects, as alluded to in this thesis, introduce some statistical dependence between the pulses. This statistical dependence renders the tradition of following Gaussian distributive models as useless, because the Central Limit Theorem based reasoning can no longer stand up to highly nonlinear behaviour.

Also, as mentioned in the thesis as an alternative to Extreme Value Theory, the study of other statistical models which dont impose shape dependent assumptions on the underlying physical configuration should be a key issue for the future of the statistical modelling of these systems. Distributions such as the Gamma Distribution and the Beta Distribution (as mentioned in the thesis) or other distributions such as the Logistic Distribution, provide the flexibility needed to account for increasingly complex physical behaviour.

This page has been left intentionally blank

Bibliography

1. Wilson, J. and J.F.B.Hawkes, *Lasers: Principles and Applications*. 1987: Prentice Hall.
2. Chesnoy, J. and J. Jerpahagnon, *Introduction to Undersea Fibre Communication*, in *Undersea Fibre Communication Systems*, J. Chesnoy, Editor. 2002, Academic Press.
3. Agrawal, G.P., *Fiber-Optic Communication Systems*. 3rd ed. 2002, New York: Wiley.
4. Riley, K.F., M.P. Hobson, and S.J. Bence, *Mathematical Methods for Physics and Engineering*. 2002, Cambridge: Cambridge University Press.
5. Andrews, L.C., R. Askey, and R. Roy, *Special Functions*. 1999, Cambridge: Cambridge Press.
6. Hammond, P., *Electromagnetism for Engineers: an Introductory Course*. 1986, Oxford: Pergamon.
7. Mignien, G., *Method of splicing optical fibres disposed in a layer in a cable*, USPTO, Editor. 1980, Compagnie Lyonnaise de Transmission Optiques: United States of America.
8. Miya, T., Y. Terunuma, T. Hosakak, and T. Miyashita. *An Ultimate Low Loss Single-mode fiber at 1.55 \mu m.* in *Optical Society of America, Topical Meeting on Optical Fiber Communication*. 1979.
9. Desurvire, E., *Erbium-doped Fibre Amplifiers: Principles and Applications*. 2001, New York: Wiley.
10. Mears, R.J., L. Reekie, I.M. Jauncey, and D.N. Payne, *Low-noise optical amplifier operating at 1.54 \mu m.* Electronics Letters, 1987. **23**: p. 1026 - 1028.
11. Boscolo, S.A., S.K. Turitsyn, and K.J. Blow, *All-Optical Passive Quasi-Regeneration in Transoceanic 40 Gbit/s Return-to-Zero Transmission Systems with Strong Dispersion Management.* Optics Communications, 2002. **205**(4-6): p. 277 - 280.

12. Li, T., *The impact of optical amplifiers on long-distance lightwave telecommunications.* Proceedings of the IEEE, 1993. **81**: p. 1568 - 1579.

13. Bolland, P. *Enhancing Capacity on Long Haul and Undersea Systems.* in *Asia-Pacific Optical Communications*. 2008. Hangzhou, China.

14. Leclerc, O., B. Lavigne, D. Chiaroni, and E. Desurvire, *All-Optical Regeneration: Principles and WDM Implementation*, in *Optical Fiber Telecommunications*, I.P. Kaminow and T. Li, Editors. 2002.

15. Becker, P.C., N.A. Olsson, and J.R. Simpson, *Erbium Doped Fibre Amplifiers: Fundamentals and Technology*. 1999, London: Academic Press.

16. Bjarklev, A., *Optical Fiber Amplifiers*. 1993, Norwood, MA: Artech House.

17. Balland, G., R.M. Paski, and R.A. Baker. *TAT-12/13 Intergration development tests - interim results.* in *Proceedings of SubOptic*. 1993.

18. Chesnoy, J., O. Gautheron, L. Le Gourrierec, and V. Lemaire, *Alcatel Telecomm Review 3Q98*. 1998.

19. Sab, O.A. and O. Gautheron, *Ultra-Long-Haul Undersea Transmission*, in *Undersea Fibre Communication Systems*, J. Chesnoy, Editor. 2002.

20. Dutton, H.J.R., *IBM Special Report: Understanding Optical Communications*. 2007.

21. Libert, J.F. and G. Waterworth, *Cable Technology*, in *Undersea Fibre Communications*, J. Chesnoy, Editor. 2001.

22. Hamilton, B., *Undersea Wye Connection for a Undersea Cable System*, USPTO, Editor. 1970, Bell Telephone Laboratories: USA.

23. Agrawal, G.P., *Nonlinear Fibre Optics*. 3rd ed. 2001: Harcourt Press.

24. Smith, R.G., *Optical Power Handling Capacity of Low Loss Optical Fibres as Determined by Stimulated Raman and Brillouin Scattering.* Applied Optics, 1972. **11**(11): p. 2489-2494.

25. Stolen, R.H., E.P. Ippen, and A.R. Tynes, *Raman Oscillation in Glass Optical Waveguides* Applied Physics Letters, 1972. **20**(62): p. 62-64.

26. Ippen, E.P. and R.H. Stolen, *Stimulated Brillouin Scattering in Optical Fibres.* Applied Physics Letters, 1972. **21**(12): p. 539-541.

27. Boyd, R.W., *Nonlinear Optics*. 1992, San Diego, CA, USA: Academic Press.

28. Cotter, D., *Observation of stimulated Brillouin scattering in low-loss silica fibre at 1.3 \mu m.* Electronics Letters, 1982. **18**(12): p. 495-496.

29. Brandon, E. and J.P. Blondel, *Unpeatered Transmission*, in *Undersea Fiber Communication Systems*, J. Chesnoy, Editor. 2002, Academic Press: Orlando.

30. Marcuse, D., A.R. Chraplyvy, and R.W. Tkach, *Effects of fibre nonlinearity on long-distance transmission.* Journal of Lightwave Technology, 1991. **9**: p. 356 - 361.

31. Forghieri, F., R.W. Tkach, and A.R. Chraplyvy, *Fibre nonlinearities and their impact on transmission systems*, in *Optical Fibre Communications*, I.P. Kaminow and T.L. Koch, Editors. 1997, Academic Press.

32. Bergano, N.S., *Undersea Amplified Lightwave System Design*, in *Optical Fibre Telecommunications*, T.L. Koch and I.P. Kaminow, Editors. 1997.

33. Mamyshev, P.V. *All-optical data regeneration based on self-phase modulation effect.* in *European Conference on Optical Communications*. 1998. Madrid, Spain.

34. Chraplyvy, A.R., D. Marcuse, and P. Henry, *Carrier-induced phase noise in angle modulated optical fiber systems.* Journal of Lightwave Technology, 1984. **2**(1): p. 6-10.

35. Killey, R., V. Mikhailov, S. Appatthurai, and P. Bayvel, *Characterization of Intrachannel Nonlinear Distortion in Ultra-High Bit-Rate Transmission Systems*, in *Optical Communication: Theory and Techniques*, E. Forestieri, Editor. 2005, Springer: New York.

36. Essiambre, R.J., B. Mikkelsen, and G. Raybon, *Intra-channel Cross-Phase Modulation and Four-Wave Mixing in High-Speed TDM Systems.* Electronics Letters, 1997. **35**(18): p. 1576 - 1578.

37. Wei, X. and L. Liu, *Analysis of intrachannel four-wave mixing in differential phase shift-keying transmission with large dispersion.* Optics Letters, 2003. **28**(23): p. 2300 - 2302.

38. Striegler, A.G. and B. Schmauss, *Fiber-based compensation of IXPM-induced timing jitter.* IEEE Photonics Technology Letters, 2004. **16**(11): p. 2574-2576.

39. Charlet, G. and S. Bigo, *Upgrading WDM Undersea Systems to 40 Gbit/s Channel Bitrate.* IEEE Transactions, 2006. **94**(5): p. 935-951.

40. Wabnitz, S. and F. Neddam, *Pulse Interactions and Collisions in Asymmetric Higher-Order Dispersion Managed Fiber Link.* Optics Communications, 2000. **183**(5-6): p. 395-405.

41. Ablowitz, M.J. and T. Hirooka, *Intrachannel Pulse Interactions in Dispersion Managed Transmission Systems: Energy Transfer.* Optics Letters, 2002. **27**(3): p. 203-205.

42. Agrawal, G.P., *Lightwave Technology: Telecommunication Systems.* 2005: John Wiley & Sons.

43. Lam, D.K.W., B.K. Garside, and K.O. Hill, *Dispersion Cancellation using Optical Fiber Filters.* Optics Letters, 1982. **7**(6): p. 291-293.

44. Yariv, A., D. Fekete, and D.M. Pepper, *Compensation for Channel Dispersion by Nonlinear Optical Phase Conjugation* Optics Letters, 1979. **4**(2): p. 52.

45. Watanabe, S., T. Naito, and T. Chikama, *Compensation of chromatic dispersion in single mode fibre by optical phase conjugation.* IEEE Photonics Technology Letters, 1993. **5**: p. 92-95.

46. Ho, K.-P., *Phase Modulated Optical Communication Systems*. 2005, New York: Springer.

47. Poole, C.D. and R.E. Wagner, *Phenomelogical Approach to Polarization Mode Dispersion in Long Single Mode Fibre*. Electronics Letters, 1986. **22**(19): p. 1029-1030.

48. Foschini, G.J. and C.D. Poole, *Statistical Theory of Polarization Dispersion in Single Mode Fibres*. Journal of Lightwave Technology, 1991. **9**(11): p. 1439-1456.

49. Yevick, D., *Multicanonical Communication System Modelling - Application to PMD Statistics*. IEEE Photonics Technology Letters, 2002. **14**: p. 1512-1514.

50. Freund, R., L. Molle, C. Caspar, J. Schwartz, S. Webb, and S. Barnes. *Mixed bit-rate and Modulation Format Upgrades of Non-slop Matched Undersea Links*. in *European Conference on Optical Communications*. 2006. Cannes, France.

51. Taneja, H., B.K. Pannaga, and A. Arora. *Low PMD Fiber by Improving Clad Ovality*. in *International Conference on Optics and Optoelectronics*. 2005. Dehradan, India.

52. Matera, F. and M. Settembre, *Compensation of polarization mode dispersion by means of the Kerr effect for nonreturn-to-zero signals*. Optics Letters, 1995. **20**(1): p. 28-30.

53. Xie, C., H. Sunnerud, M. Karlsson, and P. Andrekson, *Polarization-Mode Dispersion Induced Outages in Soliton Transmission Systems*. 2001, 2001. **13**(10): p. 1079 - 1081.

54. Mollenauer, L.F., K. Smith, J.P. Gordon, and C.R. Menyuk, *Resistance of solitons to the effects of polarization dispersion in optical fibres*. Optics Letters, 1989. **14**(21): p. 1219 - 1221.

55. Liu, X., C. Xu, and X. Wei, *Performance Analysis of Time-Polarization Multiplexed 40 Gb/s RZ-DPSK DWDM Transmission*. IEEE Photonics Technology Letters, 2004. **16**(1): p. 302-304.

56. Pilipetskii, A.N., *High-Capacity Undersea Long-Haul Systems.* IEEE Journal of Selected Topics in Quantum Electronics, 2006. **12**(4): p. 484 - 496.

57. Golovchenko, E.A., L. Rahman, B. Bakhshi, D. Kovsh, F. Idrovo, and S.M. Abbott, *Using RZ-DPSK-Based Transponders for Upgrades on Existing Long-Haul Undersea WDM Systems.* Journal of Lightwave Technology, 2008. **26**(1): p. 204 - 208.

58. Gnauck, A.H. and P.J. Winzer, *Optical Phase Shift Keyed Transmission.* Journal of Lightwave Technology, 2006. **23**(1): p. 155 - 130.

59. Xu, C., L. Liu, and L.F. Mollenauer, *Comparison of Phase Shift Keying and On-Off Keying in Long-Haul Dispersion Managed Transmission.* IEEE Photonics Technology Letters, 2003. **15**(4): p. 617 - 619.

60. K.Ishida, T. Kobayashi, J. Abe, K. Kinjo, S. Kuroda, and T. Mizuochi. *A comparitive study of 10 Gb/s RZ-DPSK and RZ-ASK Transmission over Transoceanic Distances* in *Optical Fibre Communications*. 2003.

61. Becouarn, L., G. Vareille, P. Becci, and J.F. Marcerou. *3 Tbit/s transmission (301 DPSK channels at 10.709 Gb/s) over 10270 km with a record efficiency of 0.65 bits/s Hz.* in *European Conference on Optical Communications*. 2003. Rimini, Italy.

62. Cai, J.-X., M. Nissov, C.R. Davidson, Y. Cai, A.N. Pilipetskii, H. Li, M.A. Mills, R.-M. Mu, U. Feiste, L. Xu, A.J. Lucero, D.G. Foursa, and N.S. Bergano. *Transmission of thirty-eight 40 Gbit/s channels (> 1 Tbit/s) over transoceanic distances.* in *Optical Fibre Communications*. 2002. Anaheim, California, USA.

63. Sugahara, H., K. Fukuchi, A. Tanaka, Y. Inada, and T. Ono. *6,050 km transmission of 32 x 42.7 Gb/s DWDM signals using Raman-amplified quadruple hybrid span configuration.* in *Optical Fibre Communications*. 2002. Anaheim, California, USA.

64. Tsukitani, M., M. Matsui, K. Nagayama, and E. Sasaoka. *Ultra-low nonlinearity pure-silica core fibre with an effective area of 211 mu* m^2 *and transmission loss of 0.159*

dB/km. in *European Conference on Optical Communications*. 2002. Copenhagen, Denmark.

65. Slater, B., S. Boscolo, T. Broderick, S.K. Turitsyn, R. Freund, L. Molle, C. Caspar, J. Schwartz, and S. Barnes, *Performance Analysis of 20 Gb/s RZ-DPSK Non-Slope Matched Transoceanic Undersea Links.* Optics Express, 2007. **15**(17): p. 10999 - 11007.

66. Kartalopoulos, S.V., *Optical Bit Error Rate: An Estimation Methodology*. 2004: Wiley Interscience.

67. Xu, C., X. Liu, and X. Wei, *Differential Phase Shift Keying for High Spectral Efficiency Optical Transmission.* IEEE Journal of Selected Topics in Quantum Electronics, 2003. **10**(2): p. 281 - 293.

68. Marcuse, D., *Derivation of Analytical Expressions for the Bit-Error Probability in Lightwave Systems with Optical Amplifiers.* Journal of Lightwave Technology, 1990. **8**(12): p. 1816 - 1823.

69. Primak, S., V. Kontorovich, and V. Lyandres, *Stochatistic Methods and their Applications to Communications: A Stochastic Differential Equations Approach.* 2004: Wiley.

70. Forghieri, F., R.W. Tkach, A.R. Chraplyvy, and D. Marcuse, *Reduction of four-wave mixing crosstalk in WDM systems using unequally spaced channels.* IEEE Photonics Technology Letters, 1994. **6**(6): p. 754-756.

71. Bergano, N.S., F.W. Kerfoot, and C.R. Davidson, *Margin Measurements in Optical Amplifier Systems.* IEEE Photonics Technology Letters, 1993. **5**(3): p. 304 - 306

72. Slater, B., S. Boscolo, V.K. Mezentsev, and S.K. Turitsyn, *Comparison of BER Estimation Methods in Numerical Simulation of 40 Gb/s RZ-DPSK Transmission with In-line SOAs.* IEEE Photonics Technology Letters, 2007. **19**(8): p. 607 - 609.

73. Zhang, X., Z. Qu, and G. Yang, *Probability density function of noise statistics for optically pre-amplified DPSK receivers with Mach-Zehnder interferometer demodulation.* Optics Communications, 2006. **258**(2): p. 177 - 183.

74. Ho, K.-P., *Error Probability of DPSK Signals with Intrachannel Four Wave Mixing in Highly Dispersive Transmission Systems.* IEEE Photonics Technology Letters, 2005. **17**(26): p. 789 - 791.

75. Bosco, G. and P. Poggiolini, *On the Q-factor Inaccuracy in the Performance Analysis of Optical Direct Detection DPSK Systems.* IEEE Photonics Technology Letters, 2004. **16**(2): p. 665 - 667.

76. Hiew, C.C., F.M. Abbou, H.T. Chuah, S.P. Majumdar, and A.R. Hairul, *BER Estimation of Optical WDM RZ-DPSK Systems through the Differential Phase Q.* IEEE Photonics Technology Letters, 2006. **18**(12): p. 2619 - 2621.

77. Downie, J.D., *Relationship of Q-Penalty to Eye Closure Penalty for NRZ and RZ Signals with Signal Dependent Noise.* Journal of Lightwave Technology, 2005. **23**(6): p. 2031 - 2038.

78. Downie, J.D. and A.B. Ruffin, *Analysis of Signal Distortion and Crosstalk Penalties Induced by Optical Filters in Optical Networks.* Journal of Lightwave Technology, 2003. **21**(9): p. 1876 - 1886.

79. Lee, J.-H., *Analysis and Characterization of Fiber Nonlinearities with Deterministic and Stochastic Signal Sources: Ph.D. Thesis* in *Electronic Engineering*. 2000, Virginia Polytechnic Institute and State University

80. Folland, G.B., *Fourier Analysis and its Applications*. 1992: Brooks/Cole.

81. Karpman, V.I. and E.M. Krushkal, *Modulated Waves in Nonlinear Dispersive Media.* Soviet Physics JETP, 1969. **28**(2): p. 277 - 281.

82. Hardin, R.H. and F.D. Tappert, *Applications of the Split-Step Fourier Method to the Numerical Solution of Nonlinear and Variable Coefficient Wave Equations.* SIAM Review, 1973. **15**(423): p. 423.

83. Fisher, R.A. and W. Bischel, *Numerical Studies of the Interplay between Self-Phase Modulation and Dispersion for Intense Plane Wave Laser Pulses* Journal of Applied Physics, 1975. **46**(11): p. 4921 - 4934.

84. Taha, T.R. and M.J. Ablowitz, *Analytical and Numerical Aspects of Certain Nonlinear Evolution Equations: Nonlinear Schroedinger Equation.* Journal of Computational Physics, 1984. **55**(2): p. 203 - 230.

85. Gnauck, A.H., G. Raybon, S. Chandrasekhar, J. Leuthold, C. Doerr, L. Stulz, A. Agarwal, S. Banerjee, D. Grosz, S. Hunsche, A. Kung, A. Marhelyuk, D. Maywar, M. Movassaghi, X. Liu, C. Xu, X. Wei, and D.M. Gill. *2.5 Tb/s (64 x 42.7 Gb/s) Tranmisssion over 40 x 100 km NZDSF using RZ-DPSK format and all-Raman-amplified spans.* in *Optical Fibre Communications.* 2002. Anaheim, California, USA.

86. Cai, J.-X., D.G. Foursa, L. Liu, C.R. Davidson, Y.Cai, W.W. Patterson, A.J. Lucero, B. Bakhshi, G. Mohs, P.C. Corbett, V. Gupta, W. Anderson, M. Vaa, G. Domagala, M. Mazurczyk, H. Li, S. Jiang, M. Nissov, A.N. Pilipetskii, and N.S. Bergano, *RZ-DPSK Field Trial Over 13,100 km of Installed Non-Slope Matched Undersea Fibers.* Journal of Lightwave Technology, 2005. **23**(1): p. 95 - 103.

87. Cai, J.-X., C.R. Davidson, M. Nissov, H. Li, W. Anderson, Y. Cai, L. Liu, A.N. Pilipetskii, D.G. Foursa, W.W. Patterson, P.C. Corbett, A.J. Lucero, and N.S. Bergano. *Transmission of 40 Gb/s WDM signals over 6,250 km of conventional NZ-DSF with >4 dB FEC margin.* in *Optical Fibre Communications.* 2005. Anaheim, California, USA.

88. Cai, J.-X., M. Nissov, H. Li, C.R. Davidson, W. Anderson, L. Liu, D.G. Foursa, A.N. Pilipetskii, and N.S. Bergano. *Experimental comparison of 40 Gb/s RZ-,CSRZ-, and*

NRZ-DPSK modulation formats over non-slope matched fibres. in *European Conference on Optical Communications*. 2005. Glasgow, UK.

89. Cai, J.-X., M. Nissov, W. Anderson, M. Vaa, C.R. Davidson, D.G. Foursa, and L. Liu. *Long-Haul 40 Gb/s RZ-DPSK Transmission with Long Repeater Spacing*. in *European Conference on Optical Communications*. 2005.

90. Holzloehner, R. and C.R. Menyuk, *Use of Multicanonical Monte Carlo Simulations to obtain accurate bit error rates in Optical Communication Systems.* Optics Letters, 2003. **28**(20): p. 1894-1896.

91. Nasieva, I., A. Kaliazin, and S.K. Turitsyn, *Multicanonical Monte Carlo Modelling of BER Penalty in Transmission Systems with Optical Regeneration.* Optics Communications, 2006. **262**(2): p. 246-249.

92. Berg, B.A. and T. Neuhaus, *Multicanonical Ensemble: A new approach to simulated first-order phase transitions.* Physical Review Letters, 1992. **68**(1): p. 9-12.

93. Nasieva, I., *Analysis and Optimisation of the Performance of Nonlinear Optical Communication Systems*, in *Electronic Engineering*. 2006, Aston University: Birmingham.

94. Gilks, W.R., S. Richardson, and D.J. Spiegelhalter, *Markov Chain Monte Carlo: In Practice*. 1996, London: Chapman & Hall.

95. Norris, J.R., *Markov Chains*. 1998, Cambridge: Cambridge University Press.

96. Cont, R., *Empirical Properties of Asset Returns: Stylized Facts and Statistical Issues.* IOP Quantitative Finance, 2001. **1**: p. 223 - 236.

97. Smith, R.L., *Statistics of Extremes, with Applications in Environment, Insurance and Finance*, in *Monographs on Statistics and Applied Probability 99: Extreme Values in Finance, Telecommunications and the Environment*, B. Rootzen and H. Finkelstadt, Editors. 2004, Chapman & Hall/CRC. p. 1.

98. Rice, J.A., *Mathematical Statistics and Data Analysis*. 1994: Duxbury Press.

99. Abramovich, F. and P. Bayvel, *Some Statistical Remarks on the Derivation of BER in Amplified Optical Communication Systems.* IEEE Transactions on Communications, 1997. **45**(9): p. 1032 - 1034.

100. Reiss, R.D. and M. Thomas, *Statistical Analysis of Extreme Values: from Insurance, Finance, Hydrology and other fields.* 2001, Basel: Birkhaueser-Virlag.

101. Zhang, F., C.-A. Bunge, and K. Petermann, *Statistical property of intra-channel four-wave mixing in RZ-DPSK transmission systems.* Optical Fibre Technology, 2007. **13**(1): p. 51 - 55.

102. Matyas, L., *Generalised Method of Moments Estimation: Themes in Modern Econometrics*

1999, Cambridge: Cambridge Press.

103. Ho, K.-P., L.K. Chen, and F. Tong, *Modelling of Waveform Distortion due to Optical Filtering.* IEEE Journal of Selected Topics in Quantum Electronics, 2000. **6**(2): p. 223.

104. Bigo, S. and G. Charlet. *Invited Paper: Upgrading WDM Undersea Systems to 40 Gb/s Channel Bit-rate.* in *European Conference on Optical Communications.* 2006. Cannes, France.

105. Mamyshev, P.V. and N.A. Mamysheva, *Pulse overlapped dispersion managed data transmission and intra-channel four-wave mixing.* Optics Letters, 1999. **24**(21): p. 1454 - 1456.

106. Gallion, P., *Basics of Digital Optical Communications*, in *Undersea Fibre Optic Communications*, J. Chesnoy, Editor. 2002, Elsevier: London.

Appendix A Receiver Sensitivity of RZ-DPSK and its advantage over RZ-OOK

In this appendix, we want to summarise the work of Wei et al <ref> in the study of RZ-DPSK receiver sensitivity. Firstly, we consider a linear channel with a received signal of the form;

$$F(t) = \left[\sum_{n=0}^{N-1} a_n u(t-nT) + z(t)\right] e^{-i\varpi_c t} \qquad \text{(A.1)}$$

Where ϖ_C is the angular frequency of the optical carrier, T is the bit-period, $u(t-nT)$ is the envelope function of the RZ pulse in the n-th timeslot, a_n is the complex amplitude of the n-th pulse and $z(t)$ represents a classical Gaussian zero-mean noise element. For DPSK, information is encoded in a relative phase change of the signal amplitude a_n with respect to the previous symbol a_{n-1}. For convenience $a_{n-1} = \pm 1$, from this we say that a logical zero will be represented by a phase change of π and a logical one will be represented by no phase change. The receiver performance is optimised by the inclusion of a matched optical filter with a response function of;

$$h(t) = \frac{1}{\sqrt{E_b}} u(-t) e^{i\varpi_c t} \qquad \text{(A.2)}$$

Where E_b is the energy given per bit. The filtered signal is a convolution of $F(t)$ and $h(t)$. Near the centre of the n^{th} timeslot, the filtered signal is given as;

$$F_n(t) = f_n e^{-i\varpi_c t} \qquad \text{(A.3)}$$

$$f_n = a_n \sqrt{E_b} + z_n \qquad \text{(A.4)}$$

$$z_n = \int_{(n-1/2)T}^{(n+1/2)T} z(t) u^*(t-nT) dt \qquad \text{(A.5)}$$

The filtered DPSK signal can be demodulated using a balanced optical delay interferometer, such as a Mach-Zehnder Interferometer (MZI). This device comprises a constructive and a

destructive arm, the two arms are photodiodes and measure the phase change between the signals. The two arms are given by;

$$I_{+} = \left| \frac{f_n + f_{n-1}}{2} \right|^2 \tag{A.6}$$

$$I_{-} = \left| \frac{f_n - f_{n-1}}{2} \right|^2 \tag{A.7}$$

This gives the balanced current as;

$$I_{bal} = I_{+} - I_{-} = \frac{f_n f_{n-1}^{*} + f_{n-1} f_n^{*}}{2} \tag{A.8}$$

The BER is the probability that I_{bal} has the wrong sign, using the standard relationship for BER, we can say;

$$BER = \frac{1}{2}(P(I_{bal} < 0 \mid I_{bal} > 0) + P(I_{bal} > 0 \mid I_{bal} < 0)) \tag{A.9}$$

Using the Gaussian distribution for the complex noise source z, we can say that BER is estimated from the equation;

$$BER = \frac{1}{2} e^{-\frac{E_b}{2\sigma^2}} \tag{A.10}$$

We can compare this result with the standard Gaussian estimate for BER, we can say the balanced receiver output can be given by $I_{bal} = \pm E_b$, meaning that $\mu_1 - \mu_0 = 2E_b$. The variance, in the small noise limit and for independent consecutive amplitudes is given by $\sigma_1 = \sigma_0 \approx \sqrt{2E_b \sigma}$. Due to this, Q-factor can be given as;

$$Q \approx \frac{\sqrt{E_b}}{\sqrt{2}\sigma} \tag{A.11}$$

For RZ-OOK, we can say that the distance of separation between symbols in RZ-OOK can be given as $\sqrt{2E_b}$, whereas the separation for RZ-DPSK is $2\sqrt{E_b}$. The corresponding BER estimate for RZ-OOK is given by [67];

$$BER = \left(\frac{\sigma^2}{2\pi E_b}\right)^{1/4} e^{-\frac{E_b}{4\sigma^2}} \qquad \text{(A.12)}$$

Equations (A.10) and (A.12) demonstrate a 3-dB (OSNR) benefit in receiver sensitivity between RZ-DPSK and RZ-OOK. In simple terms, we can can use approximately half the power for RZ-DPSK signals to achieve the same BER (Q-factor) as RZ-OOK transmission over the same transmission distance. This is simply understood when we consider that the symbol separation for RZ-OOK is $\sqrt{2E_b}$ and for RZ-DPSK the symbol is $2\sqrt{E_b}$. If we square these quantities to obtain the separation in optical power, the 3-dB difference is explain explicitly. A simple method of examining such a difference is by studying the BER evolution of a standard linear system. Consider a chain of amplifiers comprising 25 km of SMF followed by an amplifier configured to compensate exactly for the losses in the preceding fibre section. If we propagate pulses over 100 spans of this simple system (2500 km), we can examine how the BER behaves for increasing power for the two formats mentioned (RZ-OOK and RZ-DPSK);

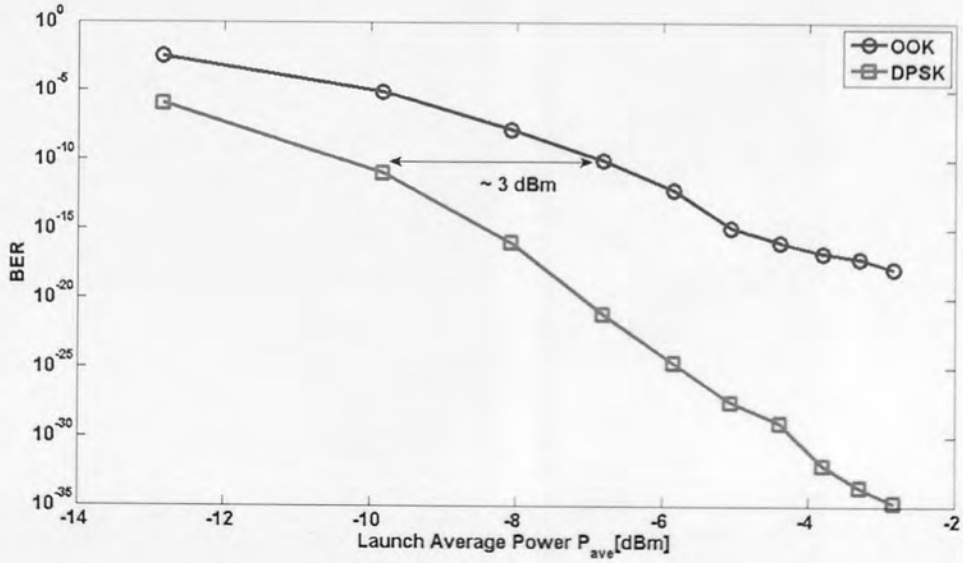

Figure A.1: BER evolution for a linear system with increasing launch average power at 40 Gb/s over 2500 km SMF

The definition of receiver sensitivity (as given in [106]) is the amount of power needed to attain a BER ~ 10^{-9}. For our linear configuration, we can study the evolution of the BER with respect to either launched or received power as in Figure A.1. We see that for a BER ~ 10^{-9}, a difference of around 3 dBm is required for RZ-OOK to achieve this level of BER. This confirms the standard result we were trying to prove in this appendix.

Appendix B: Publications

1 T. Broderick "Power Law Statistics in the Analysis of Optical Communication Systems" submitted to Physics Letters A 2009

2 T. Broderick "Estimation of Bit Error Rate in Pseudo-linear Differential Phase Shift Keyed Transmission Links" Optics Communications 2009 **282** pp 1455-1462

3 T. Broderick "A Simple Measure of Nonlinearity for Differential Phase Shift Keyed Transmission Links" submitted to Journal of Optical and Quantum Electronics 2008

4 T. Broderick, S.A. Boscolo & W.M.Wong "Optimisation and Statistical Analysis of 21.4 Gb/s RZ-DPSK WDM Non-Slope Matched Transmission" accepted for the 2009 SPIE Special Volume on Optical Technology in Communications

5 T. Broderick & S.A.Boscolo "Simple Eye Closure Penalty Estimate for Amplitude Noise Degraded Signals" SPIE Proceedings 7134 2008

6 T. Broderick, S.A.Boscolo & B.Slater "Bit-error rate performance of 20 Gbit/s WDM RZ-DPSK non-slope matched undersea transmission systems" SPIE Special Volume on Optical Technologies for Telecommunications 2007, **7026**

7 T. Broderick, B. Slater, S.A. Boscolo & S.K.Turitsyn " Statistical Analysis of RZ-DPSK Fibre Communication Channels" Proceedings of XVI International Workshop on Optical Waveguide Theory and Numerical Modelling Copenhagen, Denmark PO-01.O4

8 B. Slater, S. Boscolo, T. Broderick, S.K.Turitsyn, R.Freund, L.Molle, C.Caspar, J. Schwartz & S. Barnes " Performance analysis of 20 Gb/s RZ-DPSK non-slope matched transoceanic undersea links" Optics Express **15** (17), 2007 pp 10999 - 11007